Study of Peristaltic Transport of Dusty Fluids

By:

Hadia Tariq
Reg. No. 52-FBAS/PHDMA/F15

Department of Mathematics and Statistics
Faculty of Basic and Applied Sciences
International Islamic University, Islamabad
Pakistan
2020

Study of Peristaltic Transport of Dusty Fluids

By:

Hadia Tariq
Reg. No. 52-FBAS/PHDMA/F15

Department of Mathematics and Statistics
Faculty of Basic and Applied Sciences
International Islamic University, Islamabad
Pakistan
2020

Study of Peristaltic Transport of Dusty Fluids

By:

Hadia Tariq
Reg. No. 52-FBAS/PHDMA/F15

Supervised By:

Dr. Ambreen Afsar Khan

Department of Mathematics and Statistics
Faculty of Basic and Applied Sciences
International Islamic University, Islamabad
Pakistan
2020

Study of Peristaltic Transport of Dusty Fluids

By:

Hadia Tariq
Reg. No. 52-FBAS/PHDMA/F15

A Thesis
Submitted in the Partial Fulfillment of the
Requirements for the Degree of
DOCTOR OF PHILOSOPHY
IN
MATHEMATICS

Supervised By:

Dr. Ambreen Afsar Khan

Department of Mathematics and Statistics
Faculty of Basic and Applied Sciences
International Islamic University, Islamabad
Pakistan
2020

Dedication

I dedicate
this thesis to
My Parents

Muhammad Shafi Tariq (Father)
Mian Muhammad Sabir (Father-in-Law)
Mrs. Nafeesa Tariq (Mother)
Mrs. Shamim Sabir (Mother-in-Law)

Author's Declaration

I, **Hadia Tariq, Reg. No. 52-FBAS/PHDMA/F15** hereby state that my Ph.D. thesis titled: **Study of Peristaltic Transport of Dusty Fluids** is my own work and has not been submitted previously is own work and has not been submitted previously by me for taking any degree from this university, **International Islamic University, Sector H-10, Islamabad, Pakistan** or anywhere else in the country/world.

At any time if my statement is found to be incorrect even after my graduation the university has the right to withdraw my Ph.D. degree.

(Hadia Tariq)
Reg. No. 52-FBAS/PHDMA/F15
Dated: 15 October, 2020

Plagiarism Undertaking

I solemnly declare that research work presented in the thesis titled: **Study of Peristaltic Transport of Dusty Fluids** is solely my research work with no significant contribution from any other person. Small contribution/help wherever taken has been duly acknowledged and that complete thesis has been written by me.

I understand the zero tolerance policy of the HEC and University, **International Islamic University, Sector H-10, Islamabad, Pakistan** towards plagiarism. Therefore, I as an Author of the above titled thesis declare that no portion of my thesis has been plagiarized and any material used as reference is properly referred/cited.

I undertake that if I am found guilty of any formal plagiarism in the above titled thesis even after award of Ph.D. degree, the university reserves the rights to withdraw/revoke my Ph.D. degree and that HEC and the University has the right to publish my name on the HEC/University Website on which names of students are placed who submitted plagiarized thesis.

Student/Author Signature: 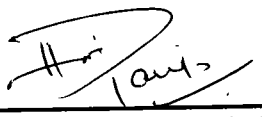

Name: **(Hadia Tariq)**

Certificate of Approval

This is to certify that the research work presented in this thesis, entitled: **Study of Peristaltic Transport of Dusty Fluids** was conducted by **Ms. Hadia Tariq,** Reg. No. **52-FBAS/PHDMA/F15** under the supervision of **Dr. Ambreen Afsar Khan** no part of this thesis has been submitted anywhere else for any other degree. This thesis is submitted to the **Department of Mathematics & Statistics, FBAS, IIU, Islamabad** in partial fulfillment of the requirements for the degree of **Doctor of Philosophy in Mathematics, Department of Mathematics & Statistics, Faculty of Basic & Applied Science, International Islamic University, Sector H-10, Islamabad, Pakistan.**

Student Name: Hadia Tariq **Signature:** _____

Examination Committee:

a) **External Examiner 1:**
Name/Designation/Office Address **Signature:** _____

Prof. Dr. Masood Khan
Professor of Mathematics,
Department of Mathematics,
Quaid-i-Azam University, Islamabad.

b) **External Examiner 2:**
Name/Designation/Office Address) **Signature:** _____

Dr. Nabeela Kousar
Associate Professor
Department of Mathematics,
Air University, Islamabad.

c) **Internal Examiner:**
Name/Designation/Office Address) **Signature:** _____

Dr. Khadija Maqbool
Assistant Professor

Supervisor Name:
Dr. Ambreen Afsar Khan **Signature:** _____

Name of HOD:
Dr. Maleeha Rashid **Signature:** _____

Name of Dean:
Prof. Dr. Muhammad Irfan Khan **Signature:** _____

Acknowledgement

My grateful thanks to **Allah Almighty** for giving me an opportunity, courage, health and chance to continue and complete this degree.

My sincere thanks and appreciation to my supervisor **Dr. Ambreen Afsar Khan** for her assistance, support and guidance which resulted in the completion of my thesis. She has always been there for me, making sure that I worked to the best of my ability and potential.

I extend my acknowledgement to **Dr. Khadija Maqbool, Dr. Maliha Rashid** and **Dr. Sajida** for their support throughout the process of this innovative task.

I am grateful to my family especially to my daughter **Manal Asif** and husband **Mian Muhammad Asif** who gave me much space, time and support to continue my studies and complete this degree. My parents have always been a source of energy, inspiration and encouragement and my siblings have always been there to support and help me whenever I needed.

I render my gratitude to my research fellows **Maryam Aziz, Rabia Batool** and **Naeema Manzoor** who helped me out and encouraged me to fulfill my research work. My dearest friend **Zainab Yousuf** for her moral support and last but not the least, I would especially mention my household helper **Ibnan Bilal**. His contribution has been immense and irreplaceable.

(Hadia Tariq)

Preface

Dusty fluids are important due to their involvement and application in the environmental sciences, engineering and physical sciences. Examples of such fluids in different fields are fallouts of pollutants in air, mixture of micro molecules of fibers exclusions in paper making, ignition and impulsion in rockets, polluted water, many juice products with pulp, paints with different suspensions, impurified crude oil etc. Many industries also utilize peristaltic pumps at different situations while processing and dealing with such fluids. This dissertation focuses on the flow of dusty fluid flowing through different geometries such as symmetric channel, asymmetric channel, curved channel and tube. These channels are considered to be exhibiting peristaltic manner. Different body forces like MHD and porosity have been added to the momentum equation, to study the dusty fluid impact in different situations. Heat transfer analysis has also been investigated. A system of coupled equations for both fluid and solid particles are derived for each case. These equations are non-linear in nature thus stream function conversions have been taken into account. Different boundary conditions such as slip condition, no slip condition, wall properties have been employed for distinct situation. Regular perturbation technique has been implemented to get the solutions. Graphical representation of the results is included to demonstrate the solutions.

Chapter one includes the basic definitions, laws and dimensionless numbers that have been used in this research. A brief literature review is also part of this chapter to give an insight to the concept of peristalsis and the related researches that have been done.

Chapter two includes effect of wall properties on the dusty Walter's B fluid model flowing through a symmetric passage. The results of the coupled equations are obtained by employing perturbation technique. The concluded outcomes are shown graphically. Impact of parameters on velocity, streamline patterns and flow rate are exhibited through graphs. This study can help researchers to understand the elastic properties of paints, polymers and molten plastic. The results obtained in this study are issued in the **Journal of Brazilian Society of Mechanical Sciences and Engineering (2018) 40:368.**

Chapter three is about the second-grade dusty fluid flowing through an asymmetric porous channel. The coupled equations are modelled. Regular perturbation method has been imposed to the system of equations to get the solutions. Streamline patterns and pressure rise graphs are found to demonstrate the influence of distinct parameters. Outcomes of this study are publication in the **Journal of Porous Media (2020) 23(9):883.**

Chapter four deals with the dusty Jeffrey fluid flowing past a symmetric passage under the influence of wall properties. The wave number in this study has been taken small, therefore the impact of both relaxation and retardation times are involved. In past, no effort is made to study the Jeffrey fluid with retardation time. Regular perturbation technique has been adopted to get the results for fluid and solid particles. Flow rate streamline patterns and velocity graphs are included to show the impact of different parameters. The results of this study are submitted in **Arabian Journal for Science and Engineering.**

Chapter five is the extension of chapter two. The motivation of this study is to investigate the MHD impact on the dusty Walter's B fluid model flowing through an

inclined asymmetric channel. The impact of heat transfer on such fluid has also been examined. DSolver command in Mathematica has been used to get the results and has been demonstrated graphically. Influence of distinct parameters on velocity and pressure are shown through graphs. The results of research are published in **Arabian Journal for Science and Engineering 44(9), 7799 – 7808 (2019).**

Chapter six is about the dusty second-grade fluid flowing past a tube. The tube is considered to be symmetric. Coupled equations have been solved by using build-in command DSolver in Mathematica. Influence of diverse parameters on the velocity, pressure rise, pressure gradient and streamline patterns have been shown. The outcomes of this research are published in **Journal of Mechanical Engineering Research 11(2), 11 – 25 (2020).**

Chapter seven deals with the study of dusty fluid with variable density of dust particles. Till date, no research study has been conducted in which the dust particles' number density is varying or not a constant. This research is conducted to note the behavior of dusty fluid with variable number density. The calculations of the coupled equations have been demonstrated through graphs. Slip condition is imposed to the boundaries to note down their behavior too. Streamline patterns and velocity graphs are included to validate the influence of parameters on such fluid. This research is accepted to be published in **Arabian Journal for Science and Engineering (2020).**

Chapter eight deals with the dusty fluid flowing through an endoscope. No effort has been made till now, to observe the flow of dusty fluid in such situation. An initial insight has been obtained by using long wavelength approximation. The obtained results are illustrated through graphs. Velocity, pressure rise and streamline patterns

graphs are included to show the effect of different parameters involved. This research study is accepted for publication in **SN Applied Sciences**.

Chapter nine is about dusty second-grade fluid flowing through a curved asymmetric channel. In previously available research articles, no attempt has been made to study such fluid in a curved channel. This research can be helpful to know the behavior of dusty fluid flowing through the curved channel as many glandular ducts, tubes are curved in nature. The results are shown through graphs. Velocity and contour graphs show the effect of involved parameters. The outcomes of this study are submitted in **Archive of Applied Mechanics**.

Contents

Chapter 1

Introduction

This chapter includes the basic definitions and concepts, fundamental laws, mathematical models and non-dimensional numbers associated to the research presented in this thesis. A comprehensive literature survey has been included to provide a better understanding to the readers.

1.1 Peristalsis

Originated from the Greek word *peristaltikos*, the wave like motion forming sinusoidal patterns, produced in the walls of tubes, channels, muscles or passages is termed as peristalsis. These sinusoidal waves are produced naturally in the biological systems. The blood flow through the veins, the esophagus, the ureters, small intestine and many more systems within the living beings exhibit the peristaltic movement. These successive waves result in the flow of the fluid or food in the desired direction. This natural mechanism inspired engineers to develop the peristaltic pumps, finger pumps and roller pumps. These pumps are extensively used in many industries e.g. oil refineries, food manufacturing factories, paper industries, sewage treatment plants and many other industries utilizes this mechanism. Many life-saving machines like dialysis machine, heart-lung machine have peristaltic pumps fixed in them.

1.2 Pumping

Pumping is an important phenomenon in peristalsis. To analyze the pumping features, the difference of time averaged flux with difference in pressure across one wavelength is observed. For inertial free peristaltic flow, the linear relation between ΔP_λ (pressure rise per wavelength) and fixed frame flux can be obtained by using the relation between wave frame and fixed frame flux. The flow pumped by peristaltic waves can also be measured by this relation.

1.3 Trapping

In a wave frame, a bolus can be defined as a volume of fluid enclosed by streamlines. When a bolus is transported at the wave speed, then this phenomenon is termed as trapping. The trapped bolus, as a whole move at the peristaltic wave speed as if surrounded by the wave. Food bolus movement in gastrointestinal track and thrombus formation in blood may be caused due to this physical phenomenon.

1.4 Dusty Fluid

Dusty fluid can be defined as a fluid having solid spherical particles suspended in it. Infected urine, pollutant fall outs in the air, various paints having powder and glitters, juices with pulp granules, impurified crude oil are few examples of such fluid.

1.5 Magnetohydrodynamic (MHD)

In fluid dynamics, the interaction of electromagnetic fluids and electrically conducting fluids are said to be under MHD effects. The study of the motion of magnetic field in the fluid is termed as magnetohydrodynamics (MHD). The set of Maxwell's equations connect the magnetic and electric field to their sources, current density and charge density.

$$\nabla . E = \frac{\rho_v}{\epsilon_0}, \qquad \text{(Gauss's Law of Electricity)}$$

$$\nabla . B = 0, \qquad \text{(Gauss's Law of Magnetism)}$$

$$\nabla \times E = -\frac{\partial B}{\partial t}, \qquad \text{(Faraday's Law)}$$

$$\nabla \times B = \mu_0 J + \mu_0 \epsilon_0 \frac{\partial E}{\partial t}, \qquad \text{(Ampere's Law)}$$

where

E is electric field, B is the magnetic field, J is current density, ρ_v is volume charge density, μ_0 is permeability of free space, ϵ_0 is permittivity for fixed space.

1.6 Porous Media

A surface having pores in it is said to be porous medium or surface. Many materials like soil, sand is porous as they allow air or fluid pass through them. In living beings, lungs, gall bladder and small blood vessels are porous. Elshehawey et al. [1] were the first who started work in porous medium with the fluid exhibiting peristaltic manner.

1.7 Dimensionless Numbers

The dimensionless numbers that are commonly studied in fluid mechanics and are used in this dissertation are defined below.

1.7.1 Reynolds Number

Inertial force proportional to the viscous force is defined as Reynolds number. It is denoted by Re.

$$Re = \frac{\text{Interial Force}}{\text{Viscous Force}}.$$

Reynolds number helps to predict the nature of the flow. The flow of the fluid is considered to be laminar if $Re < 2400$. If $2400 < Re \leq 4000$, the flow is said to be transitional while it is said to be turbulent if $Re > 4000$.

1.7.2 Prandtl Number

Prandtl number is proportion between the viscous diffusivity and thermal diffusivity. It is signified by Pr.

$$Pr = \frac{\text{viscous diffusivity}}{\text{thermal diffusivity}}.$$

1.7.3 Froude Number

It is the relation between the inertial forces and the gravitational forces. It is signified by F_r.

$$F_r = \frac{\text{interial forces}}{\text{gravitational forces}}.$$

Its significance is to analyze the nature of the flow where free surface is present.

1.7.4 Hartmann Number

Electromagnetic forces proportional to the viscous forces is defined as Hartmann number. It is denoted by Ha or H.

$$Ha = \frac{\text{electromagnetic force}}{\text{viscous force}}.$$

1.8 Basic Equations

1.8.1 Law of Conservation of Mass

Antoine Laurent Lavoisier derived this law. This law states that mass quantity in a closed system is neither formed or destroyed by physical transformation or any chemical reaction. It means that the mass remains unchanged. Continuity equation is the mathematical expression for this law. For the compressible fluids where ρ is not constant, this equation is written as

$$\frac{\partial \rho}{\partial t} + \nabla.(\rho\, \boldsymbol{V}) = 0, \tag{1.1}$$

where V is the velocity of the fluid.

In case of incompressible fluids where ρ is a constant, continuity equation reduces to

$$\nabla.\boldsymbol{V} = 0. \tag{1.2}$$

The equation of continuity for the dust particles is

$$\frac{\partial N}{\partial t} + \nabla.(N\, \boldsymbol{V}) = 0, \tag{1.3}$$

where N is the number density of the dust particles.

1.8.2 Law of Conservation of Momentum

Isaac Newton derived this fundamental law of physics. The momentum of a system remains unchanged unless an external force act on it. Mathematically, this law is expressed in equation of motion. For fluid, this equation is written as

$$\rho\left(\frac{\partial \boldsymbol{V}}{\partial t} + (\mathbf{V}.\nabla)\,\boldsymbol{V}\right) = -\nabla P + \nabla.S + \rho \boldsymbol{f}, \tag{1.4}$$

where $\boldsymbol{S}$ is the extra stress tensor and $\rho \boldsymbol{f}$ is the body force.

For the dust particles, the momentum equation is written as

$$mN\left(\frac{\partial \boldsymbol{V}_s}{\partial t} + (\boldsymbol{V}_s.\nabla)\boldsymbol{V}_s\right) = mN\boldsymbol{g} + kN(\boldsymbol{V} - \boldsymbol{V}_s). \tag{1.5}$$

In the above equation, the last terms represent the force due to the relative motion of the fluid and solid particles. Solid particles mass is denoted by m, the acceleration due to gravity is signified by $\boldsymbol{g}$ and Stokes's resistance co-efficient is given by k.

1.9 Methodology

The fluids models that are investigated in this study have been obtained by using Navier-Stokes equations. The coupled equations for 2-dimensional flows are non-linear in nature. The convective part of the Navier-Stokes equations causes non-linearity thus making the system of equations difficult to be solve. By taking stream functions into account, number of independent variables can be reduced but the non-linear nature of equations holds. Perturbation method can be applied to equations that are non-linear in nature. This technique is used to get an approximate result of the system of the equations. A small parameter is involved in this method that determines the validity and accuracy of the solution.

To get the analytical and numerical results of the system of the equations, DSolver and NDSolvers are build-in commands in Mathematica software are used. In this study, few solutions of the models are obtained by undertaking these commands.

1.10 Literature Survey

The mechanism of peristalsis has impact on pumping, pressure, trapping, reflux and the velocity of the fluid. The importance of peristalsis in both biological systems and

industrial applications have attracted many researchers and scientists to study it in different situations. Latham [2] was perhaps the primary researcher who experimentally investigated the peristaltic movement. Burn and Parkes [3] adopted the perturbation method to present the analytic solution of the problem by using small amplitude ratio. Fung and Yin [4] used the laboratory frame of reference for mathematical modelling of peristaltic flow. Shapiro et al. [5] relaxed the small amplitude approximation by using infinite wavelength approximation. Yin and Fung [6] verified experimentally that finite Reynolds number and finite wavelength is valid approximation. Newtonian fluid with peristaltic movement was investigated by Barton and Raynor [7], in flexible tubes. A bioengineering model of peristaltic fluid was suggested by Lykoudis [8]. Lew et al. [9] presented a study compromising of mathematical model of peristaltic activity of chyme. Tong and Vawter [10] studied the behavior of peristaltic pumping by applying finite difference method. Li [11] studied the peristaltic pumping under long wavelength approximation. He considered the geometry as cylindrical tube. The Poiseuille flow of the peristaltic transport of the fluid was studied by Mittra and Prasad [12]. Liron [13] examined the efficiency of peristaltic motion of the fluids in a living body. The impact of wall curvature on the peristaltic pumping was studied by Jaffrin [14]. He also investigated the inertial effects on it. The influence of peristalsis on the non-uniform tubes was studied by Gupta and Seshadri [15]. Vishnyakov et al. [16] studied the viscoplastic fluid exhibiting the peristaltic manner. The axial and gradient pressures were discussed in their article. Manero et al. [17] experimented the peristaltic motion of the fluid flowing past oscillating pipes. This study includes the investigations based on distinct values of amplitudes and frequencies of oscillation. In 1983, Srivastava et al. [18] considered physiological fluids exhibiting peristaltic motion under long wavelength and low

Reynolds number assumption. They further assumed the viscosity is variable. Bohme and Friedrich [19] presented their study with inertial free viscoelastic fluid flowing through a duct whose walls were exhibiting the peristaltic motion. Two-layered fluid flowing through a non-uniform tube was examined by Srivastava and Srivastava [20]. Takabatake and Ayukawa [21] studied the peristaltic flow numerically by using finite difference technique. Pozrikidis [22] presented the streamline patterns of distinct parameters like channel width, amplitude of the wave, phase difference in his study. Considering the walls of the tubes to be induced by peristaltic waves, Li and Brasseur [23] examined pressure and shear stress of unsteady fluid. Provost and Schwarz [24] studied the flow of fluid through axisymmetric tube. Later, Siddiqui and Schwarz [25] observed the peristaltic movement of the fluid flowing through a tube up to second order. This article discusses pressure gradient and streamline patterns of the fluid for different parameters. Few more studies in this context are [26 – 36].

The study of peristaltic transport in the existence of magnetic field has a vital role in connection to various problems involving the movement of conductive physiological fluid for example blood and saline. Krzeminski et al. [37] carried out a study to examine the impact of MHD on the fluid. Streamline graphs described the consequences of various parameters involved. Later, Afifi and Gad [38] considered the MHD impact on the fluid flowing through a porous channel. Mekheimer and Al-Arabi [39] considered planer porous passage and performed their study to check the impact of MHD on the fluid. In another study, Mekheimer [40] investigated the influence of MHD on the fluid flowing through a channel that was inclined. Few relevant studies are [41 – 49].

The exchange of thermal energy between physical systems, their generation, use and conversion is termed as heat transfer. Many industrial systems utilize heat transfer

along with peristalsis, thus attracting researchers to investigate its influence in different situations. Vajravelu et al. [50] studied the heat transfer impact on the fluid. The geometry considered in this study was a vertical annulus. Heat transfer examination in a curved passage was surveyed by Ali et al. [51]. Srinivas and Kothandapani [52] explored the heat and mass transfer of the fluid by assuming a symmetric porous passage. With the slip on the boundaries, the heat transfer impact on the peristaltic flow of the fluid was studied by Hayat et al. [53]. For the fluid flowing through a rectangular duct, heat and mass transfer was investigated by Ellahi et al. [54]. For an asymmetric passage, Sinha et al. [55] performed a study that investigates the MHD impact as well as heat transfer. Few related studies are [56 – 65].

When the flow of the molecules at the boundaries of the channel have no stationary motion then this phenomenon is referred as slip condition. Makinde and Reddy [66] studied impact of slip on the fluid flowing through a porous medium. Ebaid and Aly [67] observed the slip effects on the peristaltic nanofluids. Hayat et al. [68] considered the passage to be porous and surveyed the slip condition on the boundaries. Considering Jeffrey fluid flowing through a rectangular duct, the slip condition was studied by Ellahi and Hussain [69]. Fractional Burger's model was implemented on viscoelastic fluid to examine the slip impact on it by Tripathi et al. [70]. El-Shehawy et al. [71] studied Maxwell fluid model with slip condition. Nadeem and Akram [72] considered MHD Jeffrey fluid flowing past an asymmetric passage to examine the slip conditions on it. Hayat and Mahmood [73] examined the slip condition on third grade fluid.

In supra discussion the wall is presumed flexible but infact the wall become excited by smooth muscle contraction which controls its deformation. Therefore, walls are

elastic in nature. Mitra and Prasad [74] were first to study wall properties impact on the peristaltic flow of the fluid. Hayat and Hina [75] studied the MHD Maxwell fluid under wall properties effect. Srinivas et al. [76] examined the impression of wall properties on the fluid under MHD effect flowing through a symmetric channel. Hayat et al. [77] explored the consequences of wall properties on third grade fluid. The geometry undertaken in this study was a curved channel. They deduced that the velocity profile was not symmetric about the central line. Shahzadi et al. [78] examined the variable viscosity impact on the peristaltic flow of the fluid under the influence of wall properties. Hina et al. [79] presented a study on pseudoplastic fluid. This study includes the impact of wall properties on such fluid flowing past a curved channel. Hayat et al. [80] discussed the effect of wall properties on the viscous fluid. Micropolar fluid and effects of wall properties on it was examined by Muthu et al. [81].

In 1962, Saffman [82] introduced the system of coupled equations to investigate the flow of the dusty fluid in different situations. Later Nayfeh [83] continued this study and examined the flow of dusty fluid in a rigid pipe. The flow of dusty fluid flowing past a narrow passage was first studied by Charya [84]. The effects of the dust particles on the fluid velocity and pressure were discussed in his article. Srinivasacharya et al. [85] observed the wall properties impact on the dusty fluid exhibiting peristaltic behavior. By considering a flexible passage, Kumar et al. [86] examined peristaltic dusty fluid flowing through it. Ramamurthy and Rao [87] performed a study on dusty fluid by considering the Reynolds number to be large. The effect of MHD on dusty fluid was studied by Rathod and Kulkarni [88]. The impact of chemical reaction on dusty fluid was investigated by Muthuraj et al. [89]. They also deduced the results of heat and mass transfer. Hayat et al. [90] studied the radiative and Joule heating impact

on dusty fluid. Thermal radiation effects on viscoelastic dusty fluid was surveyed by Bhatti et al. [91]. Madhura and Uma [92] studied dusty fluid flowing through a porous passage. By considering a rectangular passage with dusty fluid flowing through it, Gireesha et al. [93] presented this study. Ramesh et al. [94] studied dusty fluid flowing through circular cylinders. In the same aspect, few recent studies are [95 – 101].

Chapter 2

Influence of Wall Properties on the Peristaltic Flow of a Dusty Walter's B Fluid

This chapter explores the impact of wall properties on the Walter's B fluid with fine solid particles in a uniform channel. Travelling sinusoidal wave is imposed on the channel walls which induces peristaltic motion in the fluid. A regular series is employed to obtain analytic solution by taking small wave number. The phenomenon is modeled in the form of stream function for both fluid and solid particles. Impact of pertinent parameters such as viscoelastic parameter κ, wave number δ, the elastic tension i.e. rigidity of the wall (E_1), the mass characterizing parameter i.e. stiffness of the wall (E_2) and the damping nature of the wall (E_3) are discussed through graphs for both fluid and dust particles. It is observed that the size of the trapped bolus increases on the right-hand side of the channel for both fluid and solid particles by increasing viscoelastic parameter. The flow rate of fluid particles surges by increasing viscoelastic parameter while it declines for solid particles.

2.1 Problem Formulation

Consider two-dimensional unsteady Walter's B fluid having fine dust particles whose number density N is assumed to be constant through a symmetric channel. In the coordinate system x-axis is along the walls and y-axis is perpendicular to it. See Fig. 2.1.

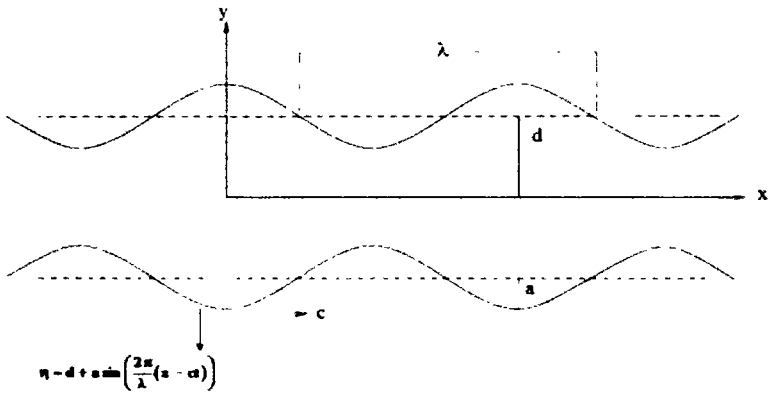

Figure 2.1: Depicts the geometry of the peristaltic transport of channel walls.

The channel wall equation is given by

$$y = \eta(\bar{X}, \bar{t}) = d + \mathrm{a}\sin\frac{2\pi}{\lambda}(\bar{X} - c\bar{t}), \tag{2.1}$$

where a is the amplitude of the wave, d half width of the channel, t the time, c the wave velocity and λ the wavelength.

The equation of motion for fluid and solid particles can be written as

For Fluid

$$\bar{\nabla}.\bar{V} = 0, \tag{2.2}$$

$$\frac{d}{dt}\bar{V} = \nabla\bar{p} + \nabla.\bar{S} + kN(\bar{V}_S - \bar{V}). \tag{2.3}$$

For Solid particles

$$\bar{\nabla}.\bar{V}_S = 0, \tag{2.4}$$

$$\frac{d}{dt}\bar{V}_s = \frac{k}{m}(\bar{V} - \bar{V}_S). \tag{2.5}$$

$\bar{V}$ and $\bar{V}_s$ represent the fluid velocity and solid particles, ρ the density and $\bar{S}$ the extra stress tensor. The mass of dust granules is m, k is the resistance co-efficient and N is

number density of solid particles, assumed to be a constant here. The constitutive relation of Walter's B fluid model is defined as

$$\bar{S} = 2\alpha_0 e - 2k_0 \frac{De}{Dt}, \tag{2.6}$$

$$\frac{De}{Dt} = \frac{\partial e}{\partial t} + \bar{V}.\nabla e - e\nabla\bar{V} - (\nabla\bar{V})^T e, \tag{2.7}$$

where e is rate of stress tensor and α_0 (limiting viscosity of shear stress) and k_0 (short memory co-efficient) are expressed as below

$$\alpha_0 = \int_0^\infty O(\tau)\, d\tau, \tag{2.8}$$

$$k_0 = \int_0^\infty \tau O(\tau) d\tau, \tag{2.9}$$

where the relaxation time is denoted by τ and $O(\tau)$ is the distribution function.

$$\int_0^\infty \tau^n O(\tau) d\tau, n \geq 2. \tag{2.10}$$

The governing equations in the form of component for fluid and solid particles are

$$\frac{\partial u}{\partial x} + \frac{\partial v}{\partial y} = 0, \tag{2.11}$$

$$\rho\left(\frac{\partial}{\partial t} + u\frac{\partial}{\partial x} + v\frac{\partial}{\partial y}\right)u = -\frac{\partial p}{\partial x} + \frac{\partial S_{xx}}{\partial x} + \frac{\partial S_{xy}}{\partial y} + kN(u_s - u), \tag{2.12}$$

$$\rho\left(\frac{\partial}{\partial t} + u\frac{\partial}{\partial x} + v\frac{\partial}{\partial y}\right)v = -\frac{\partial p}{\partial y} + \frac{\partial S_{xy}}{\partial x} + \frac{\partial S_{yy}}{\partial y} + kN(v_s - v), \tag{2.13}$$

where

$$S_{xx} = \alpha_0(4u_x) - k_0\left(4u_{xt} + 4uu_{xx} + 4vu_{xy} - 8u_x^2 - 4v_x u_y - 4v_x^2\right), \tag{2.14}$$

$$S_{xy} = \alpha_0(2u_y + 2v_x)$$

$$- k_0(2u_{yt} + 2v_{xt} + 2uu_{xy} + 2uv_{xx} + 2vu_{yy} + 2vv_{xy} - 6u_x u_y$$

$$- 2u_y v_y - 2u_x u_x - 6v_x v_y), \tag{2.15}$$

$$S_{yy} = \alpha_0(4v_y) - k_0(4v_{yt} + 4uv_{xy} + 4vv_{yy} - 4u_y^2 - 4v_x u_y - 8v_y^2). \tag{2.16}$$

For the dust particles

$$\frac{\partial u_s}{\partial x} + \frac{\partial v_s}{\partial y} = 0, \tag{2.17}$$

$$\frac{\partial u_s}{\partial t} + u_s\frac{\partial u_s}{\partial x} + v_s\frac{\partial u_s}{\partial y} = \frac{k}{m}(u - u_s), \tag{2.18}$$

$$\frac{\partial v_s}{\partial t} + u_s\frac{\partial v_s}{\partial x} + v_s\frac{\partial v_s}{\partial y} = \frac{k}{m}(v - v_s). \tag{2.19}$$

For flexible wall, the ruling equation of motion is

$$L(\eta) = p - p_0, \tag{2.20}$$

here L represent the movement of the stretched membrane with damping forces and it is defined as

$$L = -T\frac{\partial^2}{\partial x^2} + m'\frac{\partial^2}{\partial t^2} + C\frac{\partial}{\partial t}, \tag{2.21}$$

where T is tension, m' is mass per unit area, C is damping force co-efficient, p_0 pressure on the external wall.

It is considered that the walls of the passage are inextensible and $p_0 = 0$, thus the horizontal displacement of the wall is zero. The no-slip boundary conditions are

$$u = 0, \quad u_s = 0, \quad at\ y = \pm\eta, \tag{2.22}$$

$$\frac{\partial P}{\partial x} = \frac{\partial}{\partial x}L(\eta) = \mu\left(\frac{\partial S_{xx}}{\partial x} + \frac{\partial S_{xy}}{\partial y}\right) - \rho\left(\frac{\partial u}{\partial t} + u\frac{\partial u}{\partial x} + v\frac{\partial u}{\partial y}\right) + kN(u_s - u).$$

$$at\ y = \pm\eta \qquad (2.23)$$

Let us define the following stream functions and non-dimensional parameters

$$u = \frac{\partial \psi}{\partial y}, \quad v = -\frac{\partial \psi}{\partial x}, \quad u_s = \frac{\partial \varphi}{\partial y}, \quad v_s = -\frac{\partial \varphi}{\partial x}, \quad \bar{y} = \frac{y}{d},$$

$$\bar{\psi} = \frac{\psi}{\nu}, \quad \bar{\varphi} = \frac{\varphi}{\nu}, \quad \bar{x} = \frac{x}{\lambda}, \quad \bar{p} = \frac{d^2 p}{\alpha_0 \lambda c}, \quad \bar{S} = \frac{d^2}{\alpha_0 \nu^2 \rho} S,$$

$$\bar{t} = \frac{ct}{\lambda}, \quad \delta = \frac{d}{\lambda}, \quad \kappa = \frac{k_0 \nu}{\alpha_0 d^2}. \qquad (2.24)$$

The compatibility equations for the fluid and the dust particles after using the transformation and dropping the bar become

$$\delta\left[\frac{\partial}{\partial y}\left(\frac{\partial^2 \psi}{\partial t \partial y} + \frac{\partial \psi}{\partial y}\frac{\partial^2 \psi}{\partial x \partial y} - \frac{\partial \psi}{\partial x}\frac{\partial^2 \psi}{\partial y^2}\right) + \delta^2 \frac{\partial}{\partial x}\left(\frac{\partial^2 \psi}{\partial t \partial x} + \frac{\partial \psi}{\partial y}\frac{\partial^2 \psi}{\partial x^2} - \frac{\partial \psi}{\partial x}\frac{\partial^2 \psi}{\partial x \partial y}\right)\right]$$

$$= \delta \frac{\partial^2}{\partial x \partial y}(S_{xx} - S_{yy}) + \left(\frac{\partial^2}{\partial y^2} - \delta^2 \frac{\partial^2}{\partial x^2}\right) S_{xy}$$

$$+ A(\nabla_1^2 \varphi - \nabla_1^2 \psi), \qquad (2.25)$$

$$\delta\left[\frac{\partial}{\partial t}\nabla_1^2 \varphi + \frac{\partial \varphi}{\partial y}\nabla_1^2 \varphi - \frac{\partial \varphi}{\partial x}\nabla_1^2 \varphi\right] = B[\,\nabla_1^2 \psi - \nabla_1^2 \varphi], \qquad (2.26)$$

where $\nabla_1^2 = \left(\delta^2 \frac{\partial^2}{\partial x^2} + \frac{\partial^2}{\partial y^2}\right)$ is the non-dimensional operator and $A = \frac{kNd^2}{\mu}$ and $B = \frac{kd^2}{m\nu}$ are non-dimensional parameters.

$$S_{xx} = 4\delta\frac{\partial^2\psi}{\partial x\partial y}$$

$$-\kappa\delta^2\left[4\frac{\partial^3\psi}{\partial x\partial y\partial t}+4\frac{\partial\psi}{\partial y}\frac{\partial^3\psi}{\partial x^2\partial y}-4\frac{\partial\psi}{\partial x}\frac{\partial^3\psi}{\partial x\partial y^2}-8\left(\frac{\partial^2\psi}{\partial x\partial y}\right)^2\right.$$

$$\left.+4\frac{\partial^2\psi}{\partial y^2}\frac{\partial^2\psi}{\partial x^2}-4\delta^2\left(\frac{\partial^2\psi}{\partial x^2}\right)^2\right], \tag{2.27}$$

$$S_{xy} = \left(2\frac{\partial^2\psi}{\partial y^2}-2\delta^2\frac{\partial^2\psi}{\partial x^2}\right)$$

$$-\kappa\left[2\delta^2\frac{\partial^3\psi}{\partial t\partial x\partial y}-2\delta^3\frac{\partial^3\psi}{\partial t\partial x^2}+2\delta\frac{\partial\psi}{\partial y}\frac{\partial^3\psi}{\partial x\partial y^2}-2\delta^3\frac{\partial\psi}{\partial y}\frac{\partial^3\psi}{\partial x^3}\right.$$

$$-2\delta\frac{\partial\psi}{\partial x}\frac{\partial^3\psi}{\partial y^3}+2\delta^3\frac{\partial\psi}{\partial x}\frac{\partial^3\psi}{\partial x^2\partial y}-4\delta\frac{\partial^2\psi}{\partial x\partial y}\frac{\partial^2\psi}{\partial y^2}$$

$$\left.-4\delta^3\frac{\partial^2\psi}{\partial x^2}\frac{\partial^2\psi}{\partial x\partial y}\right], \tag{2.28}$$

$$S_{yy} = 4\delta\frac{\partial^2\psi}{\partial x\partial y}$$

$$-\kappa\left[4\delta^2\frac{\partial^3\psi}{\partial t\partial x\partial y}-4\delta^2\frac{\partial\psi}{\partial y}\frac{\partial^3\psi}{\partial x^2\partial y}+4\delta^2\frac{\partial\psi}{\partial x}\frac{\partial^3\psi}{\partial x\partial y^2}-4\frac{\partial^2\psi}{\partial y^2}\right.$$

$$\left.+4\frac{\partial^2\psi}{\partial x^2}\frac{\partial^2\psi}{\partial y^2}\quad-8\delta^2\frac{\partial^2\psi}{\partial x\partial y}\right]. \tag{2.29}$$

The geometry of the walls in the non-dimensional form is

$$y = \pm\eta = \pm\big(1+\epsilon sin2\pi(x-t)\big), \tag{2.30}$$

The non-dimensional form of the boundary conditions is

$$\frac{\partial\psi}{\partial y} = 0,\quad \frac{\partial\varphi}{\partial y} = 0, \qquad at\ y = \pm\eta, \tag{2.31}$$

$$\nabla_1^2 \frac{\partial \psi}{\partial y} - \delta \left[\frac{\partial}{\partial t} \frac{\partial \psi}{\partial y} + \frac{\partial \psi}{\partial y} \frac{\partial}{\partial x} \frac{\partial \psi}{\partial x} - \frac{\partial}{\partial x} \frac{\partial}{\partial y} \frac{\partial \psi}{\partial y} \right] + A \left[\frac{\partial \varphi}{\partial y} - \frac{\partial \psi}{\partial y} \right]$$

$$= \left[E_1 \frac{\partial^3}{\partial x^3} + E_2 \frac{\partial^3}{\partial x \partial t^2} + E_3 \frac{\partial^2}{\partial x \partial t} \right] \eta, \quad at\ y = \pm\eta. \tag{2.32}$$

where $E_1 = \frac{Td^4}{\alpha_0 \nu \rho}$ is tension membrane parameter, $E_2 = \frac{m'd^2}{\alpha_0 \lambda^3 \rho}$ is mass characterizing parameter and $E_3 = \frac{cd^3}{\alpha_0 \lambda^2 \nu \rho}$ signifies the damping parameter.

2.2 Method of Solution

The perturbation technique for small geometric parameter ($\delta \ll 1$) is used to get the solution.

$$\left.\begin{aligned} \psi &= \psi_0 + \delta\psi_1 + \delta^2\psi_2 + \cdots \\ \varphi &= \varphi_0 + \delta\varphi_1 + \delta^2\varphi_2 + \cdots \end{aligned}\right\}. \tag{2.33}$$

2.2.1 Zeroth Order System

$$\frac{\partial^2}{\partial y^2}(S_{0xy}) + A\left(\frac{\partial^2 \varphi_0}{\partial y^2} - \frac{\partial^2 \psi_0}{\partial y^2}\right) = 0, \tag{2.34}$$

$$B\left(\frac{\partial^2 \psi_0}{\partial y^2} - \frac{\partial^2 \varphi_0}{\partial y^2}\right) = 0, \tag{2.35}$$

where

$$S_{0xy} = 2\frac{\partial^2 \psi_0}{\partial y^2}, \tag{2.36}$$

with

$$\frac{\partial \psi_0}{\partial y} = 0, \frac{\partial \varphi_0}{\partial y} = 0, \qquad at \quad y = \pm\eta, \tag{2.37}$$

$$\frac{\partial^3\psi_0}{\partial y^3} + A\left[\frac{\partial\varphi_0}{\partial y} - \frac{\partial\psi_0}{\partial y}\right] = \left[E_1\frac{\partial^3}{\partial x^3} + E_2\frac{\partial^3}{\partial x\partial t^2} + E_3\frac{\partial^2}{\partial x\partial t}\right]\eta, \quad at\ y = \pm\eta. \quad (2.38)$$

2.2.2 First Order System

$$\frac{\partial}{\partial y}\left(\frac{\partial^2\psi_0}{\partial t\partial y} + \frac{\partial\psi_0}{\partial y}\frac{\partial^2\psi_0}{\partial x\partial y} - \frac{\partial\psi_0}{\partial x}\frac{\partial^2\psi_0}{\partial y^2}\right)$$

$$= \frac{\partial^2}{\partial x\partial y}(S_{0xx} - S_{0yy}) + \frac{\partial^2}{\partial y^2}(S_{1xy}) + A\left(\frac{\partial^2\varphi_1}{\partial y^2} - \frac{\partial^2\psi_1}{\partial y^2}\right), \quad (2.39)$$

$$B\left(\frac{\partial^2\psi_1}{\partial y^2} - \frac{\partial^2\varphi_1}{\partial y^2}\right) = \frac{\partial^3\varphi_0}{\partial t\partial y^2} + \frac{\partial\varphi_0}{\partial y}\frac{\partial^3\varphi_0}{\partial x\partial y^2} - \frac{\partial\varphi_0}{\partial x}\frac{\partial^3\varphi_0}{\partial y^3}, \quad (2.40)$$

where

$$S_{0xx} = 0, \quad (2.41)$$

$$S_{0yy} = \kappa\left[4\left(\frac{\partial^2\psi_0}{\partial y^2}\right)^2\right], \quad (2.42)$$

$$S_{1xy} = 2\frac{\partial^2\psi_1}{\partial y^2} - \kappa\left[2\frac{\partial\psi_0}{\partial y}\frac{\partial^3\psi_0}{\partial x\partial y^2} - 2\frac{\partial\psi_0}{\partial x}\frac{\partial^3\psi_0}{\partial y^3} - 4\frac{\partial^2\psi_0}{\partial x\partial y}\frac{\partial^2\psi_0}{\partial y^2}\right], \quad (2.43)$$

with

$$\frac{\partial\psi_1}{\partial y} = 0, \quad \frac{\partial\varphi_1}{\partial y} = 0, \quad at\ y = \pm\eta, \quad (2.44)$$

$$\frac{\partial^3\psi_1}{\partial y^3} + A\left[\frac{\partial\varphi_1}{\partial y} - \frac{\partial\psi_1}{\partial y}\right] = \frac{\partial^2\psi_0}{\partial t\partial y} + \frac{\partial\psi_0}{\partial y}\frac{\partial^2\psi_0}{\partial x\partial y} - \frac{\partial\psi_0}{\partial x}\frac{\partial^2\psi_0}{\partial y^2}, \quad at\ y = \pm\eta. \quad (2.45)$$

2.2.3 Second Order System

$$\frac{\partial}{\partial y}\left(\frac{\partial^2\psi_1}{\partial t\partial y}+\frac{\partial\psi_1}{\partial y}\frac{\partial^2\psi_0}{\partial x\partial y}+\frac{\partial\psi_0}{\partial y}\frac{\partial^2\psi_1}{\partial x\partial y}-\frac{\partial\psi_1}{\partial x}\frac{\partial^2\psi_0}{\partial y^2}-\frac{\partial\psi_0}{\partial x}\frac{\partial^2\psi_1}{\partial y^2}\right)$$

$$=\frac{\partial^2}{\partial x\partial y}(S_{1xx}-S_{1yy})+\frac{\partial^2}{\partial y^2}(S_{2xy})-\frac{\partial^2}{\partial x^2}(S_{0xy})$$

$$+A\left[\left(\frac{\partial^2\varphi_2}{\partial y^2}+\frac{\partial^2\varphi_0}{\partial x^2}\right)-\left(\frac{\partial^2\psi_2}{\partial y^2}+\frac{\partial^2\psi_0}{\partial x^2}\right)\right], \tag{2.46}$$

$$B\left[\left(\frac{\partial^2\psi_2}{\partial y^2}+\frac{\partial^2\psi_0}{\partial x^2}\right)-\left(\frac{\partial^2\varphi_2}{\partial y^2}+\frac{\partial^2\varphi_0}{\partial x^2}\right)\right]$$

$$=\frac{\partial^3\varphi_1}{\partial t\partial y^2}+\frac{\partial\varphi_1}{\partial y}\frac{\partial^3\varphi_0}{\partial x\partial y^2}+\frac{\partial\varphi_0}{\partial y}\frac{\partial^3\varphi_1}{\partial x\partial y^2}-\frac{\partial\varphi_1}{\partial x}\frac{\partial^3\varphi_0}{\partial y^3}-\frac{\partial\varphi_0}{\partial x}\frac{\partial^3\varphi_1}{\partial y^3},$$

(2.47)

where

$$S_{1xx}=4\frac{\partial^2\psi_0}{\partial x\partial y}+8\kappa\left(\frac{\partial^2\psi_0}{\partial x\partial y}\right)^2, \tag{2.48}$$

$$S_{1yy}=8\kappa\frac{\partial^2\psi_0}{\partial y^2}\frac{\partial^2\psi_1}{\partial x^2}-4\frac{\partial^2\psi_0}{\partial x\partial y}, \tag{2.49}$$

$$S_{2xy}=\left(2\frac{\partial^2\psi_2}{\partial y^2}-2\frac{\partial^2\psi_0}{\partial x^2}\right)$$

$$-\kappa\left[2\frac{\partial\psi_1}{\partial y}\frac{\partial^3\psi_0}{\partial x\partial y^2}+2\frac{\partial\psi_0}{\partial y}\frac{\partial^3\psi_1}{\partial x\partial y^2}-2\frac{\partial\psi_0}{\partial x}\frac{\partial^3\psi_1}{\partial y^3}-2\frac{\partial\psi_1}{\partial x}\frac{\partial^3\psi_0}{\partial y^3}\right.$$

$$-4\frac{\partial^2\psi_0}{\partial x\partial y}\frac{\partial^2\psi_1}{\partial y^2}$$

$$\left.-4\frac{\partial^2\psi_1}{\partial x\partial y}\frac{\partial^2\psi_0}{\partial y^2}\right], \tag{2.50}$$

with boundary conditions

$$\frac{\partial\psi_2}{\partial y}=0,\frac{\partial\varphi_2}{\partial y}=0, \qquad at\ y=\pm\eta, \tag{2.51}$$

$$\frac{\partial^3\psi_2}{\partial y^3}+\frac{\partial^3\psi_0}{\partial y\partial x^2}+A\left(\frac{\partial\varphi_2}{\partial y}-\frac{\partial\psi_2}{\partial y}\right)$$

$$=\left(\frac{\partial^2\psi_0}{\partial t\partial x}+\frac{\partial\psi_0}{\partial y}\frac{\partial^2\psi_1}{\partial x\partial y}+\frac{\partial\psi_1}{\partial y}\frac{\partial^2\psi_0}{\partial x\partial y}-\frac{\partial\psi_0}{\partial x}\frac{\partial^2\psi_1}{\partial y^2}-\frac{\partial\psi_1}{\partial x}\frac{\partial^2\psi_0}{\partial y^2}\right),$$

$$at\ y=\pm\eta. \tag{2.52}$$

The solutions are obtained by using the DSolver in Mathematica and are illustrated through graphs.

2.3 Results and Discussion

This portion includes the discussion on the impact of different parameters on the fluid and solid particles. The rigidity of the wall that rely on the wall tension is given by E_1 and E_2 denotes the stiffness of the wall. E_3 is dissipative nature of the wall i.e. the elasticity is determined by it. The viscoelastic property of the fluid is symbolized by κ while the wave number is denoted by δ. Figs. 2.2 – 2.4 show the velocity graphs of the fluid. Figs. 2.5 – 2.9 depict the consequences of various parameters on the flow rate of fluid. Figs. 2.10 – 2.14 are the contour graphs of viscoelastic parameter, wave number and wall parameters in the fluid. Figs. 2.15 – 2.17 portray the effects of different parameters on the velocity of solid particles. Figs. 2.18 – 2.22 render the influence of different parameters on the flow rate of the solid particles. Figs. 2.23 – 2.27 represent the contour graphs of the fine solid particles.

Fig. 2.2 describes the effects of E_1, E_2 and E_3 on the velocity of the fluid. It can be clearly observed that the increase in the parameters also increases the velocity of the fluid. It can be observed from Fig. 2.3 that there is slight growth in the fluid velocity with the increase in the wave number δ. The parameter κ has significant impact on the velocity of the fluid. It can be perceived from Fig. 2.4 that the fluid velocity

intensifies with the increase in κ. Figs. 2.5 – 2.7 depict that by increasing the values of E_1, E_2 and E_3, the fluid's flow rate rises too. The impact of δ on the fluid's flow rate can be detected in Fig. 2.8. The flow rate strengthens with the increase in wave number. Fig. 2.9 points out that when κ is increased, the flow rate of the fluid particles is reduced. Fig. 2.10 shows the behavior of trapped bolus under the different values of δ. Fig. 2.11 shows that the trapped bolus expands as the viscoelastic parameter increases. Figs. 2.12 – 2.14 show that the boluses expand in the channel's right side as the values of wall properties are enhanced.

The impact of different parameters on the velocity of the solid particles can be seen in Fig. 2.15. The rise in the tension parameter (E_1), the mass parameter (E_2) and the damping parameter (E_3) also increase the velocity of the solid particles. Fig. 2.16 show that there is growth in the velocity of the solid particles as δ is increased. Fig. 2.17 shows that as κ is increased the velocity of the dust particles is also increased. Figs. 2.18 and 2.19 show that the flow rate of the dust particles is enhanced as E_1 and E_2 are increased. There is slight decrease in the flow rate of the solid particles as we increase the values of E_3. It can be seen in Fig. 2.20. The consequences of δ on the flow rate of the dust particles can be seen in Fig. 2.21. The magnitude of trapping bolus increases as δ is increased. Fig. 2.22 reveals that the flow rate of the solid particles decreases as the viscoelastic parameter κ changes. Fig. 2.23 shows that the trapped bolus expands on the right side of the passage as the viscoelastic parameter (κ) increases while it compresses on the left side of the passage. Fig. 2.24 depicts that with the increase in δ the trapped bolus increases too. Figs. 2.25 – 2.27 show that the wall parameters are expanding the size of the bolus. Fig. 2.28 depicts the comparison of the flow rate for E_1 between the present work and the previously published work by Srinivasacharya et. al. [85].

2.4 Graphs

For Fluid

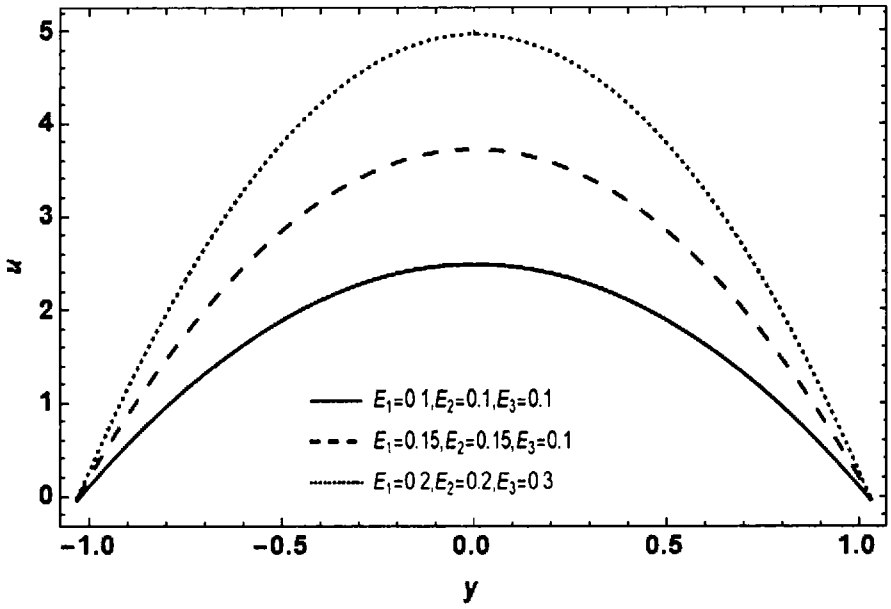

Figure 2.2: Influence of E_1, E_2 and E_3 on velocity with A=1, B = 1, δ = 0.01, ϵ = 0.1, κ = 0.1.

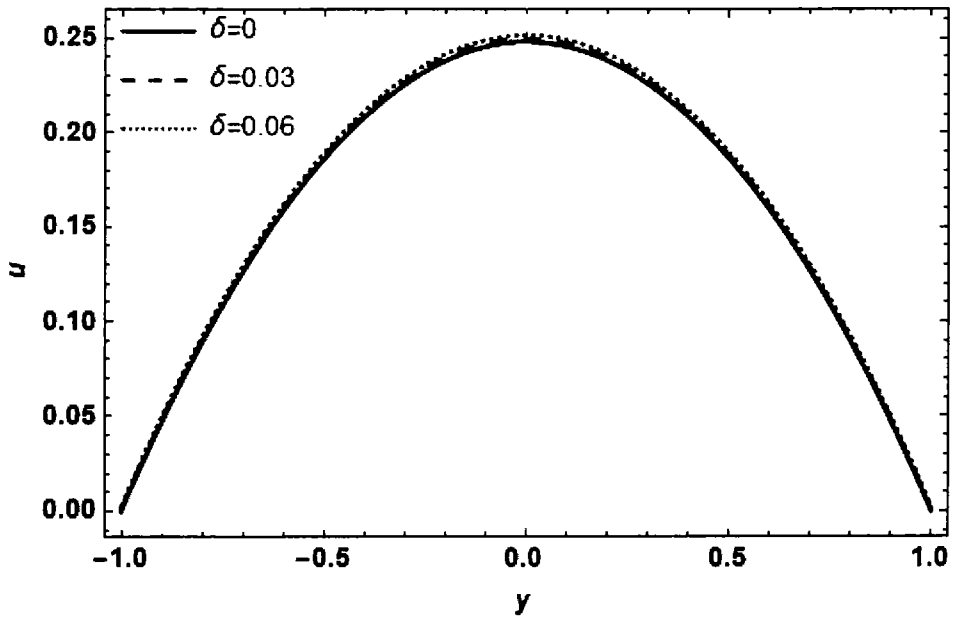

Figure 2.3: Influence of δ on velocity with ϵ = 0.1, E_2 = 0.01, A= 0.5, E_3 = 0.01, B = 0.1, κ = 0.01, E_1 = 0.01.

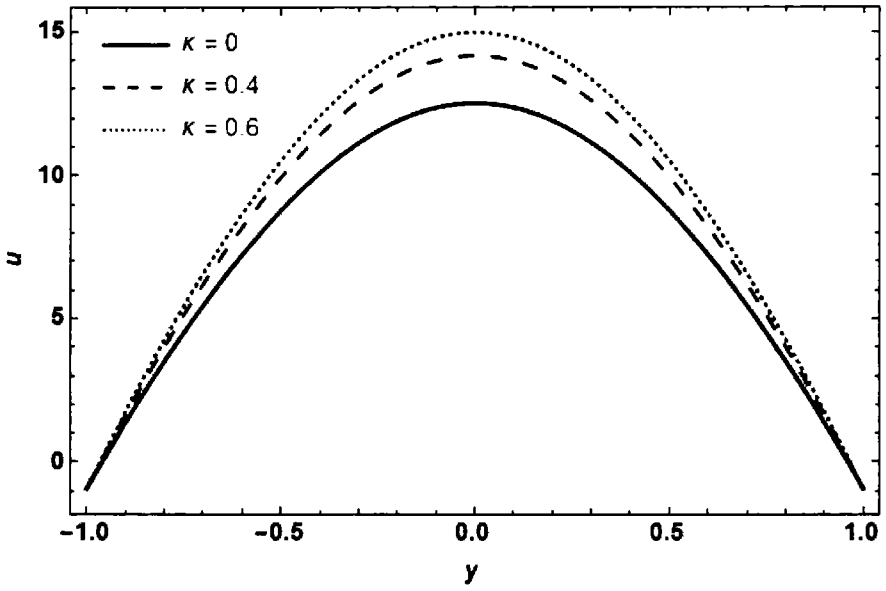

Figure 2.4: Influence of κ on velocity with $E_1 = 0.5$, $E_2 = 0.5$, $A = 1$, B = 1, $E_3 = 0.5$, $\epsilon = 0.1$, $\delta = 0.01$.

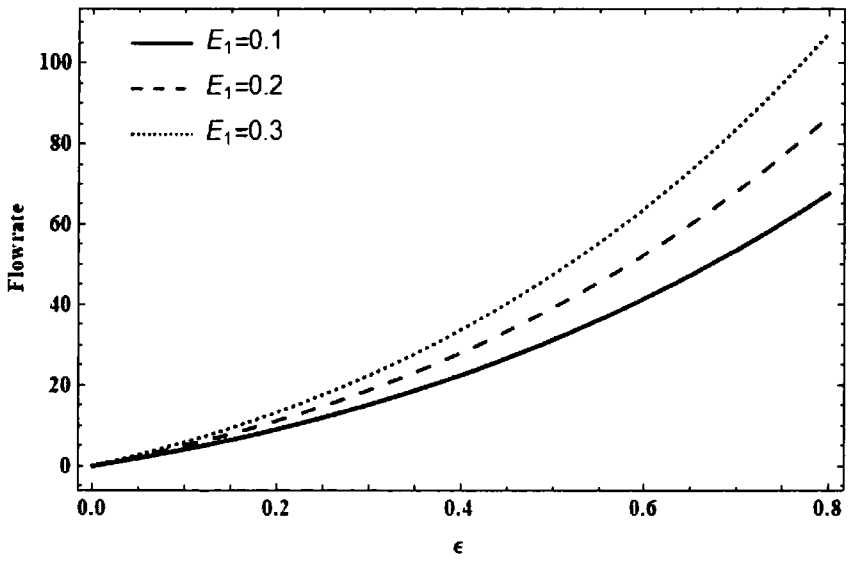

Figure 2.5: Influence of E_1 on the flow rate with $E_2 = 0.35$, $B = 1$, $E_3 = 0.25$, $A = 0.1$, $\delta = 0.01$ and $\kappa = 0.9$.

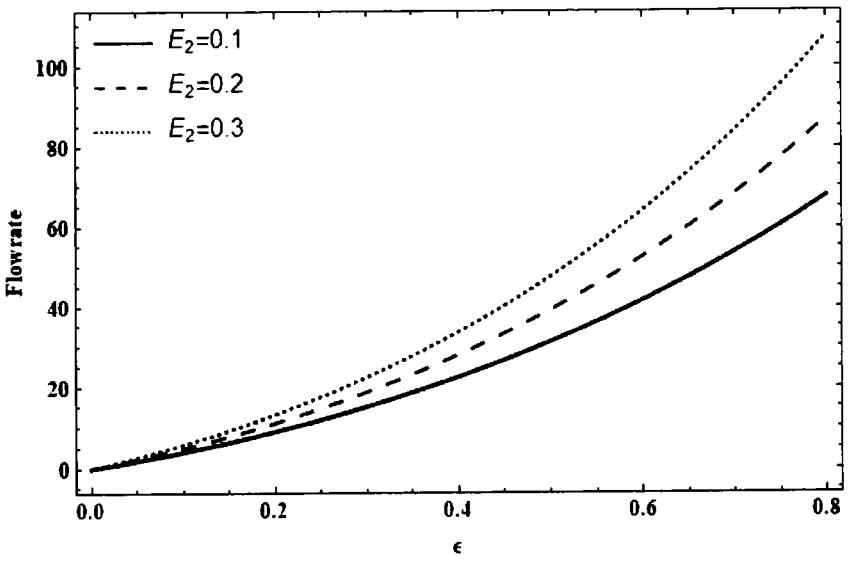

Figure 2.6: Influence of E_2 on the flow rate with $E_1 = 0.35$, $B = 0.1$, $E_3 = 0.25$, $A = 0.1$, $\delta = 0.01$ and $\kappa = 0.9$.

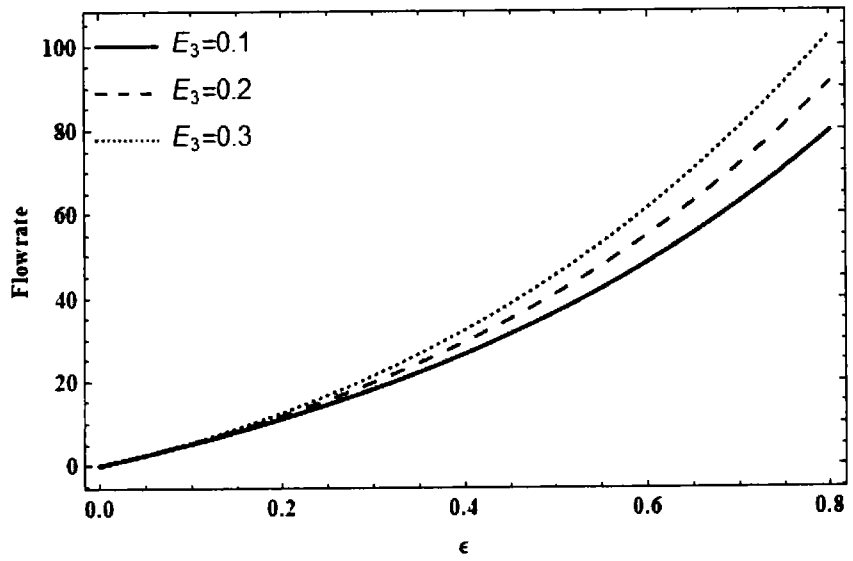

Figure 2.7: Influence of E_3 on the flow rate with $E_1 = 0.35$, $B=0.1$, $E_2 = 0.25$, $A = 0.1$, $\delta = 0.01$ and $\kappa = 0.9$.

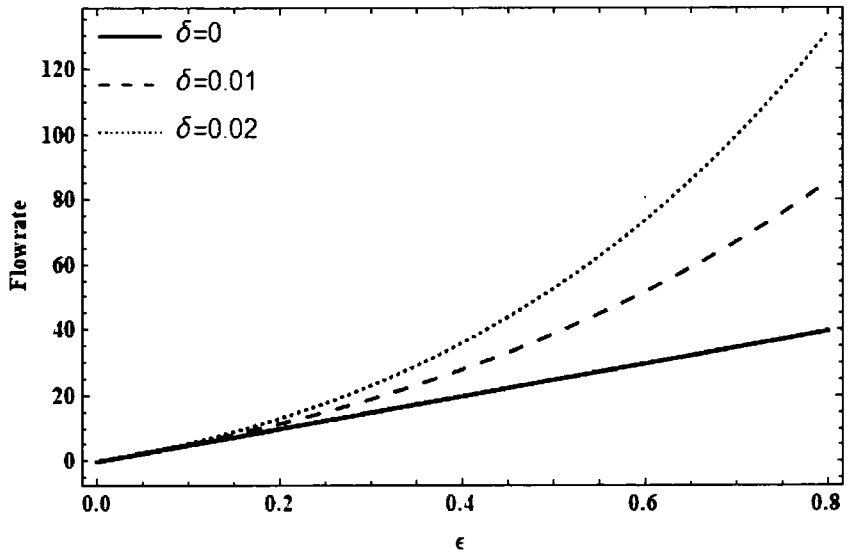

Figure 2.8: Influence of δ on the flow rate with $E_1 = 0.35$, $B = 0.1$, $E_2 = 0.25$, $A = 0.1$, $E_3 = 0.15$ and $\kappa = 0.9$.

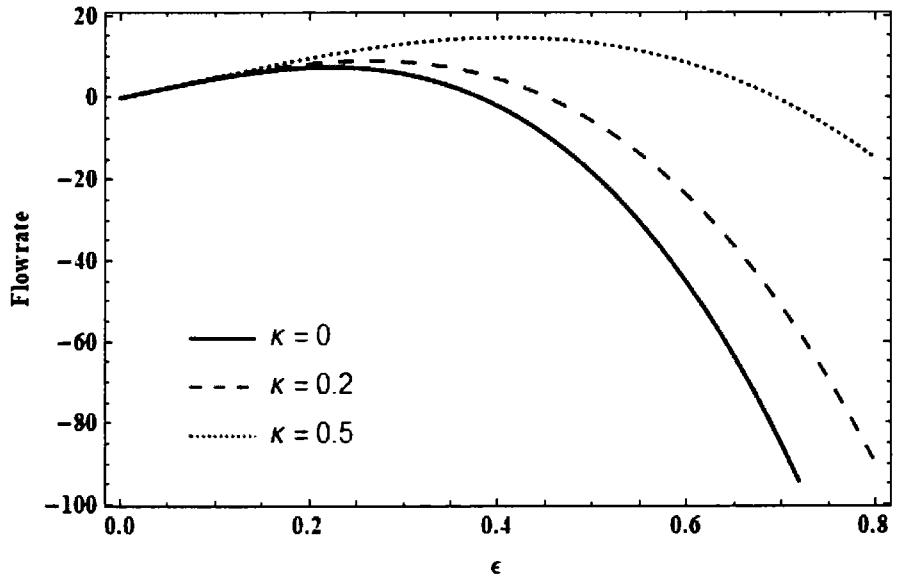

Figure 2.9: Influence of κ on the flow rate with $E_1 = 0.35$, $B = 0.1$, $E_2 = 0.25$, $A = 0.1$, $E_3 = 0.15$ and $\delta = 0.01$.

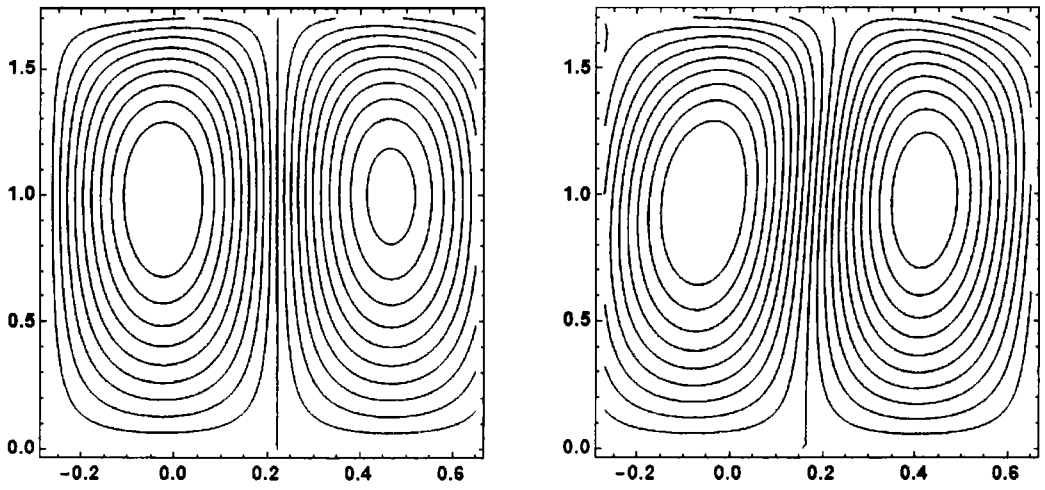

(i) $\delta = 0$ (ii) $\delta = 0.04$

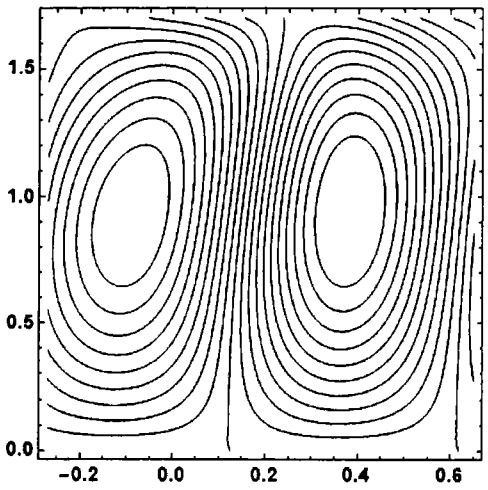

(iii) $\delta = 0.08$

Figure 2.10: Influence of δ on contour patterns with $E_1 = 0.1$, $B = 2$, $E_2 = 0.25$, $E_3 = 0.4$, $A = 2$, $\epsilon = 0.01$ and $\kappa = 0.1$.

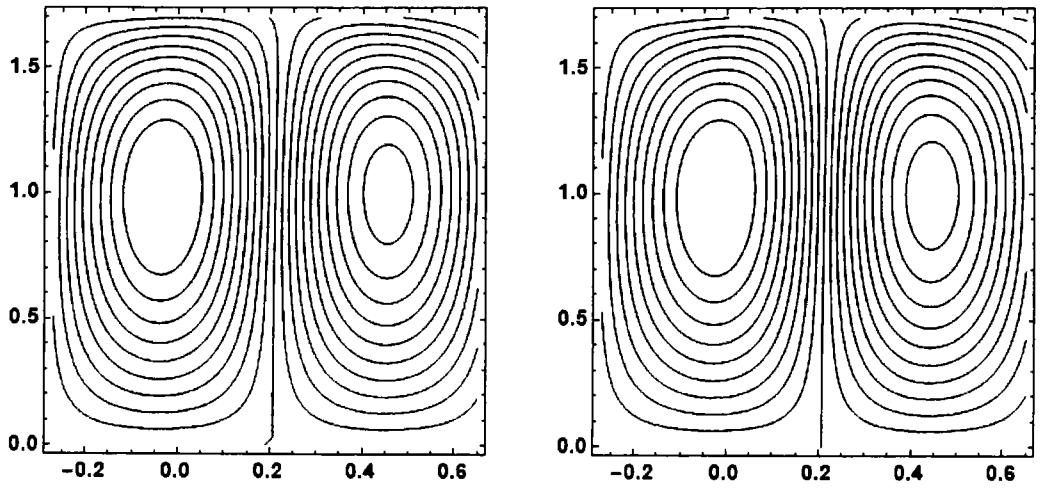

(i) $\kappa = 0$ (ii) $\kappa = 1$

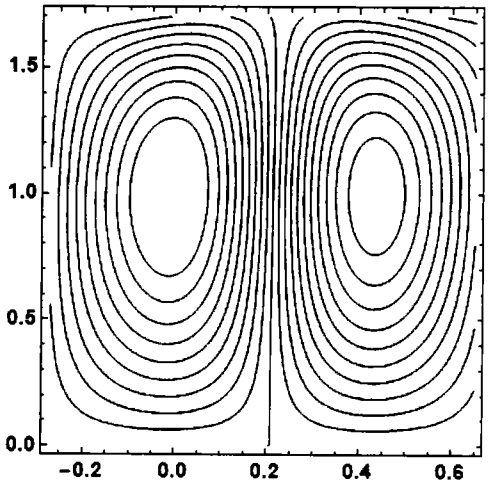

(iii) $\kappa = 2$

Figure 2.11: Influence of κ on contour patterns with $E_1 = 0.1$, $B = 2$, $E_2 = 0.25$, $E_3 = 0.4$, $A = 2$, $\epsilon = 0.01$, $\delta = 0.01$.

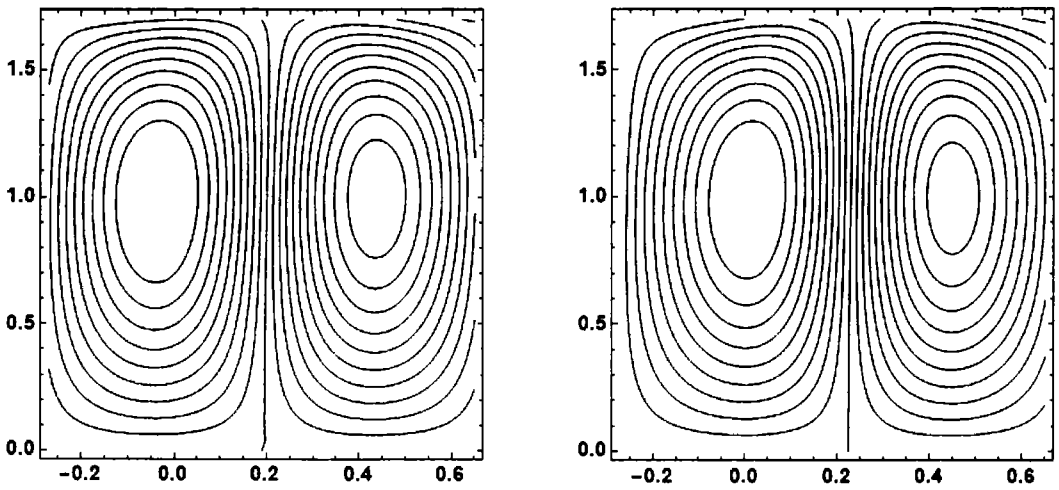

(i) $E_1 = 0$ (ii) $E_1 = 0.5$

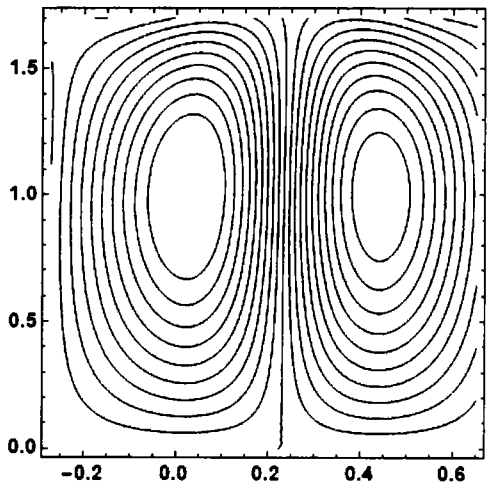

(iii) $E_1 = 1$

Figure 2.12: Influence of E_1 on contour patterns with $E_2 = 0.25, E_3 = 0.4,$

$A = 2, B = 2, \epsilon = 0.01, \delta = 0.01, \kappa = 1.$

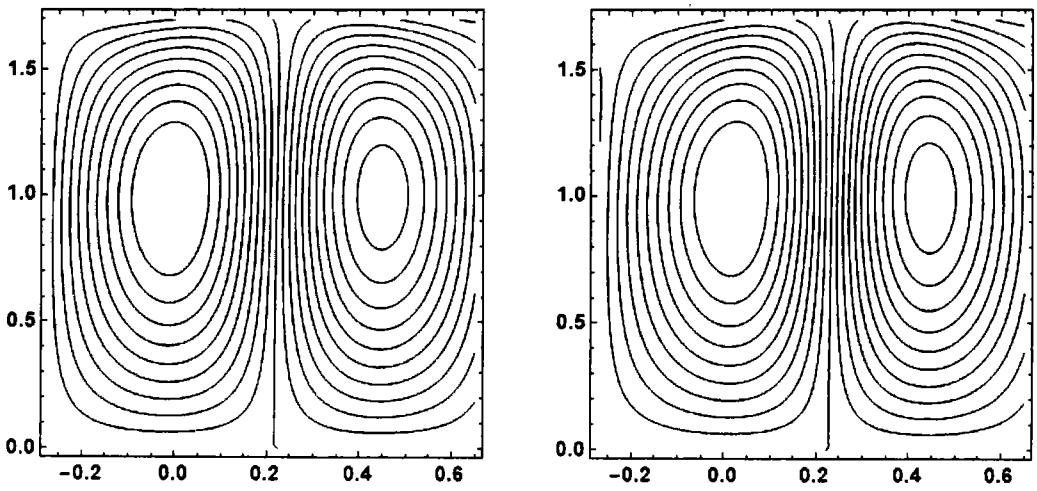

(i) $E_2 = 0$ (ii) $E_2 = 0.5$

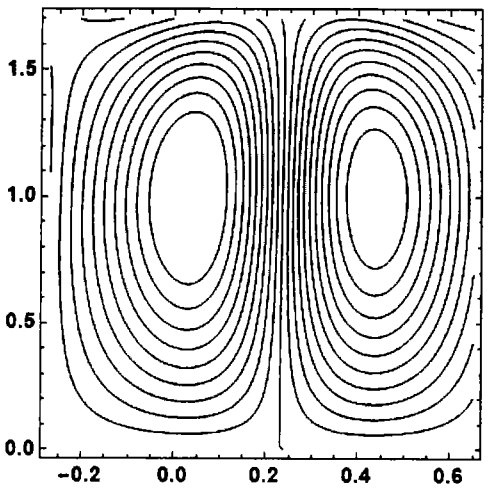

(iii) $E_2 = 1$

Figure 2.13: Influence of E_2 on contour patterns with $E_1 = 0.5$, $E_3 = 0.4$,

$A = 2, B = 2, \epsilon = 0.01, \delta = 0.01, \kappa = 1.$

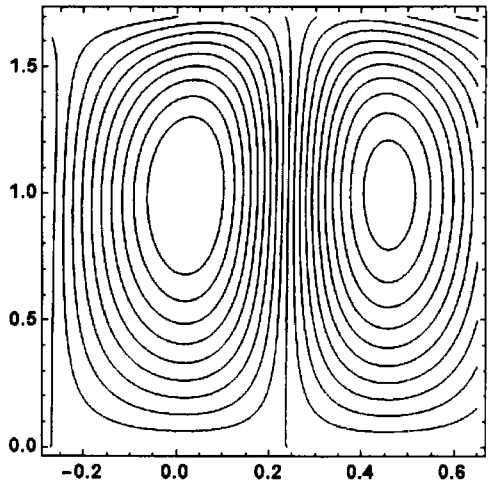

(i) $E_3 = 0$

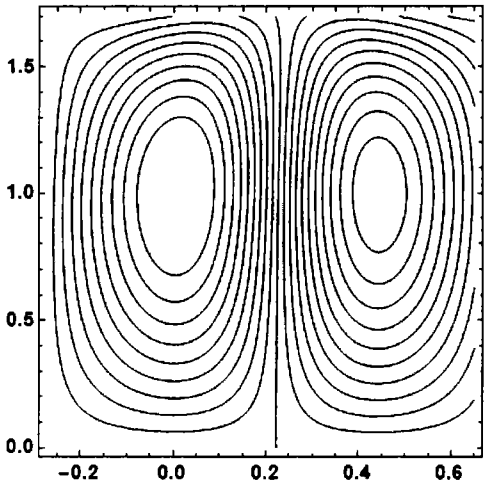

(ii) $E_3 = 0.5$

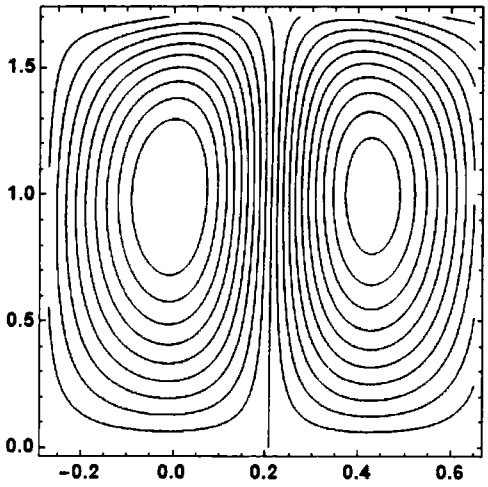

(iii) $E_3 = 1$

Figure 2.14: Influence of E_3 on contour patterns with $E_1 = 0.5$, $E_2 = 0.35$,

$A = 2, R = 2, \epsilon = 0.01, \delta = 0.01, \kappa = 1.$

Graphs of Solid Particles

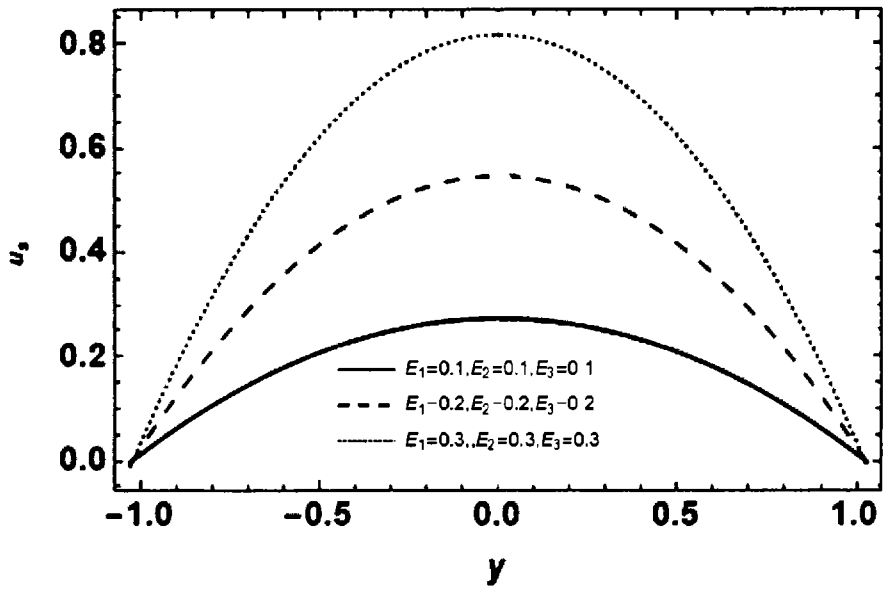

Figure 2.15: Influence of E_1, E_2 and E_3 on velocity with $\delta = 0.01$, $A = 1$, $B = 1$, $\epsilon = 0.01$ and $\kappa = 0.1$.

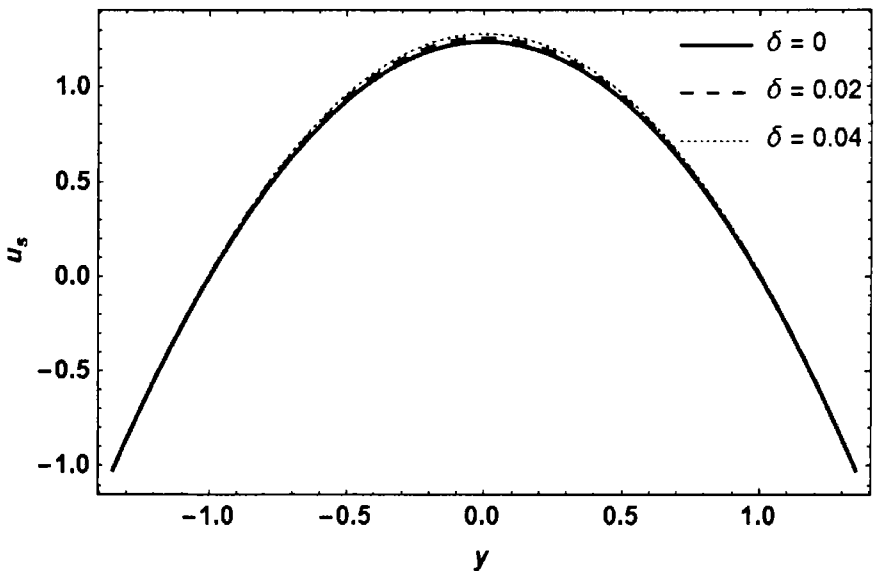

Figure 2.16: Influence of δ on velocity with $E_1 = 0.5$, $E_2 = 0.5$, $A = 1$, $B = 1$, $E_3 = 0.5$, $\epsilon = 0.01$ and $\kappa = 0.01$.

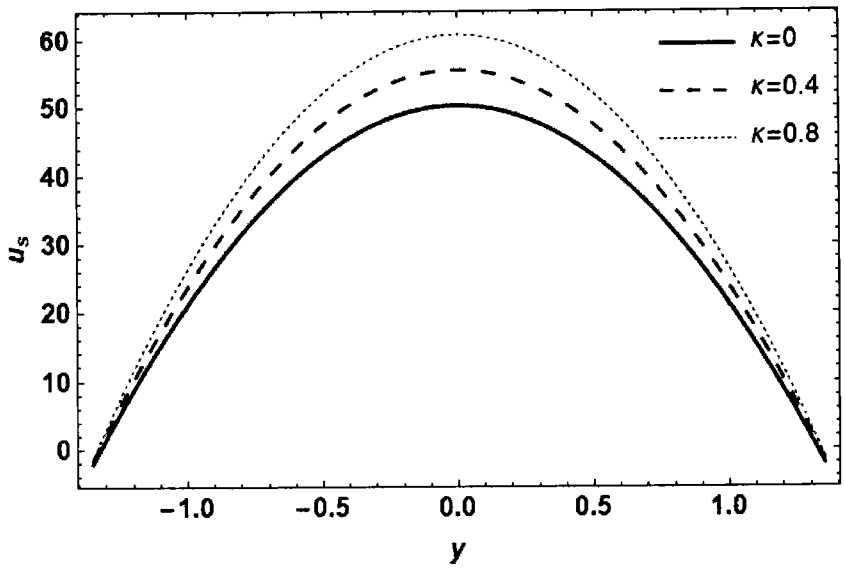

Figure 2.17: Influence of κ on velocity with $E_1 = 1$, $E_2 = 1$, $A = 0.1$, $B = 1$, $E_3 = 1$, $\epsilon = 0.1$ and $\delta = 0.01$.

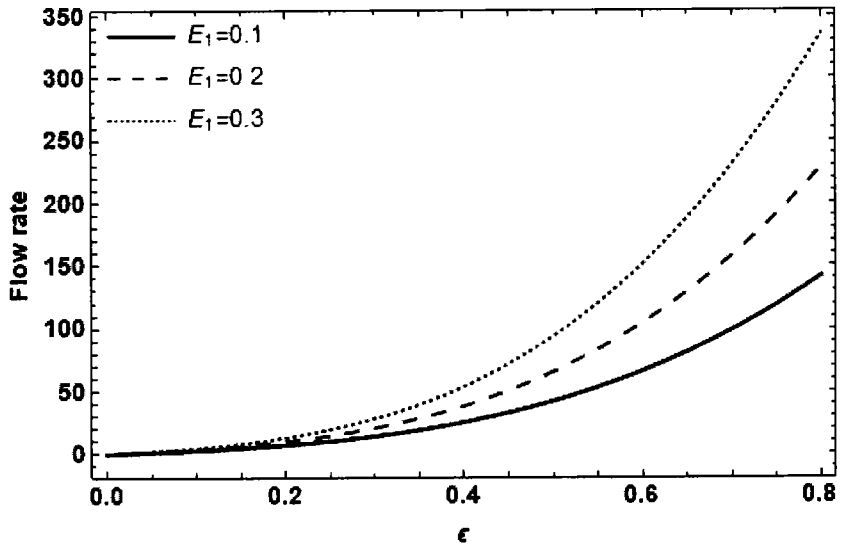

Figure 2.18: Influence of E_1 on flow rate with $E_2 = 0.25$, $E_3 = 0.35$, $A = 0.1$, $B = 1$, $\delta = 0.01$ and $\kappa = 0.9$.

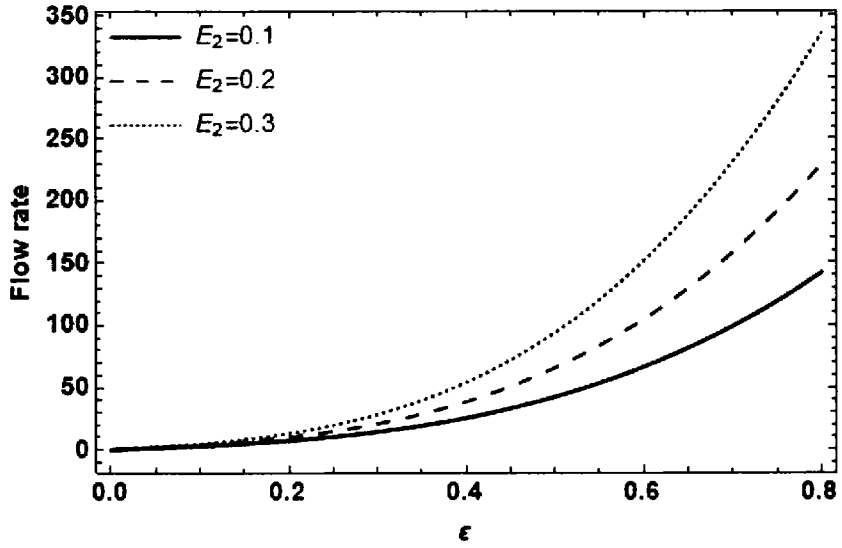

Figure 2.19: Influence of E_2 on the flow rate with $E_1 = 0.25$, $E_3 = 0.35$, $A = 0.1$, $B = 1$, $\delta = 0.01$ and $\kappa = 0.9$.

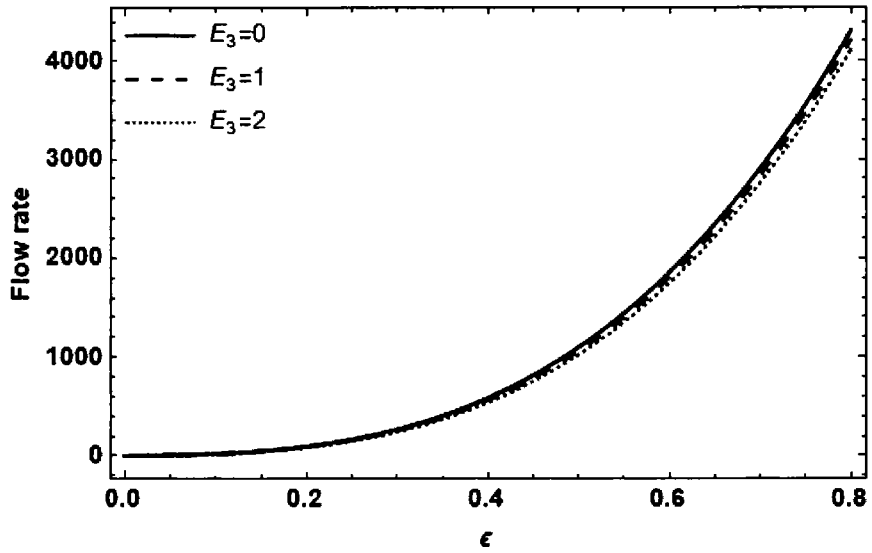

Figure 2.20: Influence of E_3 on the flow rate with $E_1 = 1$, $E_2 = 1$, $A = 1$, $B = 1$, $\delta = 0.01$ and $\kappa = 0.9$.

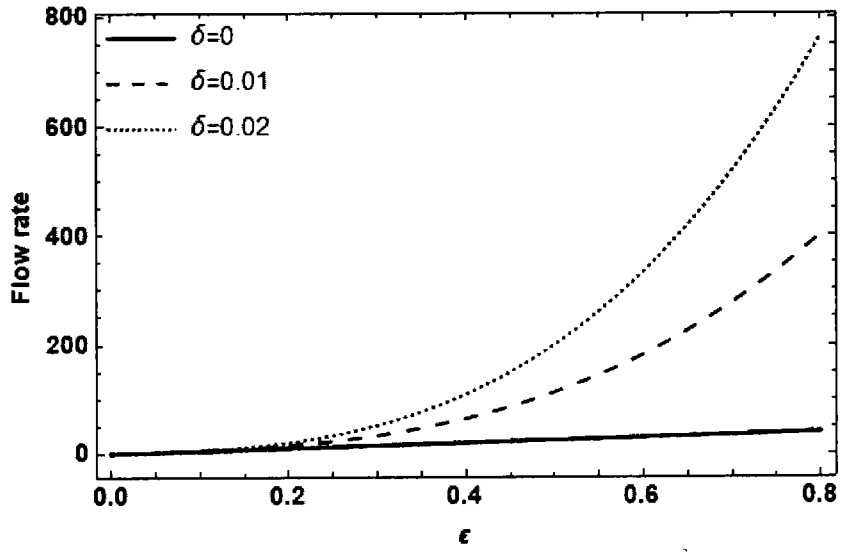

Figure 2.21: Influence of δ on the flow rate with $E_1 = 0.25$, $B = 0.1$, $E_2 = 0.35$, $A = 0.1$, $E_3 = 0.15$ and $\kappa = 0.9$.

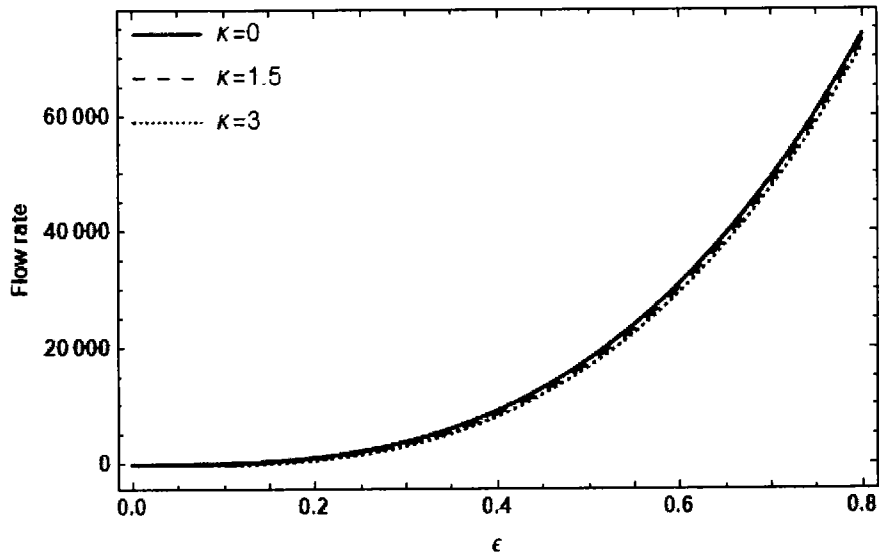

Figure 2.22: Influence of κ on the flow rate with $E_1 = 1.25$, $B = 1$, $E_2 = 1$, $A = 3$, $E_3 = 1$ and $\delta = 0.1$.

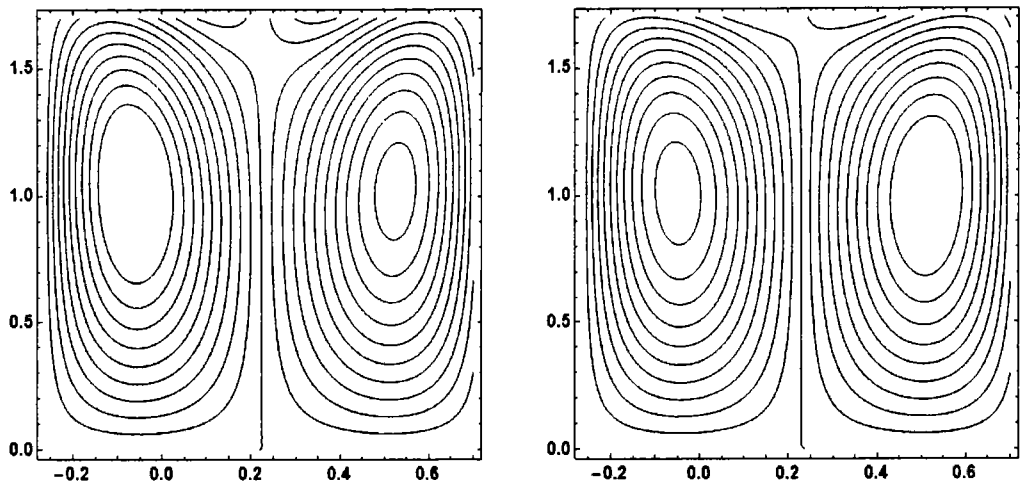

(i) $\kappa = 0$ (ii) $\kappa = 1$

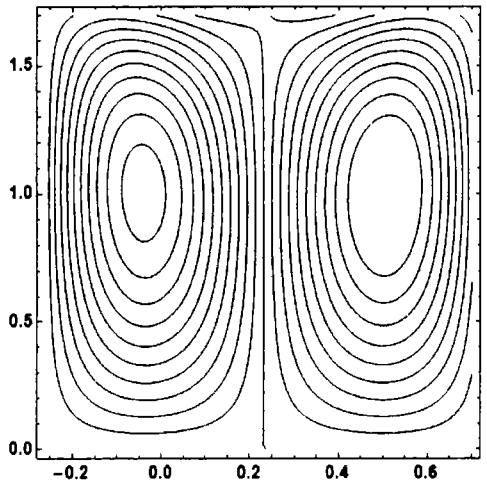

(iii) $\kappa = 2$

Figure 2.23: Influence of κ on contour patterns with $E_1 = 1$, $E_2 = 1$, $E_3 = 1$, $A = 0.5$, $B = 2$, $\epsilon = 0.01$ and $\delta = 0.01$.

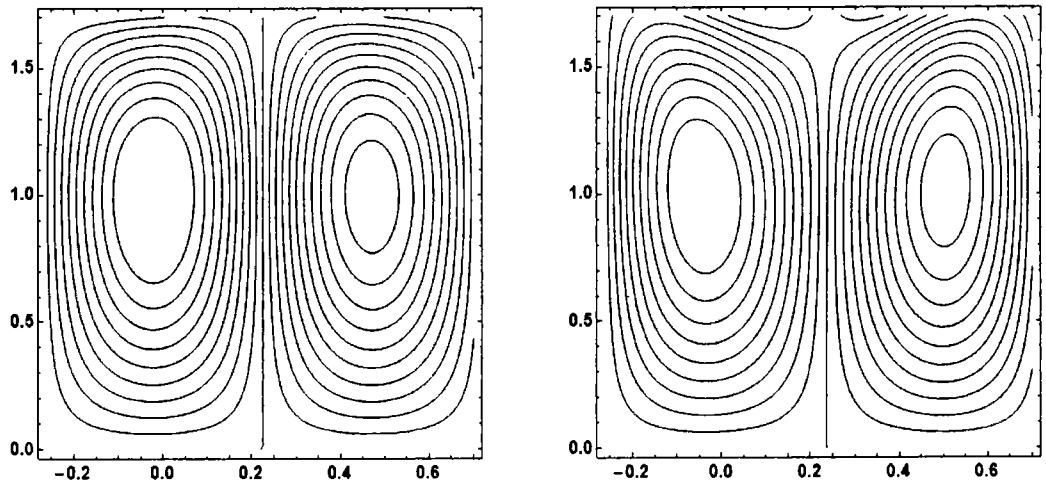

(i) $\delta = 0$ (ii) $\delta = 0.05$

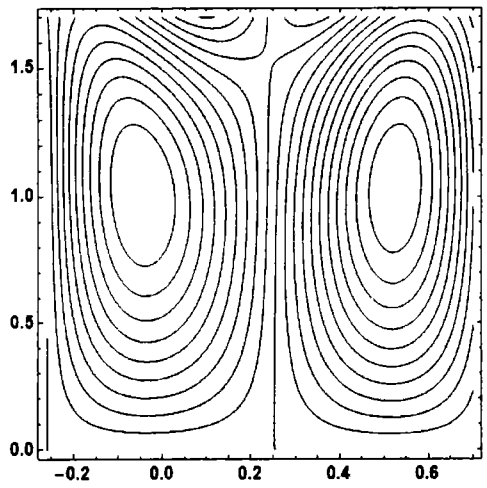

(iii) $\delta = 0.1$

Figure 2.24: Influence of δ on the contour patterns with E_1 =0.1, E_2 = 0.25, E_3 = 0.5,A = 2, B = 2, ϵ = 0.01 and κ = 0.05.

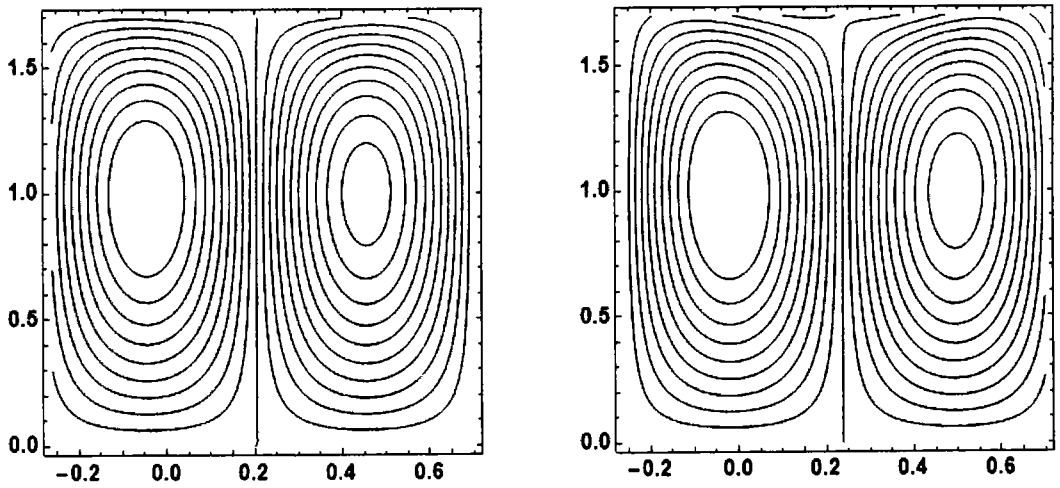

(i) $E_1 = 0$ (ii) $E_1 = 0.5$

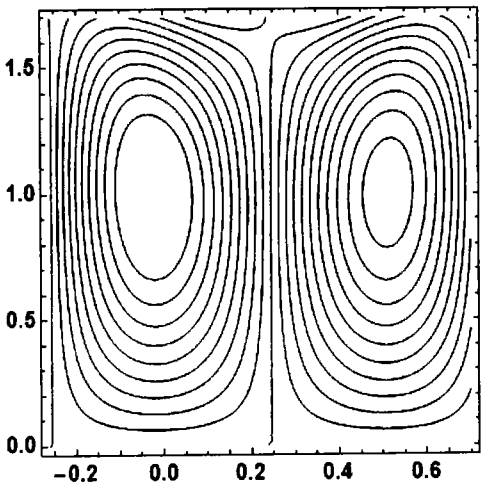

(iii) $E_1 = 1$

Figure 2.25: Influence of E_1 on the contour patterns with $\delta = 0.01$, $E_2 = 0.25$, $E_3 = 0.5$, $A = 2$, $B = 2$, $\epsilon = 0.01$ and $\kappa = 0.1$.

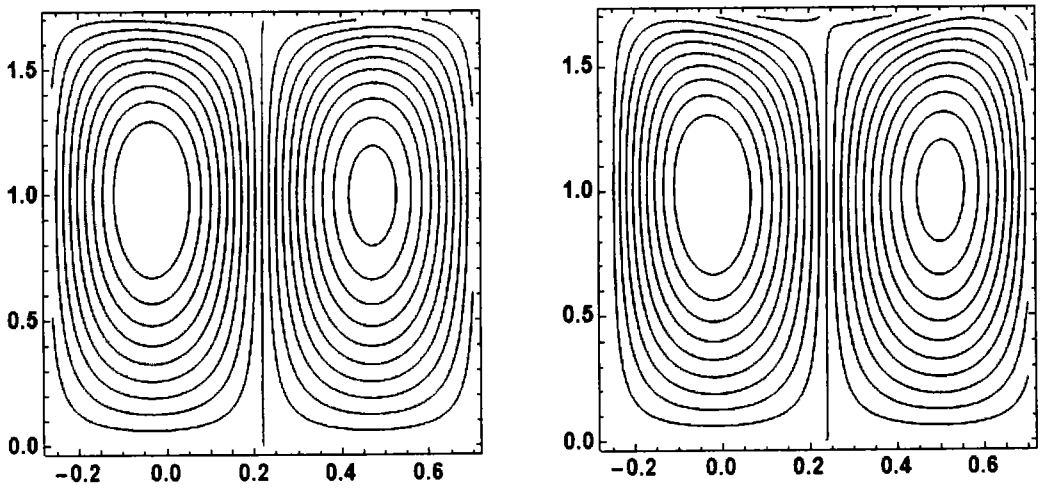

(i) $E_2 = 0$ (ii) $E_2 = 0.5$

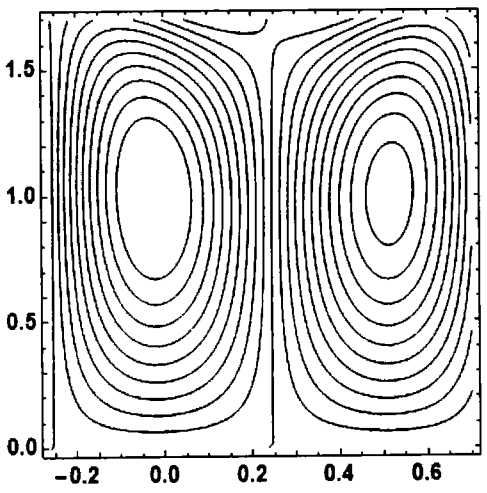

(iii) $E_2 = 1$

Figure 2.26: Influence of E_2 on the contour patterns with $\delta = 0.01$, $E_1 = 0.25$, $E_3 = 0.5$, $A = 2$, $B = 2$, $\epsilon = 0.01$ and $\kappa = 0.1$.

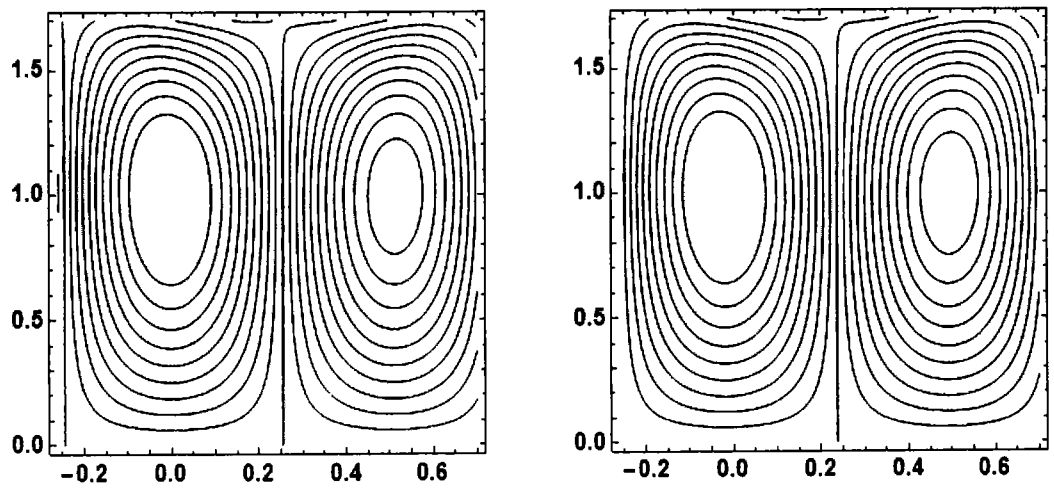

(i) $E_3 = 0$ (ii) $E_3 = 0.5$

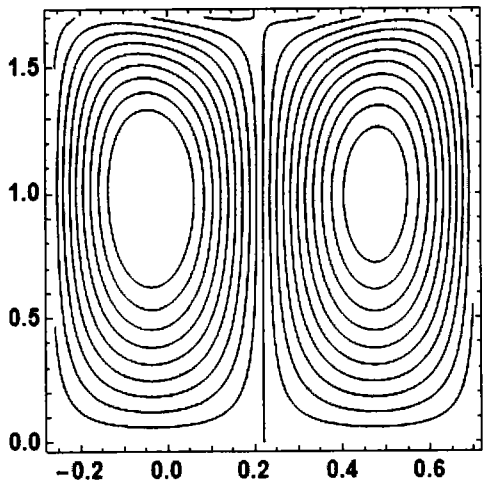

(iii) $E_3 = 1$

Figure 2.27: Influence of E_3 on the contour patterns with $\delta = 0.01$, $E_1 = 0.25$, $E_2 = 0.35$, $A = 2$, $B = 2$, $\epsilon = 0.01$ and $\kappa = 0.1$.

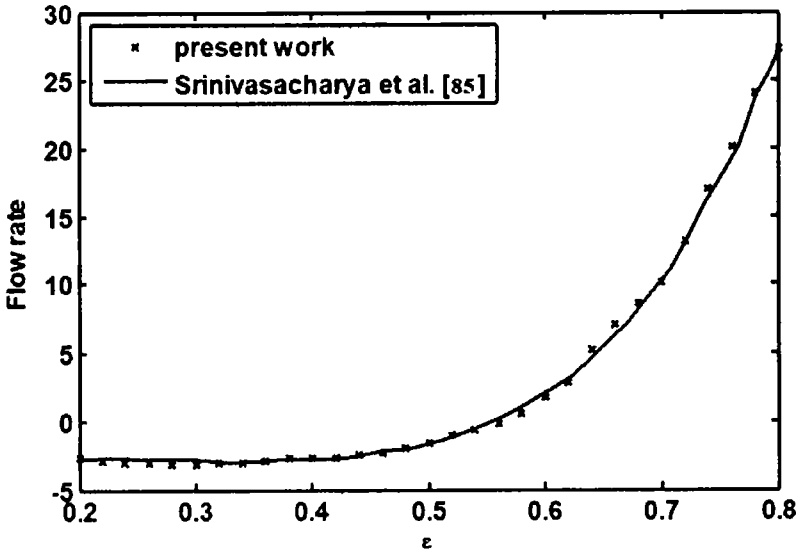

Figure 2.28: Comparison of flow rate of the fluid for E_1 between present work and Srinivasacharya et. al. [85].

2.5 Conclusion

In this study, dusty Walter's B fluid flaunting the peristaltic motion has been analyzed under the influence of wall properties. The wave number has been assumed small and the results are analyzed for different parameters. The significant features of this study are

- For the solid particles, the size of the bolus increases on the right-hand side as the viscoelastic parameter κ is increased.
- As the wave number δ is enlarged, the trapped bolus expands for both fluid and solid particles.
- The velocity enhances by increasing the values of different parameters.
- The flow rate of fluid and solid particles increases as values of E_1, E_2 and δ is increased.

Chapter 3

Peristaltic Flow of Second-Grade Dusty Fluid through a Porous Medium in an Asymmetric Channel

In this chapter, the effect of wall slip conditions on the dusty second-grade fluid through a porous asymmetric channel has been studied. The passage asymmetry is generated because of peristaltic wave train on channel walls of different phases and amplitude. An analytical solution of the situation is gained by applying regular perturbation technique under small wave number approximation. The stream functions for both fluid and solid particles and the pressure gradient are calculated and illustrated graphically.

3.1 Problem Formulation

Assuming the peristaltic motion of a second-grade fluid with a mixture of dust particles through a porous medium in an asymmetric channel of width $d_1 + d_2$. Peristaltic waves are assumed to travel along the walls of the channel. The shape of the travelling waves is given by

$$H_1(X,t) = d_1 + a_1 sin\left[\frac{2\pi}{\lambda}(X - ct)\right], \tag{3.1}$$

$$H_2(X,t) = -d_2 - a_2 sin\left[\frac{2\pi}{\lambda}(X - ct) + \phi\right], \tag{3.2}$$

where the upper and lower walls amplitude is denoted by a_1, a_2 respectively. The geometry of the problem is given in Fig. 3.1.

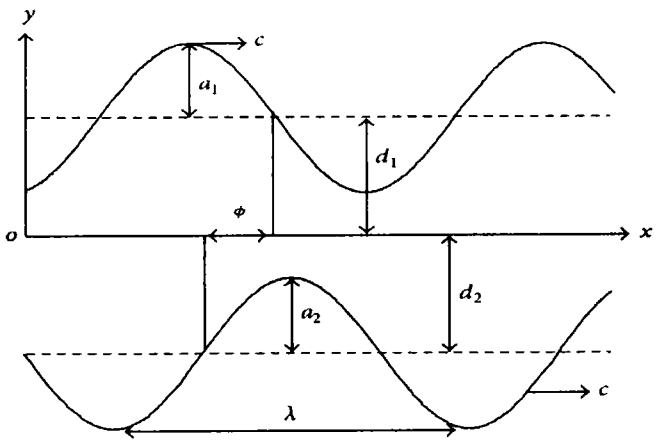

Figure. 3.1: Geometry of an asymmetric channel.

The ruling equations in the form of component for fluid and solid particles are

$$\frac{\partial U}{\partial X}+\frac{\partial V}{\partial Y}=0, \tag{3.3}$$

$$\rho\left(\frac{\partial U}{\partial t}+U\frac{\partial U}{\partial X}+V\frac{\partial U}{\partial Y}\right) = -\frac{\partial P}{\partial X}+\frac{\partial}{\partial X}(S_{XX})+\frac{\partial}{\partial Y}(S_{XY})+kN(U_s-U)-\frac{\mu}{k_1}(U), \tag{3.4}$$

$$\rho\left(\frac{\partial V}{\partial t}+U\frac{\partial V}{\partial X}+V\frac{\partial V}{\partial Y}\right) = -\frac{\partial P}{\partial Y}+\frac{\partial}{\partial X}(S_{XY})+\frac{\partial}{\partial Y}(S_{YY})+kN(V_s-V), \tag{3.5}$$

$$\frac{\partial U_s}{\partial X}+\frac{\partial V_s}{\partial Y}=0, \tag{3.6}$$

$$U_s\frac{\partial U_s}{\partial X}+V_s\frac{\partial U_s}{\partial Y}=\frac{k}{m}(U-U_s), \tag{3.7}$$

$$U_s\frac{\partial V_s}{\partial X}+V_s\frac{\partial V_s}{\partial Y}=\frac{k}{m}(V-V_s), \tag{3.8}$$

here k_1 denotes the permeability of the porous medium and N is the number density of solid particles and it is taken as a constant.

The relationship between moving and fixed frames are given below

$$p(x) = P(X,t),\ y = Y,\ x = X - ct,\ v = V,\ u = U - c,\ u_s = U_s - c, v_s = V_s. \tag{3.9}$$

In the wave frame of reference, the governing equations for the fluid particles are

$$\frac{\partial u}{\partial x} + \frac{\partial v}{\partial y} = 0, \tag{3.10}$$

$$\rho\left(u\frac{\partial u}{\partial x} + v\frac{\partial u}{\partial y}\right) = -\frac{\partial p}{\partial x} + \frac{\partial S_{xx}}{\partial x} + \frac{\partial S_{xy}}{\partial y} + kN(u_s - u) - \frac{\mu}{k_1}(u + c), \tag{3.11}$$

$$\rho\left(u\frac{\partial v}{\partial x} + v\frac{\partial v}{\partial y}\right) = -\frac{\partial p}{\partial y} + \frac{\partial S_{xy}}{\partial x} + \frac{\partial S_{yy}}{\partial y} + kN(v_s - v) - \frac{\mu}{k_1}(v). \tag{3.12}$$

The governing equations for the solid particles are

$$\frac{\partial u_s}{\partial x} + \frac{\partial v_s}{\partial y} = 0, \tag{3.13}$$

$$u_s\frac{\partial u_s}{\partial x} + v_s\frac{\partial u_s}{\partial y} = \frac{k}{m}(u - u_s), \tag{3.14}$$

$$u_s\frac{\partial v_s}{\partial x} + v_s\frac{\partial v_s}{\partial y} = \frac{k}{m}(v - v_s), \tag{3.15}$$

where

$$S_{xx} = 2\mu\frac{\partial u}{\partial x} + \alpha_1\left[2\left(u\frac{\partial^2 u}{\partial x^2} + v\frac{\partial^2 u}{\partial x\partial y}\right) + 4\left(\frac{\partial u}{\partial x}\right)^2 + 2\frac{\partial u}{\partial x}\frac{\partial v}{\partial x} + 2\left(\frac{\partial v}{\partial x}\right)^2\right]$$

$$+ \alpha_2\left[4\left(\frac{\partial u}{\partial x}\right)^2 + \left(\frac{\partial u}{\partial y} + \frac{\partial v}{\partial x}\right)^2\right],$$

$$S_{xy} = \mu\left(\frac{\partial u}{\partial y} + \frac{\partial v}{\partial x}\right) + \alpha_1\left[u\left(\frac{\partial^2 u}{\partial x\partial y}\right) + v\frac{\partial^2 u}{\partial x^2} + u\frac{\partial^2 v}{\partial x^2} - 2\frac{\partial v}{\partial x}\frac{\partial u}{\partial x} + 2\frac{\partial v}{\partial x}\frac{\partial v}{\partial x}\right],$$

$$S_{yy} = 2\mu\frac{\partial v}{\partial y} + \alpha_1\left[2\left(u\frac{\partial^2 v}{\partial x\partial y} + v\frac{\partial^2 v}{\partial y^2}\right) + 4\left(\frac{\partial v}{\partial y}\right)^2 + 2\frac{\partial u}{\partial y}\frac{\partial v}{\partial x} + 2\left(\frac{\partial u}{\partial x}\right)^2\right] +$$

$$\alpha_2\left[4\left(\frac{\partial v}{\partial y}\right)^2 + \left(\frac{\partial u}{\partial y} + \frac{\partial v}{\partial x}\right)^2\right]. \qquad (3.16)$$

Introducing the non-dimensional variables and stream functions for fluid and solid particles

$$u = \frac{\partial \psi}{\partial y}, \quad v = -\delta\frac{\partial \psi}{\partial x}, \quad u_s = \frac{\partial \varphi}{\partial y}, \quad v_s = -\delta\frac{\partial \varphi}{\partial x}, \quad p^* = \frac{pd_1^2}{\mu\lambda c}, \quad \alpha_2^* = \frac{\alpha_2 c}{\mu d_1},$$

$$x^* = \frac{x}{\lambda}, y^* = \frac{y}{d_1}, b = \frac{a_2}{d_1}, \quad d = \frac{d_2}{d_1}, \quad Re = \frac{\rho c d_1}{\mu},$$

$$\delta = \frac{d}{\lambda}, \quad \psi^* = \frac{\psi}{cd_1}, \quad \varphi^* = \frac{\varphi}{cd_1}, \quad \alpha_1^* = \frac{\alpha_1 c}{\mu d_1}, \quad S^* = \frac{Sd_1}{\mu c}, a = \frac{a_1}{d_1}. \qquad (3.17)$$

Using Eq. (3.17) into Eqs. (3.11) and (3.12) to get

$$Re\,\delta\left(\frac{\partial \psi}{\partial y}\frac{\partial^2 \psi}{\partial x\partial y} - \frac{\partial \psi}{\partial x}\frac{\partial^2 \psi}{\partial y^2}\right)$$

$$= -\frac{\partial p}{\partial x} + \delta\frac{\partial}{\partial x}(S_{xx}) + \frac{\partial}{\partial y}(S_{xy}) + \frac{kNd_1^2}{\mu}\left(\frac{\partial \varphi}{\partial y} - \frac{\partial \psi}{\partial y}\right)$$

$$-\frac{d_1^2}{k_1}\left(\frac{\partial \psi}{\partial y} + 1\right), \qquad (3.18)$$

$$Re\,\delta^3\left(\frac{\partial \psi}{\partial x}\frac{\partial^2 \psi}{\partial x\partial y} - \frac{\partial \psi}{\partial y}\frac{\partial^2 \psi}{\partial x^2}\right)$$

$$= -\frac{\partial p}{\partial y} + \delta^2\frac{\partial}{\partial x}(S_{xy}) + \delta\frac{\partial}{\partial y}(S_{yy}) + \delta^2\frac{kNd_1^2}{\mu}\left(\frac{\partial \psi}{\partial x} - \frac{\partial \varphi}{\partial x}\right)$$

$$+\delta^2\frac{d_1^2}{k_1}\left(\frac{\partial \psi}{\partial x}\right). \qquad (3.19)$$

The equations of the solid particles after using Eq. (3.17) and dropping the star are given as

$$\frac{\partial\varphi}{\partial y}\frac{\partial^2\varphi}{\partial x\partial y}-\delta\frac{\partial\varphi}{\partial x}\frac{\partial^2\varphi}{\partial y^2}=\frac{k}{m}\left(\frac{\partial\psi}{\partial y}-\frac{\partial\varphi}{\partial y}\right), \tag{3.20}$$

$$-\frac{\partial\varphi}{\partial y}\frac{\partial^2\varphi}{\partial x^2}+\delta\frac{\partial\varphi}{\partial x}\frac{\partial^2\varphi}{\partial x\partial y}=\frac{k}{m}\left(\frac{\partial\varphi}{\partial x}-\frac{\partial\psi}{\partial x}\right). \tag{3.21}$$

The compatibility equations for the fluid and solid particles become

$$Re\left[\delta\left(\frac{\partial\psi}{\partial y}\frac{\partial^3\psi}{\partial x\partial y^2}-\frac{\partial\psi}{\partial x}\frac{\partial^3\psi}{\partial y^3}\right)-\delta^3\left(\frac{\partial\psi}{\partial x}\frac{\partial^3\psi}{\partial x^2\partial y}-\frac{\partial\psi}{\partial y}\frac{\partial^3\psi}{\partial x^3}\right)\right]$$

$$=\delta\frac{\partial^2}{\partial x\partial y}\left(S_{xx}-S_{yy}\right)+\left(\frac{\partial^2}{\partial y^2}-\delta^2\frac{\partial^2}{\partial x^2}\right)S_{xy}+A(\nabla_1^2\phi-\nabla_1^2\psi)$$

$$-\frac{d_1^2}{k_1}(\nabla_1^2\psi), \tag{3.22}$$

$$\delta\left(\frac{\partial\varphi}{\partial y}\frac{\partial}{\partial x}\nabla_1^2\varphi-\frac{\partial\varphi}{\partial x}\frac{\partial}{\partial y}\nabla_1^2\varphi\right)=B(\nabla_1^2\psi-\nabla_1^2\varphi), \tag{3.23}$$

where $K=\frac{d_1^2}{k_1}$ is the permeability coefficient of the porous medium.

The walls in dimensionless form are

$$h_1(x)=1+\text{asin}(2\pi x), \tag{3.24}$$

$$h_2(x)=-d-bsin(2\pi x+\phi). \tag{3.25}$$

The time mean flow rate in the dimensionless form is denoted by F.

$$Q=F+1+d, \tag{3.26}$$

where

$$F=\int_{h_2(x)}^{h_1(x)}\frac{\partial\psi}{\partial y}dy, \tag{3.27}$$

The time flow rate of the solid particles, in the non-dimensional form is

$$E = \int_{h_2(x)}^{h_1(x)} \frac{\partial \varphi}{\partial y} dy, \tag{3.28}$$

it can be associated with Q_s, the dimensionless time flow in the fixed frame as

$$Q_s = E + 1 + d. \tag{3.29}$$

The pressure rise is given by

$$\Delta P = \int_0^1 \frac{\partial p}{\partial x} dx. \tag{3.30}$$

Dimensionless boundary conditions are

$$\psi = \frac{F}{2}, \quad \frac{\partial \psi}{\partial y} + \beta S_{xy} = -1, \quad \varphi = \frac{E}{2} \quad at\ y = h_1(x), \tag{3.31}$$

$$\psi = -\frac{F}{2}, \quad \frac{\partial \psi}{\partial y} - \beta S_{xy} = -1, \quad \varphi = -\frac{E}{2} \quad at\ y = h_2(x), \tag{3.32}$$

3.2 Method of Solution

The perturbation method has been adopted as a closed form solution is not possible for the non-linear differential equations. We expand ψ, φ, F, E and p as

$$\psi = \psi_0 + \delta\psi_1 + \delta^2\psi_2 + O(\delta^3), \tag{3.33}$$

$$\varphi = \varphi_0 + \delta\varphi_1 + \delta^2\varphi_2 + O(\delta^3), \tag{3.34}$$

$$F = F_0 + \delta F_1 + \delta^2 F_2 + O(\delta^3), \tag{3.35}$$

$$E = E_0 + \delta E_1 + \delta^2 E_2 + O(\delta^3), \tag{3.36}$$

$$p = p_0 + \delta p_1 + \delta^2 p_2 + O(\delta^3). \tag{3.37}$$

3.2.1 Zeroth-Order System

The system of equations for zeroth order is

$$\frac{\partial^2}{\partial y^2}(S_{0xy}) + A\left(\frac{\partial^2 \varphi_0}{\partial y^2} - \frac{\partial^2 \psi_0}{\partial y^2}\right) - K\left(\frac{\partial^2 \psi_0}{\partial y^2}\right) = 0, \tag{3.38}$$

$$B\left(\frac{\partial^2 \psi_0}{\partial y^2} - \frac{\partial^2 \varphi_0}{\partial y^2}\right) = 0, \tag{3.39}$$

$$\frac{dp_0}{dx} = \frac{\partial}{\partial y} S_{0xy} + A\left(\frac{\partial \varphi_0}{\partial y} - \frac{\partial \psi_0}{\partial y}\right) - K\left(\frac{\partial \psi_0}{\partial y} + 1\right), \tag{3.40}$$

With the component of stress tensor defined as follow

$$S_{0xy} = \frac{\partial^2 \psi_0}{\partial y^2}, \tag{3.41}$$

with

$$\psi_0 = \frac{F_0}{2}; \quad \frac{\partial \psi_0}{\partial y} + \beta S_{0xy} = -1; \quad \varphi_0 = \frac{E_0}{2} \qquad at\ y = h_1(x), \tag{3.42}$$

$$\psi_0 = -\frac{F_0}{2}; \quad \frac{\partial \psi_0}{\partial y} - \beta S_{0xy} = -1; \quad \varphi_0 = -\frac{E_0}{2} \qquad at\ y = h_2(x). \tag{3.43}$$

3.2.2 First-Order System

$$Re\left(\frac{\partial \psi_0}{\partial y}\frac{\partial^3 \psi_0}{\partial x \partial y^2} - \frac{\partial \psi_0}{\partial x}\frac{\partial^3 \psi_0}{\partial y^3}\right) = \frac{\partial^2}{\partial x \partial y}(S_{0xx} - S_{0yy}) + \frac{\partial^2}{\partial y^2}(S_{1xy}) + A\left(\frac{\partial^2 \varphi_1}{\partial y^2} - \frac{\partial^2 \psi_1}{\partial y^2}\right) - K\left(\frac{\partial^2 \psi_1}{\partial y^2}\right), \tag{3.44}$$

$$B\left(\frac{\partial^2 \psi_1}{\partial y^2} - \frac{\partial^2 \varphi_1}{\partial y^2}\right) = \frac{\partial \varphi_0}{\partial y}\frac{\partial^3 \varphi_0}{\partial x \partial y^2} - \frac{\partial \varphi_0}{\partial x}\frac{\partial^3 \varphi_0}{\partial y^3}, \tag{3.45}$$

$$\frac{dp_1}{dx} = Re\left(\frac{\partial\psi_0}{\partial y}\frac{\partial^2\psi_0}{\partial x\partial y} - \frac{\partial\psi_0}{\partial x}\frac{\partial^2\psi_0}{\partial y^2}\right) - \frac{\partial}{\partial y}(S_{1xy}) + A\left(\frac{\partial\varphi_1}{\partial y} - \frac{\partial\psi_1}{\partial y}\right) - K\left(\frac{\partial\psi_1}{\partial y}\right),$$

(3.46)

where

$$S_{1xy} = \frac{\partial^2\psi_1}{\partial y^2} + \alpha\left(2\frac{\partial^2\psi_0}{\partial x\partial y}\frac{\partial^2\psi_0}{\partial y^2} + \frac{\partial\psi_0}{\partial y}\frac{\partial^3\psi_0}{\partial x\partial y^2} - \frac{\partial\psi_0}{\partial x}\frac{\partial^3\psi_0}{\partial y^3}\right). \quad (3.47)$$

The corresponding boundary conditions are

$$\psi_1 = \frac{F_1}{2}; \quad \frac{\partial\psi_1}{\partial y} + \beta S_{1xy} = 0; \quad \varphi_1 = \frac{E_1}{2} \quad at\ y = h_1(x), \quad (3.48)$$

$$\psi_1 = -\frac{F_1}{2}; \quad \frac{\partial\psi_1}{\partial y} - \beta S_{1xy} = 0; \quad \varphi_1 = -\frac{E_1}{2} \quad at\ y = h_2(x). \quad (3.49)$$

3.3 Solution of the Problem

$$\psi = \left(A_1 y + A_2 + A_3\cosh\left[K^{\frac{1}{2}}y\right] + A_4\sinh\left[K^{\frac{1}{2}}y\right]\right) + \delta\begin{pmatrix} A_{50}y + A_{48} + (A_{49} - A_{20}y + A_{21}y^2)\cosh\left[K^{\frac{1}{2}}y\right] \\ +(A_{50} - A_{23}y + A_{24}y^2)\sinh\left[K^{\frac{1}{2}}y\right] \end{pmatrix}, \quad (3.50)$$

$$\varphi = (\psi_0 + B_1 y + B_2) + \delta(\psi_1 + B_{23}y + B_{24}), \quad (3.51)$$

$$\frac{dp}{dx} = -K(A_1 + 1) + \delta(D_1 + (D_2 + D_3 y)\cosh\left[K^{\frac{1}{2}}y\right] + (D_4 + D_5 y)\sinh\left[K^{\frac{1}{2}}y\right] + D_6\cosh\left[2K^{\frac{1}{2}}y\right] + D_7\sinh\left[2K^{\frac{1}{2}}y\right]). \quad (3.52)$$

3.4 Results and Discussion

This section includes the discussion on the contour graphs of both fluid and solid particles and pressure rise. Figs. 3.2 – 3.6 represent the consequences of different parameters on the fluid particles. Figs. 3.7 – 3.11 illustrate the behavior of parameters on the solid particles suspended in the fluid. Figs. 3.12 – 3.16 are the graphical representation of pressure rise for fluid particles.

Fig. 3.2 shows that with the increase in $\alpha_1$values, the bolus for the fluid particles expands. As the values of δ increases, we observe that the bolus expands too as shown in Fig. 3.3. Fig. 3.4(a) shows the effect of no slip on the fluid particles while Fig. 3.4(b) and Fig. 3.4(c) clearly show that with the rise in slip parameter, the bolus expands. The effect of porosity is demonstrated in Fig. 3.5. It can be observed in Fig. 3.5(a) that there is weak impact of porosity on fluid profile with minimum porosity amount. With the increase of porosity, the bolus starts expanding. Fig. 3.6 illustrates that rise in Reynolds number (Re) contracts the bolus of the fluid particles.

It can be perceived in Fig. 3.7 that increasing α_1 expands the bolus for the solid particles. Fig. 3.8 depicts that the bolus expands for solid particles by increasing δ. In Fig. 3.9(a) the no slip effects on the solid particles are illustrated while Fig. 3.9(b) and Fig. 3.9(c) show that as the slip parameter increases bolus starts to expand. The consequences of porosity parameter on solid particles can be studied in Fig. 3.10. We see that less porosity has minor effects on the flow of solid particles. As the porosity increases, Fig. 3.10(b) and Fig. 3.10(c) show effects increasing on the solid particles. Fig. 3.11 demonstrates that by increasing *Re*, the bolus increases as well.

Fig. 3.12 is the graphical representation of effects of $\alpha_1$on the pressure rise. We notice that with the increase in α_1 the pumping rate increases in the retrograde region ($\Delta P >$

0) while in the co-pumping region ($\Delta P < 0$) there is decrease in the pumping rate. Fig. 3.13 illustrates the effects of δ on the pressure rise. We noticed that as the values of δ increases, the pumping rate decreases in the retrograde region while it has opposite effect in the free pumping and co-pumping region. The consequences of slip parameter β on the pressure rise can be studied in Fig. 3.14. There is slight growth in pressure rise as the slip parameter is increased as more pressure would be required to pump the fluid. The rise of porosity parameter K has significant influence on the pressure rise. In Fig. 3.15 we observe that pressure has almost vanished as we take the K very close to zero. As the porosity parameter is increased, there is notable increase in the pressure rise as more pressure would be required to pump the fluid through porous passage. Fig. 3.16 exhibit the deviation of pressure rise for distinct values of Reynolds number (Re). With the increase in Re, the pressure is rising as well. Increase in Re means that inertial forces are dominant while viscous forces become weak. The retrograde region for pumping fluid will widen as Re is increased.

3.5 Graphs

Graphs of Fluid

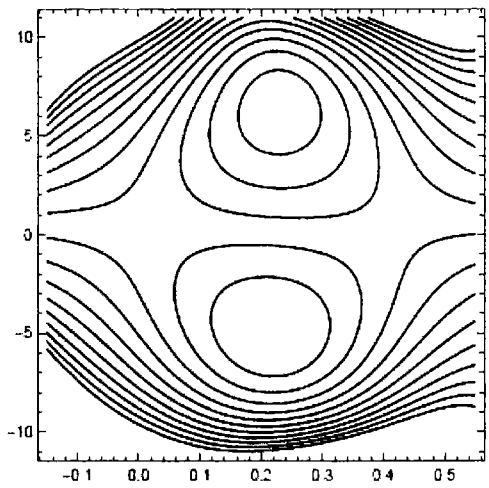

(a) $\alpha_1 = 0$

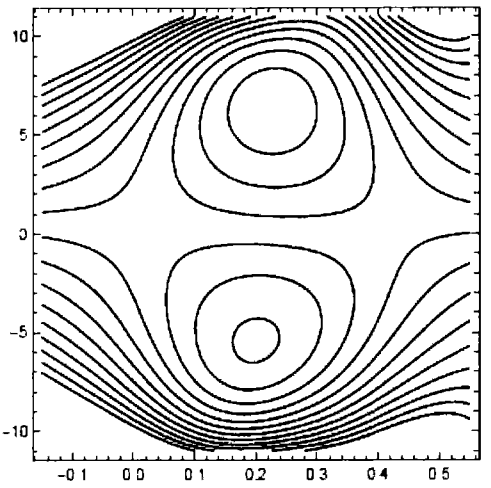

(b) $\alpha_1 = 4$

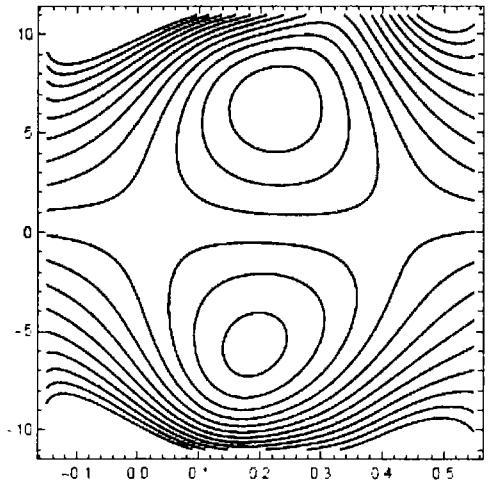

(c) $\alpha_1 = 6$

Figure 3.2: Depicts the streamline patterns of fluid particles for various values of α_1 with $b = 0.5$, $B = 0.2$, $d = 0.7$, $\phi = \frac{\pi}{6}$, $A = 0.3$, $Re = 0.15$, $\delta = 0.01$, $\beta = 0.2$, $a = 0.8$, $K = 0.1$.

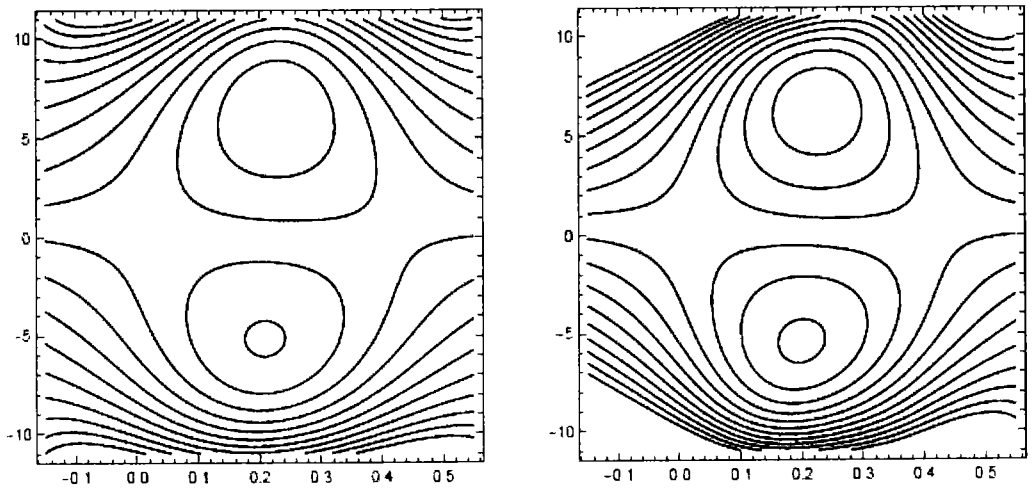

(a) $\delta = 0$ (b) $\delta = 0.4$

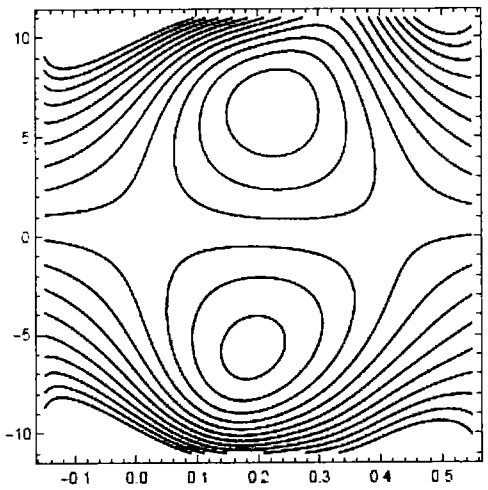

(c) $\delta = 0.6$

Figure 3.3: Depicts the streamline patterns of fluid particles for distinct values of δ with $K = 0.1$, $b = 0.5$, $d = 0.7$, $\phi = \frac{\pi}{6}$, $A = 0.2$, $B = 0.3$, $Re = 0.15$, $\alpha_1 = 2$, $a = 0.8$, $\beta = 0.2$.

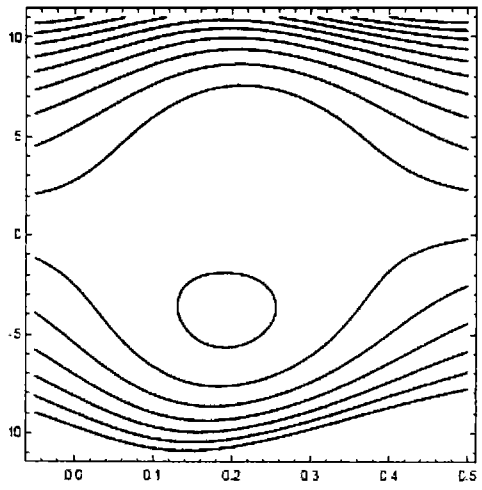

(a) $\beta = 0$

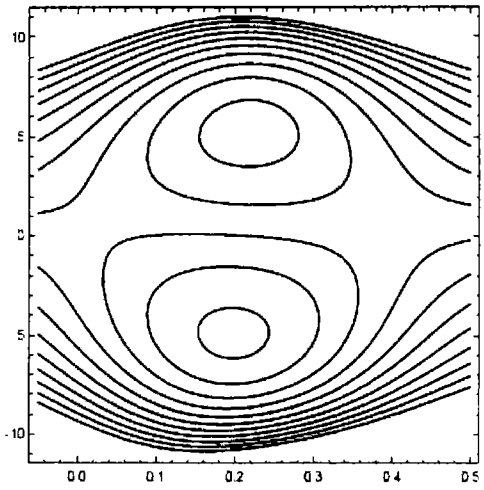

(b) $\beta = 0.2$

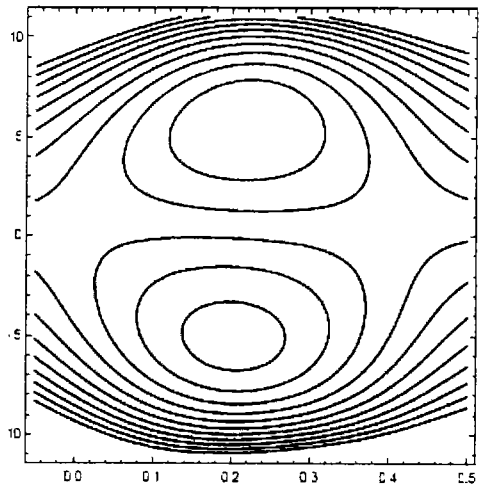

(c) $\beta = 0.3$

Figure 3.4: Depicts the streamline patterns of fluid particles for distinct values of β with $b = 0.6$, $d = 0.8$, $\phi = \frac{\pi}{6}$, $K = 0.1$, $A = 0.1$, $B = 0.1$, $Re = 0.25$, $\delta = 0.01$, $\alpha_1 = 0.1$, $a = 0.5$.

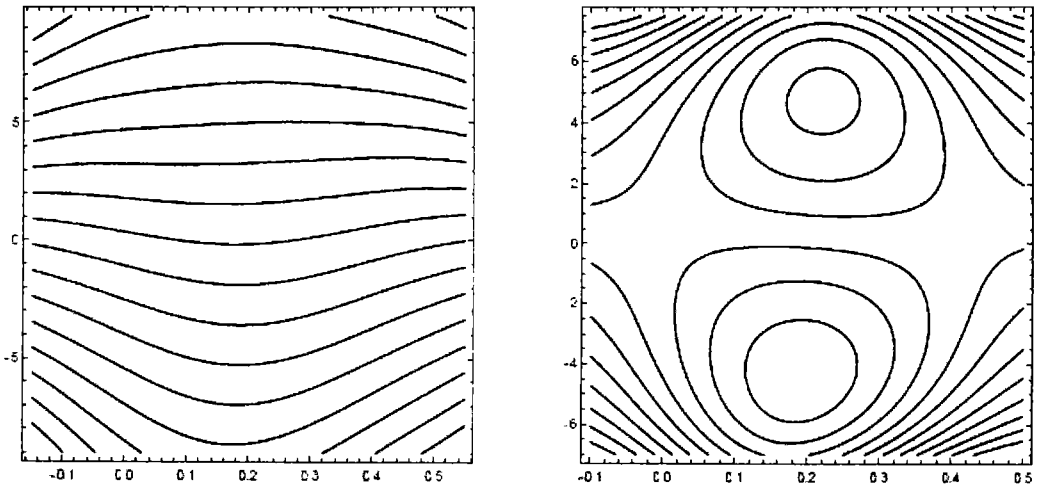

(a) K = 0.001

(b) *K = 0.2*

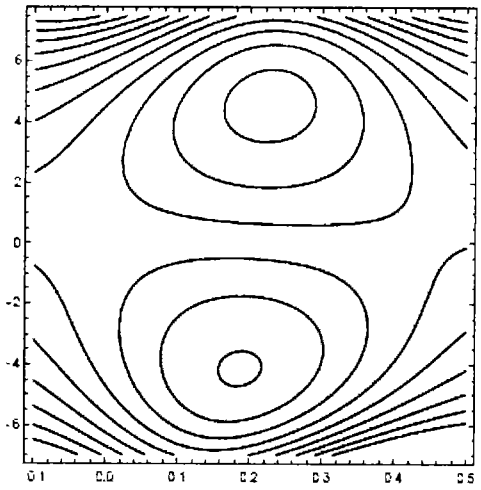

(c) *K = 0.3*

Figure 3.5: Depicts the streamline patterns of fluid particles for distinct values of K with $b = 0.6$, $d = 0.8$, $\phi = \frac{\pi}{6}$, $\alpha_1 = 0.1$, $A = 0.1$, $B = 0.1$, $Re = 0.25$, $\delta = 0.01$, $\beta = 0.1$, $a = 0.5$.

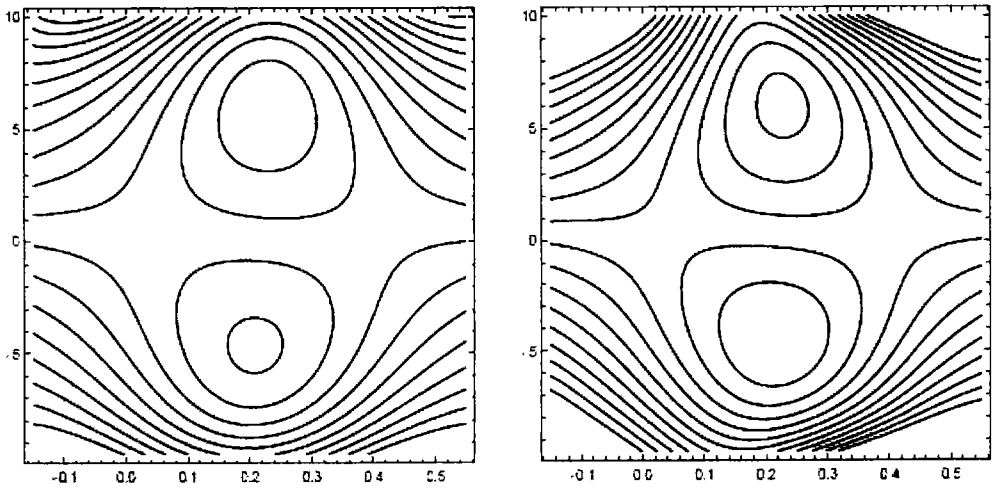

(a) *Re = 0* (b) *Re = 0.5*

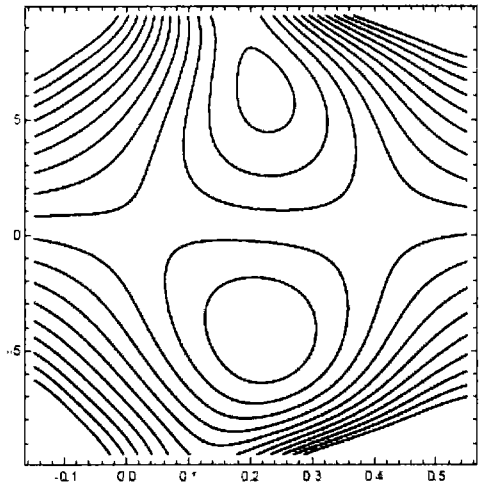

(c) *Re = 1*

Figure 3.6: Depicts the streamline patterns of fluid particles for distinct values of Reynolds number (*Re*) with $b = 0.5$, $d = 0.7$, $\phi = \frac{\pi}{6}$, $\alpha_1 = 0.1$, $A = 0.1$, $B = 0.1$, $K=0.1$, $\delta = 0.01$, $\beta = 0.1$, $a = 0.8$.

Graphs of Solid Particles

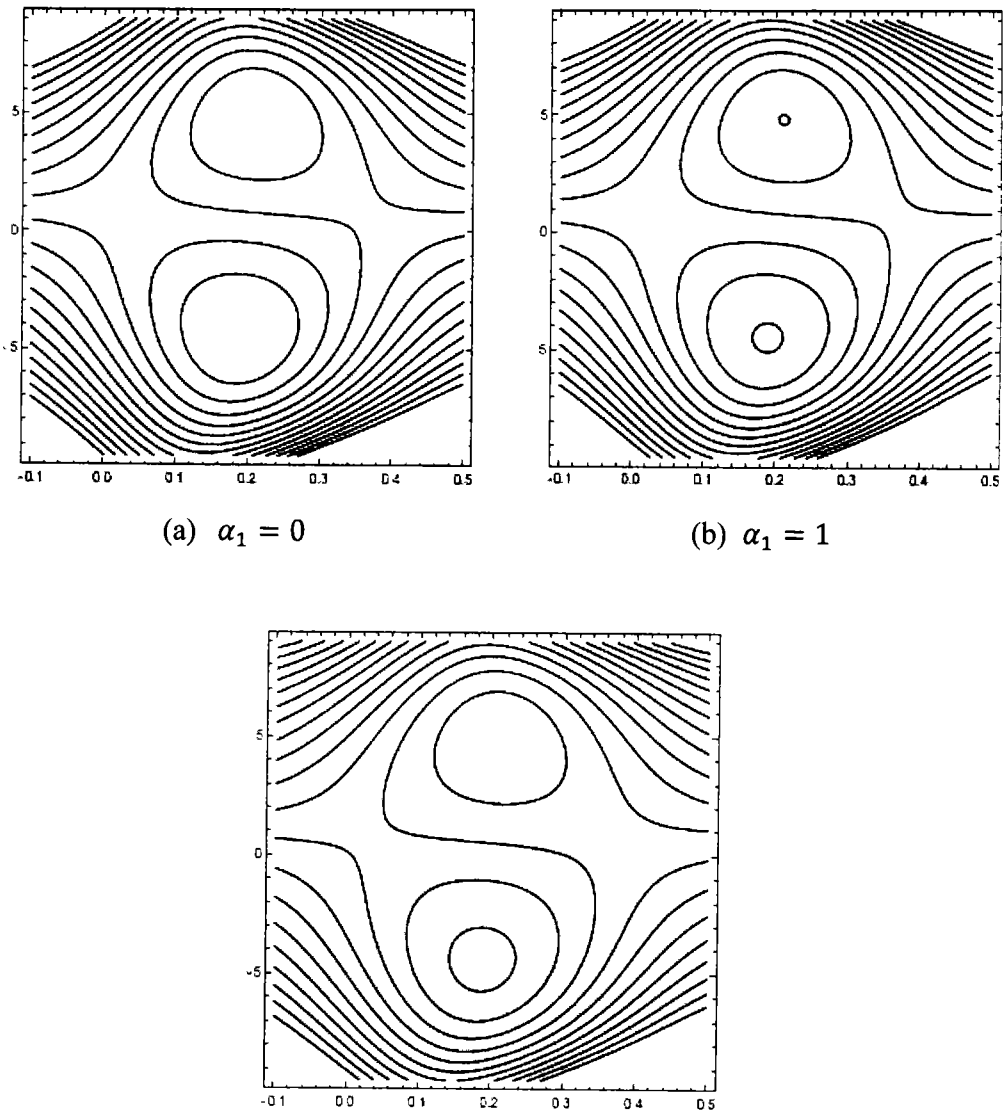

(a) $\alpha_1 = 0$ (b) $\alpha_1 = 1$

(c) $\alpha_1 = 2$

Figure 3.7: Depicts the streamline patterns of solid particles for distinct values of α_1 with $d = 0.8$, $\phi = \frac{\pi}{6}$, $K = 0.1$, $A = 0.5$, $B = 1$, $Re = 0.25$, $\delta = 0.01$, $\beta = 0.1$, $a = 0.5$, $b = 0.6$.

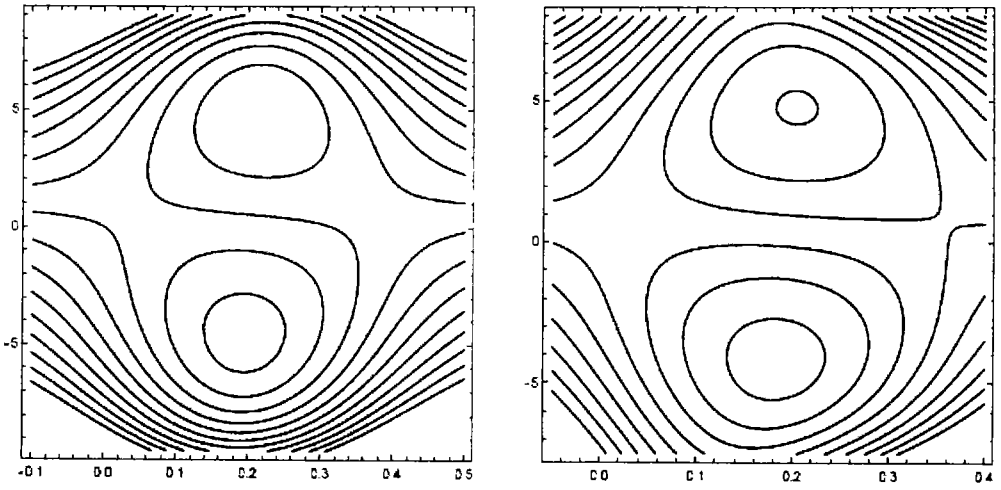

(a) $\delta = 0$ (b) $\delta = 0.02$

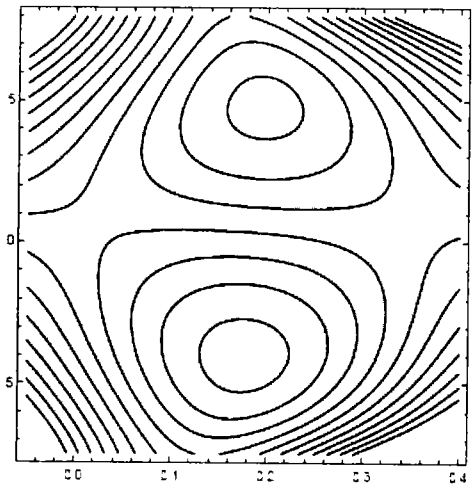

(c) $\delta = 0.03$

Figure 3.8: Depicts the streamline patterns of solid particles for distinct values of δ with $b = 0.6$, $d = 0.8$, $\phi = \frac{\pi}{6}$, $K = 0.1$, $A = 0.5$, $B = 1$, $Re = 0.25$, $\alpha_1 = 0.1$, $\beta = 0.1$, $a = 0.5$.

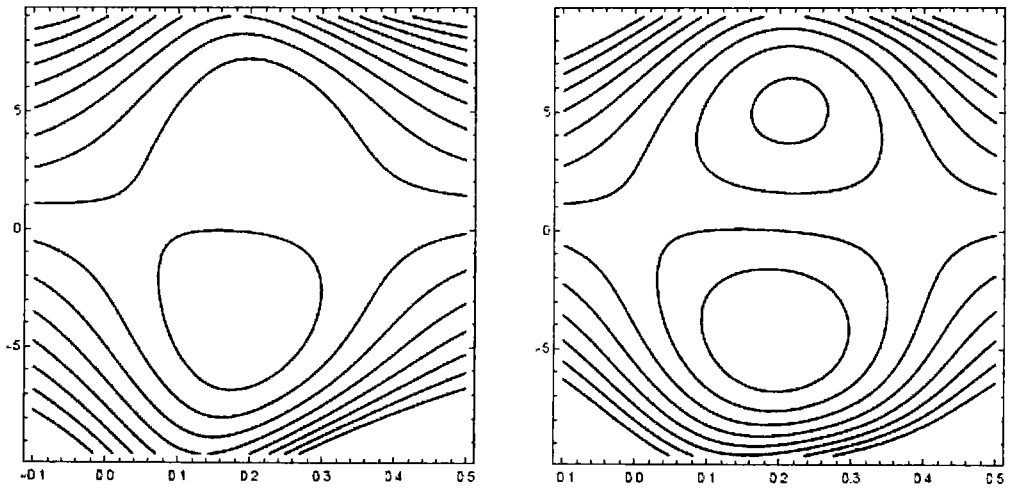

(a) $\beta = 0$ (b) $\beta = 0.2$

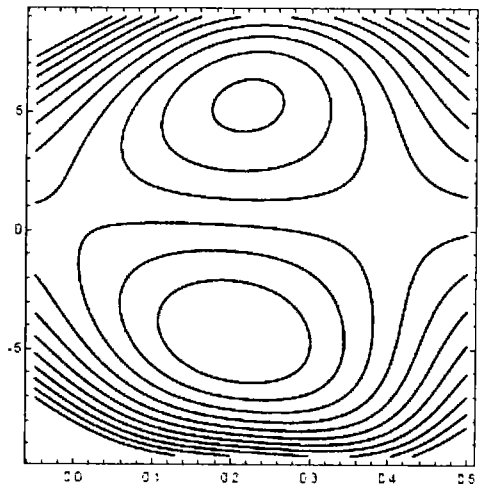

(c) $\beta = 0.3$

Figure 3.9: Depicts the streamline patterns of solid particles for distinct values of β with $Re = 0.25$, $b = 0.6$, $d = 0.8$, $\phi = \frac{\pi}{6}$, $K = 0.1$, $A = 0.5$, $B = 1$, $\delta = 0.01$, $\alpha_1 = 0.1$, $a = 0.5$.

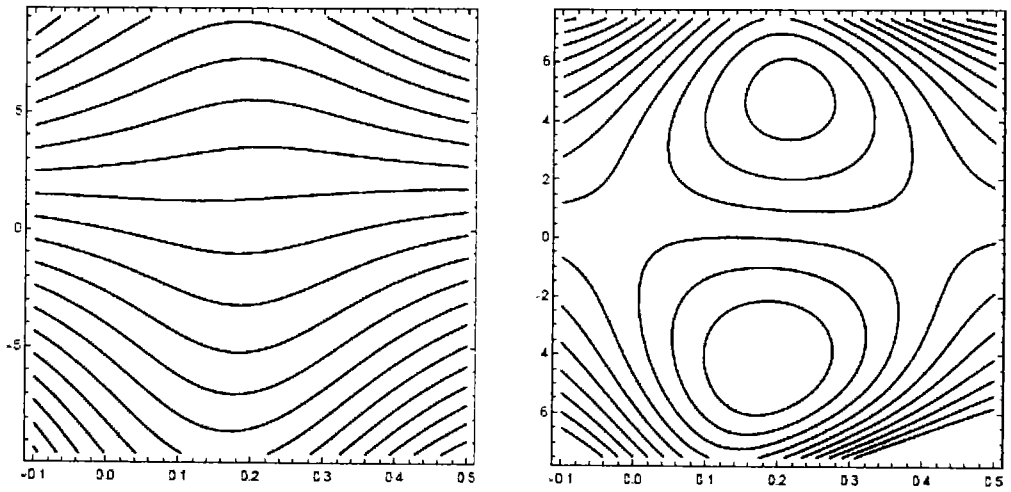

(a) K = 0.001 (b) *K = 0.2*

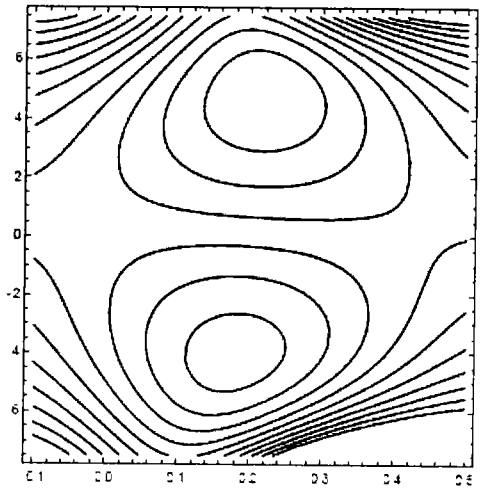

(c) K = 0.3

Figure 3.10: Depicts the streamline patterns of solid particles for distinct values of *K* with $b = 0.6$, $d = 0.8$, $\phi = \frac{\pi}{6}$, $\alpha_1 = 0.1$, $A = 0.5$, $B = 1$, $Re = 0.25$, $\delta = 0.01$, $\beta = 0.1$, $a = 0.5$.

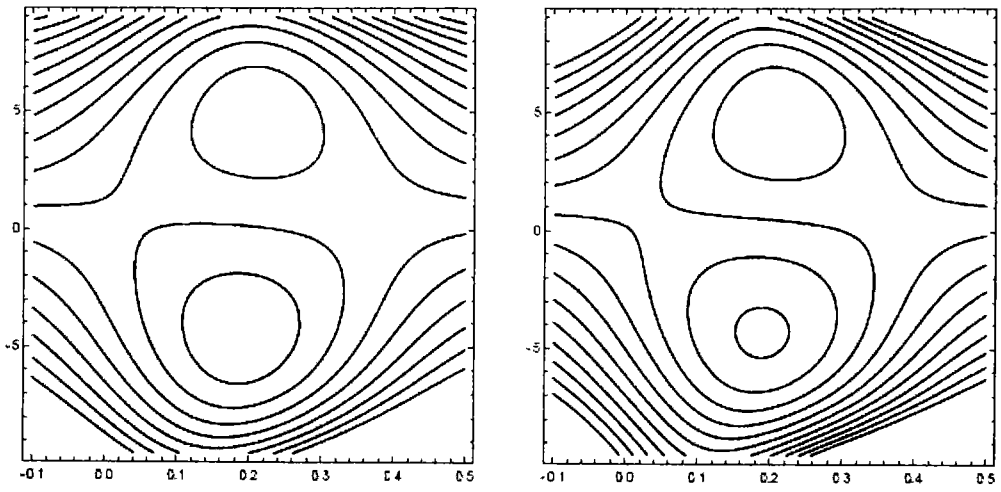

(a) Re = 0 (b) *Re = 0.5*

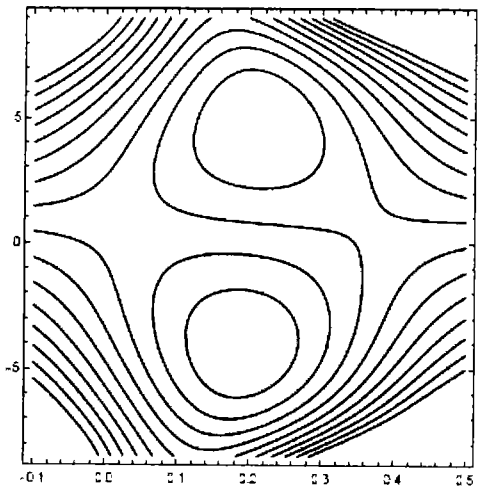

(c) *Re = 1*

Figure 3.11: Depicts the streamline patterns of solid particles for distinct values of Reynolds number (*Re*) with $b = 0.6$, $d = 0.8$, $\phi = \frac{\pi}{6}$, $\alpha_1 = 0.1$, $A = 0.5$, $B = 1$, $K = 0.1$, $\delta = 0.01$, $\beta = 0.1$, $a = 0.5$.

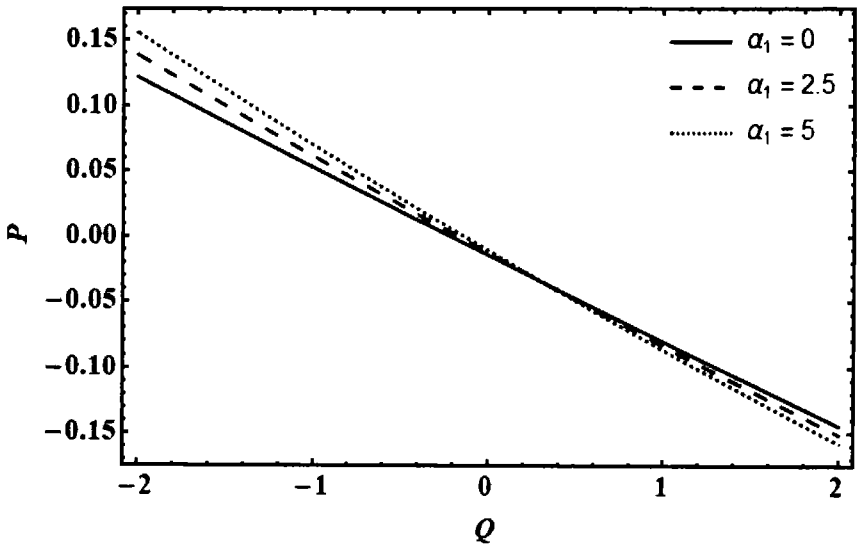

Figure 3.12: Variation of $\Delta p(P)$ with Q for distinct values of α_1 with $b = 0.6$, $\phi = \frac{\pi}{6}$, $Re = 0.25$, $A = 0.5$, $B = 1$, $K = 0.1$, $\delta = 0.01$, $x = 1$, $y = 0$, $\beta = 0.1$, $a = 0.5$, $d = 0.8$.

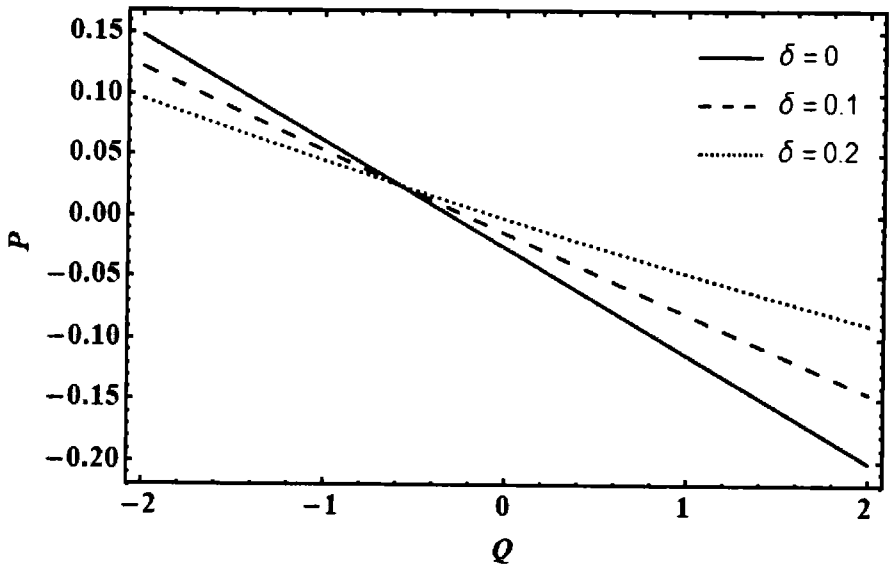

Figure 3.13: Variation of $\Delta p(P)$ with Q for distinct values of δ with $b = 0.6$, $\phi = \frac{\pi}{6}$, $Re = 0.25$, $A = 0.5$, $B = 1$, $K = 0.1$, $\alpha_1 = 0.1$, $\beta = 0.1$, $a = 0.5$, $d = 0.8$.

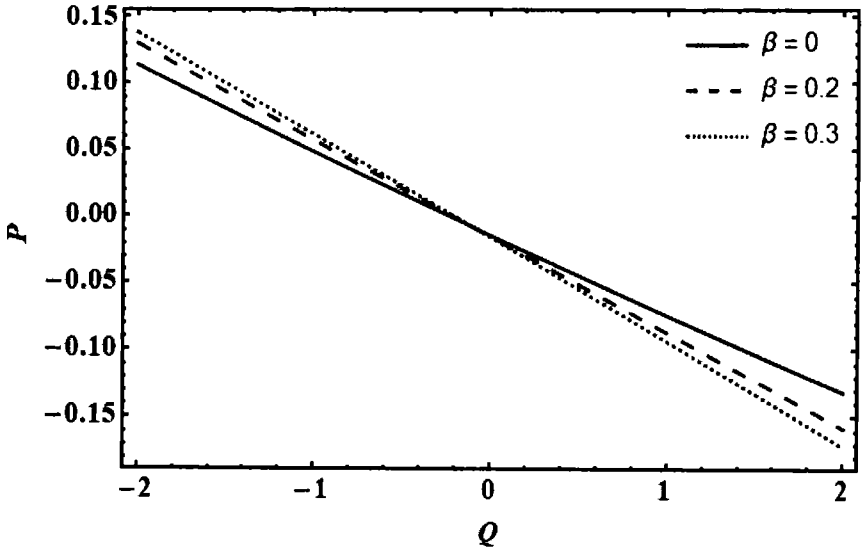

Figure 3.14: Variation of $\Delta p(P)$ with Q for distinct values of β with $b = 0.6$, $\phi = \frac{\pi}{6}$, $Re = 0.25$, $A = 0.5$, $B = 1$, $K = 0.1$, $\delta = 0.01$, $\alpha_1 = 0.1$, $a = 0.5$, $d = 0.8$.

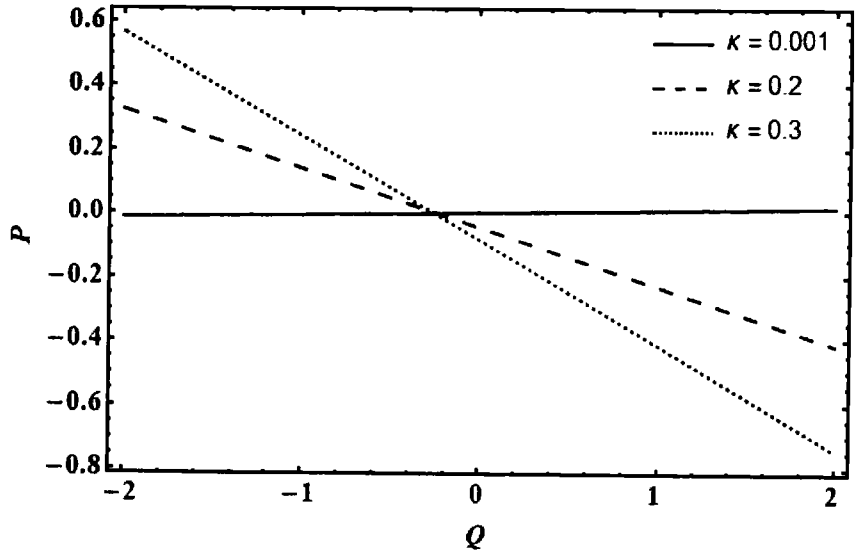

Figure 3.15: Variation of $\Delta p(P)$ with Q for distinct values of K with b = 0.6, $\phi = \frac{\pi}{6}$, $Re = 0.25$, $A = 0.5$, $B = 1$, $\alpha_1 = 0.1$, $\delta = 0.01$, $\beta = 0.1$, $a = 0.5$, $d = 0.8$.

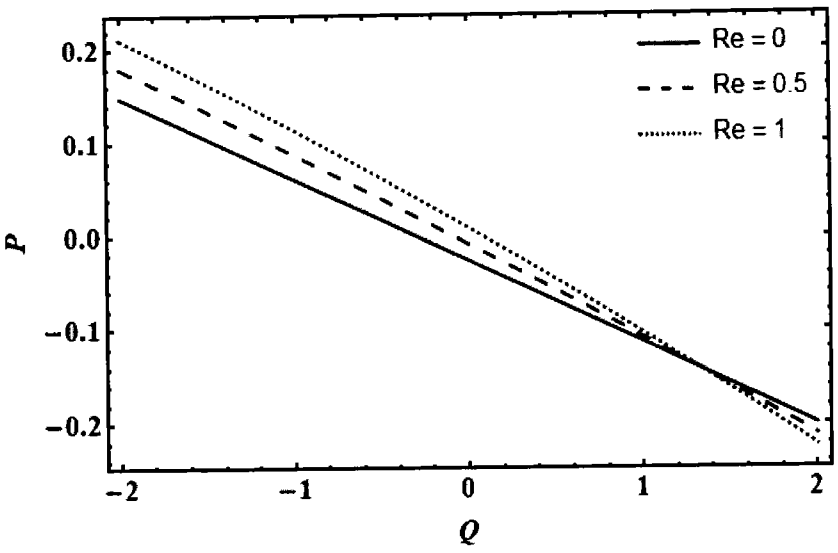

Figure 3.16: Variation of $\Delta p(P)$ with Q for distinct values of Re with $b = 0.6$, $\phi = \frac{\pi}{6}$, $K = 0.1$, $A = 0.1$, $B = 0.1$, $\alpha_1 = 0.1$, $\delta = 0.01$, $\beta = 0.1$, $a = 0.5$, $d = 0.8$.

3.6 Conclusion

In this chapter, a non-linear analysis of a second-grade dusty fluid in asymmetric channel filled with porous medium is discussed. We can draw the following conclusions.

- The pressure rise surges with an rise in α_1, β, Re and K in the retrograde region while the pumping rate declines in the co-pumping region.
- The bolus expands as α_1 and β increase for both fluid and dust particles.
- The size of the trapped bolus enhances in the lower half of the channel as Re increases for dust particles.
- With an increase of K, the size of trapped bolus increases in the upper half of the channel while it reduces in the lower half of the channel for both fluid and dust particles. This effect can be linked with the phase difference between the upper and lower walls.

Chapter 4

Small Wave Number Approximation to Peristaltic Motion of a Dusty Jeffrey Fluid

This chapter explains the consequence of the wall properties on the Jeffrey fluid consisting of the solid dust particles flaunting the peristaltic motion. The equations governing the solid particles and fluid are modeled by employing the small wave number approximation. The effect of relaxation and retardation times are also discussed. Relation of stream function is derived. Regular perturbation technique has been implemented to obtain the solutions. Streamlines graphs are included to discuss the trapping mechanism.

4.1 Problem Formulation

Considering the two-dimensional Jeffrey fluid containing fine dust particles flowing in the passage of uniform thickness $2d$. The passage walls are flexible. The velocity components along the axial and transverse direction is denoted by u and v.

The wall can be geometrically given by

$$y = \eta(\bar{X}, \bar{t}) = d + \mathrm{a}\sin\frac{2\pi}{\lambda}(\bar{X} - c\bar{t}). \tag{4.1}$$

The passage is shown in Fig. 4.1.

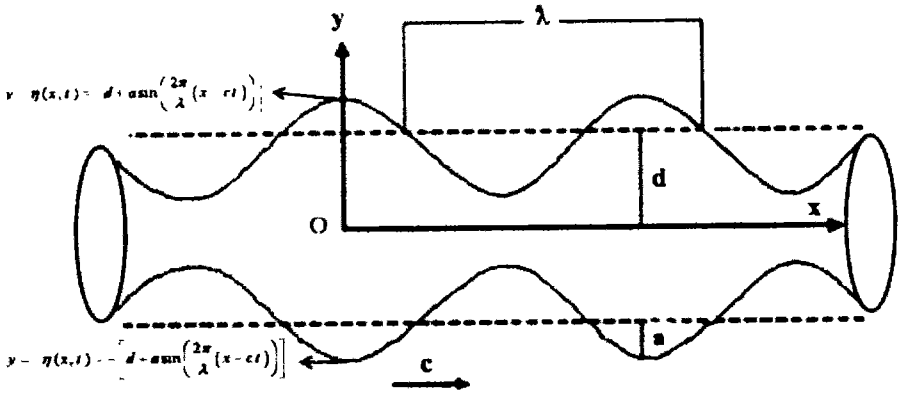

Figure 4.1: Depicts the geometry of the channel.

The continuity and the momentum equations for fluid and solid particles are

For Fluid

$$\bar{\nabla}.\bar{V}= 0, \tag{4.2}$$

$$\frac{d}{dt}\bar{V} = -\nabla\bar{p} + \nabla.\bar{S} + kN(\bar{V}_S - \bar{V}). \tag{4.3}$$

For Solid particles

$$\bar{\nabla}.\bar{V}_s= 0, \tag{4.4}$$

$$\frac{d}{dt}\bar{V}_s = \frac{k}{m}(\bar{V} - \bar{V}_S). \tag{4.5}$$

For Jeffrey fluid, the extra stress tensor $\bar{S}$ is

$$\bar{S} = \frac{\mu}{1+\lambda_1}\left(\bar{A}_1 + \Lambda\left(\frac{d}{d\bar{t}}\right)\bar{A}_1\right), \tag{4.6}$$

where the relaxation time is λ_1, Λ is the retardation time. The number density N of the dust particles is assumed to be non-varying.

The components of extra stress tensor are

$$S_{xx} = \frac{\partial u}{\partial x}\frac{2\mu}{1+\lambda_1} + \left(\frac{\partial}{\partial t}\left(\frac{\partial u}{\partial x}\right) + \left(u\frac{\partial}{\partial x} + v\frac{\partial}{\partial y}\right)\frac{\partial u}{\partial x}\right)\frac{2\mu\Lambda}{1+\lambda_1}, \tag{4.7}$$

$$S_{xy} = \frac{\mu}{1+\lambda_1}\left(\frac{\partial u}{\partial x} + \frac{\partial v}{\partial y}\right) + \frac{\mu\Lambda}{1+\lambda_1}\left(\frac{\partial}{\partial t}\left(\frac{\partial u}{\partial x} + \frac{\partial v}{\partial y}\right) + \left(u\frac{\partial}{\partial x} + v\frac{\partial}{\partial y}\right)\left(\frac{\partial u}{\partial x} + \frac{\partial v}{\partial y}\right)\right), \tag{4.8}$$

$$S_{yy} = \frac{2\mu}{1+\lambda_1}\frac{\partial v}{\partial y} + \frac{2\mu\Lambda}{1+\lambda_1}\left(\frac{\partial}{\partial t}\left(\frac{\partial v}{\partial y}\right) + \left(u\frac{\partial}{\partial x} + v\frac{\partial}{\partial y}\right)\frac{\partial v}{\partial y}\right). \tag{4.9}$$

No-slip boundary condition for the velocities are

$$u = 0, \qquad u_s = 0, \qquad at\ y = \pm\eta, \tag{4.10}$$

$$\frac{\partial P}{\partial x} = \frac{\partial}{\partial x}L(\eta) = \frac{\partial S_{xx}}{\partial x} + \frac{\partial S_{xy}}{\partial y} - \rho\left(\frac{\partial u}{\partial t} + u\frac{\partial u}{\partial x} + v\frac{\partial u}{\partial y}\right) + kN(u_s - u), \qquad y = \pm\eta. \tag{4.11}$$

Here L is the operator expressing the motion of the extended wall along with damping forces defined as

$$L = -T\frac{\partial^2}{\partial x^2} + m'\frac{\partial^2}{\partial t^2} + C\frac{\partial}{\partial t}, \tag{4.12}$$

For flexible wall, the ruling equation of motion is

$$L(\eta) = p - p_0, \tag{4.13}$$

The stream functions and the dimensionless numbers to execute a dimensionless analysis

$$u = \frac{\partial \psi}{\partial y}, \qquad v = -\frac{\partial \psi}{\partial x}, \qquad u_s = \frac{\partial \varphi}{\partial y}, \qquad v_s = -\frac{\partial \varphi}{\partial x}, \quad \bar{t} = \frac{vt}{d\lambda},$$

$$\bar{\psi} = \frac{\psi}{\nu}, \quad \bar{\varphi} = \frac{\varphi}{\nu}, \quad \bar{y} = \frac{y}{d}, \quad \bar{x} = \frac{x}{\lambda}, \quad \delta = \frac{d}{\lambda}, \quad \bar{S} = \frac{d^2}{\rho\nu^2}S. \tag{4.14}$$

After using the transformations and dropping the bar, the compatibility equations for both the solid dust granules and fluid are expressed as

$$\delta\left[\frac{\partial}{\partial y}\left(\frac{\partial^2\psi}{\partial t\partial y} + \frac{\partial\psi}{\partial y}\frac{\partial^2\psi}{\partial x\partial y} - \frac{\partial\psi}{\partial x}\frac{\partial^2\psi}{\partial y^2}\right) + \delta^2\frac{\partial}{\partial x}\left(\frac{\partial^2\psi}{\partial t\partial x} + \frac{\partial\psi}{\partial y}\frac{\partial^2\psi}{\partial x^2} - \frac{\partial\psi}{\partial x}\frac{\partial^2\psi}{\partial x\partial y}\right)\right]$$

$$= \delta\frac{\partial^2}{\partial x\partial y}(S_{xx} - S_{yy}) + \left(\frac{\partial^2}{\partial y^2} - \delta^2\frac{\partial^2}{\partial x^2}\right)S_{xy}$$

$$+A(\nabla_1^2\varphi - \nabla_1^2\psi), \tag{4.15}$$

$$\delta\left[\frac{\partial}{\partial t}\nabla_1^2\varphi + \frac{\partial\varphi}{\partial y}\nabla_1^2\varphi - \frac{\partial\varphi}{\partial x}\nabla_1^2\varphi\right] = B[\,\nabla_1^2\psi - \nabla_1^2\varphi], \tag{4.16}$$

The components of the extra stress tensor are transformed as

$$S_{xx} = \frac{\partial^2\psi}{\partial x\partial y}\left(1 + \lambda_2\delta\left(\frac{\partial}{\partial t} - \frac{\partial\psi}{\partial x}\frac{\partial}{\partial y} + \frac{\partial\psi}{\partial y}\frac{\partial}{\partial x}\right)\right)\frac{2\delta}{1+\lambda_1}, \tag{4.17}$$

$$S_{xy} = \frac{1}{1+\lambda_1}\left(\lambda_2\delta\left(\frac{\partial}{\partial t} - \frac{\partial\psi}{\partial x}\frac{\partial}{\partial y} + \frac{\partial\psi}{\partial y}\frac{\partial}{\partial x}\right) + 1\right)\left(\frac{\partial^2\psi}{\partial y^2} - \delta^2\frac{\partial^2\psi}{\partial x^2}\right), \tag{4.18}$$

$$S_{yy} = -\frac{2\delta}{1+\lambda_1}\left(1 + \lambda_2\delta\left(\frac{\partial}{\partial t} + \frac{\partial\psi}{\partial y}\frac{\partial}{\partial x} - \frac{\partial\psi}{\partial x}\frac{\partial}{\partial y}\right)\right)\frac{\partial^2\psi}{\partial x\partial y}, \tag{4.19}$$

where $\lambda_2 = \frac{\Lambda\nu}{d^2}$ is the retardation parameter.

The dimensionless moving boundary is

$$y = \pm\eta = \pm\big(1 + \epsilon sin2\pi(x - t)\big). \tag{4.20}$$

The non-dimensional form of the boundary conditions is

$$\frac{\partial\psi}{\partial y} = 0, \qquad \frac{\partial\varphi}{\partial y} = 0, \qquad at \qquad y = \pm\eta, \tag{4.21}$$

$$\nabla_1^2 \frac{\partial \psi}{\partial y} - \delta \left[\frac{\partial}{\partial t} \frac{\partial \psi}{\partial y} + \frac{\partial \psi}{\partial y} \frac{\partial}{\partial x} \frac{\partial \psi}{\partial x} - \frac{\partial}{\partial x} \frac{\partial}{\partial y} \frac{\partial \psi}{\partial y} \right] + A \left[\frac{\partial \varphi}{\partial y} - \frac{\partial \psi}{\partial y} \right]$$

$$= \left[E_1 \frac{\partial^3}{\partial x^3} + E_2 \frac{\partial^3}{\partial x \partial t^2} + E_3 \frac{\partial^2}{\partial x \partial t} \right] \eta, \qquad at\ y = \pm\eta. \tag{4.22}$$

4.2 Method of Solution

Assuming the small wave number ($\delta \ll 1$), the perturbation technique is applied to get the results through DSolver in Mathematica.

$$\left.\begin{aligned} \psi &= \psi_0 + \delta\psi_1 + \delta^2\psi_2 + \cdots \\ \varphi &= \varphi_0 + \delta\varphi_1 + \delta^2\varphi_2 + \cdots \end{aligned}\right\}. \tag{4.23}$$

4.2.1 Zeroth Order System

The zeroth order system is

$$\frac{\partial^2}{\partial y^2}(S_{0xy}) + A\left(\frac{\partial^2 \varphi_0}{\partial y^2} - \frac{\partial^2 \psi_0}{\partial y^2} \right) = 0, \tag{4.24}$$

$$B\left(\frac{\partial^2 \psi_0}{\partial y^2} - \frac{\partial^2 \varphi_0}{\partial y^2} \right) = 0, \tag{4.25}$$

with

$$S_{0xy} = \frac{1}{1+\lambda_1}\left(\frac{\partial^2 \psi_0}{\partial y^2} \right), \tag{4.26}$$

with

$$\frac{\partial \psi_0}{\partial y} = 0, \frac{\partial \varphi_0}{\partial y} = 0, \qquad at\ y = \pm\eta, \tag{4.27}$$

$$\frac{\partial^3 \psi_0}{\partial y^3} + A\left[\frac{\partial \varphi_0}{\partial y} - \frac{\partial \psi_0}{\partial y} \right] = \left[E_1 \frac{\partial^3}{\partial x^3} + E_2 \frac{\partial^3}{\partial x \partial t^2} + E_3 \frac{\partial^2}{\partial x \partial t} \right] \eta,$$

$$at \qquad y = \pm\eta. \qquad (4.28)$$

4.2.2 First Order System

The system of first order equations for the fluid and solid particles is

$$\frac{\partial}{\partial y}\left(\frac{\partial^2\psi_0}{\partial t\partial y}+\frac{\partial\psi_0}{\partial y}\frac{\partial^2\psi_0}{\partial x\partial y}-\frac{\partial\psi_0}{\partial x}\frac{\partial^2\psi_0}{\partial y^2}\right)$$

$$=\frac{\partial^2}{\partial x\partial y}(S_{0xx}-S_{0yy})+\frac{\partial^2}{\partial y^2}(S_{1xy})+A\left(\frac{\partial^2\varphi_1}{\partial y^2}-\frac{\partial^2\psi_1}{\partial y^2}\right), \qquad (4.29)$$

$$B\left(\frac{\partial^2\psi_1}{\partial y^2}-\frac{\partial^2\varphi_1}{\partial y^2}\right)=\frac{\partial^3\varphi_0}{\partial t\partial y^2}+\frac{\partial\varphi_0}{\partial y}\frac{\partial^3\varphi_0}{\partial x\partial y^2}-\frac{\partial\varphi_0}{\partial x}\frac{\partial^3\varphi_0}{\partial y^3}, \qquad (4.30)$$

with

$$S_{0xx}=0, \qquad (4.31)$$

$$S_{1xy}=\frac{1}{1+\lambda_1}\left(\frac{\partial^2\psi_1}{\partial y^2}\right.$$

$$\left.+\lambda_2\left(\frac{\partial}{\partial t}\left(\frac{\partial^2\psi_0}{\partial y^2}\right)+\left(\frac{\partial\psi_0}{\partial y}\frac{\partial}{\partial x}-\frac{\partial\psi_0}{\partial x}\frac{\partial}{\partial y}\right)\frac{\partial^2\psi_0}{\partial y^2}\right)\right), \qquad (4.32)$$

$$S_{0yy}=0. \qquad (4.33)$$

with

$$\frac{\partial\psi_1}{\partial y}=0, \qquad \frac{\partial\varphi_1}{\partial y}=0, \qquad at\ y=\pm\eta, \qquad (4.34)$$

$$\frac{\partial S_{1xy}}{\partial y}+\frac{\partial S_{0xx}}{\partial x}+A\left(\frac{\partial\varphi_1}{\partial y}-\frac{\partial\psi_1}{\partial y}\right)=\frac{\partial^2\psi_0}{\partial t\partial y}-\frac{\partial\psi_0}{\partial x}\frac{\partial^2\psi_0}{\partial y^2}+\frac{\partial\psi_0}{\partial y}\frac{\partial^2\psi_0}{\partial x\partial y},$$

$$at\ y=\pm\eta. \qquad (4.35)$$

4.2.3 Second Order System

Second order system of the coupled equations is

$$\frac{\partial}{\partial y}\left(\frac{\partial^2\psi_1}{\partial t\partial y}+\frac{\partial\psi_1}{\partial y}\frac{\partial^2\psi_0}{\partial x\partial y}+\frac{\partial\psi_0}{\partial y}\frac{\partial^2\psi_1}{\partial x\partial y}-\frac{\partial\psi_1}{\partial x}\frac{\partial^2\psi_0}{\partial y^2}-\frac{\partial\psi_0}{\partial x}\frac{\partial^2\psi_1}{\partial y^2}\right)$$

$$=\frac{\partial^2}{\partial x\partial y}(S_{1xx}-S_{1yy})+\frac{\partial^2}{\partial y^2}(S_{2xy})-\frac{\partial^2}{\partial x^2}(S_{0xy})$$

$$+A\left[\left(\frac{\partial^2\varphi_2}{\partial y^2}+\frac{\partial^2\varphi_0}{\partial x^2}\right)-\left(\frac{\partial^2\psi_2}{\partial y^2}+\frac{\partial^2\psi_0}{\partial x^2}\right)\right], \tag{4.36}$$

$$B\left[\left(\frac{\partial^2\psi_2}{\partial y^2}+\frac{\partial^2\psi_0}{\partial x^2}\right)-\left(\frac{\partial^2\varphi_2}{\partial y^2}+\frac{\partial^2\varphi_0}{\partial x^2}\right)\right]$$

$$=\frac{\partial^3\varphi_1}{\partial t\partial y^2}+\frac{\partial\varphi_1}{\partial y}\frac{\partial^3\varphi_0}{\partial x\partial y^2}+\frac{\partial\varphi_0}{\partial y}\frac{\partial^3\varphi_1}{\partial x\partial y^2}-\frac{\partial\varphi_1}{\partial x}\frac{\partial^3\varphi_0}{\partial y^3}$$

$$-\frac{\partial\varphi_0}{\partial x}\frac{\partial^3\varphi_1}{\partial y^3}, \tag{4.37}$$

with

$$S_{1xx}=\frac{2}{1+\lambda_1}\left(\frac{\partial^2\psi_0}{\partial x\partial y}\right), \tag{4.38}$$

$$S_{1yy}=-\frac{2}{1+\lambda_1}\left(\frac{\partial^2\psi_0}{\partial x\partial y}\right), \tag{4.39}$$

$$S_{2xy}=\frac{1}{1+\lambda_1}\left(\left(\frac{\partial^2\psi_2}{\partial y^2}-\frac{\partial^2\psi_0}{\partial x^2}\right)\right.$$

$$\left.+\lambda_2\left(\frac{\partial}{\partial t}\left(\frac{\partial^2\psi_1}{\partial y^2}\right)+\left(\frac{\partial\psi_1}{\partial y}\frac{\partial}{\partial x}-\frac{\partial\psi_1}{\partial x}\frac{\partial}{\partial y}\right)\frac{\partial^2\psi_1}{\partial y^2}\right)\right), \tag{4.40}$$

with boundary conditions

$$\frac{\partial\psi_2}{\partial y}=0, \qquad \frac{\partial\varphi_2}{\partial y}=0, \qquad at\ y=\pm\eta, \tag{4.41}$$

$$\frac{\partial S_{1xx}}{\partial x}+\frac{\partial S_{2xy}}{\partial y}+A\left(\frac{\partial \varphi_2}{\partial y}-\frac{\partial \psi_2}{\partial y}\right)$$

$$=-\frac{\partial^2\psi_0}{\partial y^2}\frac{\partial \psi_1}{\partial x}+\frac{\partial^2\psi_0}{\partial t\partial x}+\frac{\partial \psi_1}{\partial y}\frac{\partial^2\psi_0}{\partial x\partial y}+\frac{\partial^2\psi_1}{\partial x\partial y}\frac{\partial \psi_0}{\partial y}-\frac{\partial^2\psi_1}{\partial y^2}\frac{\partial \psi_0}{\partial x},$$

$$at\ y=\pm\eta. \quad (4.42)$$

Solutions of the above-mentioned equations are obtained through DSolver and demonstrated through graphs.

4.3 Results and Discussions

This section compromises a detailed discussion on the graphs of the both solid particles and the fluid. Three main parameters of the wall i.e., E_1, E_2 and E_3 represent the wall rigidity, the mass identifying parameter and elasticity of the wall respectively. λ_1 is the relaxation time while λ_2 is retardation time and wave number is denoted by δ. Figs. 4.2 – 4.7 show the impacts of different attributes on the flow rate of the fluid. Figs. 4.8 – 4.11 render the consequences of parameters on the fluid's velocity profile. Figs. 4.12 – 4.14 are the streamline compositions of the fluid with variation in different parameters. The effect of the parameters on the amount of the flow rate of the solid granules are shown in Figs. 4.15 – 4.20. The effects of the various attributes on the velocity of the dust particles are given in Figs. 4.21 – 4.24. Figs. 4.25 – 4.27 exhibit the influence of parameters on the streamline patterns of the dust particles.

Fig. 4.2 displays that the flow rate of the fluid grows as E_1 is increased. Increase in E_1 increases the rigidity of the wall thus fluid can flow more efficiently through the passage. Fig. 4.3 displays the effect of E_2 on the flow rate. It has the same effect on the fluid flow rate as E_1 has i.e., the flow rate enhances as the values for E_2 is increased. The rate of flow grows as the elasticity of the wall is increased as observed in Fig. 4.4.

The growth in the wave number δ, increases the fluid's rate of flow and it can be witnessed in Fig. 4.5. Increase in the wave number causes decrease in the amplitude of the wave thus resulting growth in the fluid flow. Fig. 4.6 shows that by increasing λ_1, the fluid's flow rate increases. The retardation parameter is denoted by λ_2 and the rate of the fluid's flow enhances with the increase in λ_2 and it is illustrated in Fig. 4.7. The impact of the relaxation time (λ_1) on the fluid's velocity is shown in Fig. 4.8. The velocity of the fluid decays as the values of the relaxation time (λ_1) is increased. This indicates more time is required by the particles to come back to the equilibrium system from perturbated system. Fig. 4.9 shows the fluid velocity being affected by the retardation time (λ_2). The rise in the retardation time intensifies elasticity and since elasticity and viscosity are inversely corelated to each other so the decline in viscosity boosts the fluid velocity. Fig. 4.10 shows the impact of wave number (δ) on the fluid velocity profile. The fluid velocity rises as δ increases. Fig. 4.11 is detailed illustration of effects of three parameters E_2, E_1 and E_3 on the fluid's velocity. The velocity of the fluid rises as the values of the three parameters is enlarged. Fig. 4.12 exhibits that the contraction in bolus on the left part of the channel as λ_1 is increased while it expands on the right side. Fig. 4.13 shows that the left and right bolus pushed each other with the growth in λ_2. Fig. 4.14 demonstrates that with the increase in δ (wave number), the trapped bolus compresses each other.

Figs. 4.15 – 4.16 show that as the values of E_2 and E_1 are increased the rate of flow of the solid grains is increased. Fig. 4.17 depicts that E_3 has reverse impact on the flow rate of the dust particles i.e., as E_3 increases, the rate of the flow decreases. Fig. 4.18 shows that as the values of λ_1 is increased, the flow rate decays for the solid particles. A similar impact can be noticed in Fig. 4.19. The rate of flow is decreased as the value of the retardation time (λ_2) is increased. It can be spotted in Fig. 4.20 that as δ is

enhanced, the flow rate is also increased for the solid particles. [redacted] enhanced the velocity of the solid particles intensifies near the walls of the channel [redacted] served in Fig. 4.21. Fig. 4.22 indicates that for solid grains, the velocity is decre[redacted] as the relaxation time (λ_1) is increased. It can be seen in Fig. 4.23 that as the v[redacted]s of λ_2 are increased, the solid dust particles velocity is increased. Fig. [redacted] is a comprehensive illustration of the influence of three parameters E_1, E_2 an[redacted] on the velocity of the solid particles. The velocity rises by increasing E_3, E_2 and E[redacted]g. 4.25 depicts that the bolus expands at left while it contracts at right part of the [redacted]nnel as we increase the values of λ_2. The bolus can be observed shrinking in the [redacted]portion while it expands in the right portion of the passage in Fig. 4.26 as λ_1 ar[redacted]larged. The consequences of wave number [redacted] the contour outlines of the solid [redacted]icles is given in Fig. 4.27. It can be observed tha[redacted]d bolus moves [redacted]ds right as wave number is increased.

4.4 Graphs

Graphs of Fluid

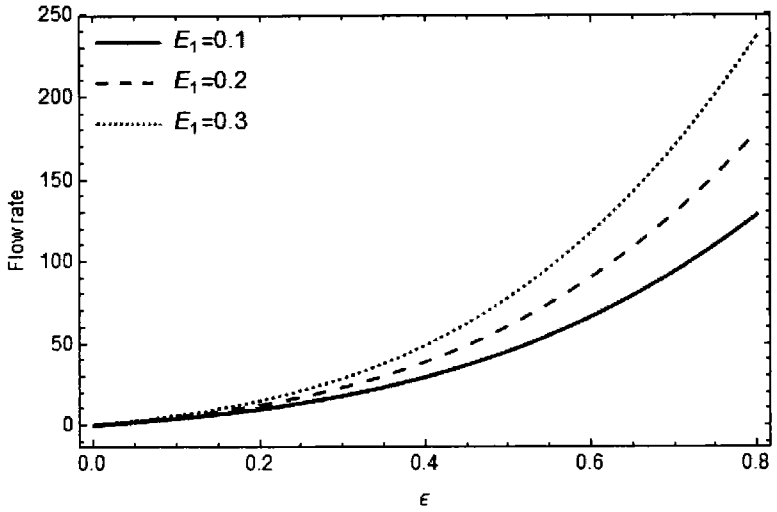

Figure 4.2: Depicts the significance of E_1 on the fluid flow rate with $\delta = 0.01$, $E_2 = 0.35$, $A = 1$, $\lambda_2 = 1$, $B = 1$, $E_3 = 0.35$, $\lambda_1 = 1$.

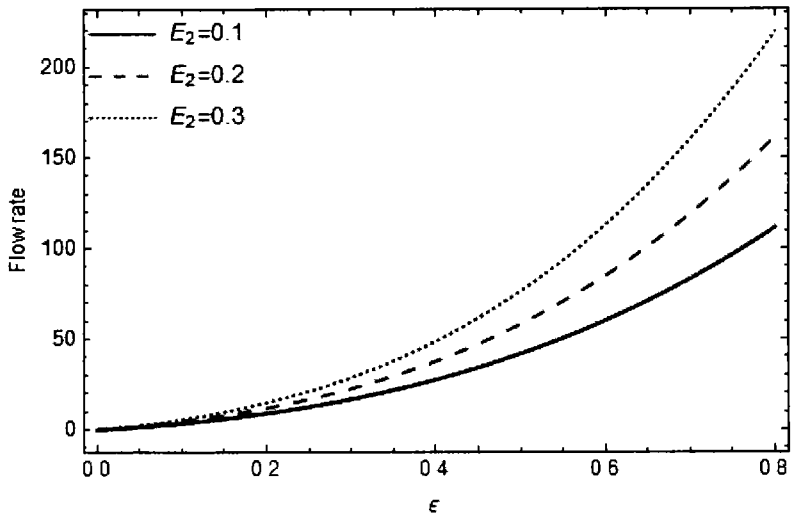

Figure 4.3: Depicts the significance of E_2 on the fluid flow rate with $\delta = 0.01$, $E_1 = 0.25$, $A = 1$, $\lambda_2 = 3$, $B = 1$, $E_3 = 0.35$, $\lambda_1 = 1$.

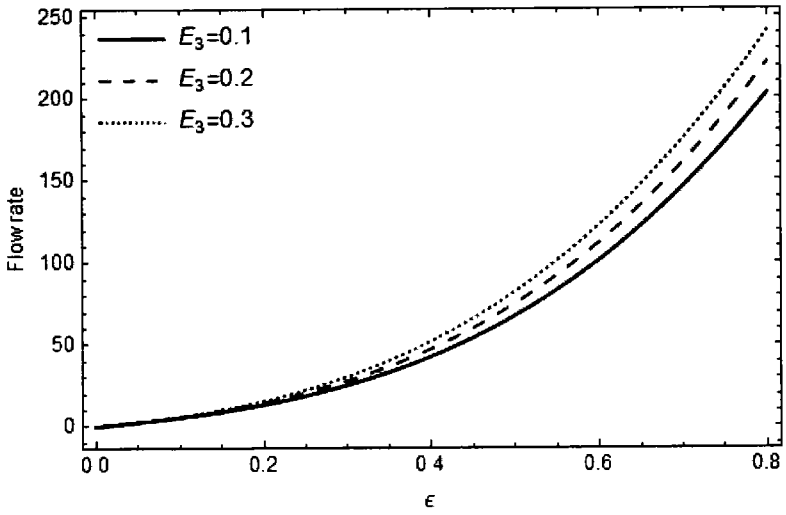

Figure 4.4: Depicts the significance of E_3 on the fluid flow rate with $\delta = 0.01$, $E_1 = 0.25$, $A = 1$, $\lambda_2 = 3$, $B = 1$, $E_2 = 0.35$, $\lambda_1 = 1$.

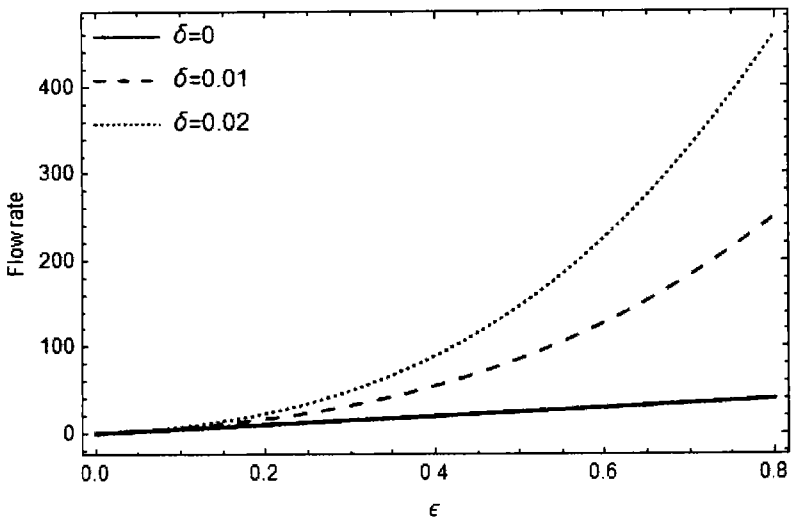

Figure 4.5: Depicts the significance of δ on the fluid flow rate with $E_3 = 0.35$, $E_1 = 0.25$, $A = 1$, $\lambda_2 = 3$, $B = 1$, $E_2 = 0.35$, $\lambda_1 = 1$.

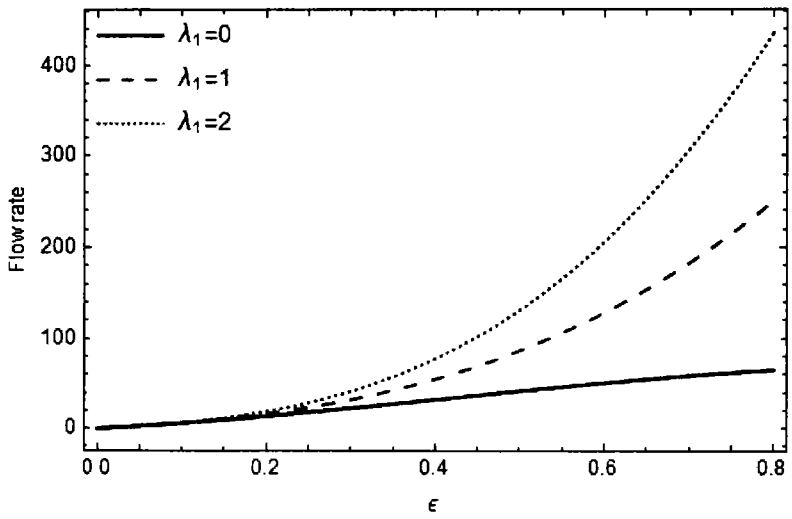

Figure 4.6: Depicts the significance of λ_1 on the fluid flow rate with $E_3 = 0.35$, $E_1 = 0.25$, $A = 1$, $\lambda_2 = 3$, $B = 1$, $E_2 = 0.35$, $\delta = 0.01$.

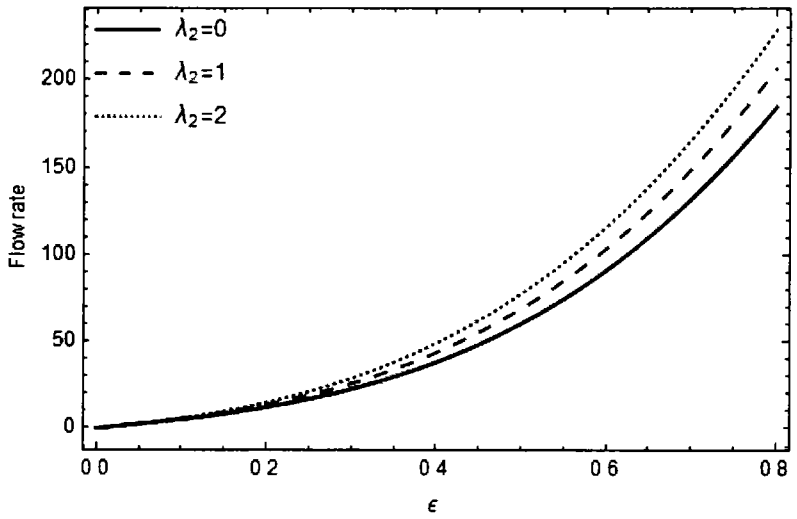

Figure 4.7: Depicts the significance of λ_2 on the fluid flow rate with $E_3 = 0.35$, $E_1 = 0.25$, $A = 1$, $\lambda_1 = 1$, $B = 1$, $E_2 = 0.35$, $\delta = 0.01$.

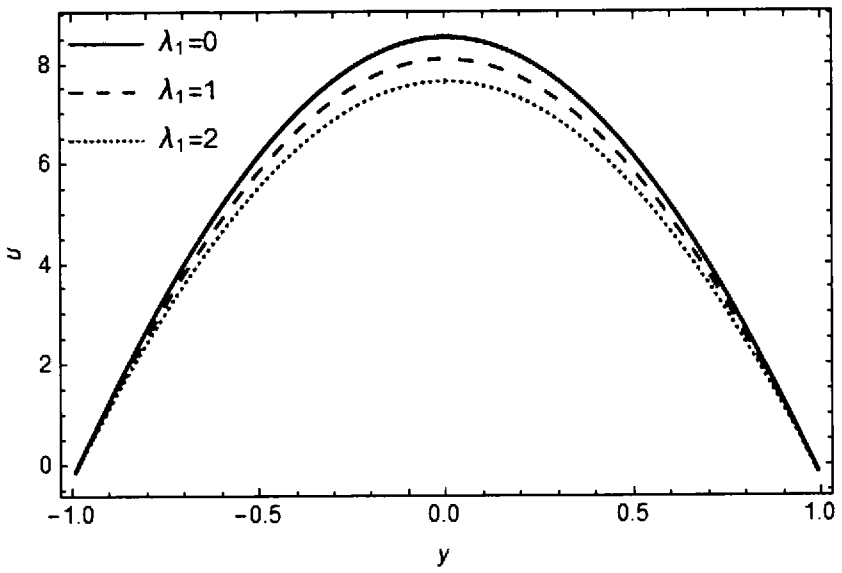

Figure 4.8: Depicts the significance of λ_1 on the fluid velocity with $E_1 = 0.35$, $E_2 = 0.25$, $A = 1$, $\lambda_2 = 1.5$, $B = 1$, $\epsilon = 0.1$, $E_3 = 0.35$, $\delta = 0.01$.

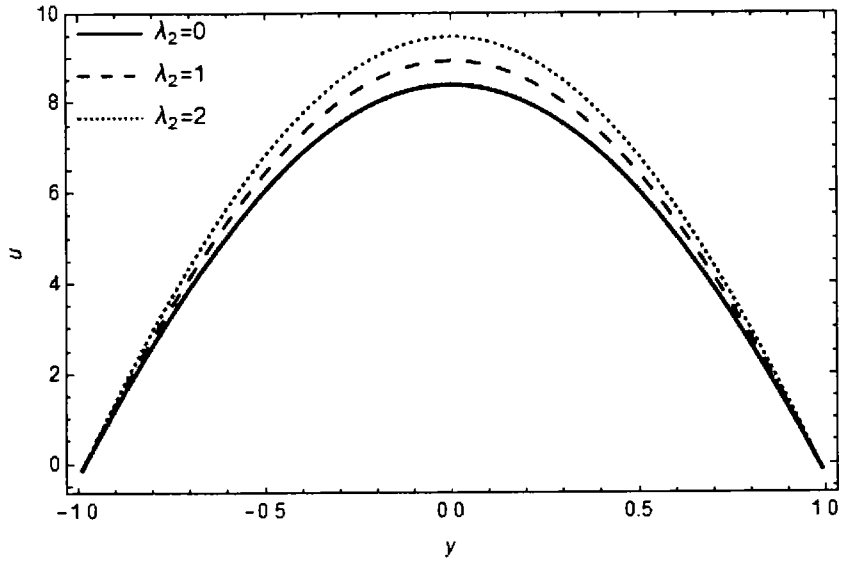

Figure 4.9: Depicts the significance of λ_2 on the fluid velocity with $E_1 = 0.35$, $E_2 = 0.25$, $A = 1$, $\lambda_1 = 3$, $B = 1$, $\epsilon = 0.1$, $E_3 = 0.35$, $\delta = 0.01$.

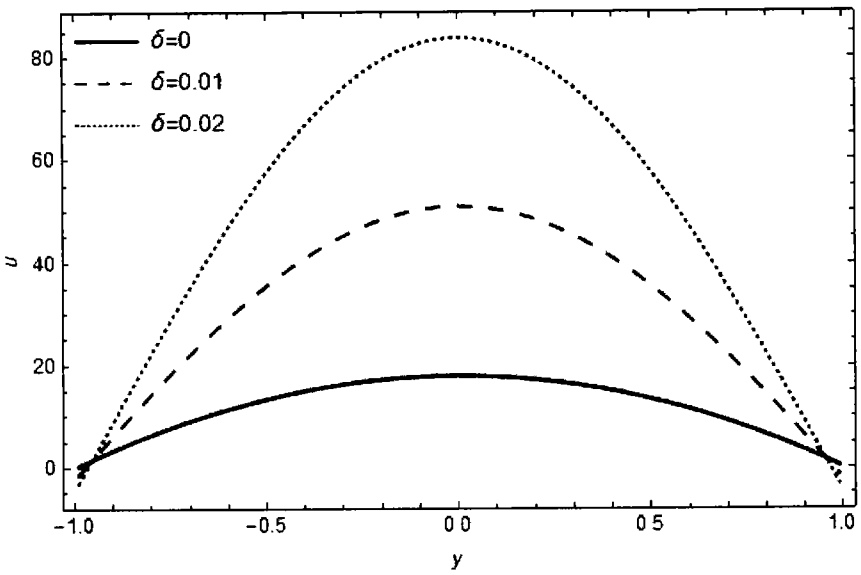

Figure 4.10: Depicts the significance of δ on the fluid velocity with $E_1 = 0.75$, $E_2 = 0.7$, $A = 5$, $\lambda_2 = 1.5$, $B = 1$, $\epsilon = 0.1$, $E_3 = 0.4$, $\lambda_1 = 2.5$.

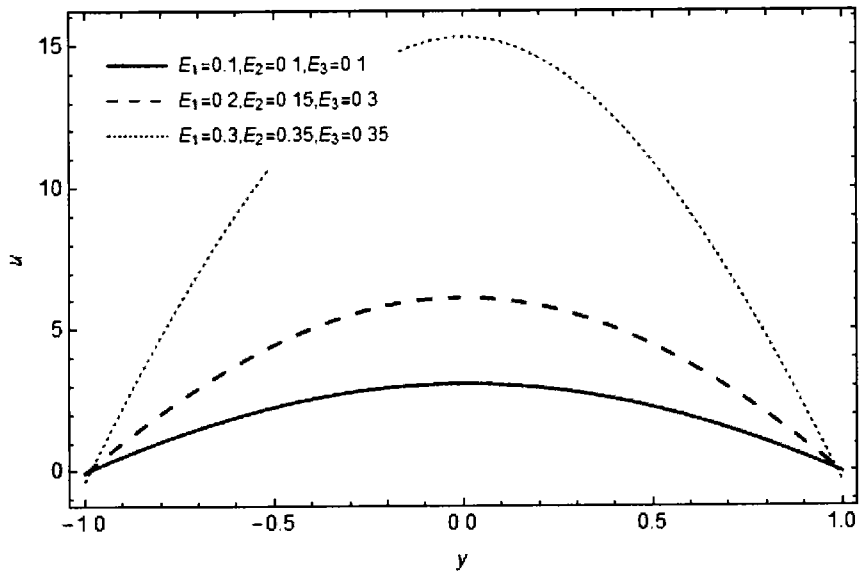

Figure 4.11: Depicts the significance of different values of E_1, E_2 and E_3 on the fluid velocity with $A = 2$, $\lambda_2 = 1.5$, $B = 3$, $\epsilon = 0.1$, $\lambda_1 = 2.5$, $\delta = 0.01$.

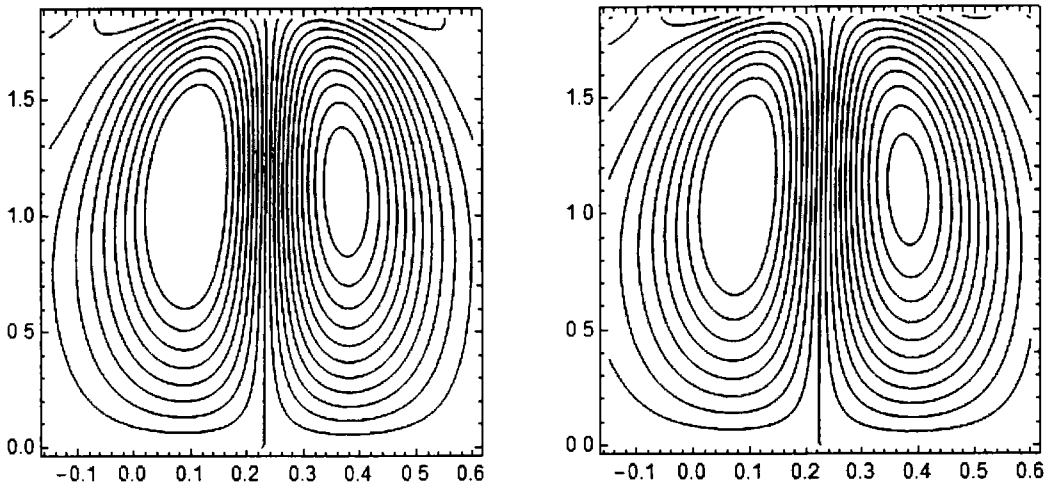

$\lambda_1 = 0$ $\lambda_1 = 0.8$

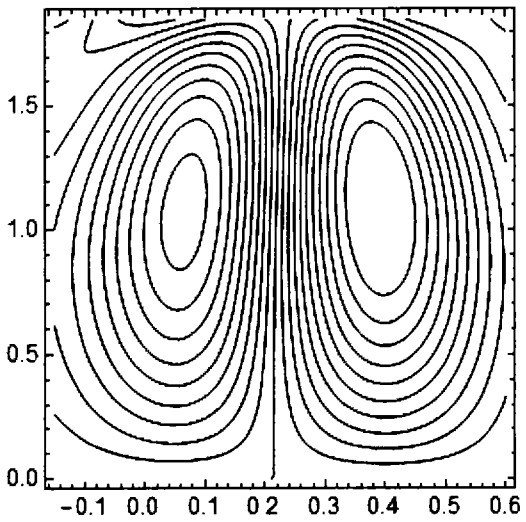

$\lambda_1 = 1.6$

Figure 4.12: Depicts the significance of λ_1 on the fluid streamline structures with E_1 = 0.5, E_2 = 0.25, A = 1, λ_2 = 1.25, B = 2, E_3 = 0.35, $\delta = 0.01$.

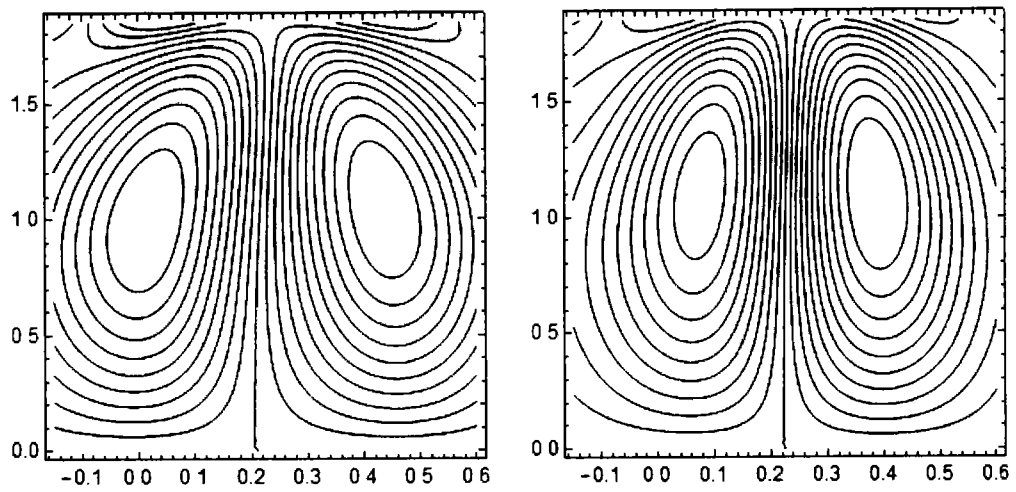

$\lambda_2 = 0$ $\lambda_2 = 0.8$

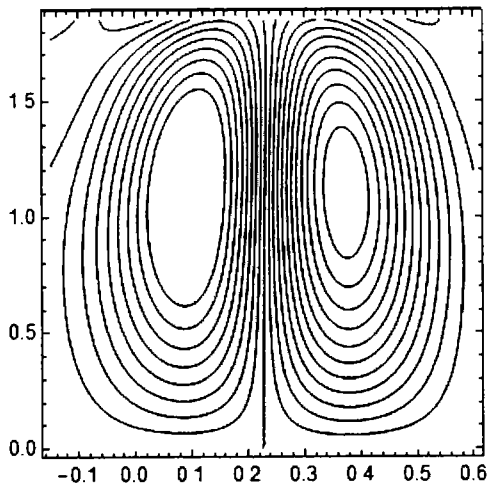

$\lambda_2 = 1.25$

Figure 4.13: Depicts the significance of λ_2 on the fluid streamline structures with E_1 = 0.5, E_2 = 0.25, δ = 0.01, A= 1, λ_1 = 0.5, B = 2, E_3 = 0.35.

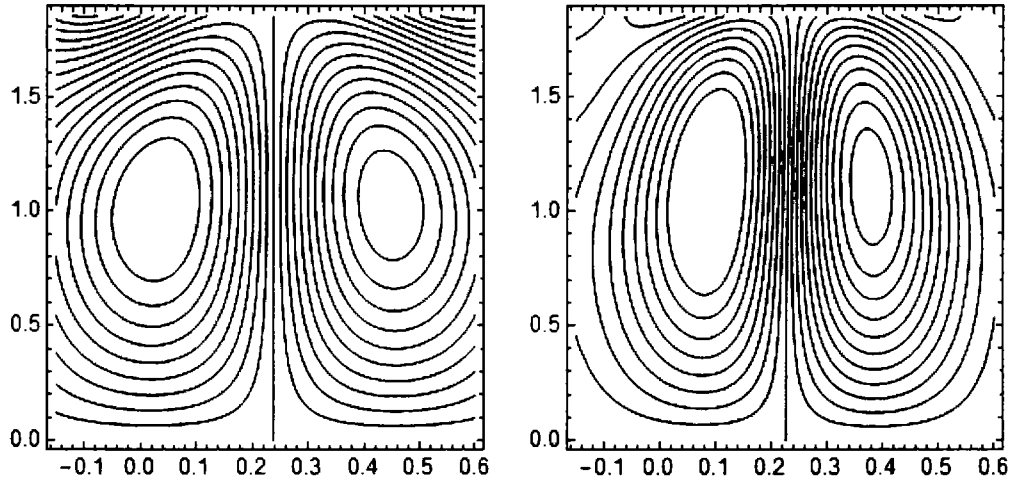

$\delta = 0$ $\delta = 0.01$

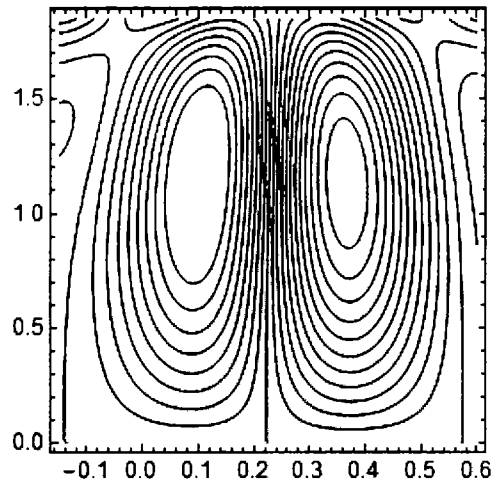

$\delta = 0.02$

Figure 4.14: Depicts the significance of δ on the fluid streamline structures with $E_1 = 0.5$, $E_2 = 0.25$, $A = 1$, $\lambda_1 = 0.5$, $B = 2$, $E_3 = 0.35$, $\lambda_2 = 1.25$.

Graphs of Solid Particles

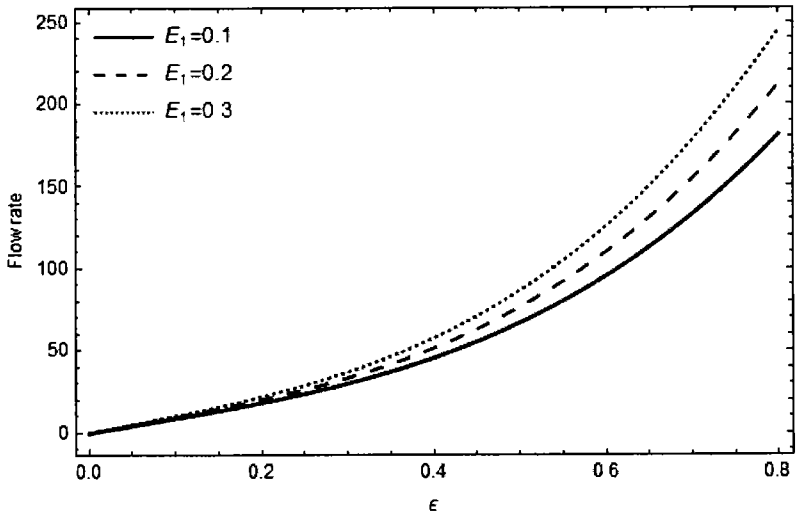

Figure 4.15: Depicts the significance of E_1 on the dust particles flow rate with E_3 = 0.25, A = 0.2, λ_1 = 0.1, B = 1, E_2 = 1, δ = 0.01, λ_2 = 0.5.

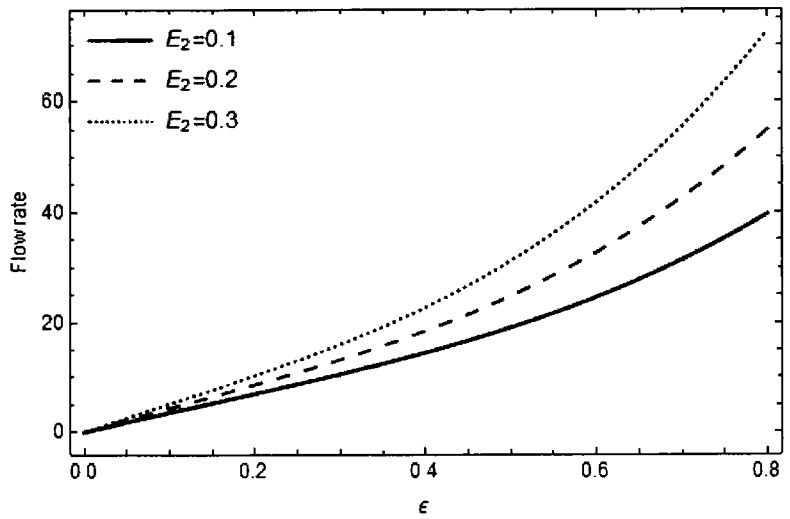

Figure 4.16: Depicts the significance of E_2 on the dust particles flow rate with E_3 = 0.25, A = 0.2, λ_1 = 0.1, B = 1, E_1 = 0.5, δ = 0.01, λ_2 = 0.5.

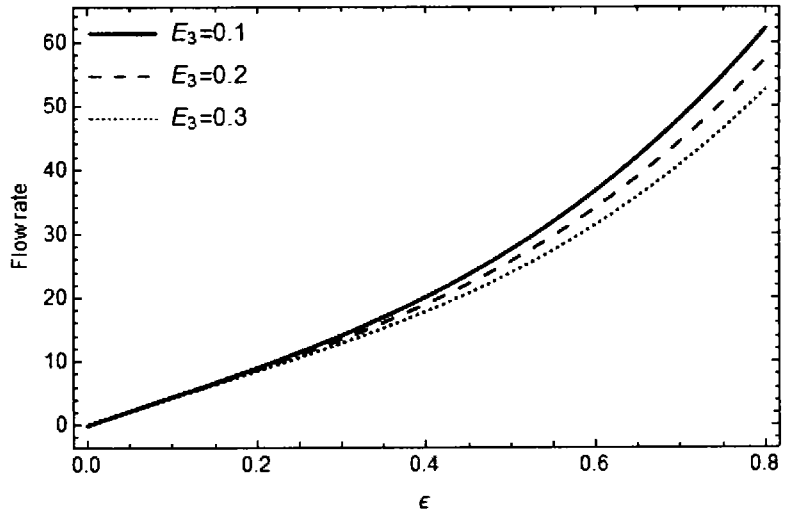

Figure 4.17: Depicts the significance of E_3 on the dust particles flow rate with E_2 = 0.2, A = 0.2, λ_1 = 0.1, B = 1, E_1 = 0.35, δ = 0.01, λ_2 = 0.5.

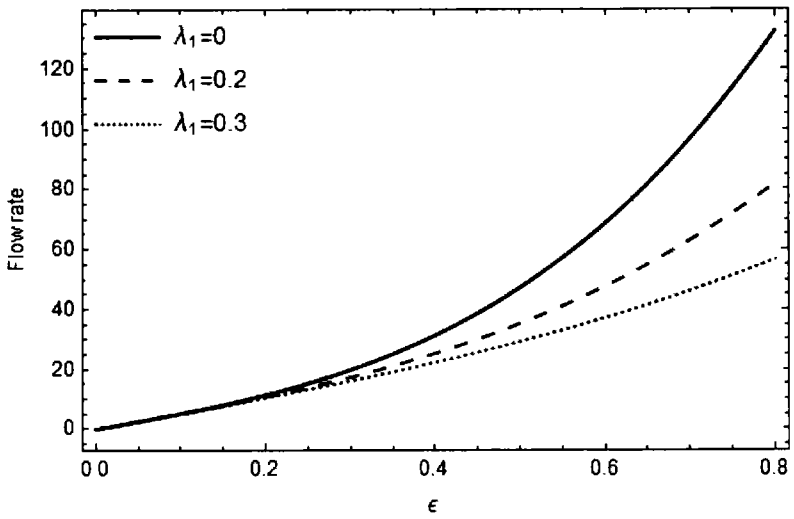

Figure 4.18: Depicts the significance of λ_1 on the dust particles flow rate with E_2 = 0.25, A = 1, E_3 = 0.5, B = 0.25, E_1 = 0.35, δ = 0.01, λ_2 = 0.5.

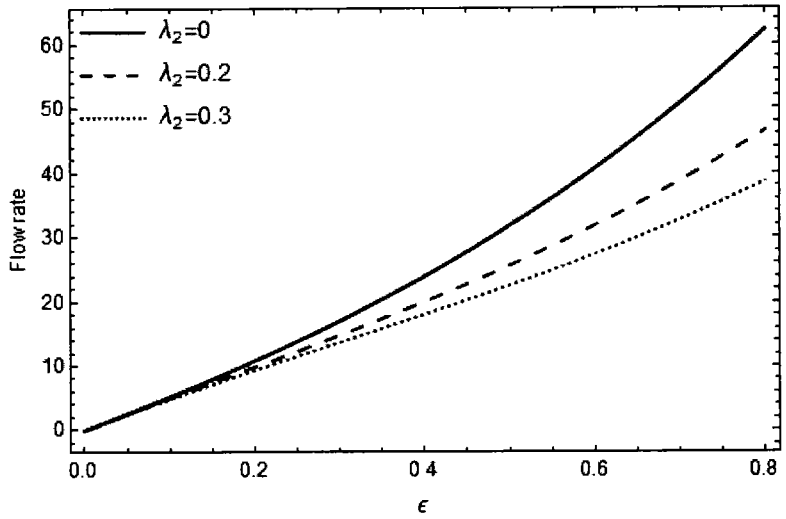

Figure 4.19: Depicts the significance of λ_2 on the dust particles flow rate with $E_2 = 0.25, A = 0.2, E_3 = 0.5, B = 1, E_1 = 0.35, \delta = 0.01, \lambda_1 = 0.2$.

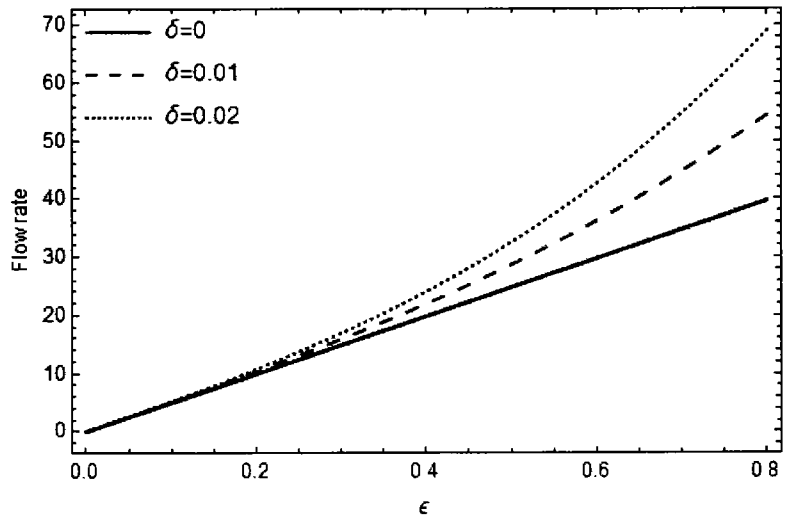

Figure 4.20: Depicts the significance of δ on the dust particles flow rate with $E_2 = 0.25, A = 0.2, E_3 = 0.5, B = 1, E_1 = 0.35, \lambda_2 = 0.1, \lambda_1 = 0.2$.

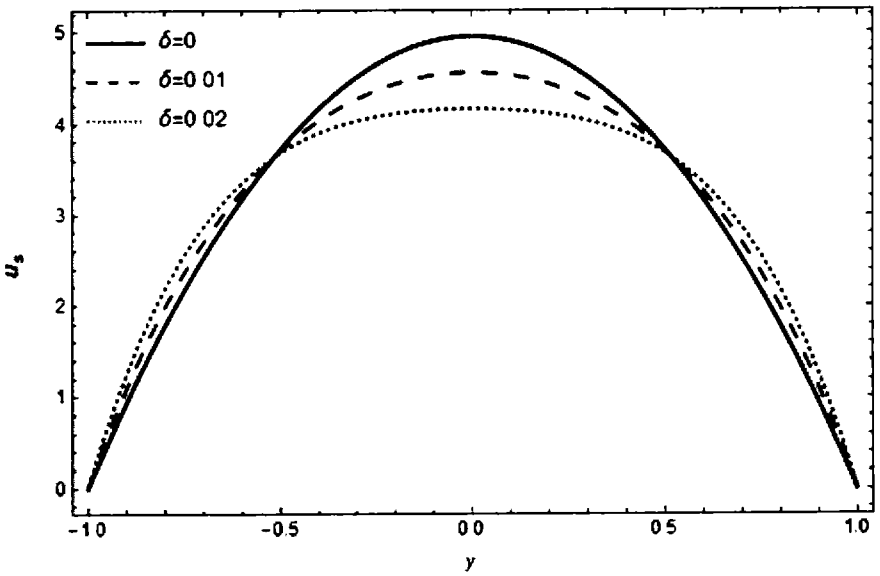

Figure 4.21: Depicts the significance of δ on solid particles velocity with $E_1 = 1$, $E_2 = 1$, $A = 1$, $\lambda_2 = 0.5$, $B = 1$, $\epsilon = 0.02$, $E_3 = 1$, $\lambda_1 = 1$.

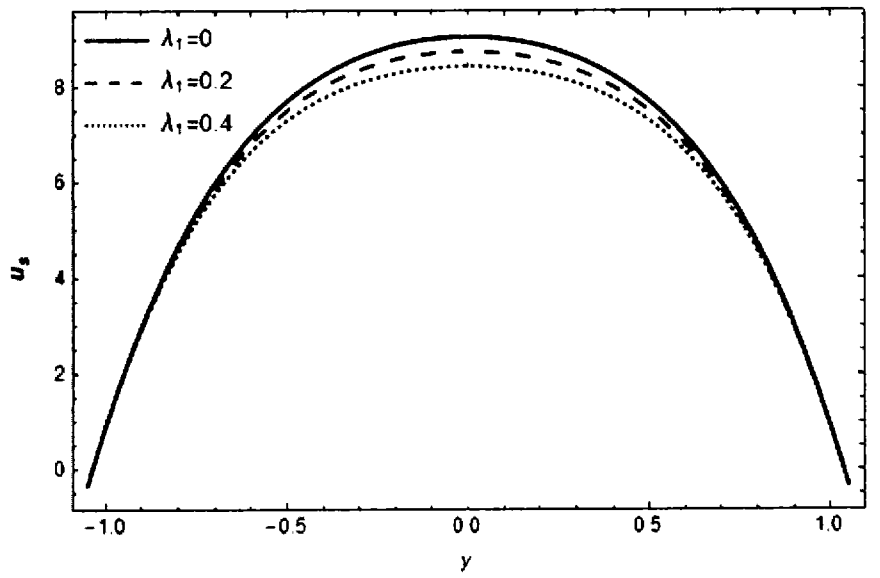

Figure 4.22: Depicts the significance of λ_1 on solid particles velocity with $E_1 = 0.5$, $E_2 = 1$, $A = 3$, $\lambda_2 = 2.5$, $B = 2.5$, $\epsilon = 0.03$, $E_3 = 0.5$, $\delta = 0.01$.

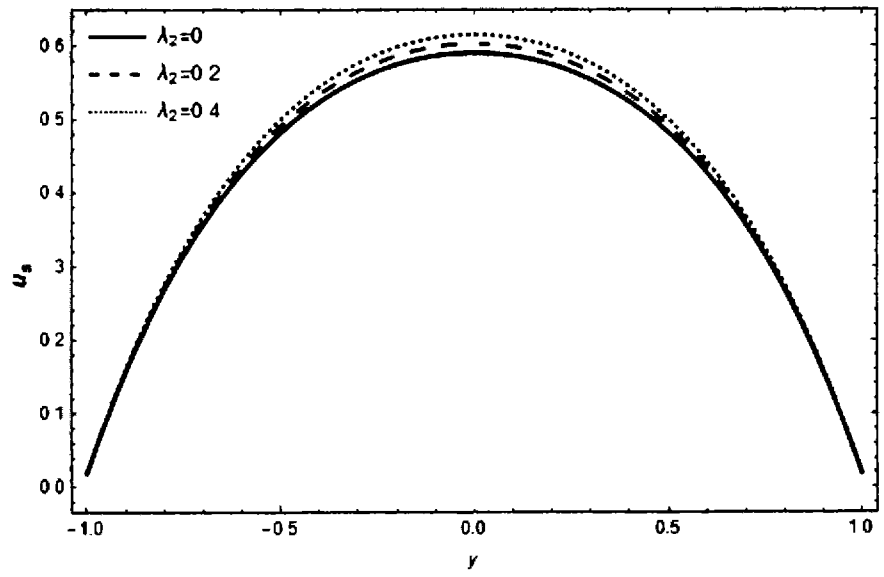

Figure 4.23: Depicts the significance of λ_2 on solid particles velocity with $E_1 = 1.5$, $E_2 = 1$, $A = 0.5$, $\lambda_1 = 0.5$, $\epsilon = 0.02$, $E_3 = 1$, $\delta = 0.01$, $B = 0.1$.

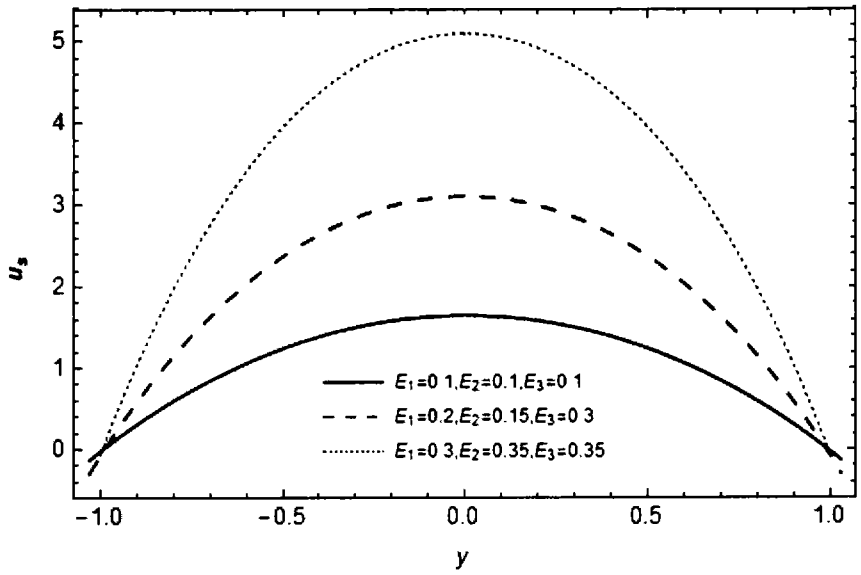

Figure 4.24: Depicts the significance of E_1, E_2 and E_3 on solid particles velocity with $A = 2$, $\lambda_2 = 1.5$, $B = 3$, $\lambda_1 = 2.5$, $\epsilon = 0.02$.

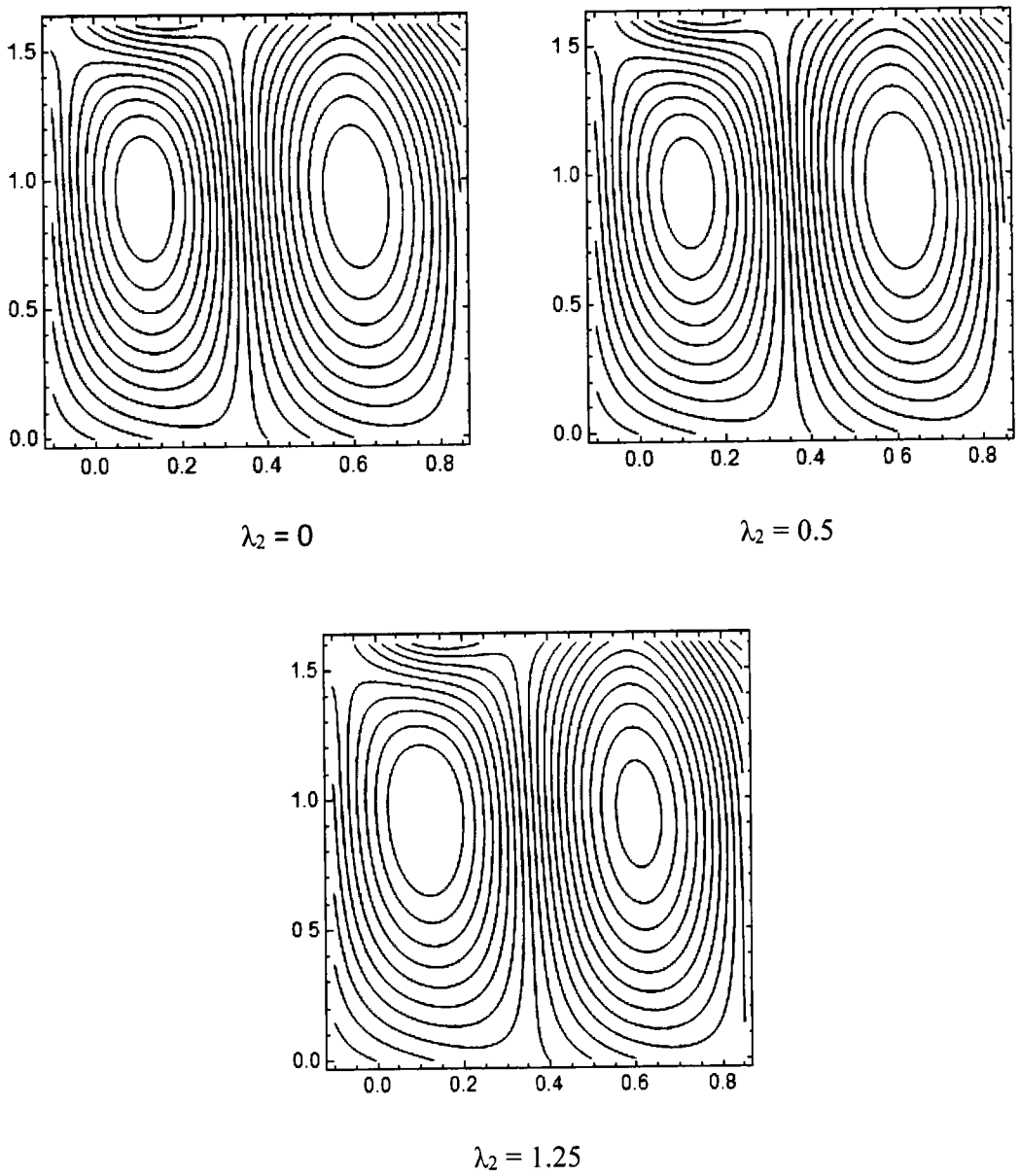

Figure 4.25: Depicts the significance of λ_2 on the solid particles streamline structures with $E_2 = 0.15$, $E_3 = 0.1$, $E_1 = 0.25$, $A = 1$, $\delta = 0.01$, $B = 2$, $\epsilon = 0.01$, $\lambda_1 = 1$.

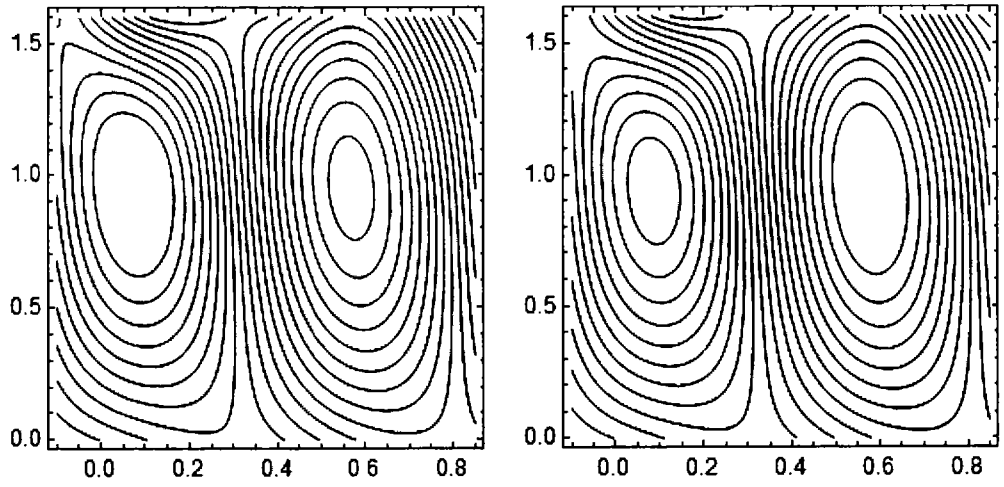

$\lambda_1 = 0$ $\lambda_2 = 0.5$

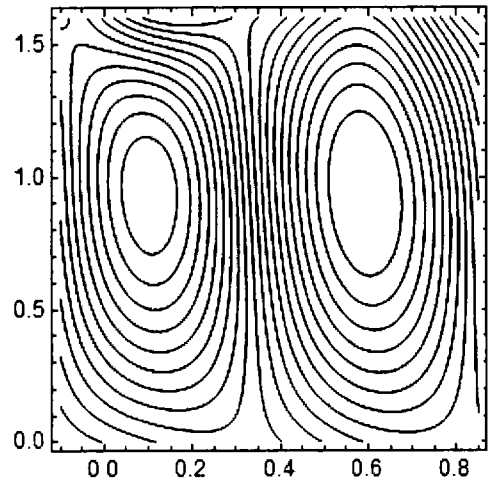

$\lambda_1 = 1.25$

Figure 4.26: Depicts the significance of λ_1 on the solid particles streamline structures with $E_2 = 0.15$, $B = 2$, $E_3 = 0.1$, $\epsilon = 0.01$, $A = 1$, $\delta = 0.01$, $\lambda_2 = 0.25$, $E_1 = 0.25$.

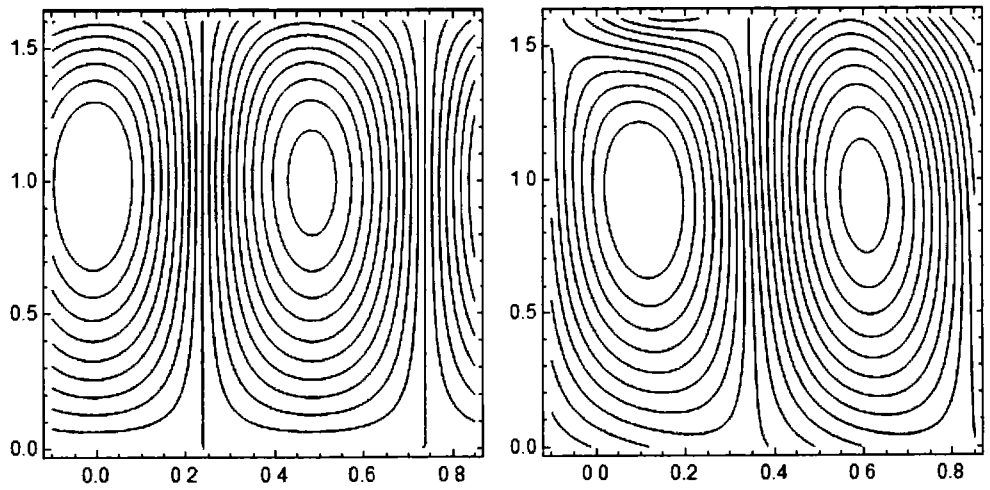

$\delta = 0$ $\delta = 0.01$

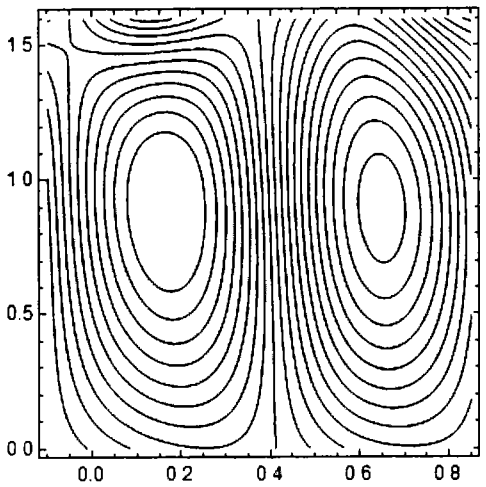

$\delta = 0.02$

Figure 4.27: Depicts the significance of δ on the solid particles streamline structures with $E_2 = 0.15$, $E_1 = 0.15$, $A = 1$, $B = 2$, $\epsilon = 0.01$, $\lambda_1 = 2$, $\lambda_2 = 1.5$, $E_3 = 0.15$.

4.5 Conclusion

In this chapter, Jeffrey fluid with the solid dust granules suspended in it have been studied under the impact of wall properties. The analytic solutions are calculated by

taking the wave number to be small. The outcomes are examined for distinct parameters. The key attributes of this study are

- As E_1, E_2 and E_3 are increasing, the solid particles velocity rises.
- The fluid flow rate increases while it decays for dust particles as the values of E_3, $\lambda_1$and λ_2 are increased.
- The fluid's velocity enhances as the values of λ_2 and δ are increased but in case of solid granules, velocity reduces for δ.
- The volume of the trapped bolus enhances on the left part for both solid and fluid as λ_2 is increased while it shrinks on the right part of the channel.
- In case of λ_1, the bolus expands at the right part of the passage while we observe that it contracts on the left side for both solid and fluid.
- For solid particles, the bolus is observed to be moving towards right part of the channel as the wave number is increased.

Chapter 5

Peristaltically Wavy Motion on Dusty Walter's B Fluid with Inclined Magnetic Field and Heat Transfer

This chapter includes the dynamics of Walter's B fluid conveying dust granules through an inclined asymmetric passage. An inclined magnetic field is imposed on the flowing fluid in order to investigate its consequences on the temperature, pressure rise and velocity. Stream functions transformation is applied to the derived equations of the dust granules and the fluid. Regular perturbation method has been carried out to interpret the non-linear equations. Graphical demonstration of various parameters is included to analyze the results.

5.1 Problem Formulation

Presuming that Walter's B fluid is incompressible and contains fine dust particles, whose number density is taken as a constant. A two-dimensional inclined asymmetric passage under the impact of constant magnetic field has been considered through which the solid particles are flowing. Both channel and magnetic field are inclined at angles γ and θ respectively. The temperature of the lower and upper walls is T_0 and T_1. The width of the channel is $d_1 + d_2$. The fluid is considered to be flowing along X-axis. Figure.5.1 depicts the geometry of the problem. The walls are described as below

$$H_1(\bar{X}, \bar{t}) = d_1 + a_1 sin\left[\frac{2\pi}{\lambda}(\bar{X} - c\bar{t})\right], \tag{5.1}$$

$$H_2(\bar{X},\bar{t}) = -d_2 - a_2 sin\left[\frac{2\pi}{\lambda}(\bar{X} - c\bar{t}) + \phi\right]. \tag{5.2}$$

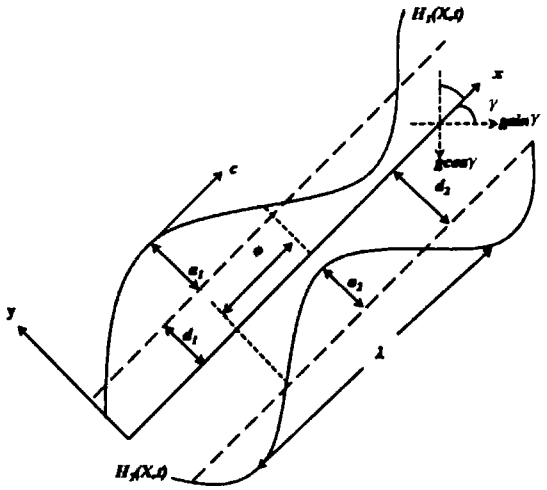

Figure. 5.1: Geometry of the channel.

The equations explaining the fluid flow are given

$$\rho\left[\frac{\partial \bar{U}}{\partial \bar{t}} + \bar{U}\frac{\partial \bar{U}}{\partial \bar{X}} + \bar{V}\frac{\partial \bar{U}}{\partial \bar{Y}}\right]$$

$$= -\frac{\partial \bar{P}}{\partial \bar{X}} + \frac{\partial \bar{S}_{\bar{X}\bar{X}}}{\partial \bar{X}} + \frac{\partial \bar{S}_{\bar{X}\bar{Y}}}{\partial \bar{Y}} + kN(\bar{U}_s - \bar{U}) + \rho g sin\gamma$$

$$- \sigma B_0^2 cos\theta(\bar{U}cos\theta - \bar{V}sin\theta), \tag{5.3}$$

$$\rho\left[\frac{\partial \bar{V}}{\partial \bar{t}} + \bar{U}\frac{\partial \bar{V}}{\partial \bar{X}} + \bar{V}\frac{\partial \bar{V}}{\partial \bar{Y}}\right] = -\frac{\partial \bar{P}}{\partial \bar{Y}} + \frac{\partial \bar{S}_{\bar{X}\bar{Y}}}{\partial \bar{X}} + \frac{\partial \bar{S}_{\bar{Y}\bar{Y}}}{\partial \bar{Y}} + kN(\bar{V}_s - \bar{V}) - \rho g cos\gamma$$

$$+\sigma B_0^2 sin\theta(\bar{U}cos\theta - \bar{V}sin\theta), \tag{5.4}$$

$$\rho\xi\left[\frac{\partial T}{\partial \bar{t}} + \bar{U}\frac{\partial T}{\partial \bar{X}} + \bar{V}\frac{\partial T}{\partial \bar{Y}}\right] = k^*\left(\frac{\partial^2 T}{\partial \bar{X}^2} + \frac{\partial^2 T}{\partial \bar{Y}^2}\right) + \bar{\Phi}. \tag{5.5}$$

The governing equations for the solid particles are described as

$$\frac{\partial \bar{U}_s}{\partial \bar{X}} + \frac{\partial \bar{V}_s}{\partial \bar{Y}} = 0, \tag{5.6}$$

$$\bar{U}_s \frac{\partial \bar{U}_s}{\partial \bar{X}} + \bar{V}_s \frac{\partial \bar{U}_s}{\partial \bar{Y}} = \frac{k}{m}(\bar{U} - \bar{U}_s), \tag{5.7}$$

$$\bar{U}_s \frac{\partial \bar{V}_s}{\partial \bar{X}} + \bar{V}_s \frac{\partial \bar{V}_s}{\partial \bar{Y}} = \frac{k}{m}(\bar{V} - \bar{V}_s). \tag{5.8}$$

The laboratory frame co-ordinates $(\bar{X}, \bar{Y})$ and the wave frame co-ordinates $(\bar{x}, \bar{y})$ are related by the transformations

$$\bar{p}(\bar{x}) = \bar{P}(\bar{X}, \bar{t}),\ \bar{y} = \bar{Y},\ \bar{x} = \bar{X} - c\bar{t},\ \bar{v} = \bar{V},\ \ \bar{u} = \bar{U} - c,\ \bar{u}_s = \bar{U}_s - c,\ \ \bar{v}_s = \bar{V}_s. \tag{5.9}$$

Initiating the following dimensionless quantities and stream functions

$$y = \frac{\bar{y}}{d_1},\quad E_r = \frac{c^2}{\xi(T_1 - T_0)},\quad x = \frac{\bar{x}}{\lambda},\quad v_s = \frac{\bar{v_s}}{c},\quad u = \frac{\bar{u}}{c},\quad \delta = \frac{d_1}{\lambda},$$

$$h = \frac{H}{d_1},\ p = \frac{d_1^2 \bar{p}}{c\lambda\alpha_0},\quad S = \frac{d_1 \bar{S}}{c\alpha_0},\quad Re = \frac{\rho c d_1}{\alpha_0},$$

$$M^2 = \frac{\sigma B_0^2 d_1}{\alpha_0},\quad F_r = \frac{c^2}{g d_1},\quad t = \frac{c\bar{t}}{\lambda},\quad P_r = \frac{\xi\alpha_0}{k^*},\quad u_s = \frac{\bar{u}_s}{c},$$

$$\mho = \frac{T - T_0}{T_1 - T_0},\quad v = \frac{\bar{v}}{c},\quad \Phi = \frac{d_1^2}{\alpha_0 c^2}\bar{\Phi},\quad u = \frac{\partial \psi}{\partial y}, u_s = \frac{\partial \varphi}{\partial y},$$

$$v = -\delta\frac{\partial \psi}{\partial x},\quad v_s = -\delta\frac{\partial \varphi}{\partial x}. \tag{5.10}$$

The ruling equations thus become after using these quantities as:

For fluid flow

$$Re\delta\left[\frac{\partial^2\psi}{\partial x \partial y}\frac{\partial \psi}{\partial y} - \frac{\partial \psi}{\partial x}\frac{\partial^2 \psi}{\partial y^2}\right]$$

$$= -\frac{\partial p}{\partial x} + \frac{\partial S_{xy}}{\partial y} + \delta\frac{\partial S_{xx}}{\partial x} + A\left(\frac{\partial \varphi}{\partial y} - \frac{\partial \psi}{\partial y}\right)$$

$$-M^2 cos\theta\left(\left(\frac{\partial\psi}{\partial y}+1\right)cos\theta+\delta\frac{\partial\psi}{\partial x}sin\theta\right)$$

$$+\frac{Re}{F_r}\,sin\gamma, \quad (5.11)$$

$$-Re\delta^3\left[\frac{\partial^2\psi}{\partial x^2}\frac{\partial\psi}{\partial y}-\frac{\partial\psi}{\partial x}\frac{\partial^2\psi}{\partial x\partial y}\right]$$

$$=-\frac{\partial p}{\partial y}+\delta^2\frac{\partial S_{xy}}{\partial x}+\delta\frac{\partial S_{yy}}{\partial y}+A\delta^2\left(\frac{\partial\psi}{\partial x}-\frac{\partial\varphi}{\partial x}\right)$$

$$+\delta M^2 sin\theta\left(\left(\frac{\partial\psi}{\partial y}+1\right)cos\theta+\delta\frac{\partial\psi}{\partial x}sin\theta\right)$$

$$-\frac{Re}{F_r}\delta\,cos\gamma, \quad (5.12)$$

$$\delta Re\left[\frac{\partial\mho}{\partial x}\frac{\partial\psi}{\partial y}-\frac{\partial\mho}{\partial y}\frac{\partial\psi}{\partial y}\right]=\frac{1}{P_r}\left[\delta^2\frac{\partial^2\mho}{\partial x^2}+\frac{\partial^2\mho}{\partial y^2}\right]+E_r\Phi, \quad (5.13)$$

$$\frac{\partial\varphi}{\partial y}\frac{\partial^2\varphi}{\partial x\partial y}-\delta\frac{\partial\varphi}{\partial x}\frac{\partial^2\varphi}{\partial y^2}=\frac{k}{m}\left(\frac{\partial\psi}{\partial y}-\frac{\partial\varphi}{\partial y}\right), \quad (5.14)$$

$$-\frac{\partial\varphi}{\partial y}\frac{\partial^2\varphi}{\partial x^2}+\delta\frac{\partial\varphi}{\partial x}\frac{\partial^2\varphi}{\partial x\partial y}=\frac{k}{m}\left(\frac{\partial\varphi}{\partial x}-\frac{\partial\psi}{\partial x}\right). \quad (5.15)$$

The compatibility equations for the fluid and solid particles is

$$\delta\,Re\left[\frac{\partial\psi}{\partial y}\frac{\partial}{\partial x}(\nabla_1^2\psi)-\frac{\partial\psi}{\partial x}\frac{\partial}{\partial y}(\nabla_1^2\psi)\right]$$

$$=\left(\frac{\partial^2}{\partial y^2}-\delta^2\frac{\partial^2}{\partial x^2}\right)S_{xy}+\delta\left(\frac{\partial^2}{\partial x\partial y}\{S_{xx}-S_{yy}\}\right)$$

$$-M^2\cos^2\theta\left(\frac{\partial^2\psi}{\partial\,y^2}\right)-2\delta M^2 sin\theta cos\theta\frac{\partial^2\psi}{\partial x\partial y}$$

$$-M^2\sin^2\theta\delta^2\left(\frac{\partial^2\psi}{\partial x^2}\right), \quad (5.16)$$

$$\delta\left(\frac{\partial\varphi}{\partial y}\frac{\partial}{\partial x}\nabla_1^2\varphi-\frac{\partial\varphi}{\partial x}\frac{\partial}{\partial y}\nabla_1^2\varphi\right)=B(\nabla_1^2\psi-\nabla_1^2\varphi). \tag{5.17}$$

The components of the extra stress tensor for the Walter's B fluid and Φ become

$$S_{xx}=4\,\delta\frac{\partial^2\psi}{\partial x\partial y}$$
$$-\kappa\left[4\,\delta^2\left(\frac{\partial^2\psi}{\partial y^2}\right)\left(\frac{\partial^2\psi}{\partial x^2}\right)+4\delta^2\frac{\partial\psi}{\partial y}\frac{\partial^3\psi}{\partial x^2\partial y}-8\delta^2\left(\frac{\partial^2\psi}{\partial y\partial x}\right)^2\right.$$
$$\left.-4\delta^4\left(\frac{\partial^2\psi}{\partial x^2}\right)^2-4\delta^2\frac{\partial\psi}{\partial y^2\partial x}\right], \tag{5.18}$$

$$S_{xy}=2\left[\frac{\partial^2\psi}{\partial y^2}-\delta^2\frac{\partial^2\psi}{\partial x^2}\right]$$
$$-\kappa\left[2\delta\frac{\partial\psi}{\partial y}\frac{\partial^3\psi}{\partial y^2\partial x}+2\delta^3\frac{\partial\psi}{\partial x}\frac{\partial^3\psi}{\partial x^2\partial y}-2\delta\frac{\partial^3\psi}{\partial y^3}\frac{\partial\psi}{\partial x}-4\delta\frac{\partial^2\psi}{\partial x\partial y}\frac{\partial^2\psi}{\partial y^2}\right.$$
$$-4\delta^3\frac{\partial^2\psi}{\partial x\partial y}\frac{\partial^2\psi}{\partial x^2}$$
$$\left.-2\delta^3\frac{\partial^3\psi}{\partial x^3}\frac{\partial\psi}{\partial y}\right], \tag{5.19}$$

$$S_{yy}$$
$$=-4\delta\frac{\partial^2\psi}{\partial x\partial y}$$
$$-\kappa\left[4\delta^2\frac{\partial\psi}{\partial x}\frac{\partial^3\psi}{\partial y^2\partial x}+4\delta^2\frac{\partial^2\psi}{\partial x^2}\frac{\partial^2\psi}{\partial y^2}-4\delta^2\frac{\partial\psi}{\partial y}\frac{\partial^2\psi}{\partial x^2\partial y}-8\delta^2\left(\frac{\partial^2\psi}{\partial y\partial x}\right)^2\right.$$
$$\left.-4\left(\frac{\partial^2\psi}{\partial y^2}\right)^2\right], \tag{5.20}$$

5.3 Method of Solution

Perturbation technique has been adopted to get the solution of the problem. Assuming the series given as

$$\psi = \psi_0 + \delta\psi_1 + \delta^2\psi_2 + O(\delta^3), \tag{5.26}$$

$$\varphi = \varphi_0 + \delta\varphi_1 + \delta^2\varphi_2 + O(\delta^3), \tag{5.27}$$

$$F = F_0 + \delta F_1 + \delta^2 F_2 + O(\delta^3), \tag{5.28}$$

$$E = E_0 + \delta E_1 + \delta^2 E_2 + O(\delta^3), \tag{5.29}$$

$$\mho = \mho_0 + \delta\mho_1 + O(\delta^2), \tag{5.30}$$

$$p = p_0 + \delta p_1 + O(\delta^2). \tag{5.31}$$

5.3.1 Zeroth-Order System

$$\frac{\partial^2}{\partial y^2}S_{0xy} + A\left[\frac{\partial^2\varphi_0}{\partial y^2} - \frac{\partial^2\psi_0}{\partial y^2}\right] - M^2\cos^2\theta\frac{\partial^2\psi_0}{\partial y^2} = 0. \tag{5.32}$$

$$B\left(\frac{\partial^2\psi_0}{\partial y^2} - \frac{\partial^2\varphi_0}{\partial y^2}\right) = 0, \tag{5.33}$$

$$\frac{1}{P_r}\frac{\partial^2\mho_0}{\partial y^2} + E_r\Phi_0 = 0, \tag{5.34}$$

$$\frac{dP_0}{dx} = \frac{\partial}{\partial y}S_{0xy} + A\left[\frac{\partial\phi_0}{\partial y} - \frac{\partial\psi_0}{\partial y}\right] - M^2\cos^2\theta\left(\frac{\partial\psi_0}{\partial y} + 1\right) + \frac{Re}{F_r}sin\gamma, \tag{5.35}$$

where

$$S_{0xy} = 2\frac{\partial^2\psi_0}{\partial y^2}, \qquad \Phi_0 = 2\left(\frac{\partial^2\psi_0}{\partial y^2}\right)^2, \tag{5.36}$$

along with the boundary conditions

$$\psi_0 = \frac{F_0}{2}, \quad \frac{\partial \psi_0}{\partial y} = -1, \quad \varphi_0 = \frac{E_0}{2}, \quad \mho_0 = 0 \quad at \quad y = h_1(x), \quad (5.37)$$

$$\psi_0 = -\frac{F_0}{2}, \quad \frac{\partial \psi_0}{\partial y} = -1, \quad \varphi_0 = -\frac{E_0}{2}, \quad \mho_0 = 1 \quad at\ y = h_2(x). \quad (5.38)$$

5.3.2 First-Order System

$$Re\left[\frac{\partial \psi_0}{\partial y}\frac{\partial}{\partial x}\left(\frac{\partial^2 \psi_0}{\partial y^2}\right) - \frac{\partial \psi_0}{\partial x}\frac{\partial}{\partial y}\left(\frac{\partial^2 \psi_0}{\partial y^2}\right)\right]$$

$$= \frac{\partial^2}{\partial y^2} S_{1xy} + \frac{\partial^2}{\partial x \partial y}\left(S_{0xx} - S_{0yy}\right) + A\left[\frac{\partial^2 \varphi_1}{\partial y^2} - \frac{\partial^2 \psi_1}{\partial y^2}\right]$$

$$- M^2 \cos^2\theta \frac{\partial^2 \psi_1}{\partial y^2} - 2M^2 \cos\theta \sin\theta \frac{\partial^2 \psi_0}{\partial x \partial y}. \quad (5.39)$$

$$B\left(\frac{\partial^2 \psi_1}{\partial y^2} - \frac{\partial^2 \varphi_1}{\partial y^2}\right) = \frac{\partial \varphi_0}{\partial y}\frac{\partial^3 \varphi_0}{\partial x \partial y^2} - \frac{\partial \varphi_0}{\partial x}\frac{\partial^3 \varphi_0}{\partial y^3}, \quad (5.40)$$

$$Re\left[\frac{\partial \mho_0}{\partial x}\frac{\partial \psi_0}{\partial y} - \frac{\partial \mho_0}{\partial y}\frac{\partial \psi_0}{\partial x}\right] = \frac{1}{P_r}\frac{\partial^2 \mho_1}{\partial y^2} + E_r \Phi_1, \quad (5.41)$$

$$\frac{dP_1}{dx} = \frac{\partial}{\partial x} S_{0xx} + \frac{\partial}{\partial y} S_{1xy} + A\left[\frac{\partial \phi_1}{\partial y} - \frac{\partial \psi_1}{\partial y}\right]$$

$$- M^2 \cos^2\theta \frac{\partial \psi_1}{\partial y} - M^2 sin\theta cos\theta \frac{\partial \psi_0}{\partial x}$$

$$- Re\left[\frac{\partial \psi_0}{\partial y}\frac{\partial^2 \psi_0}{\partial y \partial x} - \frac{\partial \psi_0}{\partial x}\frac{\partial^2 \psi_0}{\partial y^2}\right], \quad (5.42)$$

where

$$S_{0xx} = 0, \quad (5.43)$$

$$S_{0yy} = 4\kappa\left(\frac{\partial^2 \psi_0}{\partial y^2}\right)^2, \quad (5.44)$$

$$S_{1xy} = 2\left(\frac{\partial^2\psi_1}{\partial y^2}\right) - \kappa\left(-2\frac{\partial^3\psi_0}{\partial y^3}\frac{\partial\psi_0}{\partial x} - 4\frac{\partial^2\psi_0}{\partial x\partial y}\frac{\partial^2\psi_0}{\partial y^2} + 2\frac{\partial\psi_0}{\partial y}\frac{\partial^3\psi_0}{\partial x\partial y^2}\right), \quad (5.45)$$

$$\Phi_1 = 4\frac{\partial^2\psi_0}{\partial y^2}\left(\frac{\partial^2\psi_1}{\partial y^2}\right)^2 + 2\kappa\left[\frac{\partial^2\psi_0}{\partial y^2}\frac{\partial^3\psi_0}{\partial y^3}\frac{\partial\psi_0}{\partial x} - \frac{\partial^2\psi_0}{\partial y^2}\frac{\partial\psi_0}{\partial y}\frac{\partial^3\psi_0}{\partial y^2\partial x}\right]$$
$$+ 6\kappa\left[\frac{\partial^2\psi_0}{\partial x\partial y}\left(\frac{\partial^2\psi_0}{\partial y^2}\right)^2 - \frac{\partial^2\psi_0}{\partial y\partial x}\frac{\partial^2\psi_0}{\partial y^2}\right], \quad (5.46)$$

along with the boundary conditions

$$\psi_1 = \frac{F_1}{2}, \quad \frac{\partial\psi_1}{\partial y} = 0, \quad \varphi_1 = \frac{E_1}{2}, \quad \mho_1 = 0 \quad at \quad y = h_1(x), \quad (5.47)$$

$$\psi_1 = -\frac{F_1}{2}, \quad \frac{\partial\psi_1}{\partial y} = 0, \varphi_1 = -\frac{E_1}{2}, \quad \mho_1 = 0 \quad at \quad y = h_2(x). \quad (5.48)$$

The solution of these system of equations are calculated by using DSolver in Mathematica. The results are demonstrated through graphs.

5.4 Results and Discussion

The graphical demonstration of many constraints on the velocity profile of the fluid, pressure rise and temperature are deliberated in this section. Figs. 5.2 – 5.7 are the graphical presentation of the velocity of the dust particles and the fluid under the consequences of different parameters. Figs. 5.8 – 5.13 are graphs plotted to study the impact of miscellaneous attributes on the pressure rise. Figs. 5.14 – 5.17 are the temperature profile of the fluid under the effect of different parameters.

Fig. 5.2 shows the velocity of the dusty Walter's B fluid for various values of the magnetic field *(M)*. Magnetic force is a resistive force and causes resistance in the flow of the fluid. It can be concluded that M is affecting the fluid's velocity and the velocity is declining as the values of M are increased. The increase in Reynolds

number *(Re)* is rising effect on the velocity of the dusty Walter's B fluid. Fig. 5.3 shows that as the *Re* is increased, slight growth in the velocity of the fluid can be spotted. As rise in the Reynolds number can be associated with lessening of viscosity thus resulting growth in the velocity. The viscosity (κ) reduces the fluid's velocity. Fig. 5.4 clearly illustrates the property of viscosity on the velocity of the fluid. As the viscosity κ is increased, the velocity of the fluid starts decaying. The wave number is given by (δ). As the wave number is enhanced, we observe decrease in the velocity of the fluid as shown in Fig.5.5. Fig. 5.6 reveals that the rise in the viscosity parameter κ, slower down the velocity of the dust grains. Due to the drag co-efficient and the size of the particles as the magnetic field grows, a significant decreasing effect in the solid particle's velocity can be spotted in Fig. 5.7.

The effect of the magnetic field *(M)* on the pressure rise is illustrated in Fig. 5.8. This figure reveals that pressure rise increases in the retrograde region ($\Delta P > 0$) as increase in the magnetic effect slower downs the velocity of the fluid thus more pressure would be required to pump the fluid while in the co-pumping region ($\Delta P < 0$) we can observe a reverse situation. Fig. 5.9 displays the impact of the viscoelastic parameter κ on the pressure rise. It can be concluded from the figure that more pressure would be required to pump the fluid as its viscosity is increased. It can be perceived from Fig. 5.10, that with the rise in Froude number F_r, the pressure rate decreases throughout the region. Increase in Froude number is directly proportional to the speed of the fluid thus less pressure would be required to pump the fluid as it speeds up. The impact of the inclination of the passage on the pressure rise is illustrated in Fig. 5.11. As the inclination of the passage i.e. γ is increased, the rate of pumping rises throughout the region. The increase in wave number δ rises the pressure rate in the

retrograde region as demonstrated in Fig. 5.12. The pressure rises thoroughly in the region as displayed in Fig. 5.13, as the Reynolds number *(Re)* is increased.

Fig. 5.14 shows that as the Prandtl number P_r is increased, the fluid's temperature declines. With rise in Prandtl number the process of heat diffusion slower down thus the temperature declines. The influence of the inclination of the magnetic field θ on the temperature of the fluid is shown in Fig. 5.15. We observe that as the inclination of the magnetic field rises, the temperature of the fluid rises too. Fig. 5.16 exhibits that enhance in the values of M increases the temperature of the dusty Walter's B fluid. As the impact of magnetic field enhances, the velocity of the fluid weakens thus resulting in the rise in temperature. With the increase in Eckert number E_r, the temperature rise can be observed in Fig. 5.17.

5.5 Graphs

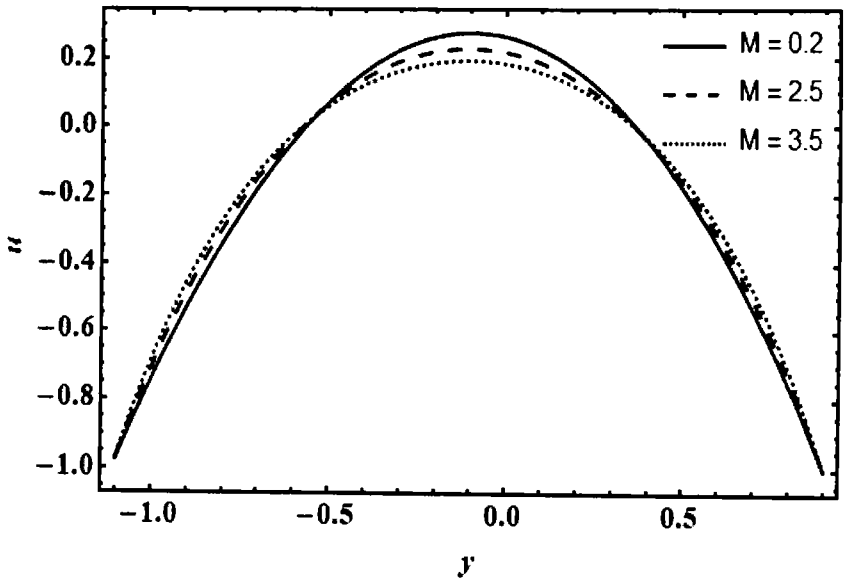

Figure 5.2: Impact of M on velocity of the fluid with $Q = 2$, $Q_s = 2$, $\phi = 0.3$, $b = 0.2$, $A = 0.1$, $Re = 5$, $d = 1.3$, $\delta = 0.2$, $\kappa = 0.1$, $\theta = \pi/6$, $a = 0.1$, $B = 1$.

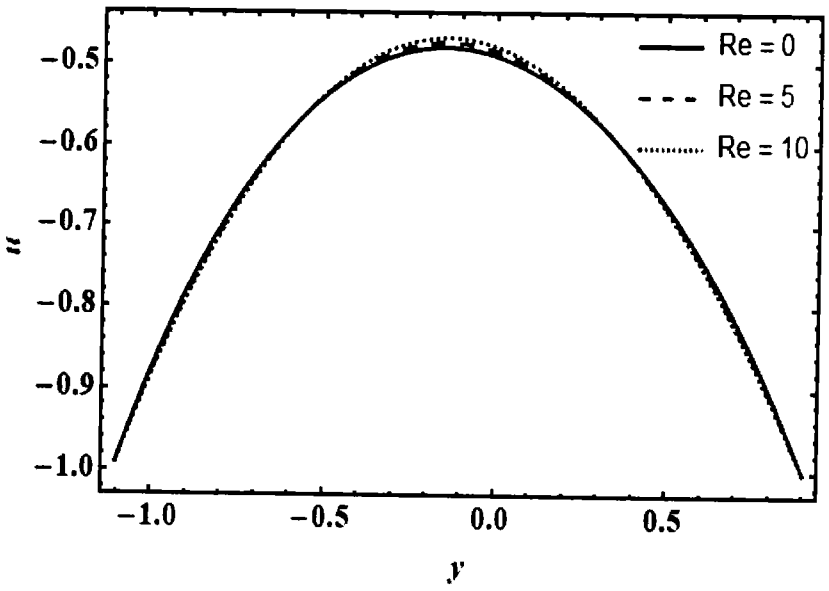

Figure 5.3: Impact of Re on velocity of the fluid with $Q = 1$, $Q_s = 1$, $\phi = 0.3$, $b = 0.2$, $A = 0.1$, $d = 1.3$, $B = 1$, $M = 1.5$, $\delta = 2$, $\kappa = 0.1$, $\theta = \pi/10$, $a = 0.1$.

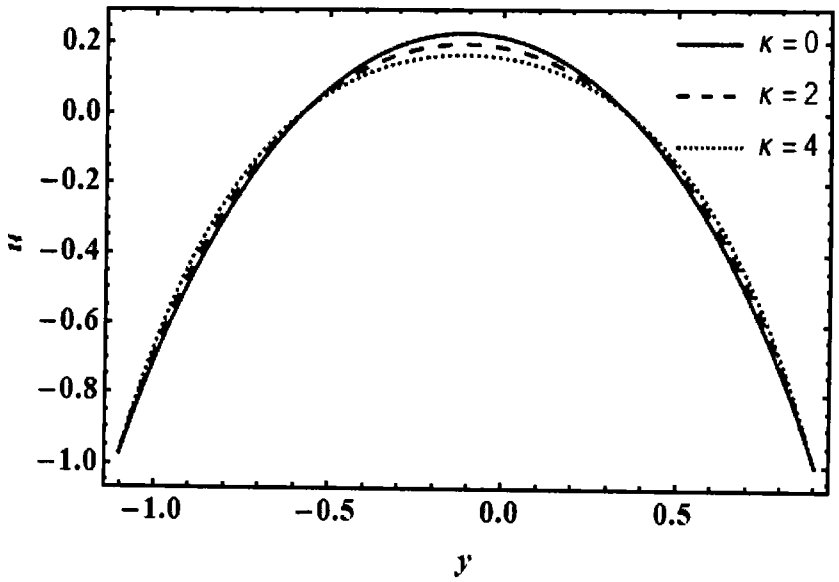

Figure 5.4: Impact of κ on velocity of the fluid with $Q = 2$, $Q_s = 2$, $\phi = 0.3$, $b = 0.2$, $A = 0.1$, $d = 1.3$, $B = 1$, $Re = 5$, $\delta = 0.2$, $M = 1.5$, $\theta = \pi/6$, $a = 0.1$.

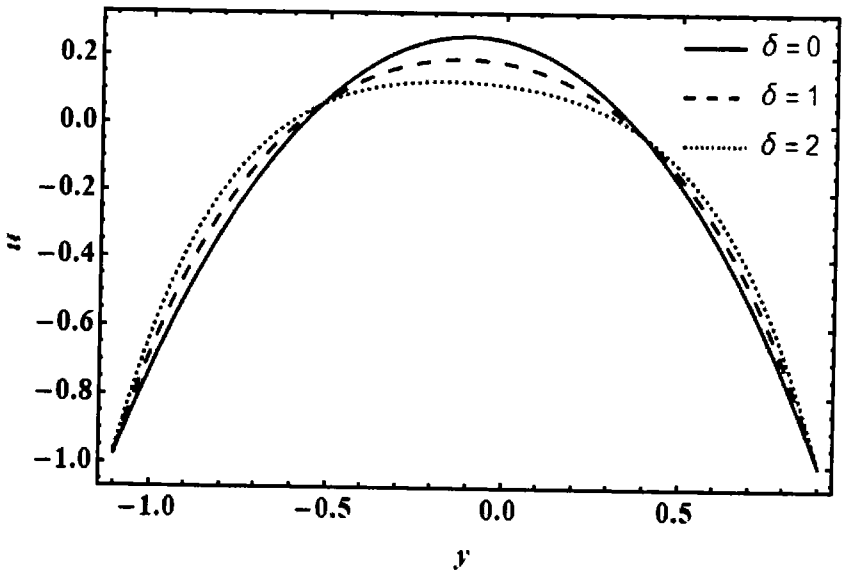

Figure 5.5: Impact of δ on velocity of the fluid with $Q = 2$, $Q_s = 2$, $\phi = 0.3$, $b = 0.2$ $A = 0.1$, $d = 1.3$, $B = 1$, $Re = 5$, $\kappa = 1$, $M = 1.5$, $\theta = \pi/6$, $a = 0.1$.

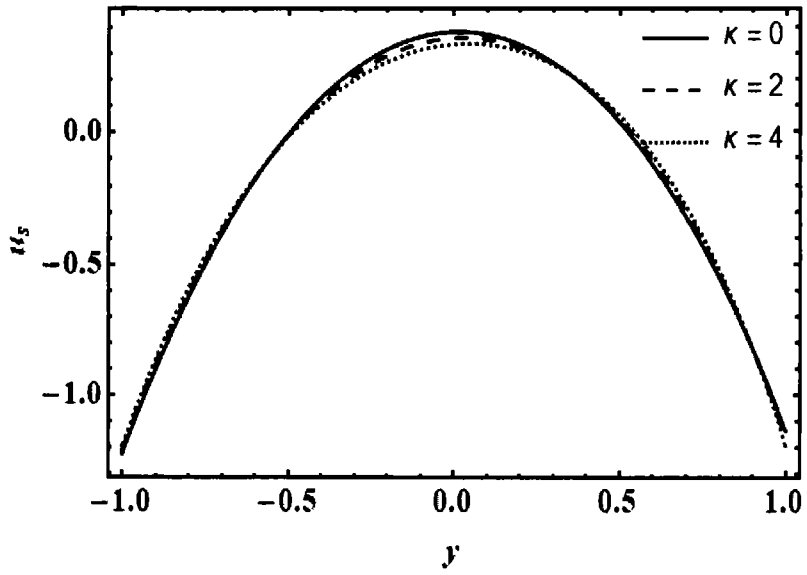

Figure 5.6: Impact of κ on velocity of the solid particles with $Q = 2$, $Q_s = 2$, $\phi = 0.3$, $b = 0.2$, $A = 0.1$, $B = 1$, $Re = 5$, $d = 1.3$, $\delta = 0.2$, $M = 1.5$, $\theta = \pi/6$, $a = 0.1$.

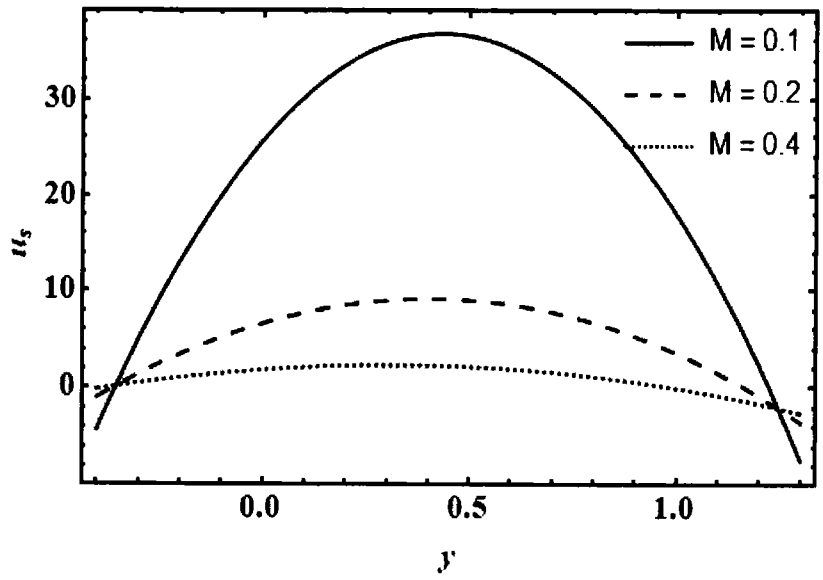

Figure 5.7: Impact of M on velocity of the solid particles with $Q = 2$, $Q_s = 2$, $\phi = 0.3$, $b = 0.2$, $A = 0.1$, $d = 1.3$, $B = 1$, $Re = 5$, $\delta = 0.2$, $M = 1.5$, $\theta = \pi/6$, $a = 0.1$.

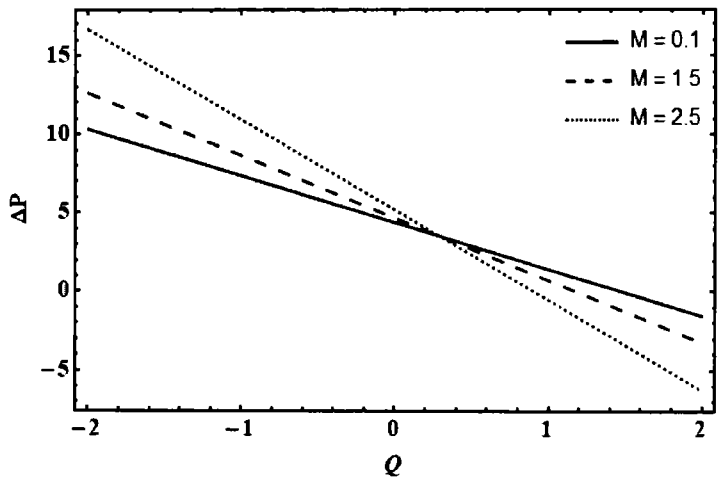

Figure 5.8: Impact of M on ΔP with $\phi = 0.3$, $b = 0.2$, $A = 0.1$, $B = 1$, $Re = 5$, $\delta = 0.01$, $\kappa = 0.2$, $\theta = \pi/6$, $a = 0.1$, $\gamma = \frac{\pi}{4}$, $F_\gamma = 1$, $d = 1.3$.

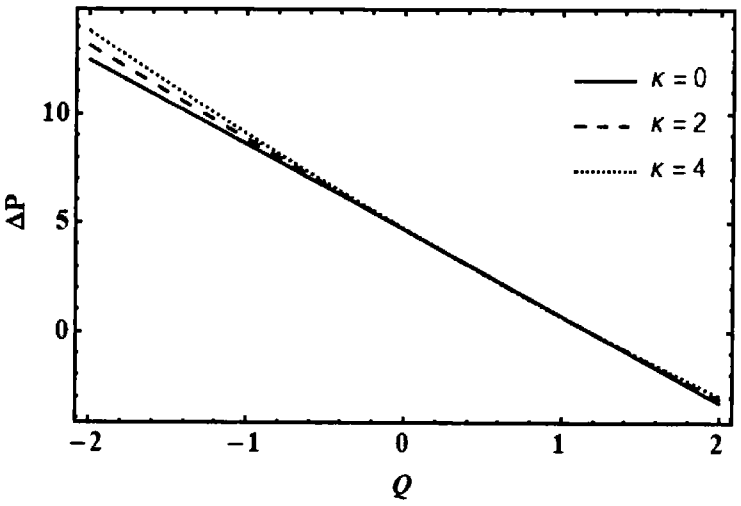

Figure 5.9: Impact of κ on ΔP with $\phi = 0.3$, $b = 0.2$, $A = 0.1$, $B = 1$, $M = 1.5$, $\delta = 0.01$, $\kappa = 0.1$, $Re = 5$, $\theta = \pi/10$, $a = 0.1$, $\gamma = \frac{\pi}{4}$, $F_\gamma = 1$, $d = 1.3$.

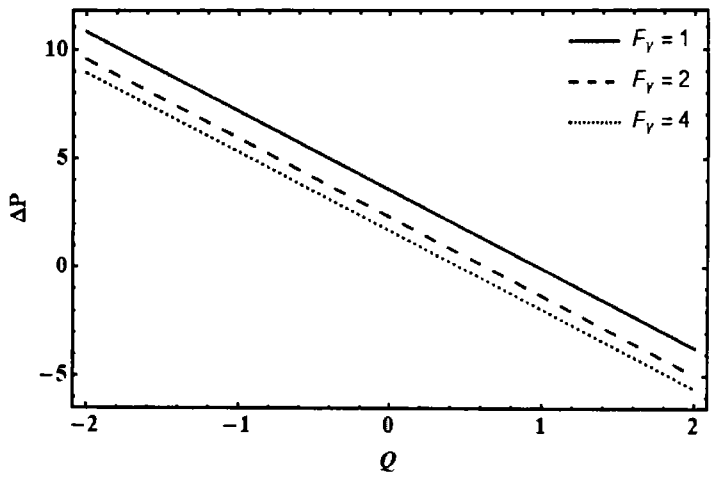

Figure 5.10: Impact of F_γ on ΔP with $\phi = 0.3$, $b = 0.2$, $A = 0.1$, $B = 1$, $Re = 5$, $\delta = 0.05$, $M = 1.5$, $\kappa = 0.5$, $\theta = \pi/6$, $a = 0.1$, $\gamma = \frac{\pi}{6}$, $d = 1.3$.

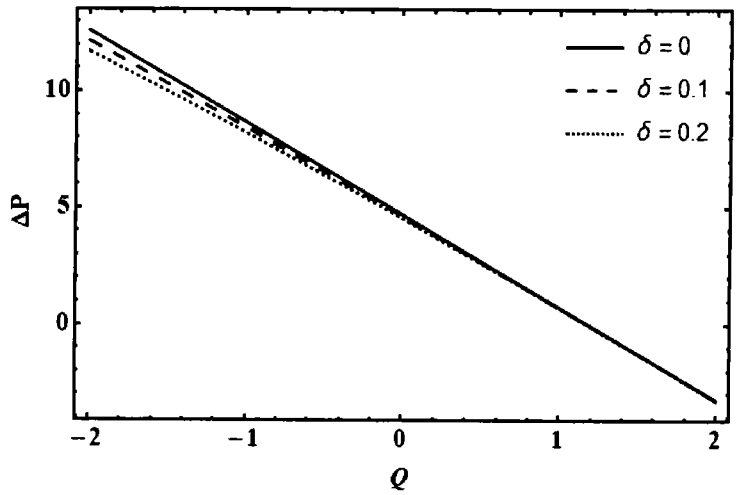

Figure 5.11: Impact of δ on ΔP with $\phi = 0.3$, $b = 0.2$, $A = 0.1$, $B = 1$, $Re = 5$, $a = 0.1$, $\kappa = 0.2$, $\theta = \pi/6$, $M = 1.5$, $\gamma = \frac{\pi}{4}$, $F_\gamma = 1$, $d = 1.3$.

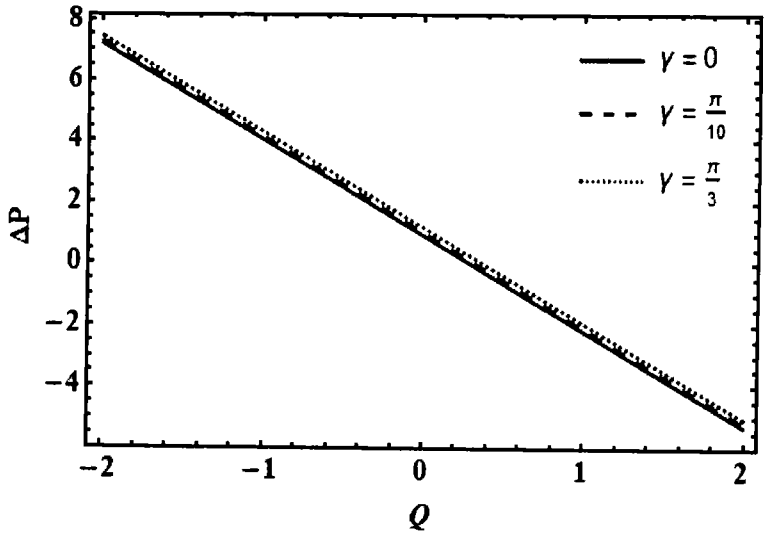

Figure 5.12: Impact of γ on ΔP with $\phi = 0.3$, $b = 0.2$, $A = 0.1$, $B = 1$, $Re = 5$, $\delta = 0.01$, $\kappa = 0.2$, $\theta = \pi/6$, $a = 0.1$, $M = 0.5$, $F_\gamma = 1$, $d = 1.3$.

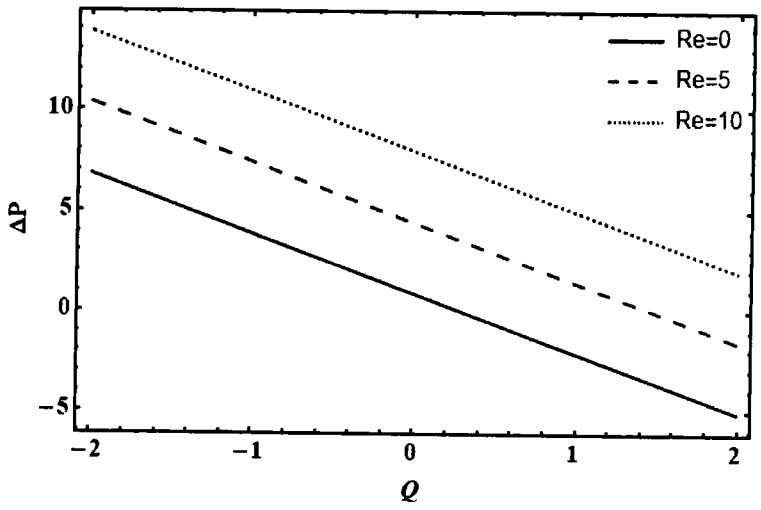

Figure 5.13: Impact of *Re* on ΔP with $\phi = 0.3$, $b = 0.2$, $A = 0.1$, $B = 1$, $M = 0.15$, $\delta = 0.01$, $\kappa = 0.2$, $\theta = \pi/6$, $a = 0.1$, $\gamma = \frac{\pi}{4}$, $F_\gamma = 1$, $d = 1.3$.

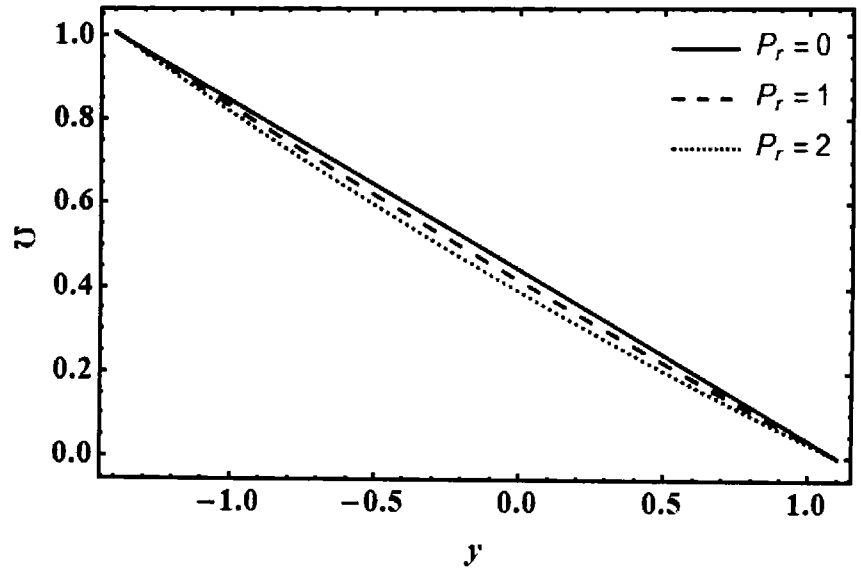

Figure 5.14: Impact of P_r on $\mho$ with $d = 1$, $Q = 2$, $Q_s = 2$, $\phi = 0.3$, $A = 0.1$, $B = 1$, $Re = 5$,$\kappa = 0.5$, $\delta = 0.1$, $M = 0.5$, $\theta = \pi/6$, $a = 0.1$, $E_c = 2.5$, $b = 0.4$.

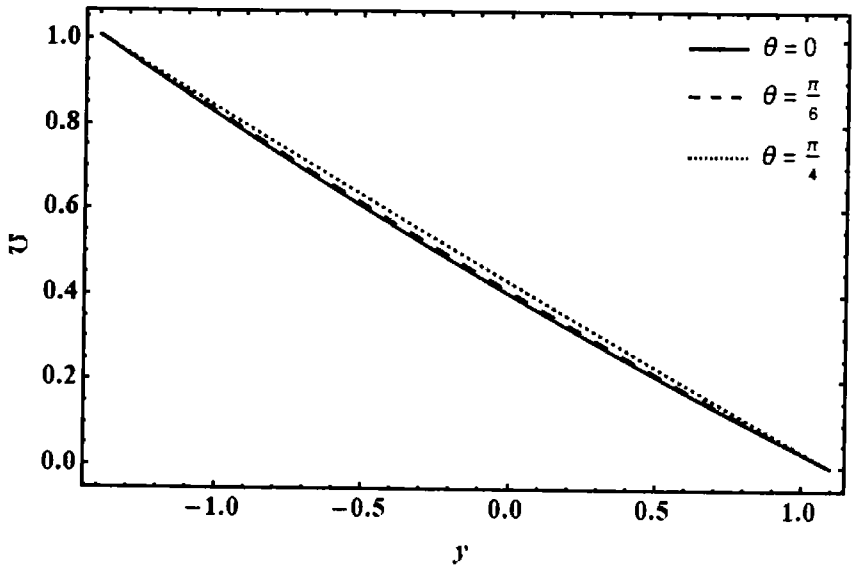

Figure 5.15: Impact of θ on $\mho$ with $d = 1$, $Q = 2$, $Q_s = 2$, $\phi = 0.3$, $A = 0.1$, $B = 1$, $Re = 5$, $\kappa = 0.5$, $\delta = 0.1$, $M = 0.5$, $P_r = 1.5$, $a = 0.1$, $E_c = 1.5$, $b = 0.4$.

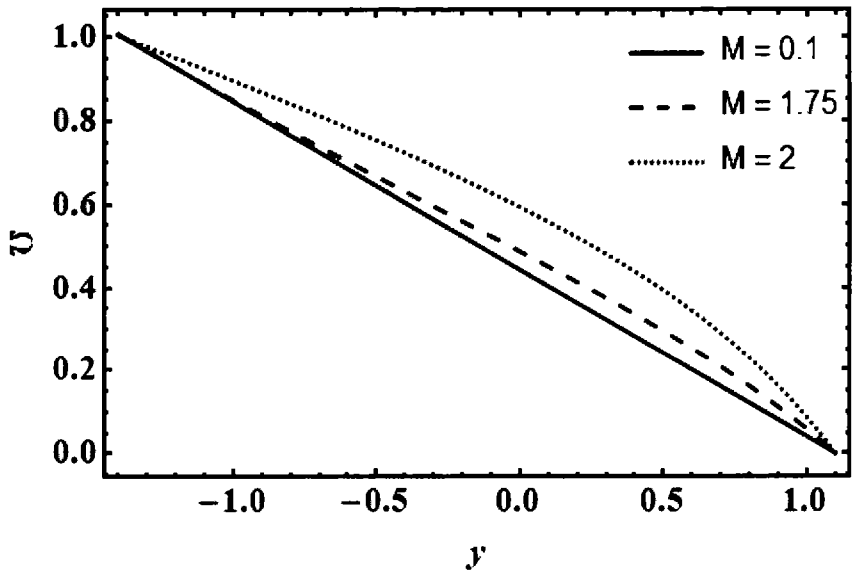

Figure 5.16: Impact of M on $\mho$ with $Q = 2$, $Q_s = 2$, $\phi = 0.3$, $b = 0.4$, $d = 1$, $A = 0.1$, $B = 1$, $Re = 5$, $\kappa = 0.5$, $\delta = 0.1$, $P_r = 1.25$, $\theta = \pi/6$, $a = 0.1$, $E_c = 0.5$.

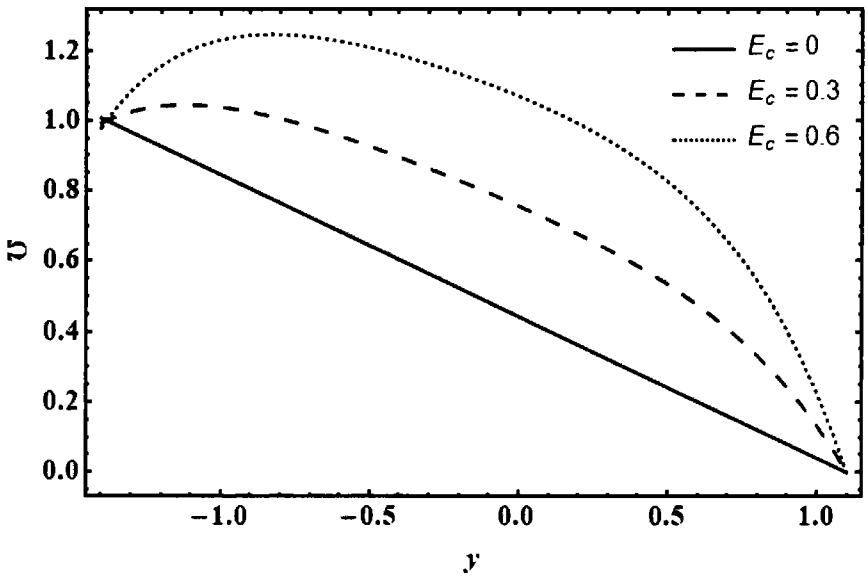

Figure 5.17: Impact of E_c on $\mho$ with $Q = 2$, $Q_s = 2$, $d = 1$, $b = 0.4$, $A = 0.1$, $B = 1$, $Re = 5$, $\kappa = 0.5$, $\delta = 0.5$, $P_r = 1$, $\theta = \pi/6$, $a = 0.1$, $M = 2.5$, $\phi = 0.3$.

5.6 Conclusion

This chapter is about Walter's B dusty fluid revealing the peristaltic motion in an inclined asymmetric passage. An inclined magnetic field is imposed to the fluid flow to examine the impact of various attributes. We concluded the following major results.

- The fluid velocity decays due to rise in the magnetic field while a reverse situation was observed as we increased the values of Reynolds number.
- By raising the viscoelastic parameter and the wave number, the fluid velocity decreases.
- The velocity of the solid granules declines with the rise in magnetic field and viscoelastic parameter.
- The pumping rate increases as M, Re, κ and δ are increased, while it decreases through all the region as Froude number F_r is increased.
- The temperature $\mho$ lowers down as P_r are increased while it enhances with the increase in M, E_c and θ.

Chapter 6

Peristaltic Transport of a Second-Grade Dusty Fluid in a Tube

This chapter intents to analyze the behavior of second-grade dusty fluid flowing through a flexible tube whose walls are induced by the peristaltic movement. Coupled equations for the fluid and solid particles have been modelled by considering small wave number approximation. Regular perturbation technique has been implemented to get the solutions and the outcomes are demonstrated through graphs. The impact of diverse parameters on the contour presentations and on the velocity of the solid grains and fluid have been illustrated.

6.1 Problem Formulation

Taking the axisymmetric flow of a second-grade fluid which contain small spherical particles in a tube of radius a. These particles are even in size. Therefore, the number density N of the solid granules are presumed to be constant. The walls of the tube are propagating with constant speed c. We select the cylindrical coordinate structure $(\bar{R}, \bar{Z})$. In the radial and axial directions, the velocity components are taken as $\bar{U}$, $\bar{W}$ for fluid and $\bar{U}_s$ and $\bar{W}_s$ for dust particles.

The wall of the tube is given as

$$\bar{R}(\bar{Z}, \bar{t}) = a + b \sin \frac{2\pi}{\lambda}(\bar{Z} - c\bar{t}). \tag{6.1}$$

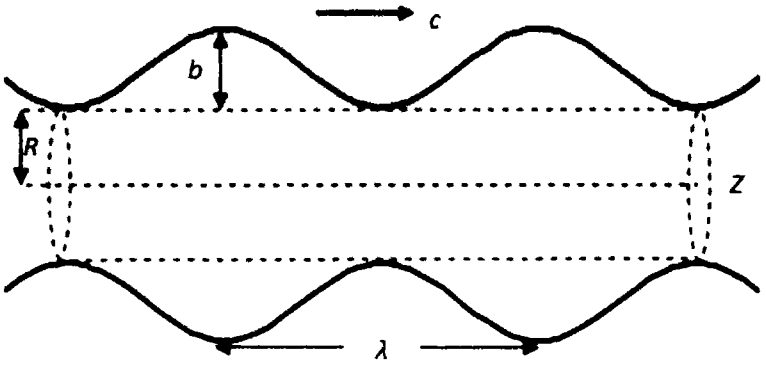

Fig. 6.1: Geometry of the tube.

In the fixed frame $(\bar{R}, \bar{Z})$, the equations expressing the movement of the fluid and the solid grains are

$$\frac{1}{\bar{R}}\frac{\partial(\bar{R}\bar{U})}{\partial\bar{R}} + \frac{\partial(\bar{W})}{\partial\bar{Z}} = 0, \tag{6.2}$$

$$\rho\frac{d}{d\bar{t}}(\bar{U}) = -\frac{\partial\bar{p}}{\partial\bar{R}} + \frac{1}{R}\frac{\partial}{\partial R}(R\bar{T}_{rr}) + \frac{\partial}{\partial\bar{Z}}(\bar{T}_{rz}) + kN(\bar{U}_s - \bar{U}), \tag{6.3}$$

$$\rho\frac{d}{d\bar{t}}(\bar{W}) = -\frac{\partial\bar{p}}{\partial\bar{Z}} + \frac{1}{R}\frac{\partial}{\partial R}(R\bar{T}_{rz}) + \frac{\partial}{\partial\bar{Z}}(\bar{T}_{zz}) + kN(\bar{W}_s - \bar{W}), \tag{6.4}$$

$$\frac{1}{\bar{R}}\frac{\partial(\bar{R}\bar{U}_s)}{\partial\bar{R}} + \frac{\partial(\bar{W}_s)}{\partial\bar{Z}} = 0, \tag{6.5}$$

$$\frac{d}{d\bar{t}}(\bar{U}) = \frac{k}{m}(\bar{U} - \bar{U}_s), \tag{6.6}$$

$$\frac{d}{d\bar{t}}(\bar{W}) = \frac{k}{m}(\bar{W} - \bar{W}_s), \tag{6.7}$$

where $\frac{d}{dt} = \left(\frac{\partial}{\partial\bar{t}} + \frac{1}{\bar{R}}\frac{\partial}{\partial\bar{R}} + \frac{\partial}{\partial\bar{Z}}\right)$.

Using the transformations mentioned below to associate the moving $(\bar{r}, \bar{z})$and fixed frames $(\bar{R}, \bar{Z})$

$$\bar{z} = \bar{Z} - c\bar{t}\,,\ \bar{r} = \bar{R}, \bar{w} = \bar{W} - c, \bar{u} = \bar{U}, \qquad \bar{w}_s = \bar{W}_s - c, \quad \bar{u}_s = \bar{U}_s, \tag{6.8}$$

and taking into account the dimensionless quantities

$$w=\frac{\bar{w}}{c},\quad r=\frac{\bar{r}}{a},\quad z=\frac{\bar{z}}{\lambda},\quad p=\frac{a^2\bar{p}}{\lambda\mu c},u_s=\frac{\bar{u}_s}{\delta c},\quad w_s=\frac{\bar{w}_s}{c},\quad t=\frac{c\bar{t}}{\lambda},$$

$$u=\frac{\bar{u}}{\delta c},\quad \delta=\frac{a}{\lambda},\quad Re=\frac{\rho ca}{\mu},\quad T=\frac{a\bar{T}}{\mu c},\quad u_s=-\frac{1}{r}\frac{\partial\varphi}{\partial z},\quad A=\frac{kNa^2}{\mu},$$

$$B=\frac{ka}{mc},\quad w=\frac{1}{r}\frac{\partial\psi}{\partial r}\quad w_s=\frac{1}{r}\frac{\partial\varphi}{\partial r},\quad \alpha_1=\frac{c\overline{\alpha_1}}{\mu a},\quad u=-\frac{1}{r}\frac{\partial\psi}{\partial z}. \tag{6.9}$$

The compatibility equations for fluid and dust particles after removing the pressure gradient are

$$Re\delta\left[\delta^2\left(-\frac{2}{r}\frac{\partial^2\psi}{\partial z^2}\frac{\partial\psi}{\partial z}-\frac{\partial^3\psi}{\partial z^3}\frac{1}{r}\frac{\partial\psi}{\partial r}+\frac{\partial\psi}{\partial z}\frac{1}{r}\right)\right.$$

$$\left.-\left(\frac{\partial\psi}{\partial z}\frac{3}{r^2}\frac{\partial^2\psi}{\partial r^2}+\frac{\partial^3\psi}{\partial r^2\partial z}\frac{1}{r}\frac{\partial\psi}{\partial r}-\frac{\partial\psi}{\partial r}\frac{3}{r^3}\frac{\partial\psi}{\partial z}-\frac{\partial\psi}{\partial r}\frac{1}{r^2}\frac{\partial^2\psi}{\partial r\partial z}-\frac{1}{r}\frac{\partial^3\psi}{\partial r^3}\frac{\partial\psi}{\partial z}\right)\right]$$

$$=\delta\frac{\partial^2}{\partial r\partial z}(rT_{rr})-r\frac{\partial}{\partial r}\left(\frac{1}{r}\frac{\partial}{\partial r}(rT_{rz})\right)+r\delta^2\left(\frac{\partial^2T_{rz}}{\partial z^2}\right)-r\delta\left(\frac{\partial^2T_{zz}}{\partial z\partial r}\right)$$

$$+A(\nabla_1^2\varphi-\nabla_1^2\psi), \tag{6.10}$$

$$\delta\left[\delta^2\left(\frac{1}{r}\frac{\partial\varphi}{\partial z}-\frac{\partial^3\varphi}{\partial z^3}\frac{1}{r}\frac{\partial\varphi}{\partial r}-\frac{\partial\varphi}{\partial z}\frac{\partial^2\varphi}{\partial z^2}\frac{2}{r}\right)\right.$$

$$\left.-\left(\frac{\partial\varphi}{\partial z}\frac{3}{r^2}\frac{\partial^2\varphi}{\partial r^2}-\frac{\partial\varphi}{\partial r}\frac{1}{r^2}\frac{\partial^2\varphi}{\partial r\partial z}-\frac{\partial\varphi}{\partial z}\frac{3}{r^3}\frac{\partial\varphi}{\partial r}-\frac{\partial^3\varphi}{\partial r^3}\frac{1}{r}\frac{\partial\varphi}{\partial z}+\frac{\partial^3\varphi}{\partial r^2\partial z}\frac{\partial v}{\partial r}\frac{1}{r}\right)\right]$$

$$=B(\nabla_1^2\phi-\nabla_1^2\psi), \tag{6.11}$$

where $\nabla_1^2=\left(\delta^2\frac{\partial^2}{\partial z^2}+\frac{\partial^2}{\partial r^2}-\frac{1}{r}\frac{\partial}{\partial r}\right)$.

Walls geometry in dimensionless configuration is

$$h=1+\phi\,sinz, \tag{6.12}$$

where the occlusion is $\phi = \frac{b}{a}$ (the amplitude proportion).

The non-dimension boundary conditions are

$$\psi = 0, \quad \varphi = 0, \quad \frac{\partial}{\partial r}\left(\frac{1}{r}\frac{\partial \psi}{\partial r}\right) = 0, \qquad at \quad r = 0, \tag{6.13}$$

$$\psi = F, \quad \varphi = E, \quad \frac{1}{r}\frac{\partial \psi}{\partial r} = -1, \qquad at \quad r = h. \tag{6.14}$$

The dimensionless time flow of the fluid and the solid granules are given as

$$Q = F + 0.5\left(1 + \frac{\phi^2}{2}\right), \tag{6.15}$$

$$Q_s = E + 0.5\left(1 + \frac{\phi^2}{2}\right), \tag{6.16}$$

where

$$F = \int_0^h \frac{\partial \psi}{\partial r} dr = \psi(h) - \psi(0), \tag{6.17}$$

$$E = \int_0^h \frac{\partial \phi}{\partial r} dr = \varphi(h) - \varphi(0). \tag{6.18}$$

The expression for the pressure rise is

$$\Delta P = \int_0^{2\pi} \frac{dp}{dr} dr. \tag{6.19}$$

6.2 Method of Solution

The equations obtained for the dust and the fluid particles are non-linear in nature.

To obtain the solution, perturbation technique has been adopted.

$$\psi = \psi_0 + \delta\psi_1 + \delta^2\psi_2 + O(\delta^3), \tag{6.20}$$

$$F = F_0 + \delta F_1 + \delta^2 F_2 + O(\delta^3), \tag{6.21}$$

$$\varphi = \varphi_0 + \delta\varphi_1 + \delta^2\varphi_2 + O(\delta^3), \tag{6.22}$$

$$F_s = F_{s0} + \delta F_{s1} + \delta^2 F_{s2} + O(\delta^3), \tag{6.23}$$

$$p = p_0 + \delta p_1 + \delta^2 p_2 + O(\delta^3). \tag{6.24}$$

6.2.1 Zeroth-Order system

$$\left(\frac{\partial^2}{\partial r^2} - \frac{1}{r}\frac{\partial}{\partial r}\right)\left[\left(rT_{0rz} - A(\varphi_0 - \psi_0)\right)\right] = 0, \tag{6.25}$$

$$\left(\frac{\partial^2}{\partial r^2} - \frac{1}{r}\frac{\partial}{\partial r}\right)\left(B(\varphi_0 - \psi_0)\right) = 0, \tag{6.26}$$

$$\frac{dp_0}{dz} = \frac{1}{r}\left(T_{0rz} + r\frac{\partial}{\partial r}(T_{0rz})\right) + \frac{A}{r}\left(\frac{\partial}{\partial r}(\psi_0 - \varphi_0)\right), \tag{6.27}$$

where

$$T_{0rz} = -\frac{1}{r}\left(\frac{1}{r}\frac{\partial\psi_0}{\partial r} + \frac{\partial^2\psi_0}{\partial r^2}\right). \tag{6.28}$$

with

$$\psi_0 = 0, \quad \varphi_0 = 0, \quad \frac{\partial}{\partial r}\left(\frac{1}{r}\frac{\partial\psi_0}{\partial r}\right) = 0, \quad at \quad r = 0, \tag{6.29}$$

$$\psi_0 = F_0, \quad \varphi_0 = E_0, \quad \frac{1}{r}\frac{\partial\psi_0}{\partial r} = -1, \quad at \quad r = h. \tag{6.30}$$

Solution of Zeroth-Order

$$\psi_0 = \frac{1}{2}r^2 a_{11} + \frac{1}{4}r^4 a_{12},$$

$$\phi_0 = \frac{a_{12}r^4}{4} + \frac{1}{2}r^2 a_{13},$$

$$a_{11} = 1 + \frac{4F_0}{h^2}, a_{12} = \frac{-2(2F_0 + h^2)}{h^4}, a_{13} = -\frac{a_{12}h^2}{2} + \frac{2F_{s0}}{h^2}.$$

This solution is same as obtained by Siddiqui and Schwarz [25].

6.2.2 First Order System

$$Re\frac{1}{r}\left(-\frac{\partial\psi_0}{\partial r}\frac{\partial^3\psi_0}{\partial r^2\partial z} + \frac{\partial\psi_0}{\partial z}\frac{3}{r^2}\frac{\partial\psi_0}{\partial r} + \frac{\partial^3\psi_0}{\partial r^3}\frac{\partial\psi_0}{\partial z} - \frac{\partial\psi_0}{\partial z}\frac{3}{r}\frac{\partial^2\psi_0}{\partial r^2} + \frac{\partial^2\psi_0}{\partial z\partial r}\frac{\partial\psi_0}{\partial r}\frac{1}{r}\right)$$

$$= A\left(\left(-\frac{1}{r}\frac{\partial}{\partial r} + \frac{\partial^2}{\partial r^2}\right)(\varphi_1 - \psi_1)\right) - r\frac{\partial}{\partial r}\left(\frac{1}{r}\frac{\partial}{\partial r}(rT_{1rz})\right) + \frac{\partial^2}{\partial z\partial r}(rT_{0rr})$$

$$-\left(r\frac{\partial^2 T_{0zz}}{\partial z\partial r}\right), \tag{6.31}$$

$$\left(\frac{1}{r}\left(-\frac{\partial\varphi_0}{\partial z}\frac{3}{r^2}\frac{\partial^2\varphi_0}{\partial r^2} + \frac{\partial\varphi_0}{\partial z}\frac{3}{r^3}\frac{\partial\varphi_0}{\partial r} + \frac{\partial^2\varphi_0}{\partial r\partial z}\frac{1}{r^2}\frac{\partial\varphi_0}{\partial r} - \frac{1}{r}\frac{\partial^3\varphi_0}{\partial z\partial r^2}\frac{\partial\varphi_0}{\partial r}\right.\right.$$

$$\left.\left. + \frac{\partial\varphi_0}{\partial z}\frac{\partial^3\varphi_0}{\partial r^3}\frac{1}{r}\right)\right) = B\left(\left(\frac{\partial^2}{\partial r^2} - \frac{1}{r}\frac{\partial}{\partial r}\right)(\varphi_1 - \psi_1)\right), \tag{6.32}$$

$$\frac{dp_1}{dz} = \left(\frac{\partial T_{0zz}}{\partial z}\right) + \frac{1}{r}\left(\frac{\partial}{\partial r}(rT_{1rz})\right) + \frac{A}{r}\left(\frac{\partial\psi_1}{\partial r} - \frac{\partial\varphi_1}{\partial r}\right)$$

$$- Re\left(\frac{\partial\psi_0}{\partial z}\frac{1}{r^3}\frac{\partial\psi_0}{\partial r} - \frac{\partial\psi_0}{\partial z}\frac{\partial^2\psi_0}{\partial r^2}\frac{1}{r^2} + \frac{\partial\psi_0}{\partial r}\frac{\partial^2\psi_0}{\partial r\partial z}\frac{1}{r^2}\right), \tag{6.33}$$

where

$$T_{1rz} = \frac{1}{r}\left(-\frac{\partial^2\psi_1}{\partial r^2} + \frac{\partial\psi_1}{\partial r}\frac{1}{r}\right)$$

$$+ \alpha_1\left[\frac{2}{r^2}\frac{\partial^2\psi_0}{\partial r\partial z}\frac{\partial^2\psi_0}{\partial r^2} + \frac{1}{r^2}\frac{\partial\psi_0}{\partial r}\frac{\partial^3\psi_0}{\partial r^2\partial z} - \frac{1}{r^2}\frac{\partial\psi_0}{\partial z}\frac{\partial^3\psi_0}{\partial r^3} - \frac{\partial\psi_0}{\partial z}\frac{\partial\psi_0}{\partial r}\frac{1}{r^4}\right.$$

$$\left. + \frac{1}{r^3}\frac{\partial\psi_0}{\partial z}\frac{\partial^2\psi_0}{\partial r^2} - \frac{\partial\psi_0}{\partial r}\frac{\partial^2\psi_0}{\partial r\partial z}\frac{3}{r^3}\right], \tag{6.34}$$

$$T_{0rr} = \alpha_1 \left[\frac{\partial}{\partial r}\left(-\frac{1}{r}\frac{\partial \psi_0}{\partial r}\right)\right]^2, \tag{6.35}$$

$$T_{0zz} = -\alpha_1 \left[\frac{\partial}{\partial r}\left(-\frac{1}{r}\frac{\partial \psi_0}{\partial r}\right)\right]^2. \tag{6.36}$$

with

$$\psi_1 = 0, \quad \varphi_1 = 0, \quad \frac{\partial}{\partial r}\left(\frac{1}{r}\frac{\partial \psi_1}{\partial r}\right) = 0, \qquad at \quad r = 0, \tag{6.37}$$

$$\psi_1 = F_1, \quad \varphi_1 = E_1, \quad \frac{1}{r}\frac{\partial \psi_1}{\partial r} = 0, \qquad at\ r = h. \tag{6.38}$$

Solution of First Order

$$\psi_1 = -\frac{1}{96}Aa'_{12}a_{13}r^6 - \frac{1}{576}Aa'_{12}a_{12}r^8 + \frac{1}{96}a_{11}a'_{12}r^6Re + \frac{1}{576}a'_{12}a_{12}r^8Re + \frac{1}{2}r^2b_1 + \frac{1}{4}r^4b_2,$$

$$\phi 1 = \frac{(-a'_{12}a_{13} + Bb_2)r^4}{4B} + \frac{(-a'_{12}a_{12} + 12B\left(-\frac{1}{96}Aa'_{12}a_{13}\right) + 12B\left(\frac{1}{96}a_{11}a'_{12}Re\right))r^6}{12B} + \left(-\frac{1}{576}Aa'_{12}a_{12} + \frac{1}{576}a'_{12}a_{12}Re\right)r^8 + \frac{1}{2}r^2b_3,$$

$$b_1 = \frac{576F_1 + a'_{12}h^6(-3Aa_{13} - Aa_{12}h^2 + 3a_{11}Re + a_{12}h^2Re)}{144h^2},$$

$$b_2 = \frac{-192F_1 + a'_{12}h^6(4Aa_{13} + Aa_{12}h^2 - 4a_{11}Re - a_{12}h^2Re)}{48h^4},$$

$$b_3 = \frac{1}{6Bh^2}\Bigg(a'_{12}(3a_{13}h^4 + a_{12}h^6) - 3B\Bigg(b_1 h^4 + 4\Bigg(\begin{matrix} \left(\frac{1}{96}Aa'_{12}a_{13}\right)h^6 + \left(\frac{1}{96}Rea'_{12}a_{13}\right)h^6 \\ -\left(\frac{1}{576}Aa'_{12}a_{12}\right)h^8 + \left(\frac{1}{576}Aa'_{12}a_{12}\right)h^8 - F_{s1} \end{matrix} \Bigg) \Bigg) \Bigg).$$

In the absence of solid particles, this solution is same as obtained by Siddiqui and Schwarz [25].

6.2.3 Second Order System

$$Re\frac{1}{r}\left(-\frac{\partial\psi_1}{\partial z}\frac{\partial^2\psi_1}{\partial r^2}\frac{3}{r} + \frac{\partial^3\psi_1}{\partial r^3}\frac{\partial\psi_1}{\partial z} + \frac{\partial\psi_1}{\partial z}\frac{3}{r^2}\frac{\partial\psi_1}{\partial r} - \frac{\partial^3\psi_1}{\partial z\partial r^2}\frac{\partial\psi_1}{\partial r} + \frac{\partial\psi_1}{\partial r}\frac{\partial^2\psi_1}{\partial r\partial z}\frac{1}{r}\right)$$

$$= \frac{\partial^2}{\partial z\partial r}(rT_{1rr}) + r\left(\frac{\partial^2 T_{0rz}}{\partial z^2}\right) - r\left(\frac{\partial^2 T_{1zz}}{\partial r\partial z}\right)$$

$$+ A\left(\left(\frac{\partial^2 z}{\partial r^2}\right)(\varphi_0 - \psi_0) + \left(\frac{\partial^2}{\partial r^2} - \frac{1}{r}\frac{\partial}{\partial r}\right)(\varphi_2 - \psi_2)\right)$$

$$- r\frac{\partial}{\partial r}\left(\frac{1}{r}\frac{\partial}{\partial r}(rT_{2rz})\right), \qquad (6.39)$$

$$\left(\frac{1}{r}\left(-\frac{\partial^2\varphi_1}{\partial r^2}\frac{\partial\varphi_1}{\partial z}\frac{3}{r} - \frac{\partial\varphi_1}{\partial r}\frac{\partial^3\varphi_1}{\partial r^2\partial z} + \frac{\partial\varphi_1}{\partial z}\frac{\partial^3\varphi_1}{\partial r^3} + \frac{\partial\varphi_1}{\partial r}\frac{\partial^2\varphi_1}{\partial z\partial r}\frac{1}{r} + \frac{\partial\varphi_1}{\partial z}\frac{\partial\varphi_1}{\partial r}\frac{3}{r^2}\right)\right)$$

$$= B\left(\left(\frac{\partial^2 z}{\partial r^2}\right)(\varphi_0 - \psi_0) + \left(\frac{\partial^2}{\partial r^2} - \frac{1}{r}\frac{\partial}{\partial r}\right)(\varphi_2 - \psi_2)\right), \qquad (6.40)$$

$$\frac{dp_2}{dz} = \left(\frac{\partial T_{1zz}}{\partial z}\right) + \left(\frac{1}{r}\frac{\partial}{\partial r}(rT_{1rz})\right) + \frac{A}{r}\left(\frac{\partial \psi_2}{\partial r} - \frac{\partial \varphi_2}{\partial r}\right)$$

$$- Re\left(\frac{\partial \psi_1}{\partial z}\frac{1}{r^3}\frac{\partial \psi_1}{\partial r} - \frac{1}{r^2}\frac{\partial^2 \psi_1}{\partial r^2}\frac{\partial \psi_1}{\partial z} + \frac{1}{r^2}\frac{\partial \psi_1}{\partial r}\frac{\partial^2 \psi_1}{\partial r \partial z}\right), \tag{6.41}$$

where

$$T_{2rz} = \left(-\frac{\partial^2 \psi_1}{\partial r^2}\frac{1}{r} + \frac{1}{r^2}\frac{\partial \psi_1}{\partial r} + \frac{1}{r}\frac{\partial^2 \psi_0}{\partial z^2}\right)$$

$$+ \alpha_1\left[\frac{2}{r^2}\frac{\partial^2 \psi_1}{\partial r^2}\frac{\partial^2 \psi_1}{\partial r \partial z} - \frac{1}{r^4}\frac{\partial \psi_1}{\partial z}\frac{\partial \psi_1}{\partial r} + \frac{\partial \psi_1}{\partial z}\frac{1}{r^3}\frac{\partial^2 \psi_1}{\partial r^2} - \frac{3}{r^3}\frac{\partial \psi_1}{\partial r}\frac{\partial^2 \psi_1}{\partial r \partial z}\right.$$

$$\left. - \frac{1}{r^2}\frac{\partial \psi_1}{\partial z}\frac{\partial^3 \psi_1}{\partial r^3} + \frac{\partial \psi_1}{\partial r}\frac{1}{r^2}\frac{\partial^3 \psi_1}{\partial r^2 \partial z}\right], \tag{6.42}$$

$$T_{1rr} = \left(-\frac{\partial \psi_0}{\partial z}\frac{2}{r^2} + \frac{2}{r}\frac{\partial^2 \psi_0}{\partial z \partial r}\right) - \alpha_1\left[\frac{\partial}{\partial r}\left(-\frac{1}{r}\frac{\partial \psi_1}{\partial r}\right)\right]^2, \tag{6.43}$$

$$T_{1zz} = \left(-\frac{\partial^2 \psi_0}{\partial z \partial r}\frac{2}{r}\right) + \alpha_1\left[\frac{\partial}{\partial r}\left(-\frac{1}{r}\frac{\partial \psi_1}{\partial r}\right)\right]^2. \tag{6.44}$$

with

$$\psi_2 = 0, \quad \varphi_2 = 0, \quad \frac{\partial}{\partial r}\left(\frac{1}{r}\frac{\partial \psi_2}{\partial r}\right) = 0, \quad \text{at} \quad r = 0, \tag{6.45}$$

$$\psi_2 = F_2, \quad \varphi_2 = E_2, \quad \frac{1}{r}\frac{\partial \psi_2}{\partial r} = 0, \quad \text{at } r = h. \tag{6.46}$$

These systems of equations are solved by using DSolver methodology in Mathematica software.

6.3 Results and Discussion

This section is dedicated to discuss the impact of diverse parameters on the velocity, streamline, pressure rise. Velocity of the fluid under the influence of Reynolds number

(Re), (α_1) i.e. the second-grade attribute and (δ) the wave number is presented in Figs. 6.2 – 6.4. The graphical demonstration of the pressure gradient is shown in Figs. 6.5 – 6.7. Figs. 6.8 – 6.10 are plotted to examine the pressure rise. Impact of parameters on shear stress are presented in Fig. 6.11 – 6.13. Streamline graphs hold an important role while studying the flow of the fluids. The pattern of the flow of the fluid is presented through the contour graphs. Figs. 6.14 – 6.16 show the streamline patterns of fluid under the impact of different attributes. The consequences of these parameters on the velocity of the solid grains is illustrated in Figs. 6.17 – 6.19. As the fluid contains the solid grains in it so the contour graphs for the solid grains are included as well. The contour graphs for different parameters for the solid grains are exemplified in Figs. 6.20 – 6.22.

As shown in Fig. 6.2, with the increase in wave number, the fluid flows more smoothly and efficiently in the desired direction. With the rise in the Reynolds number (Re), we see an increasing manner in the velocity at the center of the tube. As increase in Re reduces the friction force thus causing rise in the fluid velocity. Growth in α_1, enhances the velocity of the fluid as demonstrated in Fig. 6.4. The pressure gradient $\frac{dp}{dz}$ versus z is given in Figs. 6.5 – 6.7 for the impact of Re, α_1 and δ respectively. It is noted that small pressure gradient has been occurred in $z \in [1,3]$. It means that the flow can smoothly go through without imposition of large pressure gradient and large pressure gradient occurs for $z \in [3,7]$. It means greater pressure gradient is required to attain same flux to pass it. Fig. 6.8 shows the influence of φ on pressure rise. As the amplitude is increased, we conclude that more pressure is needed to pump the fluid throughout the region. The pumping rate falls in the retrograde region ($\Delta P > 0$) as the wave number increases. While a reverse situation can be observed in co-pumping region ($\Delta P < 0$). The retrograde region broadens with the increase in α_1. Pumping

rate grows with the increase in second grade parameter. Impression of different parameters on wall shear stress T_{rz} at $r = h$, are demonstrated in Figs. 6.11 – 6.13. With the increase in the parameters, it can be seen that the walls of the tube are exhibiting to and fro movement thus the peristaltic motion of the wall can be seen clearly.

Fig. 6.14 shows that as the values of the wave number (δ) is raised, the bolus in the channel get enhanced. As wave number is increased, the movement of bolus can be seen stretching towards the upward direction. The impact of Reynolds number (Re) on the streamline pattern is shown in Fig. 6.15. As the Reynolds number is increased, viscous force weakens thus we observe that the motion of the fluid gets smoother and bolus expands and move towards upward direction. The streamline patterns for the amplitude ratio (φ) is illustrated in Fig. 6.16. For $\varphi = 0$, no bolus is formed as shown in Fig. 6.16(a). As the values of φ are increased, we see a clear change in the formation and volume of the bolus. The motion of the fluid particles is towards the direction of the amplitude of the tube.

The impact of parameters like (δ), Re and (α) on the velocity of the solid grains is given in Figs. 6.17 – 6.19. We observe increase in the velocity for (δ) and for Re, growth in the velocity of the solid grains. Increase in Reynolds number refers that viscous forces are weakening thus particles may flow more smoothly but for the second-grade parameter (α_1), we observe no change in the velocity of the solid grains at least to $O(\delta^2)$. Fig. 6.20 shows the impact of (δ) on the contour patterns of the solid grains. As the wave number grow, we see an expansion in the volume of the bolus. This indicates that the movement of particles is expanding. The enlargement in the Reynolds number (Re), enhances the bolus as illustrated in Fig. 6.21. With lower viscous force, the bolus formed shows that the movement of particles get smoother.

With the rise in the amplitude of the wave, we observe that the bolus is stretched upward as illustrated in Fig. 6.22. With the increase in amplitude, the flow of the particles also moves up along the upward direction. Fig. 6.23 shows a comparison between the velocity profile obtained by perturbation technique and numerical technique. The velocity of the fluid seems to be following same pattern and ranges through both techniques.

6.4 Graphs

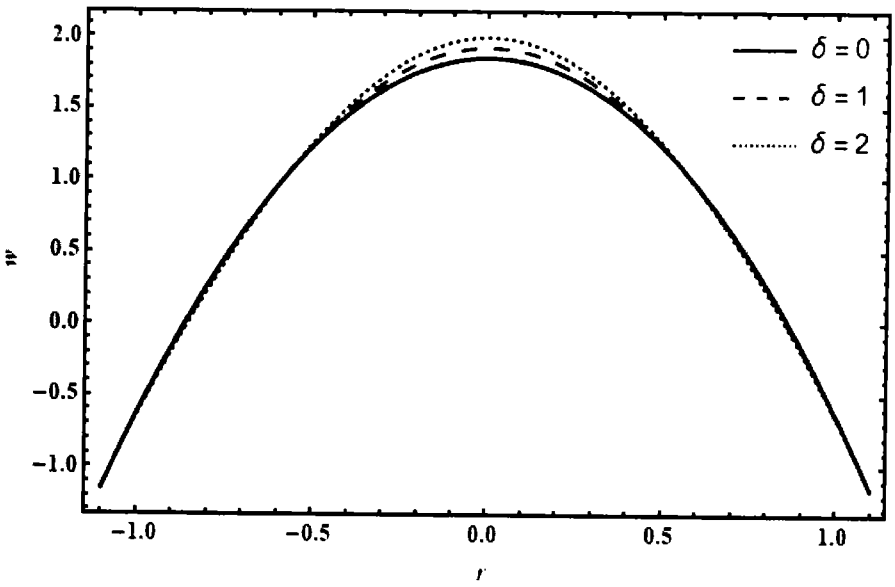

Fig. 6.2: Velocity presentation of fluid for $\phi = 0.15,\ Q = 0.75,\ \alpha_1 = 1.5, A = 1, B = 1, Re = 5, Q_s = 0.5.$

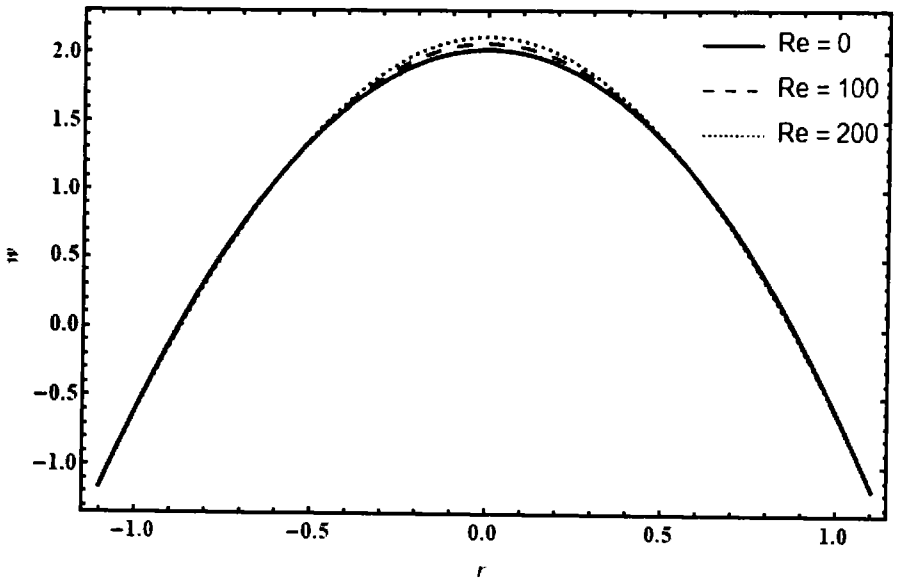

Fig. 6.3: Velocity presentation of fluid for $\phi = 0.15,\ Q = 0.75,\ \alpha_1 = 1.5, A = 1, B = 1, \delta = 0.5, Q_s = 0.5.$

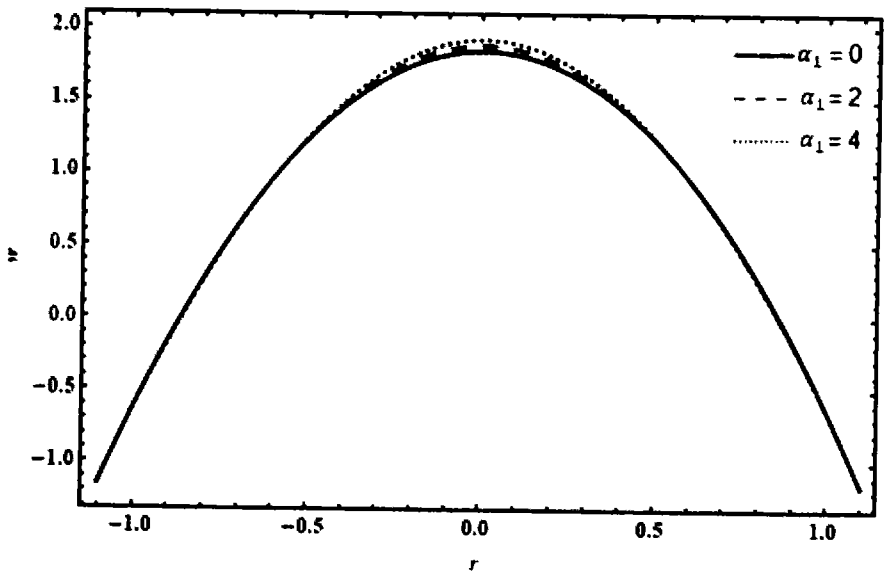

Fig. 6.4: Velocity presentation of fluid for $\phi = 0.15,\ Q = 0.75,\ Re = 5, A = 1, B = 1, \delta = 0.5, Q_s = 0.5.$

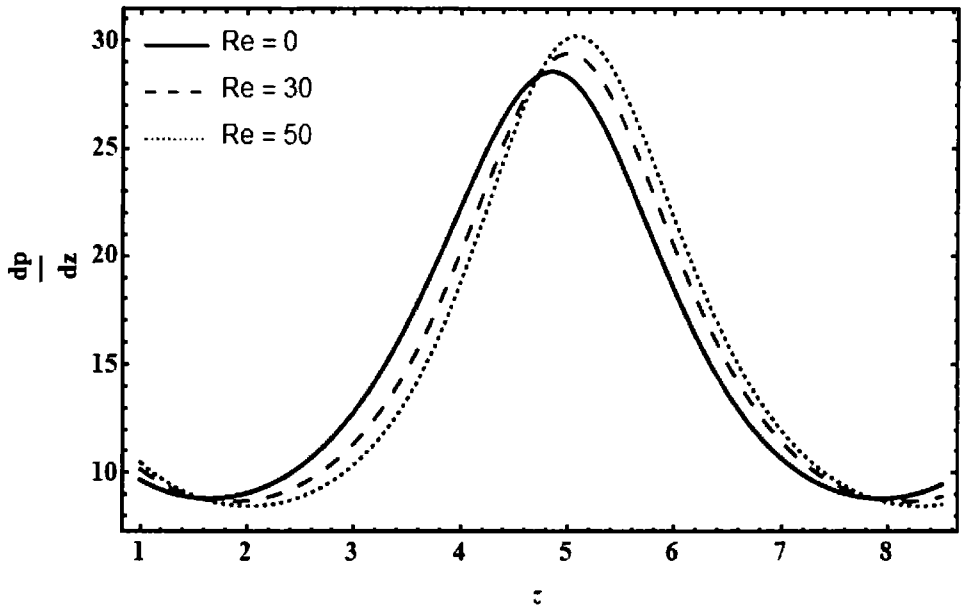

Fig. 6.5: The pressure gradient dp/dz versus z with $Q = 0.9, \alpha_1 = 1.5,\ A = 2, B = 2, \delta = 0.02, Q_s = 0.8, \phi = 0.2.$

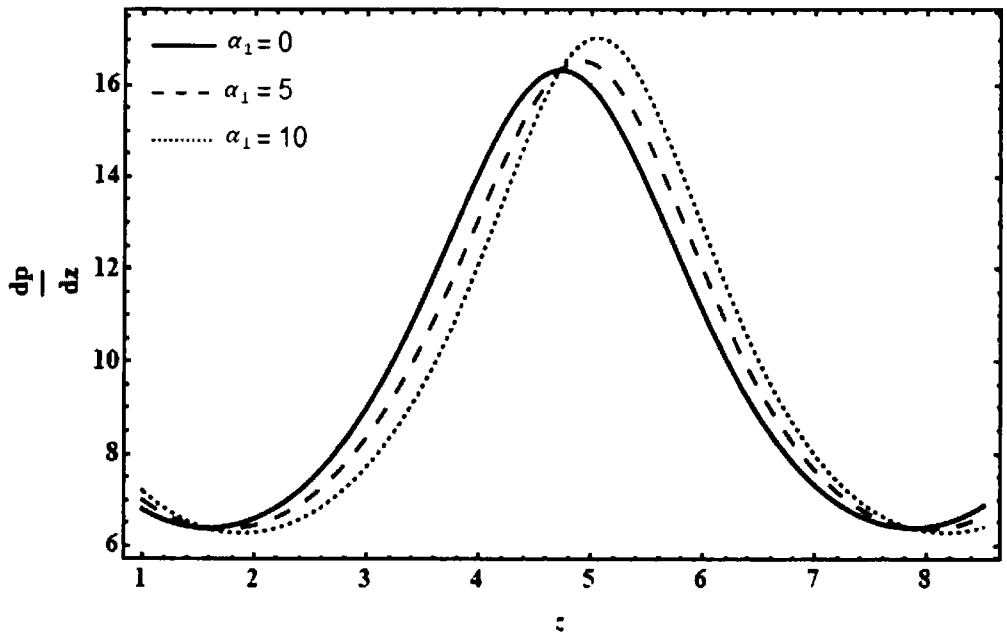

Fig. 6.6: The pressure gradient dp/dz versus z with $Q = 0.6, Re = 5\ A = 1, B = 2, \delta = 0.02, Q_s = 0.5, \phi = 0.15.$

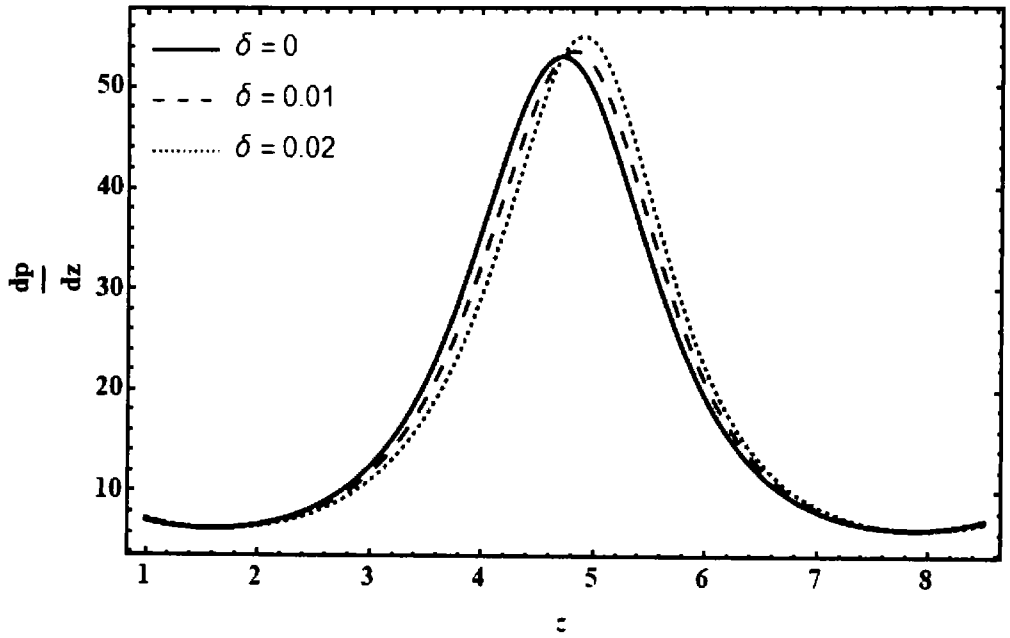

Fig. 6.7: The pressure gradient dp/dz versus z with $Q = 0.9, Re = 5\ A = 2, B = 2,$ $\alpha_1 = 1.5, Q_s = 0.8, \phi = 0.35.$

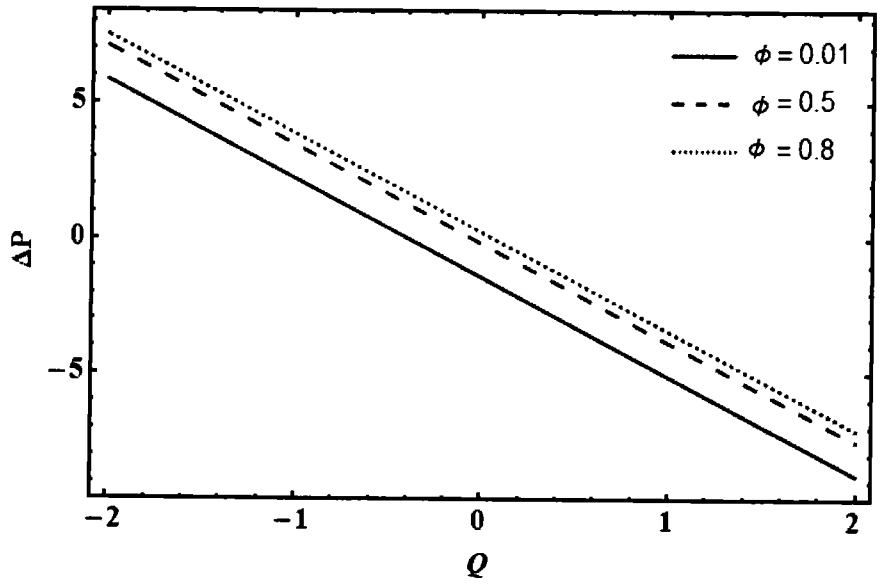

Fig. 6.8: The pressure rise ΔP versus Q with $\delta = 0.01, Re = 5\ A = 2, B = 2, \alpha_1 =$ 1.5.

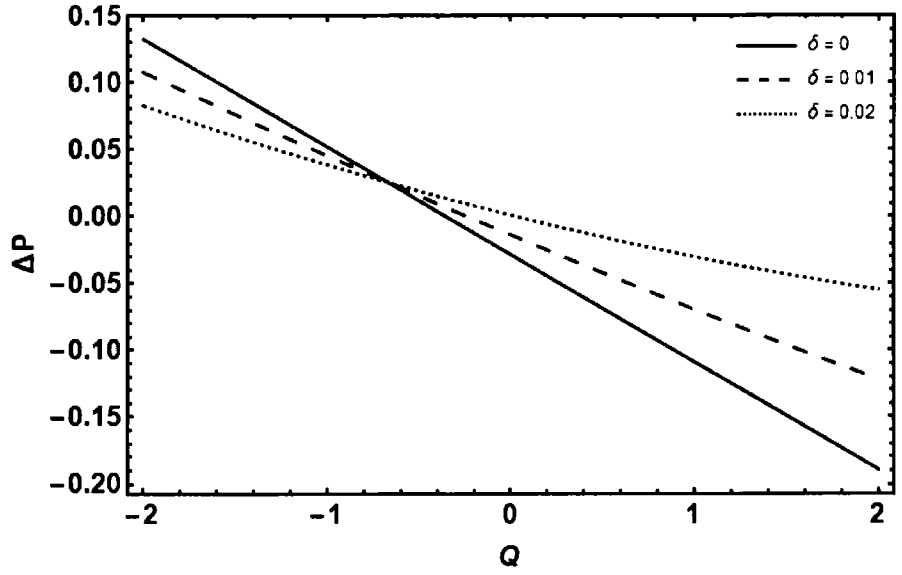

Fig. 6.9: The pressure rise ΔP versus Q with $\phi = 0.15, Re = 5\ A = 1, B = 2, \alpha_1 = 1.5$.

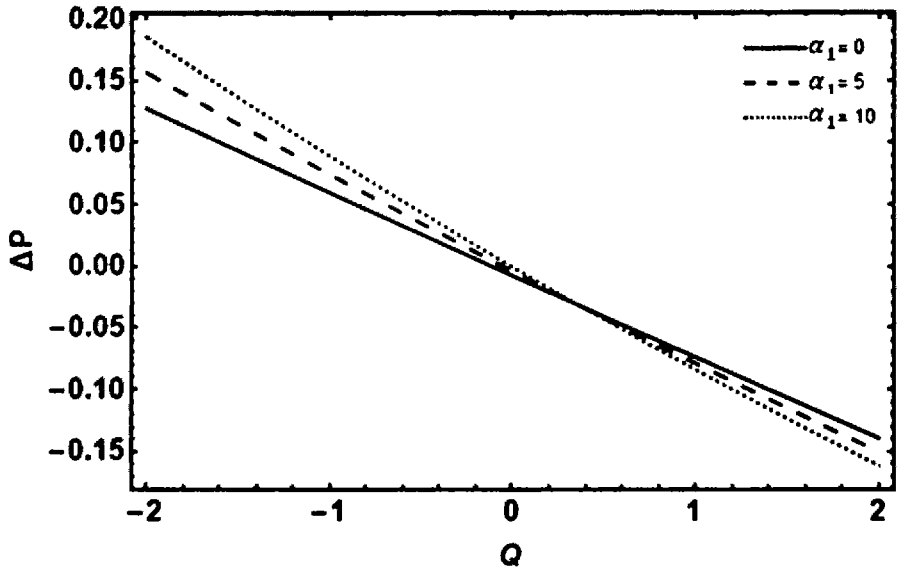

Fig. 6.10: The pressure rise ΔP versus Q with $\phi = 0.15, Re = 2.5, A = 1, B = 2, \delta = 0.01$.

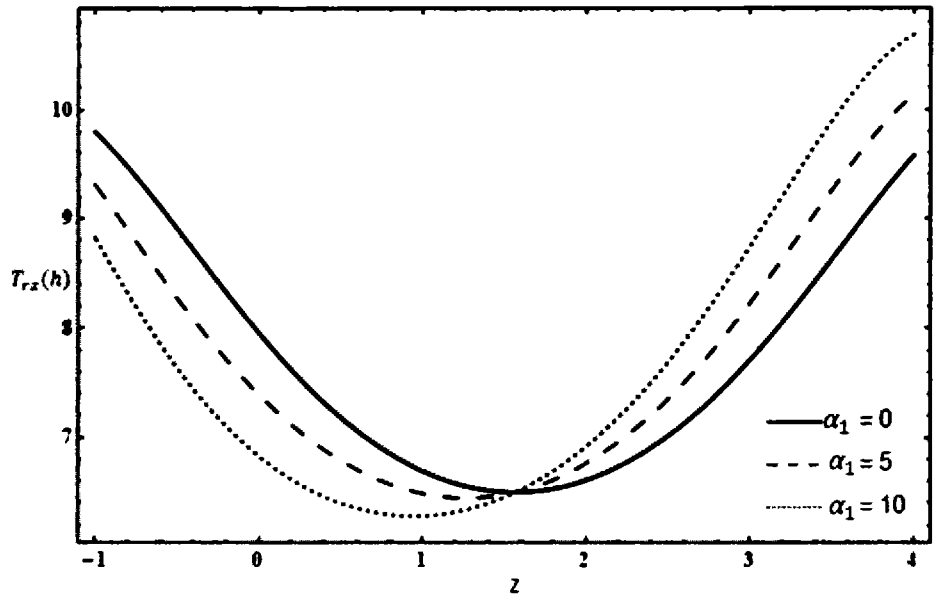

Fig. 6.11: The shear stress at wall with $\phi = 0.15, Re = 5, A = 1, B = 2, \delta = 0.01, Q = 0.8, Q_s = 0.7.$

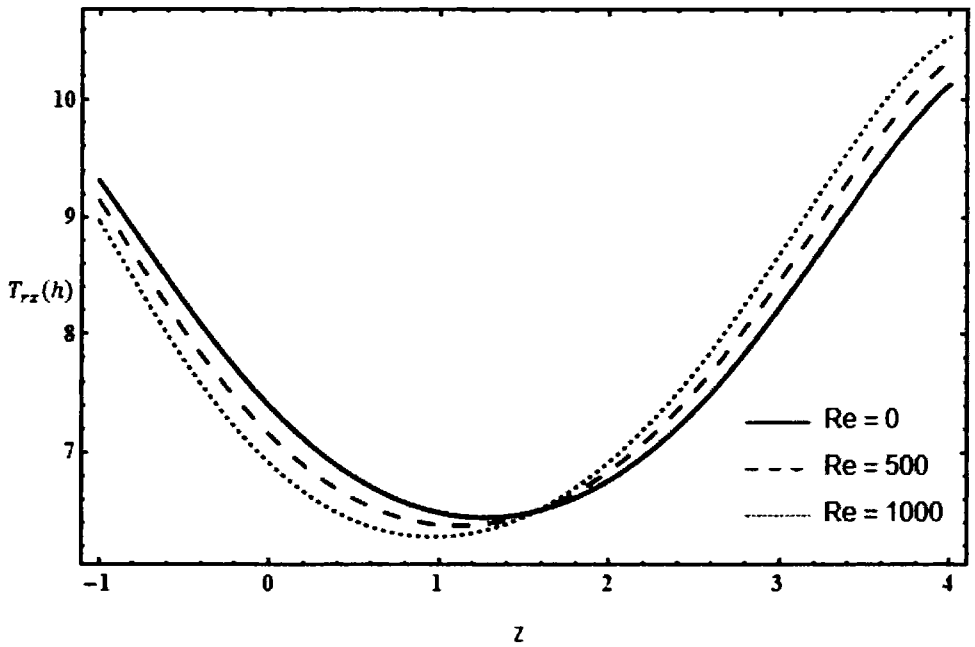

Fig. 6.12: The shear stress at wall with $\phi = 0.15, \alpha_1 = 5, A = 1, B = 2, \delta = 0.01, Q = 0.8, Q_s = 0.7.$

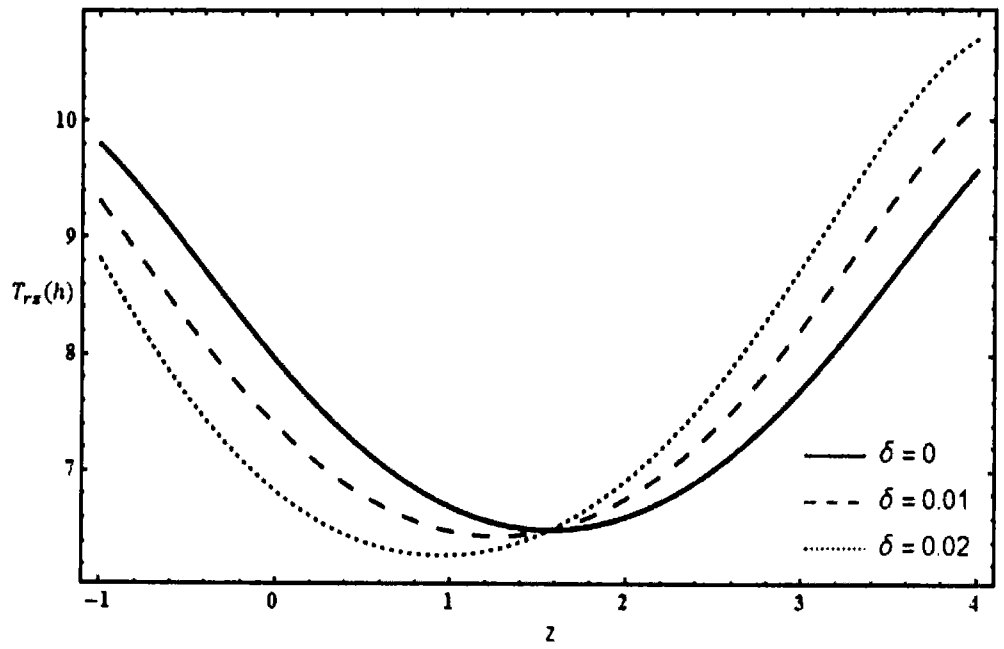

Fig. 6.13: The shear stress at wall with $\phi = 0.15, Re = 5, A = 1, B = 2, \alpha = 2, Q = 0.8, Q_s = 0.7.$

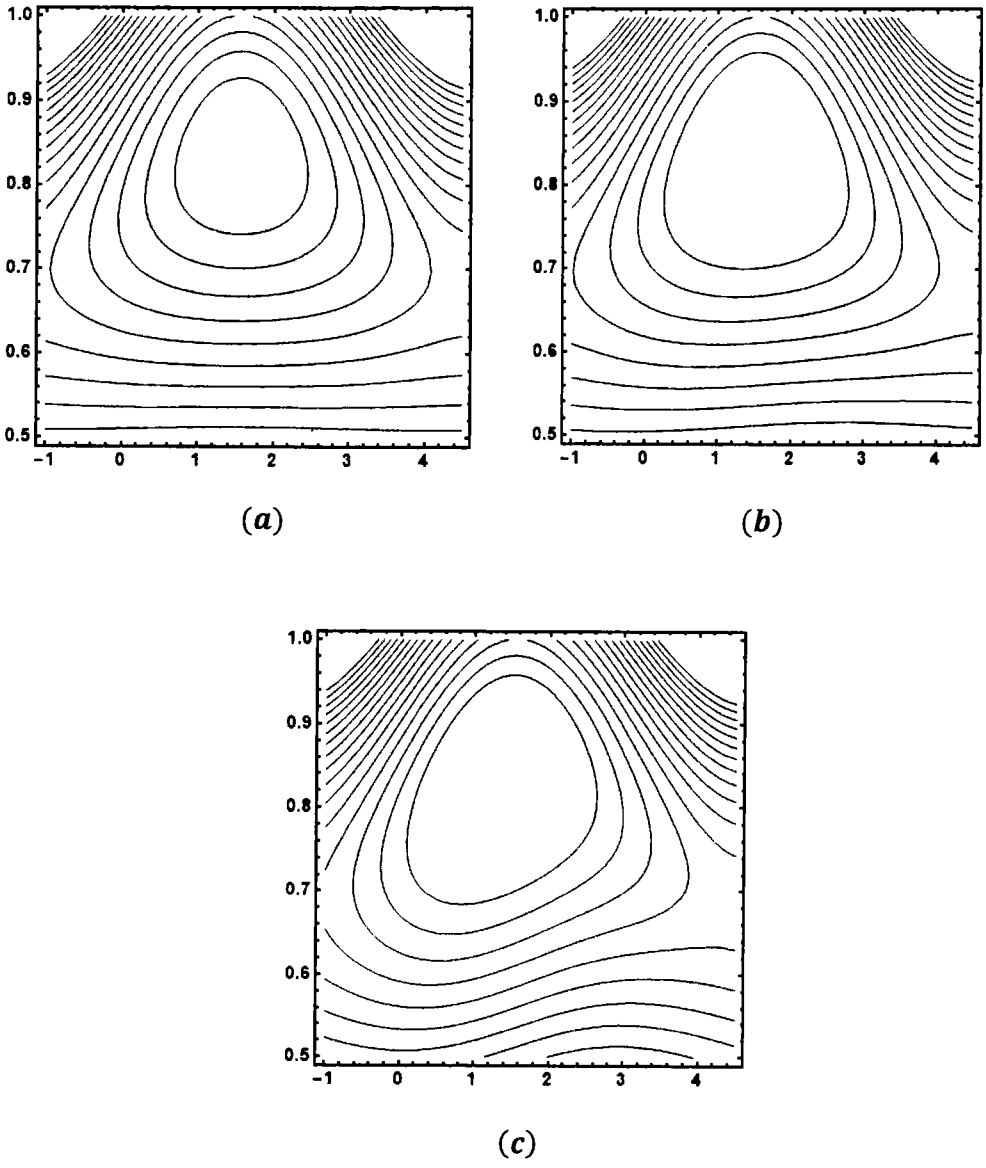

Fig 6.14: Streamline presentation of fluid for $(a)\ \delta = 0\ (b)\ \delta = 0.1\ \ (c)\ \delta = 0.5$ with $\phi = 0.12, \alpha_1 = 5, A = 1, B = 2, Re = 50, Q = 0.6, Q_s = 0.9.$

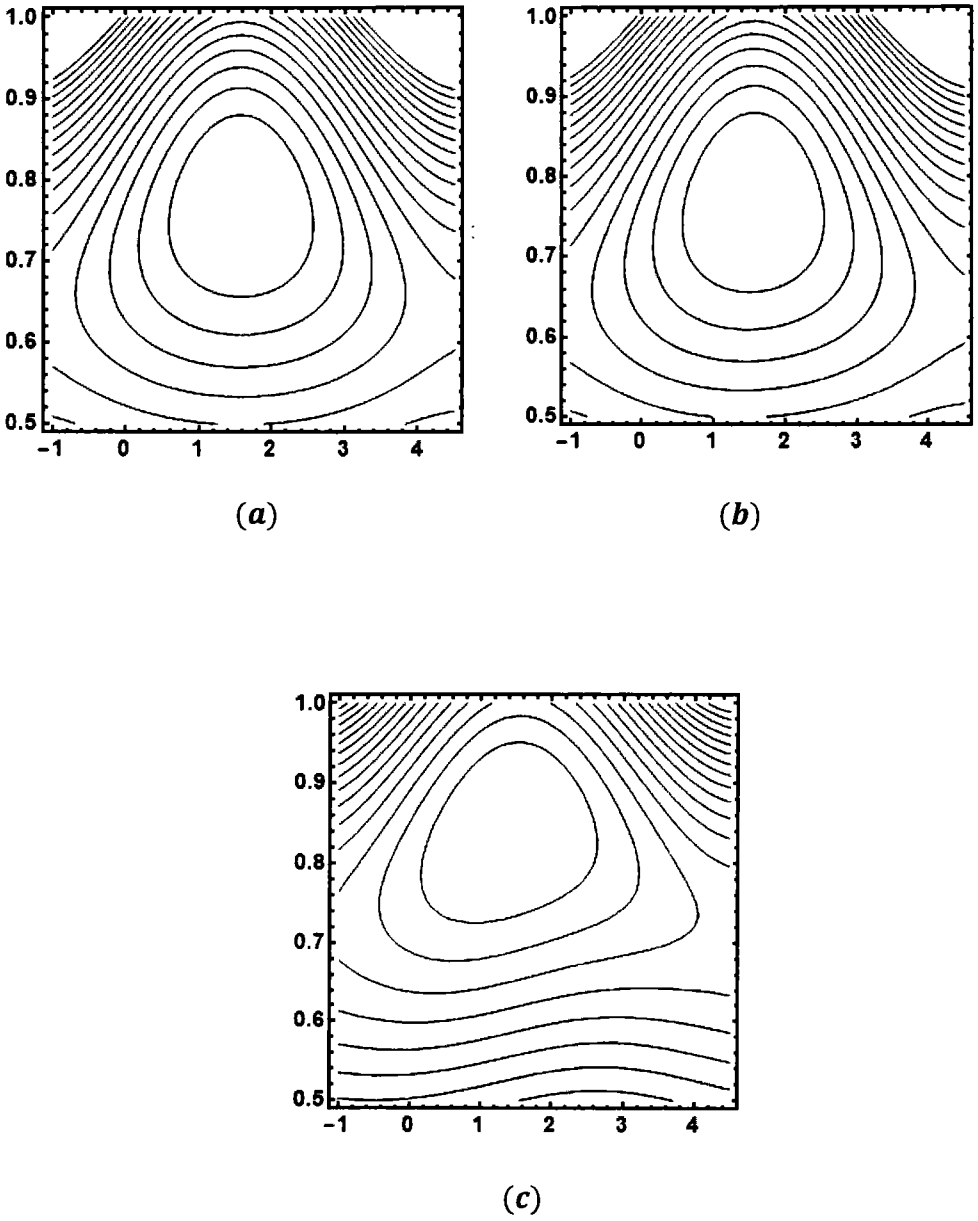

Fig. 6.15: Streamline presentation of fluid for $(a)\ Re = 0\ \ (b)\ Re = 100\ \ (c)\ Re = 200$ with $\phi = 0.1,\ \alpha_1 = 1.5, A = 1, B = 2, \delta = 0.06, Q = 0.65, Q_s = 0.6.$

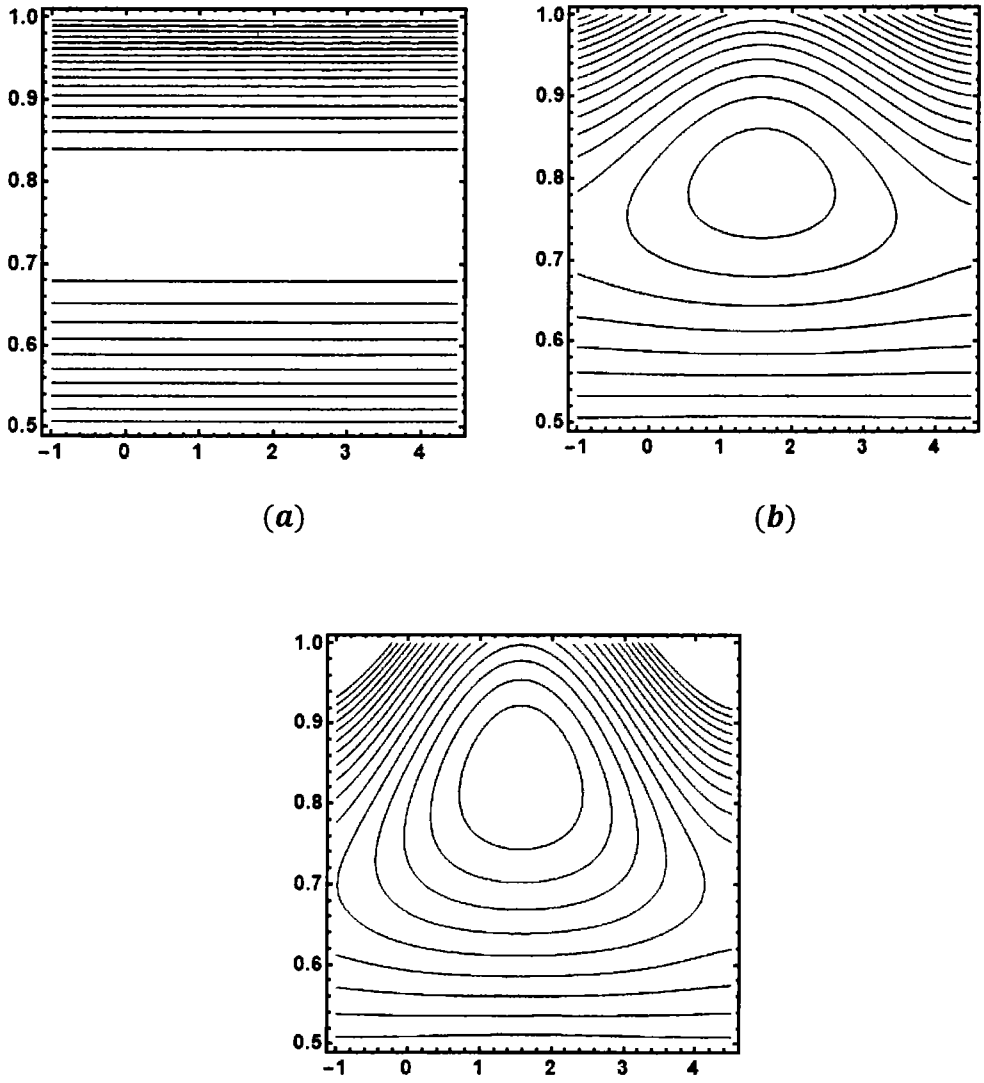

Fig. 6.16: Streamline presentation of fluid for $(a)\ \phi = 0\ (b)\ \phi = 0.05\ (c)\ \phi = 0.12$ with$Q = 0.6,\ \alpha_1 = 1.5, A = 1, B = 2, \delta = 0.06, Re = 5, Q_s = 0.9.$

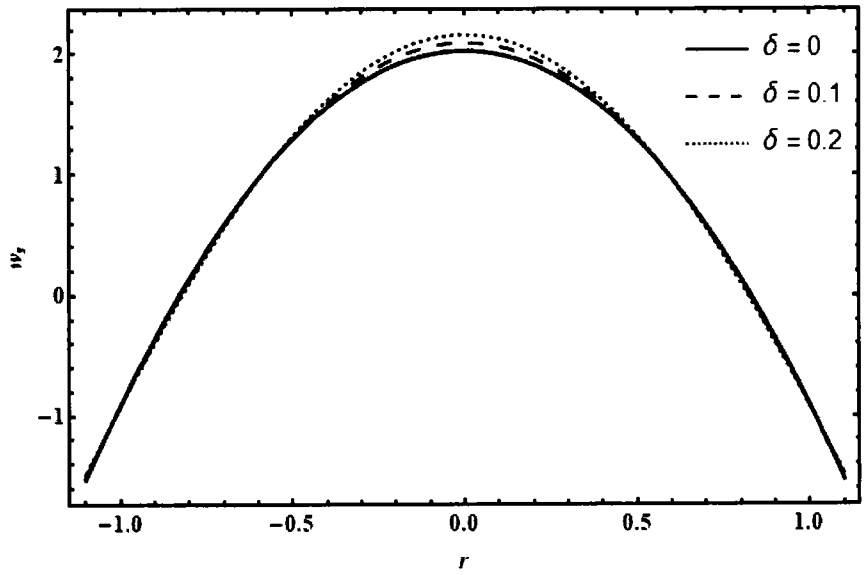

Fig. 6.17: Velocity presentation of solid grains for $\phi = 0.15,\ Q = 0.9,\ Re = 5, A = 1, B = 1, \alpha_1 = 1.5, Q_s = 0.7.$

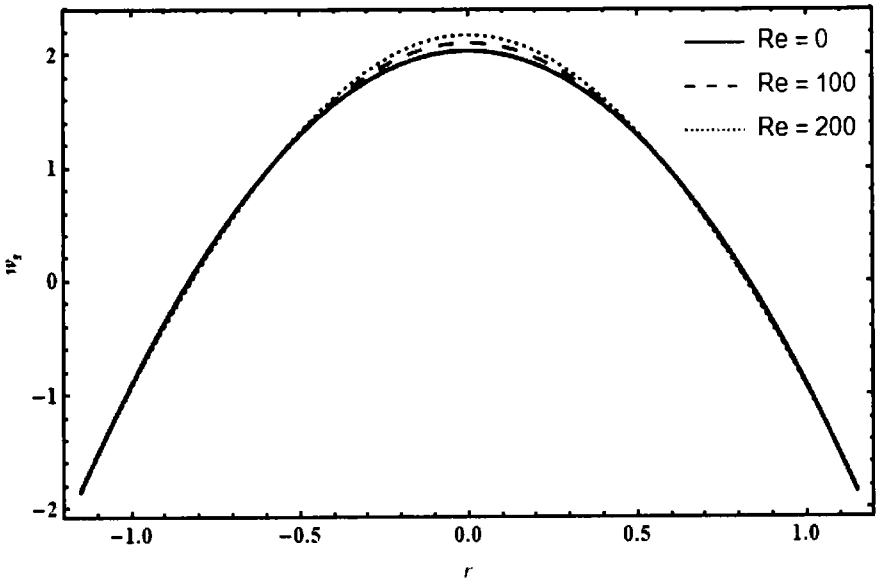

Fig. 6.18: Velocity presentation of solid grains for $\phi = 0.15,\ Q = 0.9,\ \delta = 0.5, A = 1, B = 1, \alpha_1 = 1.5, Q_s = 0.7.$

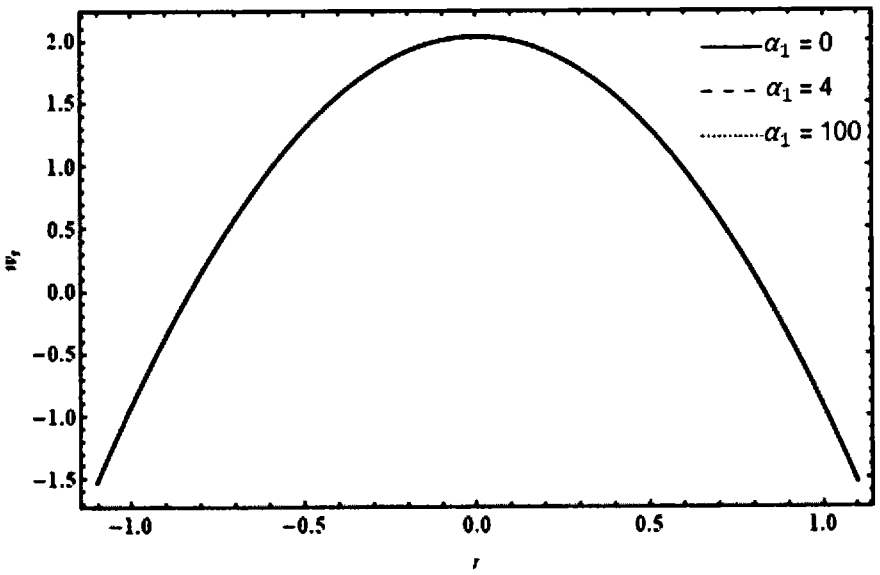

Fig. 6.19: Velocity presentation of solid grains for $\phi = 0.15,\ Q = 0.9,\ \delta = 0.5, A = 1, B = 1,\ Re = 10, Q_s = 0.7.$

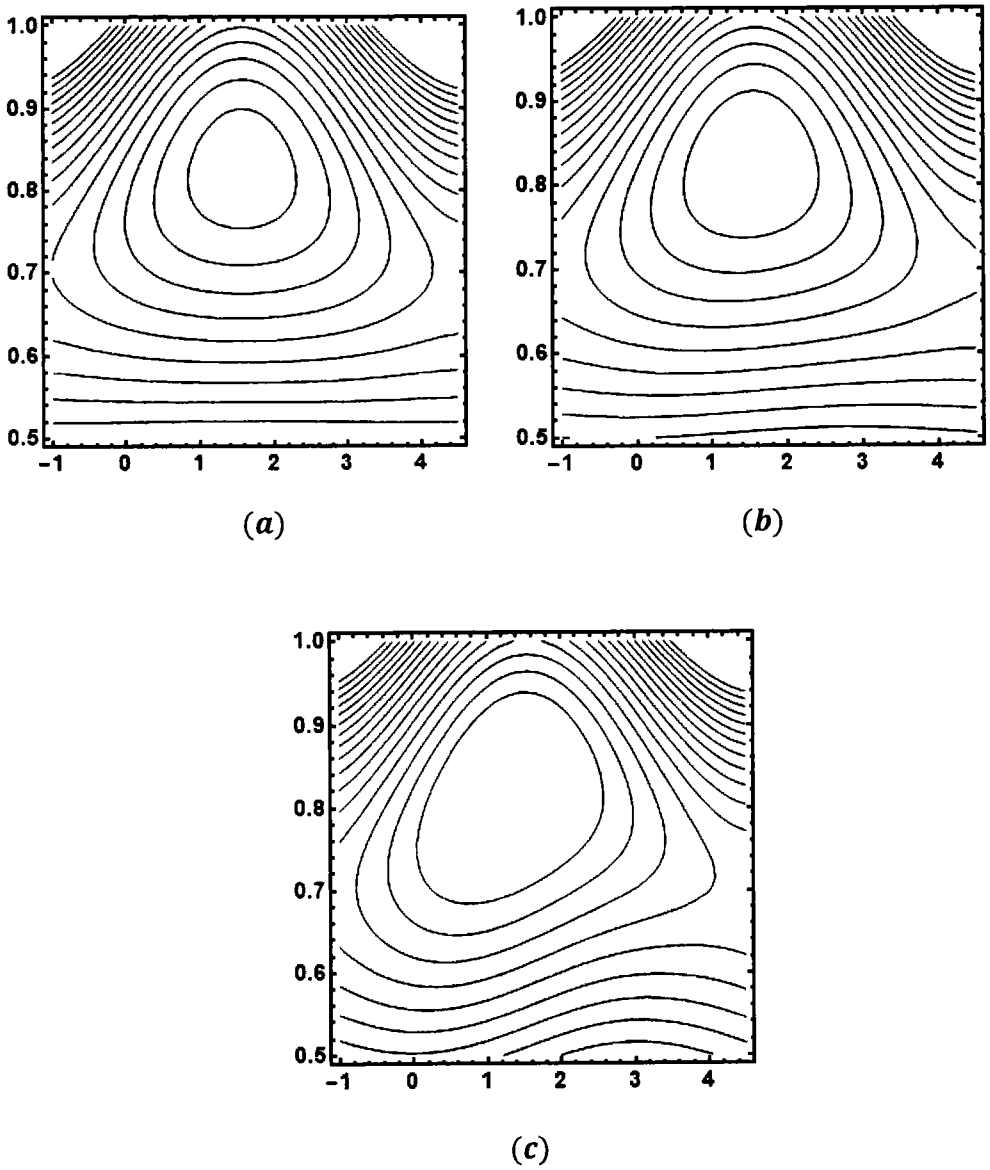

Fig. 6.20: Streamline presentation of solid grains for $(a)\ \delta = 0\ (b)\ \delta = 0.1\ (c)\ \delta = 0.5$ with $\phi = 0.1, \alpha_1 = 5, A = 1, B = 2, Re = 50, Q = 0.6, Q_s = 0.6$.

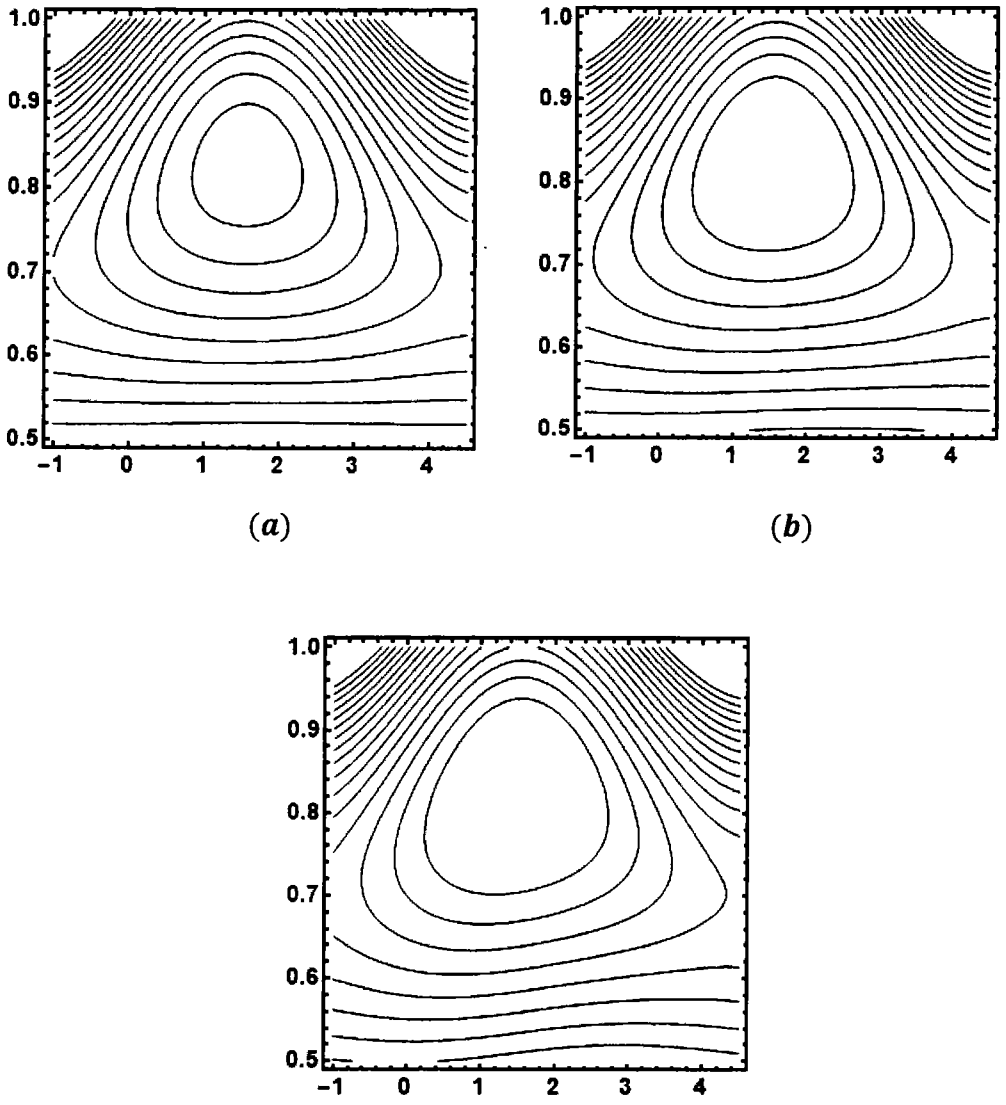

Fig. 6.21: Streamline presentation of solid grains for (a) $Re = 0$ (b) $Re = 50$ (c) $Re = 100$ with $\phi = 0.1, \alpha_1 = 1.5, A = 1, B = 2, \delta = 0.05, Q = 0.6, Q_s = 0.6$.

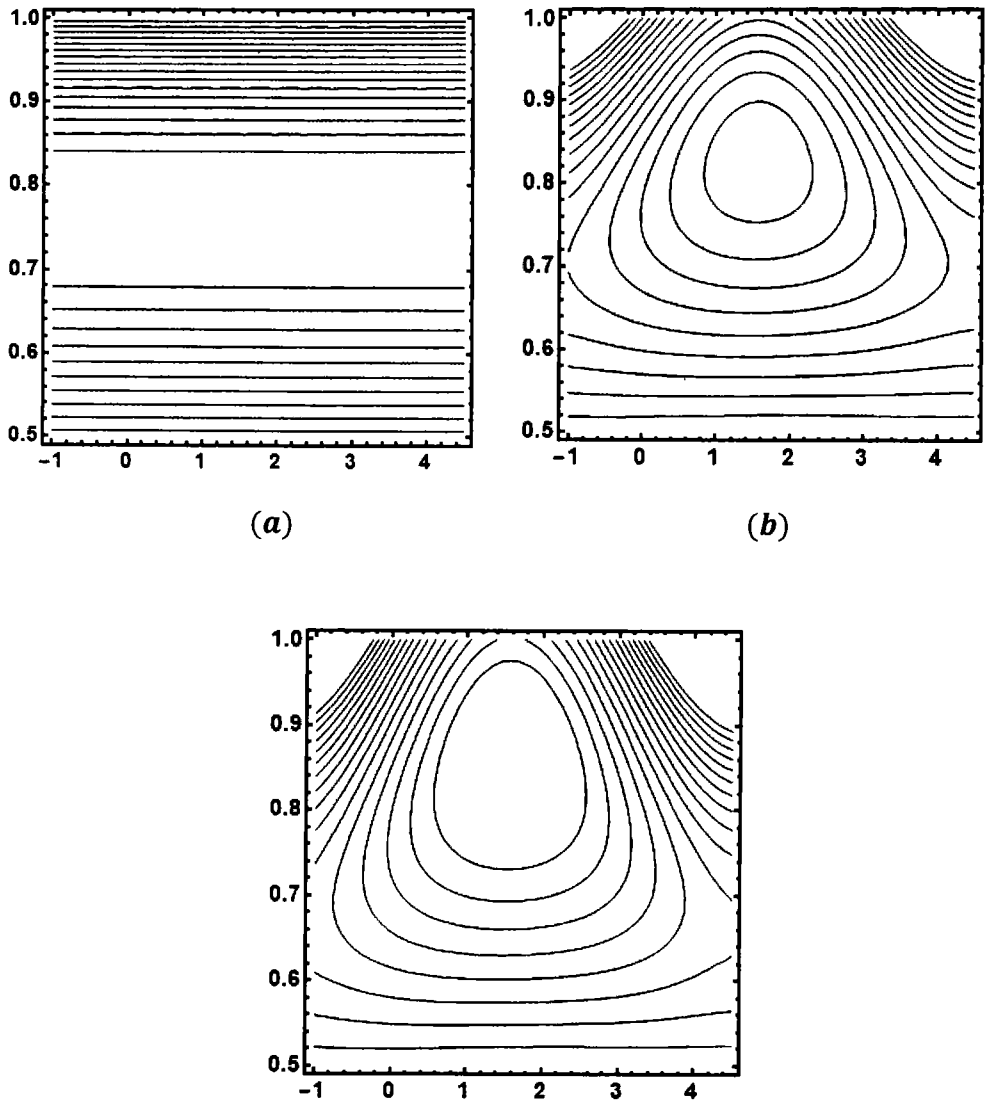

Fig. 6.22: Streamline presentation of solid grains for $(a)\ \phi = 0\ (b)\ \phi = 0.1\ (c)\ \phi = 0.15$ with $Q_s = 0.6, \alpha_1 = 1.5, A = 1, B = 2, \delta = 0.05, Q = 0.6, Re = 5.$

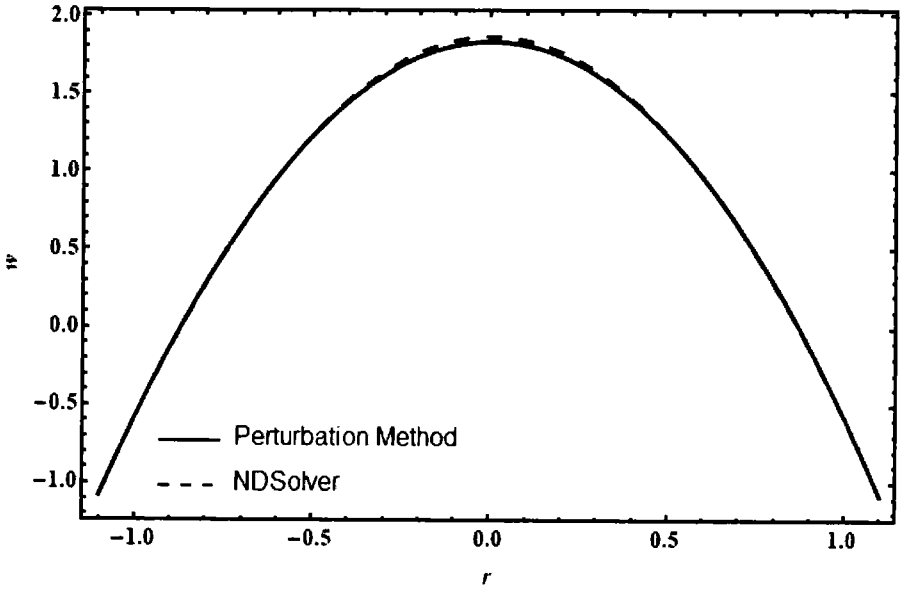

Fig. 6.23: Comparison between perturbation method and numerical method with $\varphi = 0.15, Q_s = 0.6, \alpha_1 = 0.5, A = 1, B = 2, \delta = 0.02, Q = 0.6, Re = 5.$

6.5 Conclusions

In this article, we studied the second-grade fluid containing fine dust grains in a tube. Perturbation technique up to $O(\delta^2)$ has been imposed to get the solutions. The results are shown through graphs. Following results are worth mentioning:

- The bolus expands for solid grains and fluid as the wave number enhances.
- The trapped bolus expands for dust grains and the fluid as Reynolds number *(Re)* is increased.
- The bolus is stretched to the upward direction of the channel as the amplitude ratio is increased.
- Growth in the velocity of the solid grains and the fluid for the parameter δ and Re.
- In retrograde region, pumping rate increases with the increase in α_1 and it decreases for increased values of δ.

Chapter 7

Theoretical Analysis of Peristaltic Viscous Fluid with Inhomogeneous Dust Particles

This chapter deals with the inhomogeneous behavior of the solid grains suspended in the fluid. The number density of the dust grains is taken as variable. The coupled equations for solid granules and the fluid under long wavelength have been modelled. Streamline transformations have been invoked and results are discussed through graphs.

7.1 Problem Formulation

Assuming the incompressible viscous dusty fluid flowing through an asymmetric passage. The dust particles are solid spherical particles which are not uniformly distributed in the channel and their number density $N(y)$ is dependent on y. The walls of the channel are presumed to be tempted by peristaltic wave. The amplitudes of the waves are denoted by a_1 and b_1. The width of the passage is given by $d_1 + d_2$. λ is the wave length and the phase difference is given by ϕ. The walls are defined as

$$H_1(\bar{X},\bar{t}) = d_1 + a_1 sin\left[\frac{2\pi}{\lambda}(\bar{X} - c\bar{t})\right], \tag{7.1}$$

$$H_2(\bar{X},\bar{t}) = -d_2 - a_2 sin\left[\frac{2\pi}{\lambda}(\bar{X} - c\bar{t}) + \phi\right]. \tag{7.2}$$

The ruling equations for the fluid are

$$\frac{\partial \bar{U}}{\partial \bar{X}} + \frac{\partial \bar{V}}{\partial \bar{Y}} = 0, \tag{7.1}$$

$$\frac{d}{dt}(\bar{U}) = \nu \nabla^2(\bar{U}) - \frac{1}{\rho}\frac{\partial P}{\partial x} + \frac{1}{\rho} kN(\bar{Y})(\bar{U}_s - \bar{U}), \tag{7.2}$$

$$\frac{d}{dt}(\bar{V}) = \nu \nabla^2(\bar{V}) - \frac{1}{\rho}\frac{\partial P}{\partial y} + \frac{1}{\rho} kN(\bar{Y})(\bar{V}_s - \bar{V}). \tag{7.3}$$

For the dust particles, governing equations are

$$\frac{\partial (N(\bar{Y})\bar{U}_s)}{\partial \bar{X}} + \frac{\partial (N(\bar{Y})\bar{V}_s)}{\partial \bar{Y}} = 0, \tag{7.4}$$

$$\frac{\partial \bar{U}_s}{\partial \bar{t}} + \bar{U}_s \frac{\partial \bar{U}_s}{\partial \bar{X}} + \bar{V}_s \frac{\partial \bar{U}_s}{\partial \bar{Y}} = \frac{k}{m}(\bar{U} - \bar{U}_s), \tag{7.5}$$

$$\frac{\partial \bar{V}_s}{\partial \bar{t}} + \bar{U}_s \frac{\partial \bar{V}_s}{\partial \bar{X}} + \bar{V}_s \frac{\partial \bar{V}_s}{\partial \bar{Y}} = \frac{k}{m}(\bar{V} - \bar{V}_s). \tag{7.6}$$

Using the following transformations given below to convert the fixed frame into wave frame

$$\bar{p}(\bar{x}) = \bar{P}(\bar{X}, \bar{t}), \bar{y} = \bar{Y}, \bar{x} = \bar{X} - c\bar{t}, \ \bar{v} = \bar{V}, \ \bar{u} = \bar{U} - c, \bar{u}_s = \bar{U}_s - c, \ \bar{v}_s = \bar{V}_s. \tag{7.7}$$

By introducing the non-dimensional variables and parameters

$$p = \frac{\bar{p} d_1^2}{\mu \lambda c}, \quad x = \frac{\bar{x}}{\lambda}, \quad y = \frac{\bar{y}}{d_1}, \quad u = \frac{\bar{u}}{c}, \quad v = \frac{\bar{v}}{c}, \quad N(y) = \frac{N(\bar{y})}{N_0},$$

$$S^* = \frac{S d_1}{\mu c}, \quad a = \frac{a_1}{d_1}, \quad b = \frac{a_2}{d_1}, \quad d = \frac{d_2}{d_1}, \ Re = \frac{\rho c d_1}{\mu}, \quad \delta = \frac{d}{\lambda}.$$

$$u = \frac{\partial \psi}{\partial y}, \quad v = -\delta \frac{\partial \psi}{\partial x}, \quad u_s = \frac{\partial \varphi}{\partial y}, \ v_s = -\delta \frac{\partial \varphi}{\partial x}. \tag{7.8}$$

The continuity equation of the fluid is satisfied identically and momentum equations become

$$\delta Re\left(\frac{\partial\psi}{\partial y}\frac{\partial^2\psi}{\partial x\partial y}-\frac{\partial^2\psi}{\partial y^2}\frac{\partial\psi}{\partial x}\right)$$

$$=\left(\frac{\partial^3\psi}{\partial y^3}+\delta^2\frac{\partial^3\psi}{\partial x^2\partial y}\right)+AN(y)\left(\frac{\partial\varphi}{\partial y}-\frac{\partial\psi}{\partial y}\right)-\frac{\partial p}{\partial x}, \tag{7.9}$$

$$\delta^3 Re\left(\frac{\partial\psi}{\partial x}\frac{\partial^2\psi}{\partial y\partial x}-\frac{\partial^2\psi}{\partial x^2}\frac{\partial\psi}{\partial y}\right)$$

$$=-\delta^2\left(\frac{\partial^3\psi}{\partial x\partial y^2}+\delta^2\frac{\partial^3\psi}{\partial x^3}\right)+AN(y)\delta^2\left(\frac{\partial\psi}{\partial x}-\frac{\partial\varphi}{\partial x}\right)-\frac{\partial p}{\partial y}, \tag{7.10}$$

For further investigation, we consider the density of the solid particles in the non-dimensional form as

$$N(y)=e^{-\zeta y}=1-\zeta y. \tag{7.11}$$

The compatibility equation for fluid and solid particles is

$$\delta Re\left(\frac{\partial\psi}{\partial y}\frac{\partial}{\partial x}(\nabla_1^2\psi)-\frac{\partial\psi}{\partial x}\frac{\partial}{\partial y}(\nabla_1^2\psi)\right)$$

$$=\nabla_1^4\psi+A(1-\zeta y)(\nabla_1^2\varphi-\nabla_1^2\psi)-\zeta A\left(\frac{\partial\varphi}{\partial y}-\frac{\partial\psi}{\partial y}\right). \tag{7.12}$$

$$\delta\left(\frac{\partial\phi}{\partial y}\frac{\partial}{\partial x}\nabla_1^2\varphi-\frac{\partial\phi}{\partial x}\frac{\partial}{\partial y}\nabla_1^2\varphi\right)=B(\nabla_1^2\psi-\nabla_1^2\varphi), \tag{7.13}$$

The geometry of the channel in non-dimensional form is

$$h_1=1+a\cos 2\pi x, \tag{7.14}$$

$$h_2=-d-b\cos(2\pi x+\phi). \tag{7.15}$$

7.2 Method of Solution

After adopting long wavelength and low Reynolds number assumptions, Eq. (7.12) and (7.13) reduces to

$$\frac{\partial^4\psi}{\partial y^4} + A(1-\zeta y)\left(\frac{\partial^2\varphi}{\partial y^2} - \frac{\partial^2\psi}{\partial y^2}\right) - \zeta A\left(\frac{\partial\varphi}{\partial y} - \frac{\partial\psi}{\partial y}\right) = 0, \tag{7.16}$$

$$B\left(\frac{\partial^2\psi}{\partial y^2} - \frac{\partial^2\varphi}{\partial y^2}\right) = 0, \tag{7.17}$$

with

$$\psi = \frac{F}{2}, \quad \frac{\partial\psi}{\partial y} + \beta\frac{\partial^2\psi}{\partial y^2} = -1, \quad \varphi = \frac{E}{2}, \quad at \quad y = h_1(x), \tag{7.18}$$

$$\psi = -\frac{F}{2}, \quad \frac{\partial\psi}{\partial y} - \beta\frac{\partial^2\psi}{\partial y^2} = -1, \quad \varphi = -\frac{E}{2}, \quad at \quad y = h_2(x). \tag{7.19}$$

NDSolver command in Mathematica has been taken in account to get the solutions and graphs of these equations. The impact of parameters is represented through graphs.

7.3 Results and Discussion

This section is the description of the results presented in the form of graphs. The influence of the variable density co-efficient and the slip parameter on the fluid velocity is shown in Figs. 7.1 and 7.2 respectively, while on the solid particles is presented in Figs. 7.3 and 7.4. The streamline patterns of fluid and dust particles are shown in Figs. 7.5 to 7.8.

The impact of the variable density coefficient ζ is depicted in Fig. 7.1. The density of the particle in the fluid can be defined as the proportion between the mass of the

particle to the amount of space it takes up. Increase in the density means that more dust particles are concentrated in the fluid. We can observe in the Fig. 7.1 that as the particles are increased in the fluid, the velocity increases in the region [0, 1.5] and the fluid velocity is maximum at the center of the channel. As more dust particles are concentrated in the fluid, the channel is pushed in the direction of the fluid. The slip parameter is given by β. When the flow of the molecules at the boundaries of the channel have no stationary motion then this phenomenon is referred as slip condition. It can be deduced from Fig. 7.2 that as the slip parameter is increased, the velocity decays in the center of the passage while at the boundaries of the passage it increases. Fig. 7.3 demonstrates the velocity of the dust particles. It can be perceived in the figure that as the density of the dust granules is growing, the speed of the flow is gained in the region near the lower wall. The variation of the slip parameter on the velocity of the dust granules. It can be learned from the figure that the dust particles are behaving in the similar manner as the fluid i.e. the velocity reduces at the middle of the channel while increases at the boundaries.

Fig. 7.5 is the graphical representation of streamline patterns for different values of ζ. With the increase in the density parameter, the bolus in the upper part of channel compresses and the bolus in the lower part of the channel expands thus squeezing the bolus in the upper portion. The impact of slip parameter on the streamline patterns of the fluid is shown in Fig. 7.6. The bolus enlarges as the slip is increased. For the dust particles, the trapped bolus can be seen flourishing in the lower portion of the passage as the density is growing as displayed in Fig. 7.7. The impact of slip on the dust particles streamline patterns is shown in Fig. 7.8. The bolus expands in the lower part of the channel.

7.4 Graphs

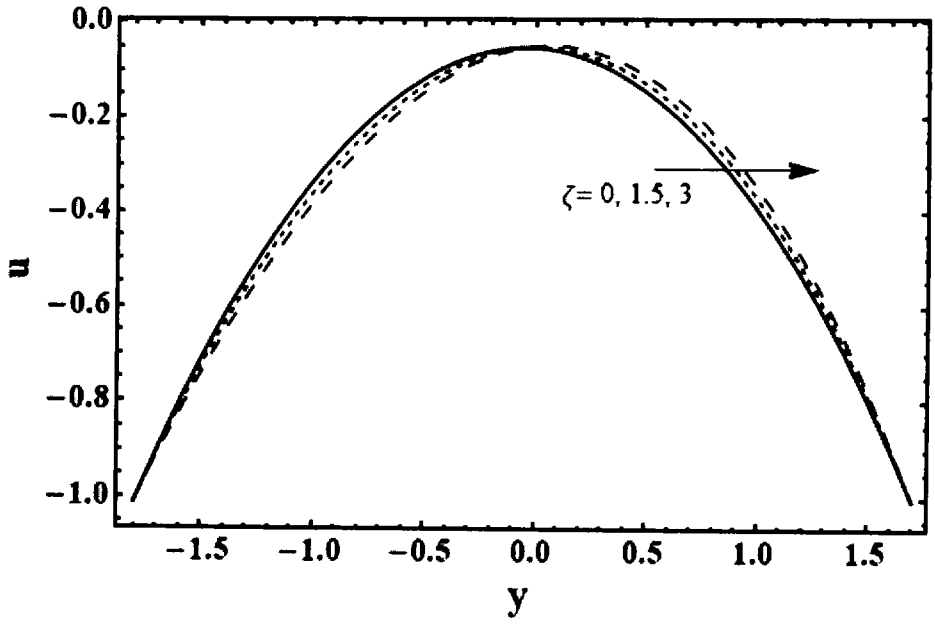

Figure 7.1: Displays the effect of ζ on velocity of the fluid with $B = 0.75, A = 1.5,$ $d = 1, b = 0.8, a = 0.6, \phi = \frac{\pi}{6}, Q = 0.9, Q_s = 0.8, \beta = 0.1.$

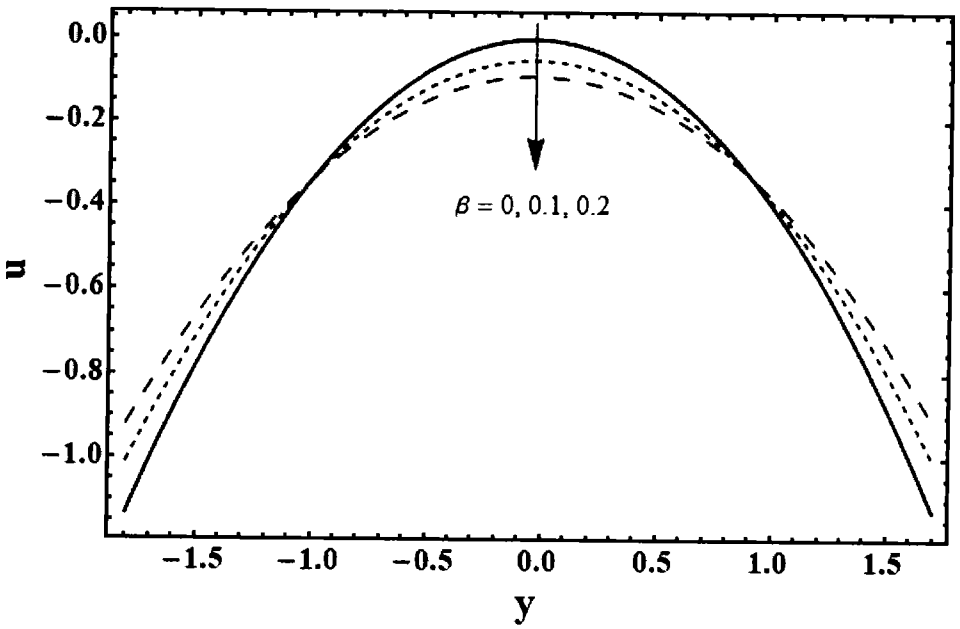

Figure 7.2: Displays the effect of β on velocity of the fluid with $B = 0.75, A =$ $1.5, d = 1, b = 0.8, a = 0.6, \phi = \frac{\pi}{6}, Q = 0.9, Q_s = 0.8, \zeta = 0.2.$

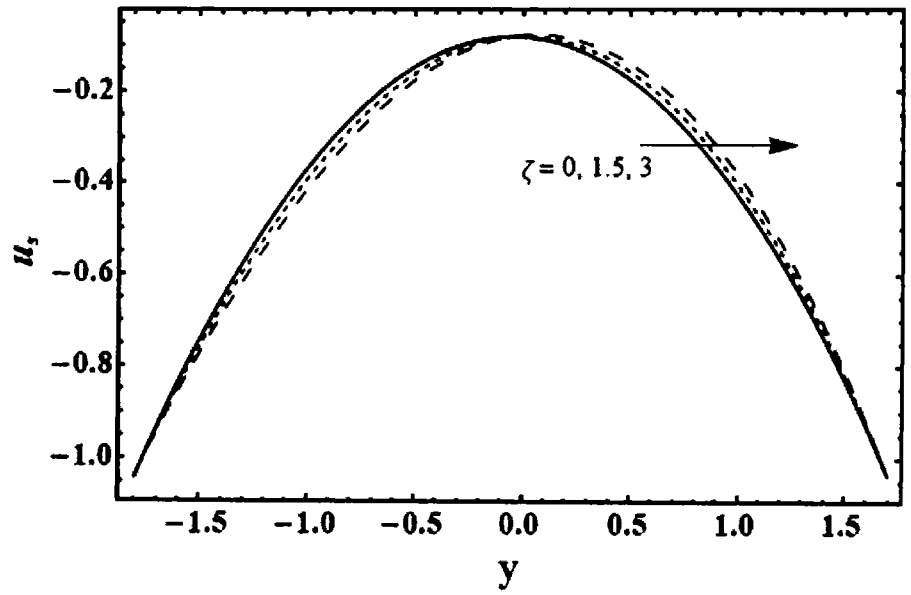

Figure 7.3: Displays the effect of ζ on velocity of the solid particles with $B = 0.75, A = 1.5, d = 1, b = 0.8, a = 0.6, \phi = \frac{\pi}{6}, Q = 0.9, Q_s = 0.8, \beta = 0.1$.

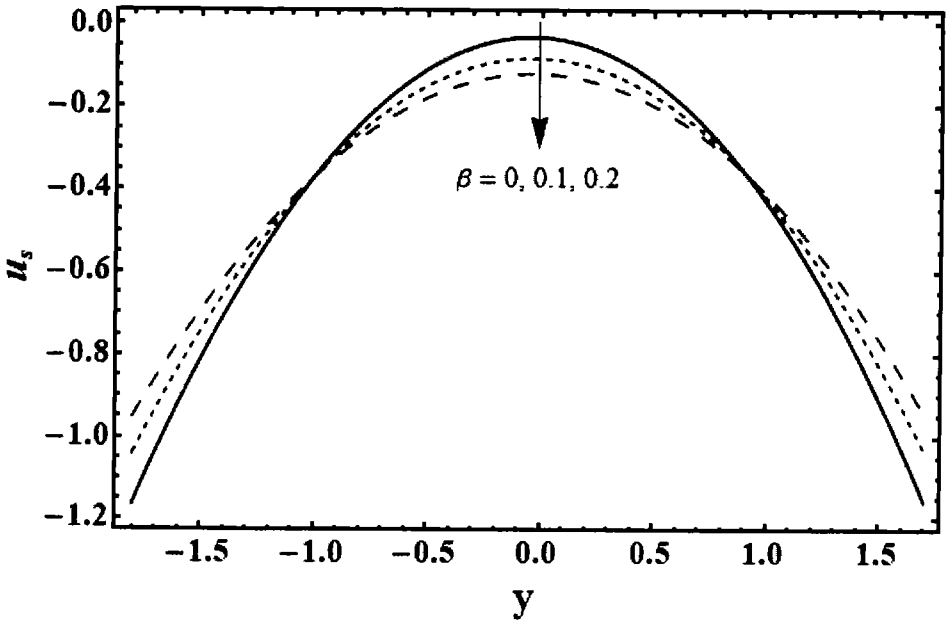

Figure 7.4: Displays the effect of β on velocity of the solid particles with $B = 0.75, A = 1.5, d = 1, b = 0.8, a = 0.6, \phi = \frac{\pi}{6}, Q = 0.9, Q_s = 0.8, \zeta = 0.2$.

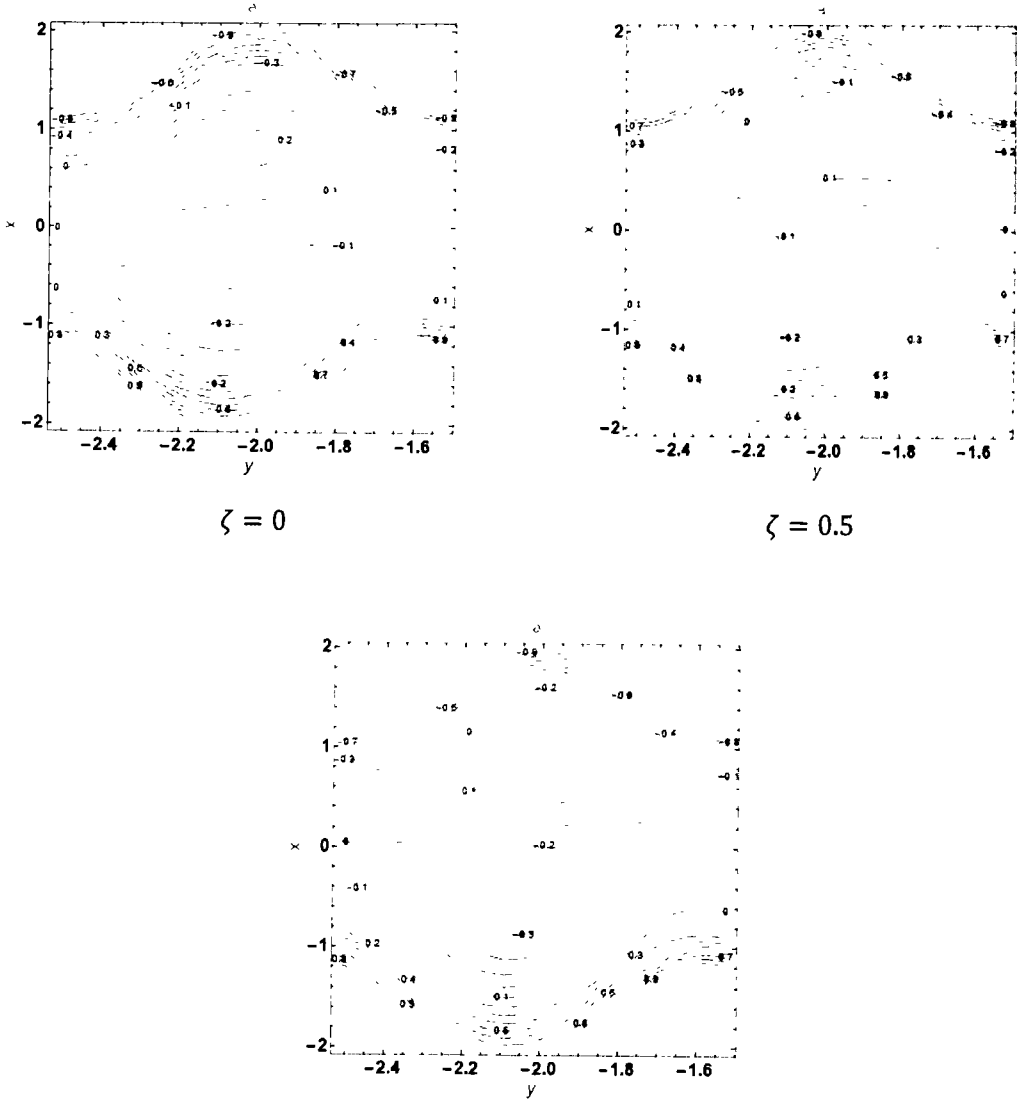

Figure 7.5: Depicts the streamline graphs of fluid for different values of ζ with $A = 1.5, B = 0.75, Q_s = 0.1, d = 1, \phi = \frac{\pi}{6}, a = 0.4, \beta = 0.1, b = 0.4, Q = 2.$

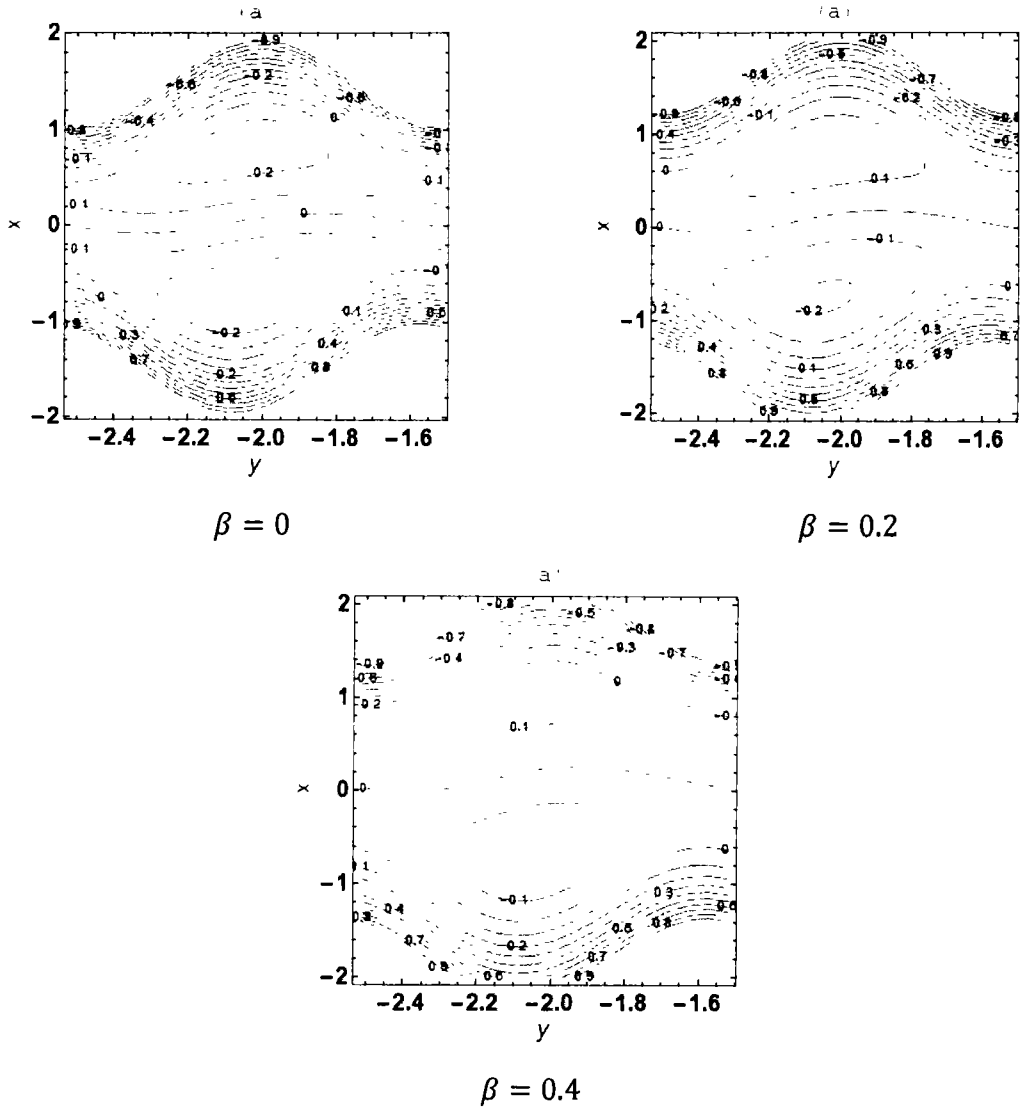

$\beta = 0$ $\beta = 0.2$

$\beta = 0.4$

Figure 7.6: Depicts the streamline pattern of fluid for different values of β with $A = 1.5, B = 0.75, Q_s = 0.1, d = 1, \phi = \frac{\pi}{6}, a = 0.4, \zeta = 0.1, b = 0.4, Q = 2.$

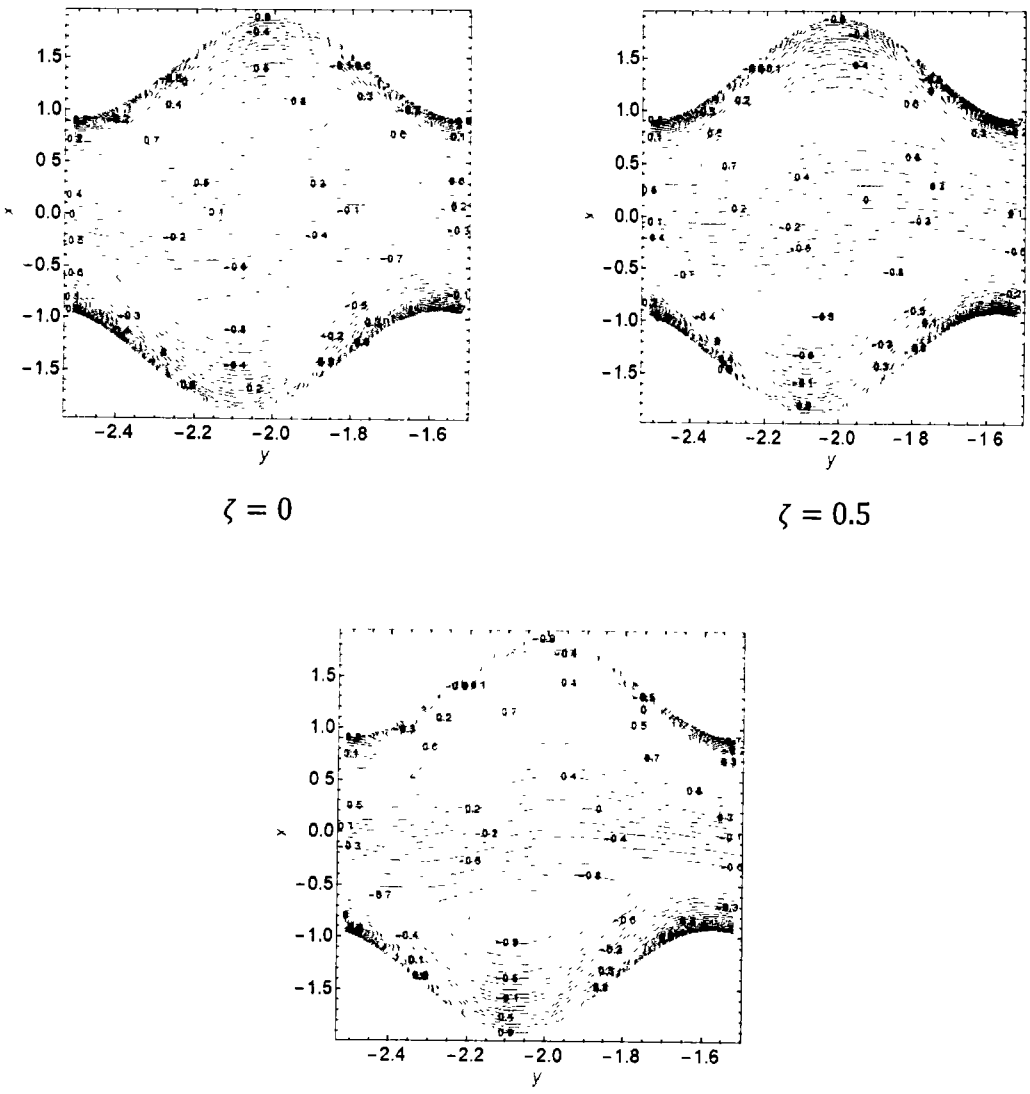

Figure 7.7: Depicts the streamline pattern of solid for different values of ζ with $A = 1.5, B = 0.75, Q_s = 3, d = 1, \phi = \frac{\pi}{6}, a = 0.4, \beta = 0.1, b = 0.4, Q = 3.$

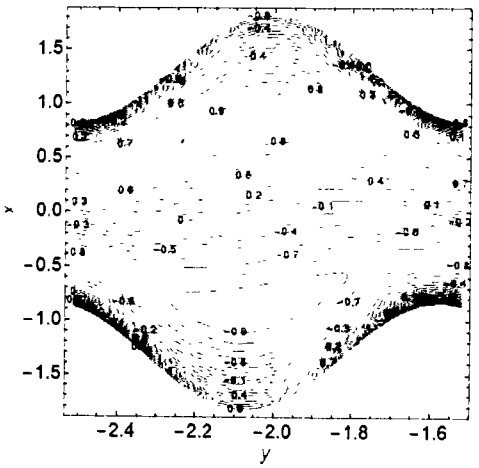

$\beta = 0$

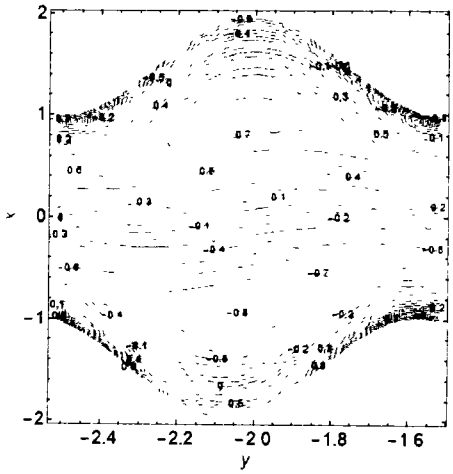

$\beta = 0.2$

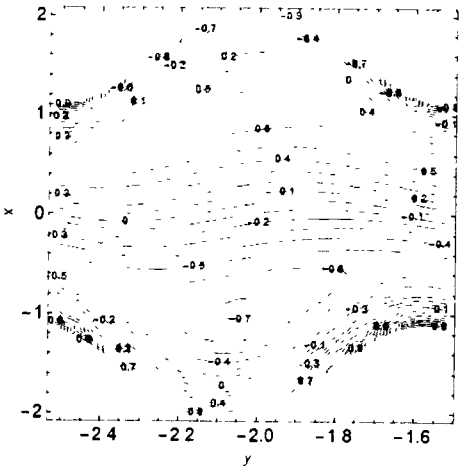

$\beta = 0.4$

Figure 7.8: Depicts the streamline pattern of solid for diverse values of β with $A = 1.5, B = 0.75, Q_s = 3, d = 1, \phi = \frac{\pi}{6}, a = 0.4, \zeta = 0.1, b = 0.4, Q = 3.$

7.5 Conclusion

Incompressible viscous fluid consisting dust particles is supposed to be flowing through an asymmetric channel. The number density of the dust grains is taken as variable. Following key results are obtained in this study:

- As the number density variable is increased, the velocity increases in the region near lower wall while it decreases in upper wall region.
- The velocity rises at the boundaries of the channel while it decreases at the center of the passage as the slip constraint is increased for the fluid as well as solid granules.
- Bolus enlarges in the lower part of the passage, with the increase in number density of dust particles.
- As the slip parameter increase, the trapped bolus broadens.

Chapter 8

Peristaltic Flow of a Dusty Electrically Conducting Fluid Through a Porous Medium in an Endoscope

The impact of MHD on peristaltic flow of a dusty fluid in an endoscope has been discussed in this chapter. The porous space inside the concentric tube is filled with an incompressible fluid. The outer tube wall is flexible while the inner tube is rigid. Coupled equations for both the solid granules and the fluid have been modelled by supposing long wavelength and low Reynolds number assumptions. The results are attained analytically and presented through graphs. The impact of different parameters on velocity, pressure rise and streamlines have been included.

8.1 Problem Formulation

Considering that viscous dusty incompressible fluid is flowing past a co-axial tube. The space between the inner and outer tube is filled up with the dusty fluid. The inner tube is rigid while the outer tube exhibits the peristaltic behavior. An even applied magnetic field B_0 makes the fluid to be electrically conducting. The induced magnetic field can be ignored for smaller magnetic Reynolds number. Cylindrical polar coordinates $(\bar{R}, \bar{Z})$ represent the radial and the centerline of the tubes. Mathematically two walls can be described as

$$r_1 = a_1, \tag{8.1}$$

$$r_2 = a_2 + b\sin\frac{2\pi}{\lambda}(z - ct), \tag{8.2}$$

a_1 is the radius of the inner tube and outer tube's radius is a_2. To avoid unsteady flow the transformation given below has been taken into account.

$$V = v + c, \qquad U = u, \qquad R = r, \qquad Z = z + ct. \tag{8.3}$$

The ruling equations of the dusty MHD fluid and the dust granules flowing past a porous tube are given as

$$\frac{\partial v}{\partial z} + \frac{u}{r^2} + \frac{\partial u}{\partial r} = 0, \tag{8.4}$$

$$\rho\left(u\frac{\partial u}{\partial r} + v\frac{\partial u}{\partial z}\right) = \mu\left(\frac{\partial^2 u}{\partial r^2} + \frac{\partial^2 u}{\partial z^2} - \frac{u}{r^2} + \frac{1}{r}\frac{\partial u}{\partial r}\right) - \frac{\partial p}{\partial r} - \frac{\mu\phi}{k_0}u + Nk(u_s - u), \tag{8.5}$$

$$\rho\left(u\frac{\partial v}{\partial r} + v\frac{\partial v}{\partial z}\right) = \mu\left(\frac{\partial^2 v}{\partial r^2} + \frac{\partial^2 v}{\partial z^2} + \frac{1}{r}\frac{\partial v}{\partial r}\right) - \frac{\partial p}{\partial z} + Nk(v_s - v) - \left(\sigma B_0^2 + \frac{\mu\phi}{k_1}\right)(v + c), \tag{8.6}$$

$$\frac{\partial v_s}{\partial z} + \frac{u_s}{r^2} + \frac{\partial u_s}{\partial r} = 0, \tag{8.7}$$

$$\rho\left(u_s\frac{\partial u_s}{\partial r} + v_s\frac{\partial u_s}{\partial z}\right) = \frac{k}{m}(u - u_s) - \frac{\partial p}{\partial r}, \tag{8.8}$$

$$\rho\left(u_s\frac{\partial v_s}{\partial r} + v_s\frac{\partial v_s}{\partial z}\right) = \frac{k}{m}(v - v_s) - \frac{\partial p}{\partial z}. \tag{8.9}$$

The relevant boundary conditions are

$$v = -c, \qquad u = 0 \qquad at \qquad r = r_1, \tag{8.10}$$

$$v = -c \qquad at \qquad r = r_2 = a_2 + b\,sin\frac{2\pi}{\lambda}z\,. \tag{8.11}$$

The non-dimensional quantities that have been employed are

$$\bar{r} = \frac{r}{a_2},\quad \bar{r_1} = \frac{r_1}{a_2} = \frac{a_1}{a_2} = \varepsilon < 1,\ \bar{z} = \frac{z}{\lambda},\ \bar{p} = \frac{a^2 p}{\lambda\mu c},\ \bar{v} = \frac{v}{c},\ \frac{1}{K} = \frac{\phi a_2^2}{k_1},\quad \bar{u} = \frac{u}{\delta c},\ \delta =$$

$$\frac{a_2}{\lambda},\ \theta = \frac{b}{a_2},\ \bar{r}_2 = \frac{r_2}{a_2} = 1 + \theta\, sin2\pi z,\ M^2 = \frac{\sigma B_0^2 a_2^2}{\mu}. \tag{8.12}$$

Under the long wavelength and low Reynolds number assumption, the system of equations after dropping the bar is given as

$$\frac{\partial v}{\partial z} + \frac{u}{r^2} + \frac{\partial u}{\partial r} = 0, \tag{8.13}$$

$$\frac{dp}{dr} = 0, \tag{8.14}$$

$$\frac{dp}{dz} = A(u_s - u) + \frac{1}{r}\frac{\partial v}{\partial r} + \frac{\partial^2 v}{\partial r^2} - l^2(v+1), \tag{8.15}$$

$$\frac{dp}{dz} = B(u - u_s), \tag{8.16}$$

with

$$v = -1, \qquad u = 0 \qquad at \qquad r = r_1, \tag{8.17}$$

$$v = -1 \qquad at \qquad r = r_2 = 1 + \theta\, sin2\pi z, \tag{8.18}$$

where $l^2 = \frac{1}{K} + M^2$.

For the laboratory frame, the rate of flow is specified by

$$\Theta = 2\pi \int_{r_1}^{r_2} V\, R\, dR. \tag{8.19}$$

By inducing Eq. (8.3) and after integration, the above equation becomes

$$\Theta = q + \pi c(r_2^2 - r_1^2), \tag{8.20}$$

where the flow rate is q in wave frame and it is described by

$$q = 2\pi \int_{r_1}^{r_2} v\, r\, dr. \tag{8.21}$$

The time-averaged flow rate is

$$\bar{Q} = \frac{1}{T}\int_0^T \Theta\, dt. \tag{8.22}$$

By inserting Eq. (8.20) into Eq. (8.22) and integration yields

$$\bar{Q} = q + \pi c\left(a_2^2 - a_1^2 + \frac{b^2}{2}\right). \tag{8.23}$$

The above equation becomes

$$\mathrm{Q} = F + \frac{1}{2}\left(1 - \varepsilon^2 + \frac{\theta^2}{2}\right), \tag{8.24}$$

where $\mathrm{Q} = \frac{\bar{Q}}{2\pi a_2^2 c}, F = \frac{q}{2\pi a_2^2 c}$ are the non-dimensional mean flows in laboratory and wave frames respectively.

The dimensionless volume flow rate is

$$F = \int_{\overline{r_1}}^{\overline{r_2}} \bar{r}\, \bar{v} dr. \tag{8.25}$$

8.2 Method of Solution

Exact solution of the Eq. (8.15) w.r.t boundary conditions Eq. (8.17) and Eq. (8.18) is

$$v(r,z) = C_1 I_0(lr) + C_2 K_0(lr) - \frac{1}{l^2}\left(\left(\frac{A}{B} - 1\right)\frac{dp}{dz} + l^2\right), \tag{8.24}$$

where modified Bessel functions of the first and second kinds are I_0 and K_0. Also,

$$C_1 = \frac{\left(K_0(l\varepsilon) - K_0(lr_2)\right)\left(\frac{A}{B} - 1\right)\frac{dp}{dz}}{l^2(I_0(lr_2)K_0(l\varepsilon) - I_0(l\varepsilon)K_0(lr_2))}, \tag{8.25}$$

$$C_2 = \frac{\left(I_0(lr_2) - I_0(l\varepsilon)\right)\left(\frac{A}{B} - 1\right)\frac{dp}{dz}}{\eta^2(I_0(lr_2)K_0(l\varepsilon) - I_0(l\varepsilon)K_0(lr_2))}. \tag{8.26}$$

The expression for $\frac{dp}{dz}$ is

$$\begin{aligned}\frac{dp}{dz} = \left(\frac{A}{B} - 1\right)^{-1} & (l^4(r_2^2 + 2F - \varepsilon^2)(I_0(lr_2)K_0(l\varepsilon) \\ & - I_0(l\varepsilon)K_0(lr_2)))(-l^2r_2^2I_2(\varepsilon r_2)K_0(\varepsilon l) \\ & - \varepsilon^2l^2I_2(\varepsilon l)K_0(lr_2) + l^2r_2^2I_0(\varepsilon l)K_2(r_2l) + \varepsilon^2l^2I_0(r_2l)K_2(l\varepsilon) - 4)^{-1}.\end{aligned} \tag{8.27}$$

If we consider $A = 4$ and $B = 2$ then similar results can be obtained as given by Afsar et al. [102].

8.3 Results and Discussion

To analyze the impact of parameters like magnetic field (M), porosity (K) and the concentration parameter (B) on the dusty fluid, graphs for pressure, velocity and streamline patterns are drawn. Figs. 8.1 and 8.2 exhibit the velocity profile of the fluid for the porous parameter α and magnetic field parameter (M). Increase in porosity results in increase of soaking in capacity of the medium thus resulting in decay of the velocity. Fig. 8.1 demonstrates that as the parameter K is enlarged, a notable decrease in the velocity can be observed. Decrease in the velocity can be observed in Fig. 8.2 by enhancing the Hartman number (M). Increase in electromagnetic force causes friction thus resulting drop in the velocity of the fluid.

Fig. 8.3 shows influence of α on the pressure rise. It can be observed the augmented pumping occurs for $0.1 < Q < 2$, no pumping occurs at $Q = 0.1$. Pressure rise of the fluid under the effect of Hartman number (M) can be seen in Fig. 8.4. The pressure rises in the pumping region with increase in (M). It can be deduced that as Hartman number is raised an additional pressure will be necessary to pump fluid. Fig. 8.5 shows the influence of concentration parameter (B) on the pressure rise of the fluid. At $Q = 0.1$, no pumping occurs, while peristaltic pumping occurs at $Q < 0.1$. As the concentration of the solid particles rises, increased pressure will be essential to pump the fluid. The radius ratio of the tube is denoted by ε. As the radius ratio is enlarged, lesser pressure is exerted by the fluid. Fig. 8.6 shows that impact of increase in ϵ as a reverse influence on the pressure rise.

Figs. 8.7 and 8.8 exhibit the trapping mechanism which is plotted as a result of contour. The streamlines in Fig. 8.7 show that influence of porous parameter. It can be concluded that with the rise in porosity the trapped bolus expands and is pushed outward. While for the magnetic parameter (M), the trapped bolus contracts.

8.4 Graphs

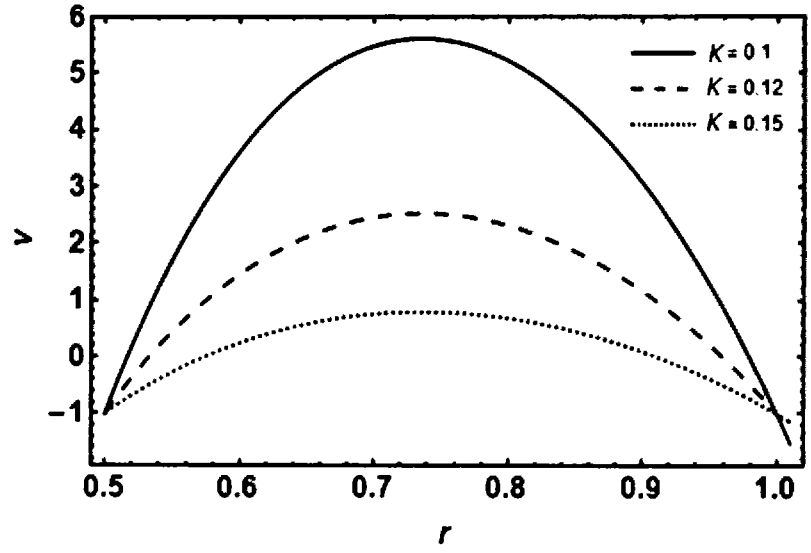

Figure 8.1: Velocity profile of the fluid for distinct values of K with $M = 0.4, \theta = 0.8, A = 2, B = 0.2, \varepsilon = 0.5, Q = 0.9$.

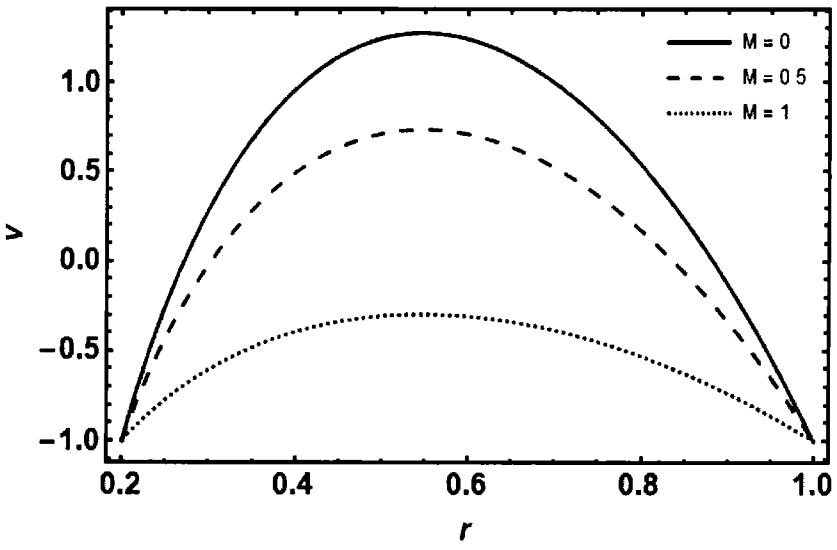

Figure 8.2: The velocity profile of the fluid for distinct values of M with $K = 0.4, \theta = 0.4, A = 2, B = 1.5, \varepsilon = 0.2, Q = 0.9$.

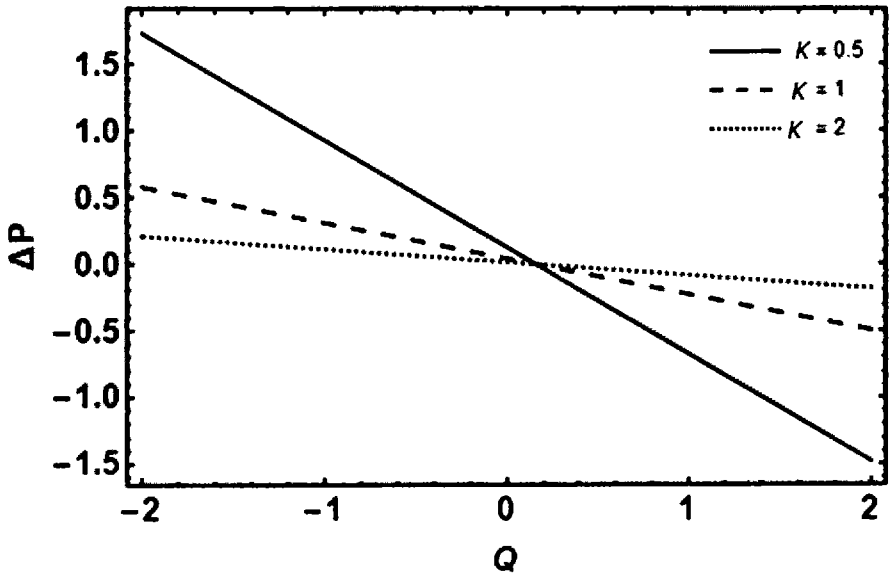

Figure 8.3: The pressure rise for distinct of K with $\varepsilon = 0.4, \theta = 0.8, A = 2, B = 0.2, M = 0.4$.

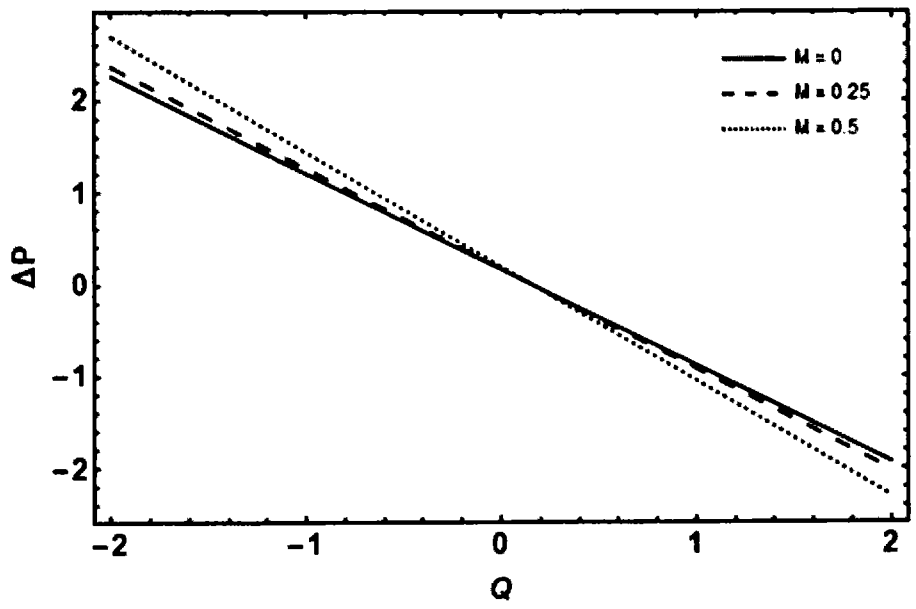

Figure 8.4: The pressure rise for distinct values of M with $K = 0.4, \theta = 0.8, A = 2, B = 0.2, \varepsilon = 0.5$.

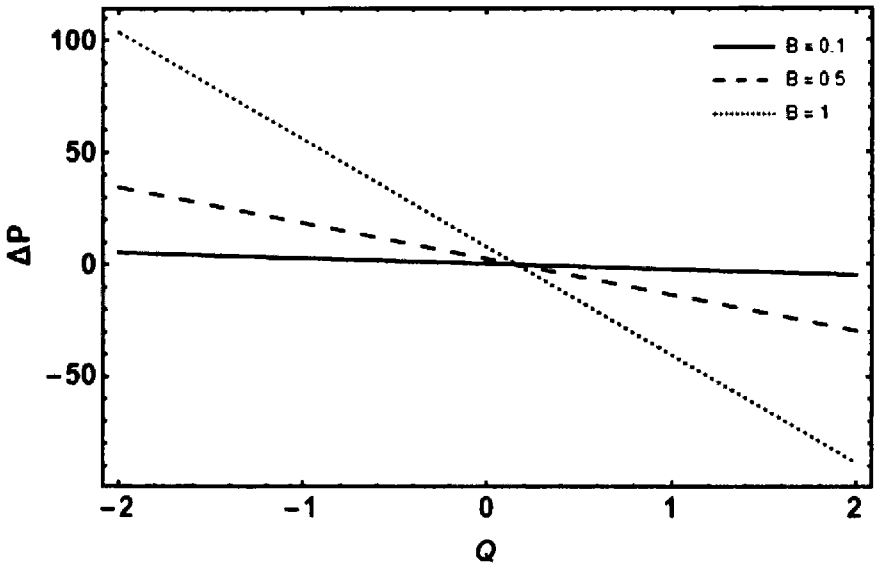

Figure 8.5: The pressure rise for distinct values of B with $K = 0.4, \theta = 0.8, A = 2, M = 0.5, \varepsilon = 0.2$.

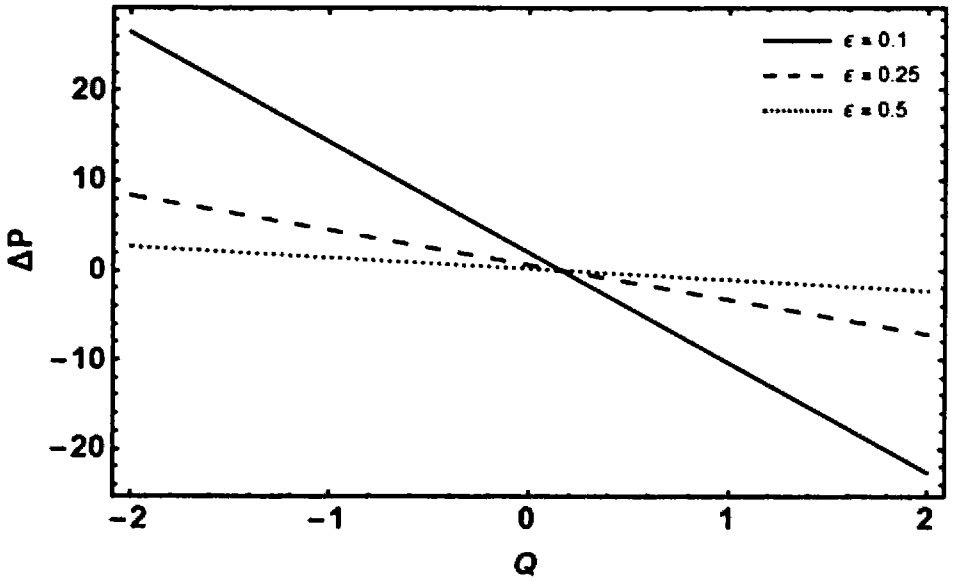

Figure 8.6: The pressure rise for distinct values of ϵ with $K = 0.4, \theta = 0.8, A = 2, B = 0.2, M = 0.5$.

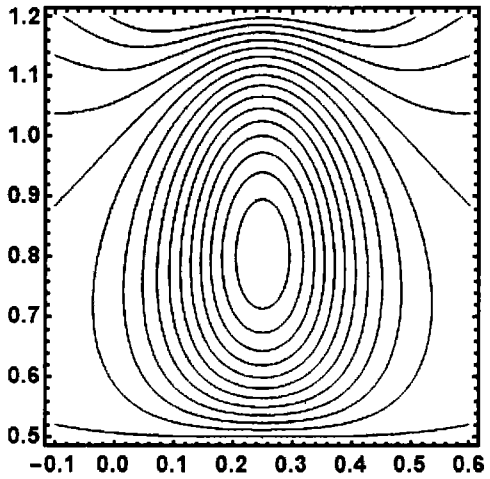

$K = 0.1$

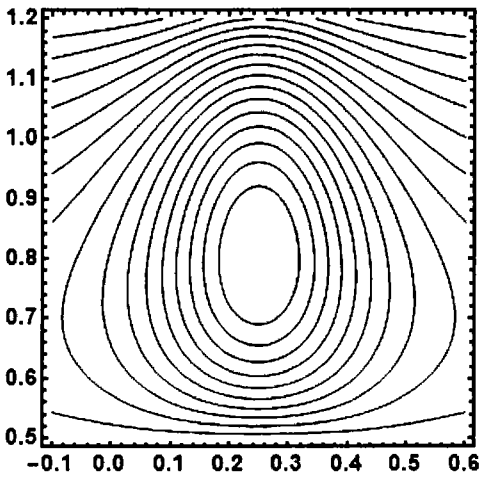

$K = 0.2$

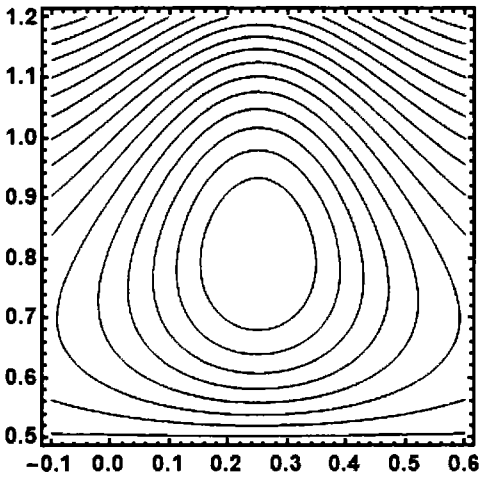

$K = 0.4$

Figure 8.7: Contour graphs of the fluid for distinct values of K with $M = 0.5, \theta = 0.15, A = 2, B = 3, \varepsilon = 0.5, Q = 1.5$.

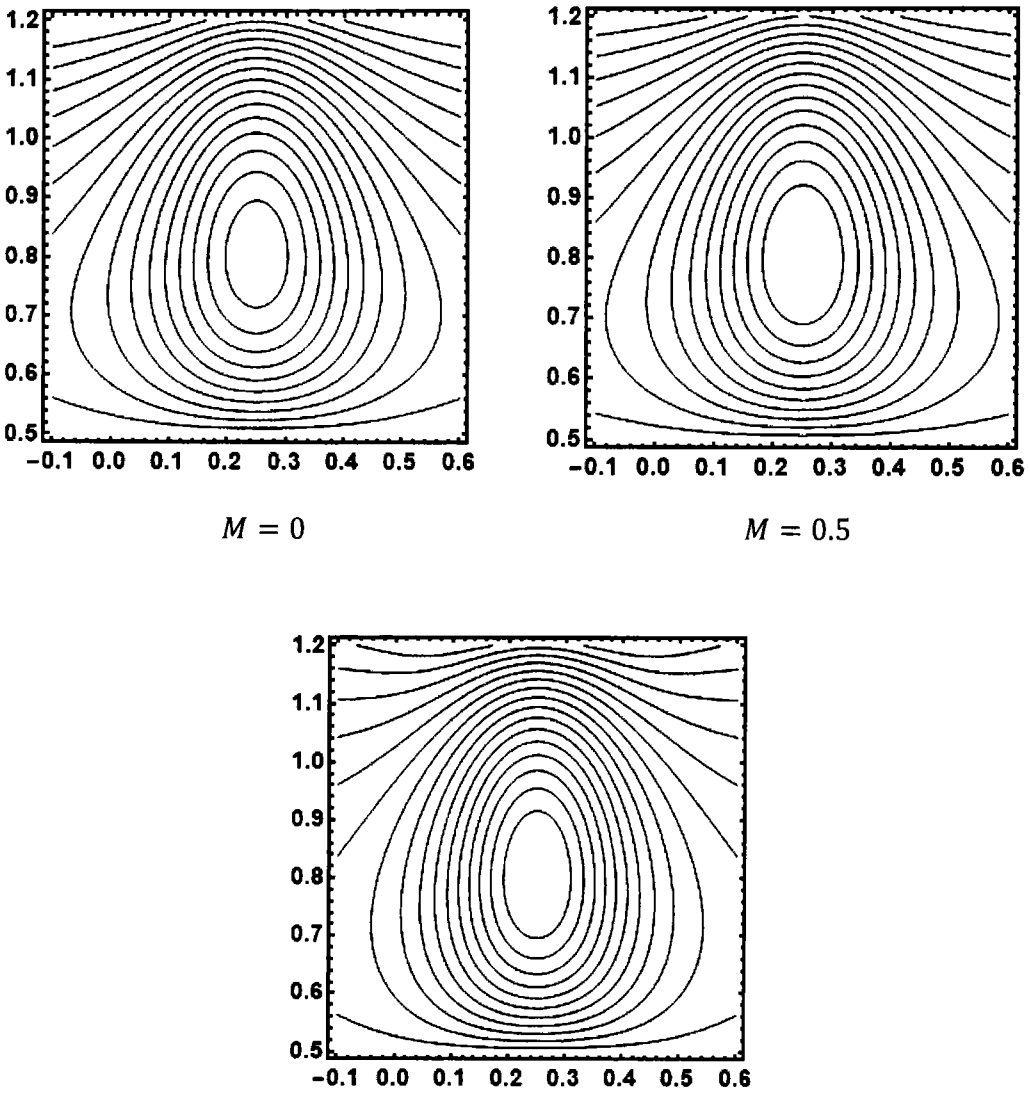

Figure 8.8: Contour graphs of the fluid for distinct values of M with $K = 0.2, \theta = 0.15, A = 2, B = 3, \varepsilon = 0.5, Q = 1.5$.

8.5 Conclusion

The chapter describes the peristaltic flow of dusty fluid through a porous annulus. The exact solution for pressure gradient and axial velocity are found. The conclusions that are worth mentioning are

- The velocity of the fluid decays for K i.e. the porous parameter.
- Increase in pressure rise can be spotted for M and B. They stimulate the motor activity of the wall.
- The trapped bolus inflated by increasing porous parameter.
- The trapped bolus compresses by increasing in M.

Chapter 9

Peristaltic Flow of a Second-Grade Dusty Fluid in a Curved Channel

The chapter addresses the peristaltic flow of dusty second-grade fluid flowing through a curved configuration. Coupled equations for dust granules and fluid have been derived by using small wave number approximation. The solutions are attained analytically and the concluded results are explained through graphs.

9.1 Problem Formulation

A two-dimensional curved channel whose thickness $2a$ is taken. A second-grade dusty fluid is flowing in a curved channel with the radial (r) and axial (a) velocities of the fluid and dust granules are given by u, v, u_s, v_s. Mathematically, the channel upper and lower walls are described as

$$H_1(\bar{X}, \bar{t}) = d_1 + a_1 sin\left[\frac{2\pi}{\lambda}(\bar{X} - c\bar{t})\right], \tag{9.1}$$

$$H_2(\bar{X}, \bar{t}) = -d_2 - a_2 sin\left[\frac{2\pi}{\lambda}(\bar{X} - c\bar{t}) + \phi\right]. \tag{9.2}$$

The continuity equation for the fluid and dust particles is

$$\left(R\frac{\partial}{\partial \bar{x}} + \frac{\partial}{\partial \bar{r}}(R + \bar{r})\right)\bar{V} = 0, \tag{9.3}$$

$$\left(\frac{\partial}{\partial \bar{r}}(R + \bar{r}) + R\frac{\partial}{\partial \bar{x}}\right)\bar{V}_s = 0. \tag{9.4}$$

The governing equations of momentum are given as

$$\rho\left(\frac{\partial \bar{V}}{\partial t} + (\bar{V}.\nabla)\bar{V}\right) = -\nabla\bar{P} + \nabla\bar{T} + kN(\bar{V}_s - \bar{V}), \tag{9.5}$$

$$\left(\frac{\partial \bar{V}_s}{\partial t} + (\bar{V}_s.\nabla)\bar{V}_s\right) = \frac{k}{m}(\bar{V} - \bar{V}_s), \tag{9.6}$$

For second-grade fluid, extra stress tensor is specified by $\bar{T}$.

$$\bar{T} = \mu\overline{A_1} + \alpha_1\overline{A_2} + \alpha_2\overline{A_1}^2, \tag{9.7}$$

$$\overline{A_1} = (grad\,\bar{V}) + (grad\,\bar{V})^t, \tag{9.8}$$

$$\overline{A_2} = \frac{d\bar{A}_1}{dt} + \overline{A_1}(grad\,\bar{V}) + (grad\,\bar{V})^t\overline{A_1}. \tag{9.9}$$

To consider the flow to be steady, the reference frame $(\bar{R}, \bar{X})$ is converted into laboratory frame $(\bar{r}, \bar{x})$ by using the conversions expressed as

$$\bar{u}_s = U_s - c, \quad \bar{x} = \bar{X} - c\bar{t}, \quad \bar{v}_s = V_s, \quad \bar{r} = \bar{R}, \quad \bar{u} = \bar{U} - c, \quad \bar{v} = \bar{V}, \tag{9.10}$$

The dimensionless quantities and the streamline functions that have been utilized are as follow:

$$x = \frac{\bar{x}}{\lambda}, \quad r = \frac{\bar{r}}{a}, u_s = \frac{\bar{u}_s}{c}, \quad u = \frac{\bar{u}}{c}, \quad C = \frac{R}{a}, v_s = \frac{\bar{v}_s}{\delta c}, \quad \delta = \frac{a}{\lambda},$$

$$v = \frac{\bar{v}}{\delta c}, \quad r = \frac{\bar{r}}{a}, Re = \frac{\rho c a}{\mu}, \quad T = \frac{a\bar{T}}{\mu c}, \quad \alpha = \frac{c\bar{\alpha}}{\mu a}, \quad v = \frac{C}{r + C}\frac{\partial \psi}{\partial x},$$

$$u_s = -\frac{\partial \varphi}{\partial r}, u = -\frac{\partial \psi}{\partial r}, \quad v_s = \frac{C}{r + C}\frac{\partial \varphi}{\partial x}, \quad P = \frac{a^2}{\lambda\mu c}\bar{P}. \tag{9.11}$$

The resulting compatibility equations of the fluid and solid granules after removing the pressure terms are

$$Re\,\delta\left(\frac{1}{C}\frac{\partial^2\psi}{\partial r\partial x}-\frac{\partial^2\psi}{\partial r^2}\frac{\partial\psi}{\partial x}\frac{1}{r+C}+\frac{\partial\psi}{\partial x}\left(1-\frac{\partial\psi}{\partial r}\right)\frac{1}{(r+C)^2}-\left(1-\frac{\partial\psi}{\partial r}\right)\frac{1}{(C+r)}\frac{\partial^2\psi}{\partial x\partial r}\right.$$

$$+\left(\frac{C+r}{C}\right)\frac{\partial^3\psi}{\partial x\partial r^2}-\frac{\partial\psi}{\partial x}\frac{\partial^3\psi}{\partial r^3}-\left(\frac{r+C}{C}\right)\left(1-\frac{\partial\psi}{\partial r}\right)\frac{\partial^2}{\partial r^2}\left(\left\{\frac{\partial\psi}{\partial x}\frac{C}{C+r}\right\}\right)$$

$$+\delta^2\frac{C}{C+r}\frac{\partial^3\psi}{\partial x^3}+\delta^2\frac{2C^2}{(C+r)^3}\frac{\partial\psi}{\partial x}\frac{\partial^2\psi}{\partial x^2}-\delta^2\frac{\partial\psi}{\partial x}\frac{C^2}{(r+C)^2}\frac{\partial^3\psi}{\partial x^2\partial r}$$

$$\left.-\delta^2\frac{\partial^3\psi}{\partial x^3}\frac{C^2}{(r+C)^2}\left(1-\frac{\partial\psi}{\partial r}\right)-\frac{\partial^2\psi}{\partial x\partial r}\left(1-\frac{\partial\psi}{\partial r}\right)\frac{2}{C+r}\right)$$

$$=\left(\delta\frac{\partial^2}{\partial x\partial r}+\frac{\partial}{\partial x}\frac{\delta}{C+r}\right)T_{xx}$$

$$+\left[\frac{1}{C}\frac{\partial}{\partial r}\left\{\frac{1}{(C+r)}\frac{\partial}{\partial r}(C+r)^2\right\}-\delta^2\frac{C}{r+C}\frac{\partial^2}{\partial x^2}\right]T_{rx}$$

$$-\delta\frac{1}{C+r}\frac{\partial^2}{\partial x\partial r}((C+r)T_{rr})$$

$$+A\left[\left(\frac{1}{C}\frac{\partial}{\partial r}+\frac{C+r}{C}\frac{\partial^2}{\partial r^2}+\delta^2\frac{\partial^2}{\partial x^2}\right)(\psi-\varphi)\right], \qquad (9.12)$$

$$\delta\left(\frac{1}{C}\frac{\partial^2\varphi}{\partial r\partial x}-\frac{\partial\varphi}{\partial x}\frac{1}{C+r}\frac{\partial^2\varphi}{\partial r^2}+\frac{\partial\varphi}{\partial x}\left(1-\frac{\partial\varphi}{\partial r}\right)\frac{1}{(C+k)^2}-\frac{\partial^2\varphi}{\partial r\partial x}\left(1-\frac{\partial\varphi}{\partial r}\right)\frac{1}{(C+k)}\right.$$

$$+\left(\frac{r+C}{C}\right)\frac{\partial^3\varphi}{\partial x\partial r^2}-\frac{\partial^3\varphi}{\partial r^3}\frac{\partial\varphi}{\partial x}-\frac{2}{C}\left(1-\frac{\partial\varphi}{\partial r}\right)\frac{\partial^2\varphi}{\partial x\partial r}$$

$$-\frac{\partial}{\partial r}\left(\left\{-\frac{C}{(C+r)^2}\frac{\partial\varphi}{\partial x}+\frac{\partial^2\varphi}{\partial r\partial x}\frac{C}{C+r}\right\}\right)\left(\frac{C+r}{C}\right)\left(1-\frac{\partial\varphi}{\partial r}\right)+\delta^2\frac{\partial^3\varphi}{\partial x^3}$$

$$+\delta^2\frac{\partial^2\varphi}{\partial x^2}-\delta^2\frac{\partial^3\varphi}{\partial x^2\partial r}-\delta^2\frac{\partial^3\varphi}{\partial x^3}\left(1-\frac{\partial\varphi}{\partial r}\right)\left.\frac{C}{r+C}\right)$$

$$=B\left[\left(\frac{r+C}{C}\frac{\partial^2}{\partial r^2}+\frac{1}{C}\frac{\partial}{\partial r}+\delta^2\frac{\partial^2}{\partial x^2}\right)(\varphi-\psi)\right]. \qquad (9.13)$$

The elements of extra stress tensor are

$$T_{rr} = 2\delta \frac{\partial}{\partial r}\left(\frac{C}{C+r}\frac{\partial \psi}{\partial x}\right)$$

$$+ \alpha_1 \left[-2C\delta^2 \frac{\partial^2}{\partial r \partial x}\left(\frac{\partial \psi}{\partial x}\frac{1}{C+r}\right)\right.$$

$$+ \delta^2 C^2 \left(1 - \frac{\partial \psi}{\partial r}\right)\frac{2}{C+r}\frac{\partial^2}{\partial x \partial r}\left(\frac{\partial \psi}{\partial x}\frac{1}{C+r}\right)$$

$$+ 2C\delta^2 \frac{\partial^2}{\partial r^2}\left(\frac{\partial \psi}{\partial x}\frac{C}{C+r}\right)\frac{\partial \psi}{\partial x}\frac{1}{r+C} + 4\delta^2 \left(\frac{\partial}{\partial r}\left(\frac{C}{r+C}\frac{\partial \psi}{\partial x}\right)\right)^2$$

$$- 2\delta^2 \frac{C^2}{(C+r)^2}\frac{\partial^2 \psi}{\partial r^2}\frac{\partial^2 \psi}{\partial x^2} + \left(1 - \frac{\partial \psi}{\partial r}\right)\frac{2}{C+r}\frac{\partial^2 \psi}{\partial r^2}$$

$$+ \delta^4 \frac{2C^4}{(C+r)^4}\left(\frac{\partial^2 \psi}{\partial x^2}\right)^2 - \delta^2 \frac{4C^2}{(C+r)^3}\left(1 - \frac{\partial \psi}{\partial r}\right)\frac{\partial}{\partial x}\left(\frac{\partial \psi}{\partial x}\right)$$

$$\left. + \left(1 - \frac{\partial \psi}{\partial r}\right)^2 \frac{2}{(C+r)^2}\right]$$

$$+ \alpha_2 \left[4\delta^2 \left(\frac{\partial}{\partial r}\left(\frac{\partial \psi}{\partial x}\frac{C}{C+r}\right)\right)^2 \right.$$

$$\left. + \left(\frac{\partial}{\partial r}\left(-\frac{\partial \psi}{\partial r}\right) + \delta^2 \frac{\partial^2 \psi}{\partial x^2}\frac{C^2}{(r+C)^2} - \left(1 - \frac{\partial \psi}{\partial r}\right)\frac{1}{r+C}\right)^2 \right], \qquad (9.14)$$

$$T_{rx} = \left(-\frac{\partial^2\psi}{\partial r^2} + \delta^2\frac{C^2}{(r+C)^2}\frac{\partial^2\psi}{\partial x^2} - \left(1-\frac{\partial\psi}{\partial r}\right)\frac{1}{C+r}\right)$$

$$+\alpha_1\left[\delta\frac{\partial^3\psi}{\partial x\partial r^2} - \delta^3\frac{\partial^3\psi}{\partial x^3}\frac{C^2}{(C+r)^2} + \delta\frac{\partial^2\psi}{\partial x\partial r}\frac{1}{r+C}\right.$$

$$-\delta\left(1-\frac{\partial\psi}{\partial r}\right)\frac{C}{r+C}\frac{\partial^3\psi}{\partial x\partial r^2}$$

$$+\delta^3\left(1-\frac{\partial\psi}{\partial r}\right)\frac{C^2}{(C+r)^2}\frac{\partial^2}{\partial x^2}\left(\frac{C}{C+r}\frac{\partial\psi}{\partial x}\right)$$

$$+\delta\frac{C}{(C+r)^2}\left(1-\frac{\partial\psi}{\partial r}\right)\frac{\partial^2\psi}{\partial x\partial r} - \delta\frac{\partial\psi}{\partial x}\frac{C}{r+C}\frac{\partial^3\psi}{\partial r^3}$$

$$-\delta^3\frac{C^3}{(C+r)^4}\frac{\partial\psi}{\partial x}\frac{\partial}{\partial x}\left(\frac{\partial\psi}{\partial x}\right) + \delta^3\frac{C^2}{(C+r)^2}\frac{\partial\psi}{\partial x}\frac{\partial^2}{\partial r\partial x}\left(\frac{\partial\psi}{\partial x}\frac{C}{C+r}\right)$$

$$+\delta\frac{C}{(r+C)^3}\frac{\partial\psi}{\partial x}\left(1-\frac{\partial\psi}{\partial r}\right) + \delta\frac{\partial\psi}{\partial x}\frac{C}{(r+C)^2}\frac{\partial^2\psi}{\partial r^2}$$

$$+2\delta\frac{\partial}{\partial r}\left(-\frac{\partial\psi}{\partial r}\right)\frac{\partial}{\partial r}\left(\frac{\partial\psi}{\partial x}\frac{C}{C+r}\right) - 2\delta^3\frac{C^2}{(r+C)^2}\frac{\partial}{\partial r}\left(\frac{\partial\psi}{\partial x}\frac{C}{C+r}\right)\frac{\partial^2\psi}{\partial x^2}$$

$$\left.+\frac{2\delta}{C+k}\frac{\partial}{\partial r}\left(\frac{\partial\psi}{\partial x}\frac{C}{C+r}\right)\left(1-\frac{\partial\psi}{\partial r}\right)\right], \quad (9.15)$$

$$T_{xx} = -2\delta \frac{\partial}{\partial r}\left(\frac{\partial \psi}{\partial x}\frac{C}{C+r}\right)$$

$$+ \alpha_1 \left[2\delta^2 \frac{\partial^2}{\partial r \partial x}\left(\frac{\partial \psi}{\partial x}\frac{C}{C+r}\right) - \delta^2 \frac{2C}{C+r}\frac{\partial^2}{\partial r \partial x}\left(\frac{C}{C+r}\frac{\partial \psi}{\partial x}\right)\left(1 - \frac{\partial \psi}{\partial r}\right)\right.$$

$$- 2\delta^2 \frac{C}{C+r}\frac{\partial^2}{\partial r^2}\left(\frac{\partial \psi}{\partial x}\frac{C}{r+C}\right)\frac{\partial \psi}{\partial x} - 2\left(-\frac{\partial^2 \psi}{\partial r^2}\right)^2$$

$$- 2\delta^2 \frac{C^2}{(C+r)^2}\frac{\partial^2 \psi}{\partial r^2}\frac{\partial^2 \psi}{\partial x^2} + \left(1 - \frac{\partial \psi}{\partial r}\right)\frac{2}{r+C}\frac{\partial^2 \psi}{\partial r^2}$$

$$\left. + 4\delta^2 \left(\frac{\partial}{\partial r}\left(\frac{\partial \psi}{\partial x}\frac{C}{C+r}\right)\right)^2 \right]$$

$$+ \alpha_2 \left[4\delta^2 \left(\frac{\partial}{\partial r}\left(\frac{\partial \psi}{\partial x}\frac{C}{r+C}\right)\right)^2 \right.$$

$$\left. + \left(-\frac{\partial^2 \psi}{\partial r^2} + \delta^2 \frac{\partial^2 \psi}{\partial x^2}\frac{C^2}{(r+C)^2} - \left(1 - \frac{\partial \psi}{\partial r}\right)\frac{1}{r+C}\right)^2 \right]. \qquad (9.16)$$

Boundary conditions in dimensionless form are

$$\psi = -\frac{F}{2}, \qquad \frac{\partial \psi}{\partial r} = 1, \qquad \varphi = -\frac{E}{2}, \qquad at \quad r = h = 1 + \phi \sin(x),$$

(9.17)

$$\psi = \frac{F}{2}, \qquad \frac{\partial \psi}{\partial r} = 1, \qquad \varphi = \frac{E}{2}, \qquad at \quad r = -h = -(1 + \phi \sin(x)).$$

(9.18)

9.3 Method of Solution

The series solution for ψ and φ are expand as

$$\psi = \psi_0 + \delta\psi_1 + \delta^2\psi_2 + O(\delta^3), \qquad (9.19)$$

$$\varphi = \varphi_0 + \delta\varphi_1 + \delta^2\varphi_2 + O(\delta^3), \tag{9.20}$$

$$F = F_0 + \delta F_1 + \delta^2 F_2 + O(\delta^3), \tag{9.21}$$

$$E = E_0 + \delta E_1 + \delta^2 E_2 + O(\delta^3). \tag{9.22}$$

9.3.1 Zeroth Order System

$$\frac{1}{C}\frac{\partial}{\partial r}\left\{\frac{1}{(C+r)}\frac{\partial}{\partial r}(C+r)^2\right\}T_{0rx} + A\left[\left(\frac{C+r}{C}\frac{\partial^2}{\partial r^2} + \frac{1}{C}\frac{\partial}{\partial r}\right)(\psi_0 - \varphi_0)\right] = 0, \tag{9.23}$$

$$B\left[\left(\frac{C+r}{C}\frac{\partial^2}{\partial r^2} + \frac{1}{C}\frac{\partial}{\partial r}\right)(\varphi_0 - \psi_0)\right] = 0, \tag{9.24}$$

where

$$T_{0rx} = -\frac{\partial^2\psi_0}{\partial r^2} + \frac{1}{r+C}\left(\frac{\partial\psi_0}{\partial r} - 1\right), \tag{9.25}$$

with

$$\psi_0 = -\frac{F_0}{2}, \qquad \frac{\partial\psi_0}{\partial r} = 1, \qquad \varphi_0 = -\frac{E_0}{2}, \qquad at \quad r = h = 1 + \phi\sin(x), \tag{9.26}$$

$$\psi_0 = \frac{F_0}{2}, \qquad \frac{\partial\psi_0}{\partial r} = 1, \qquad \varphi_0 = \frac{E_0}{2}, \qquad at \quad r = -h = -(1 + \phi\sin(x)). \tag{9.27}$$

9.3.2 First Order System

$$Re\left(\frac{1}{C}\frac{\partial^2\psi_0}{\partial r\partial x}-\frac{\partial^2\psi_0}{\partial r^2}\frac{1}{C+r}\frac{\partial\psi_0}{\partial x}+\frac{\partial\psi_0}{\partial x}\frac{1}{(C+r)^2}\left(1-\frac{\partial\psi_0}{\partial r}\right)\right.$$

$$-\frac{1}{(r+C)}\frac{\partial^2\psi_0}{\partial x\partial r}\left(1-\frac{\partial\psi_0}{\partial r}\right)+\frac{\partial^3\psi_0}{\partial x\partial r^2}\left(\frac{C+r}{C}\right)-\frac{\partial^3\psi_0}{\partial r^3}\frac{\partial\psi_0}{\partial x}$$

$$\left.-\left(\frac{C+r}{C}\right)\frac{\partial^2}{\partial r^2}\left(\left\{\frac{C}{C+r}\frac{\partial\psi_0}{\partial x}\right\}\right)\left(1-\frac{\partial\psi_0}{\partial r}\right)-\frac{\partial^2\psi_0}{\partial x\partial r}\frac{2}{r+C}\left(1-\frac{\partial\psi_0}{\partial r}\right)\right)$$

$$=\left(\frac{1}{C+r}\frac{\partial}{\partial x}+\frac{\partial^2}{\partial x\partial r}\right)T_{0xx}+\frac{1}{C}\left[\frac{\partial}{\partial r}\left\{\frac{1}{(C+r)}\frac{\partial}{\partial r}(r+C)^2\right\}\right]T_{1rx}$$

$$-\frac{1}{C+r}\frac{\partial^2}{\partial r\partial x}\left((r+C)T_{0rr}\right)+A\left[\left(\frac{C+r}{C}\frac{\partial^2}{\partial r^2}+\frac{1}{C}\frac{\partial}{\partial r}\right)(\psi_1-\varphi_1)\right],$$

(9.28)

$$\left(\frac{1}{C}\frac{\partial^2\varphi_0}{\partial r\partial x}-\frac{\partial\varphi_0}{\partial x}\frac{\partial^2\varphi_0}{\partial r^2}\frac{1}{r+C}+\frac{1}{(C+r)^2}\left(1-\frac{\partial\varphi_0}{\partial r}\right)\frac{\partial\varphi_0}{\partial x}-\left(1-\frac{\partial\varphi_0}{\partial r}\right)\frac{\partial^2\varphi_0}{\partial x\partial r}\frac{1}{(C+r)}\right.$$

$$+\frac{\partial^3\varphi_0}{\partial x\partial r^2}\left(\frac{C+r}{C}\right)-\frac{\partial\varphi_0}{\partial x}\frac{\partial^3\varphi_0}{\partial r^3}$$

$$-\left(\frac{C+r}{C}\right)\frac{\partial}{\partial r}\left(\left\{-\frac{\partial\varphi_0}{\partial x}\frac{C}{(C+r)^2}+\frac{C}{r+C}\frac{\partial^2\varphi_0}{\partial r\partial x}\right\}\right)\left(1-\frac{\partial\varphi_0}{\partial r}\right)$$

$$\left.-\frac{2}{c}\frac{\partial^2\varphi_0}{\partial r\partial x}\left(1-\frac{\partial\varphi_0}{\partial r}\right)\right)=B\left[\left(\frac{C+r}{C}\frac{\partial^2}{\partial r^2}+\frac{1}{C}\frac{\partial}{\partial r}\right)(\varphi_1-\psi_1)\right],$$

(9.29)

where

$$T_{0xx}=\alpha_1\left[2\left(\frac{\partial^2\psi_0}{\partial r^2}\right)^2+\left(1-\frac{\partial\psi_0}{\partial r}\right)\frac{\partial^2\psi_0}{\partial r^2}\frac{2}{C+r}\right]$$

$$+\alpha_2\left[\left(-\frac{\partial^2\psi_0}{\partial r^2}-\left(1-\frac{\partial\psi_0}{\partial r}\right)\frac{1}{C+r}\right)^2\right],\qquad(9.30)$$

$$T_{0rr} = \alpha_1\left[\frac{2}{r+C}\left(1-\frac{\partial\psi_0}{\partial r}\right)+\left(1-\frac{\partial\psi_0}{\partial r}\right)^2\frac{2}{(r+C)^2}\right]$$

$$+\alpha_2\left[\left(-\frac{\partial^2\psi_0}{\partial r^2}-\frac{1}{r+C}\left(1-\frac{\partial\psi_0}{\partial r}\right)\right)^2\right], \tag{9.31}$$

$$T_{1rx} = \left[-\frac{\partial^2\psi_1}{\partial r^2}+\frac{1}{r+C}\frac{\partial\psi_1}{\partial r}\right]$$

$$+\alpha_1\left[\frac{\partial^3\psi_0}{\partial x\partial r^2}+\frac{\partial^2\psi_0}{\partial r\partial x}\frac{1}{C+r}-\left(1-\frac{\partial\psi_0}{\partial r}\right)\frac{C}{C+r}\right.$$

$$+\frac{\partial^2\psi_0}{\partial r^2}\frac{\partial\psi_0}{\partial x}\frac{C}{(C+r)^2}+\left(1-\frac{\partial\psi_0}{\partial r}\right)\frac{\partial^2\psi_0}{\partial x\partial r}\frac{C}{(r+C)^2}$$

$$-\frac{C}{C+r}\frac{\partial^3\psi_0}{\partial r^3}\frac{\partial\psi_0}{\partial x}+\frac{C}{(C+r)^3}\frac{\partial\psi_0}{\partial x}\left(1-\frac{\partial\psi_0}{\partial r}\right)$$

$$-2\frac{\partial^2\psi_0}{\partial r^2}\left(-\frac{\partial\psi_0}{\partial x}\frac{C}{(C+r)^2}+\frac{C}{C+r}\frac{\partial^2\psi_0}{\partial r\partial x}\right)$$

$$\left.+\frac{2}{C+r}\left(-\frac{C}{(C+r)^2}\frac{\partial\psi_0}{\partial x}+\frac{C}{r+C}\frac{\partial^2\psi_0}{\partial r\partial x}\right)\left(1-\frac{\partial\psi_0}{\partial r}\right)\right], \tag{9.32}$$

with

$$\psi_1 = -\frac{F_1}{2}, \qquad \frac{\partial\psi_1}{\partial r} = 0, \qquad \varphi_1 = -\frac{E_1}{2}, \qquad at \quad r = h = 1+\phi\sin(x),$$

(9.33)

$$\psi_1 = \frac{F_1}{2}, \qquad \frac{\partial\psi_1}{\partial r} = 0, \qquad \varphi_1 = \frac{E_1}{2}, \qquad at \quad r = -h = -(1+\phi\sin(x)).$$

(9.34)

Solutions are obtained by using DSolver command in Mathematica software.

9.4 Results and Discussion

This portion aims to define the impact of parameters like wave number δ, second-grade parameter α_1, Reynolds number Re and C i.e., the curvature of the passage. Figs. 9.1 – 9.7 show the streamline patterns and velocity of the fluid while Figs. 9.8 – 9.13 display the streamline patterns of the dust elements.

The streamline pattern in Fig. 9.1 displays the impact of wave number on the fluid. With the increase in the wave number, it can be seen that the trapped bolus in the upper portion of the passage increases in size while the bolus in the lower portion start moving towards the direction of the fluid flow. Reynolds number impact on the trapped bolus can be observed in Fig. 9.2. The trapped bolus in the upper part of the passage contracts with the increase in Re while the bolus in the lower part contracts and eventually vanishes. The consequence of curvature parameter C on the contour plots can be seen in Fig. 9.3. As C is increasing, it can be seen the bolus present in the upper part of the passage contracts while a bolus forms in the lower part of the passage. The trapped bolus in the upper part of the passage enhances as the second-grade parameter α_1 increases as displayed in Fig. 9.4. In Fig. 9.5, it can be seen that the velocity of the fluid decays at the center of the passage as the wavenumber increases. Wave number is inversely related to wavelength so as wave number increases, wavelength decreases thus causing more turbulence in fluid resulting in reduction of velocity. The second-grade parameter indicates the viscous nature of the fluid. As this parameter increases, the velocity decreases as demonstrated in Fig. 9.6. The increase in curvature, rises fluid velocity in the direction of the flow as indicated in Fig. 9.7.

The streamline patterns for dust granules for distant values of wave number are given in Fig. 9.8. As the wave number is increased the trapped in the upper portion of the

passage expands while the bolus in the lower part moves away in the direction of the flow. As Fig. 9.9 indicates, the bolus trapped in the lower part of the passage enhances in size as Reynolds number is increased. Impact of increase in curvature parameter C on the streamline patterns is given in Fig. 9.10. As the curvature enhances, bolus in the lower section of the passage forms and it continues increasing as C increases. In Fig. 9.11, the impact of second-grade parameter on contour patterns are presented. With the increase in α_1, the trapped bolus starts contracting. The impression of velocity under the influence of wave number is demonstrated in Fig. 9.12. Decay in the velocity can be seen in the center of the passage as the wave number increases. The impact of second-grade parameter on dust granules velocity is demonstrated in Fig. 9.13. Increase in the viscous nature of the fluid decreases the velocity.

9.5 Graphs

For Fluid

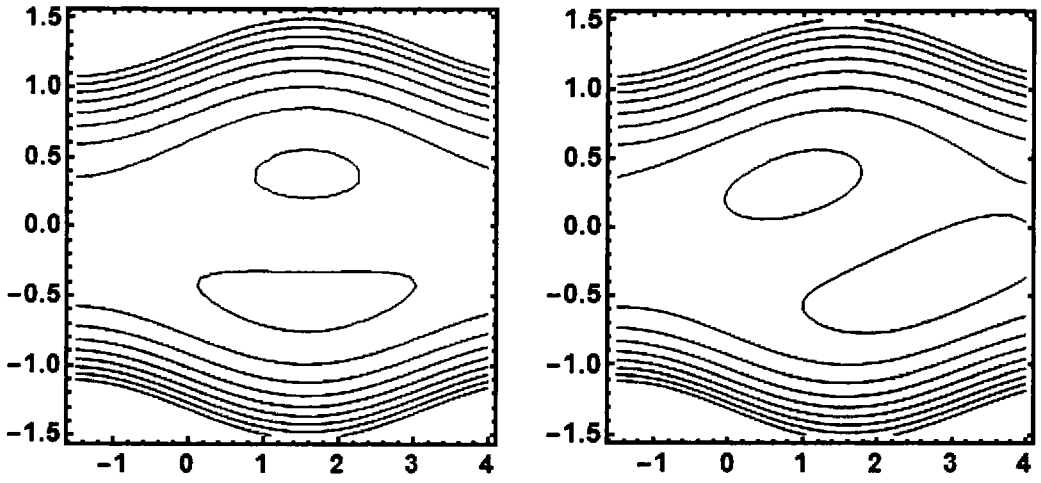

$\delta = 0$ $\delta = 0.01$

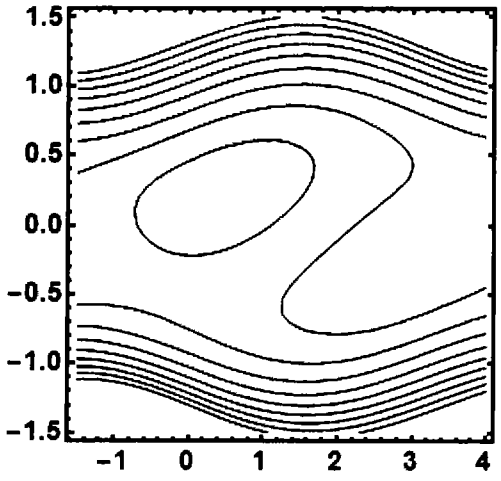

$\delta = 0.02$

Figure 9.1: The streamline patterns for the fluid for distinct values of δ with $Q = 1.5, \phi = 0.2, Q = 1.5, Q_s = 1.8, Re = 5, A = 0.8, B = 0.7, \alpha_1 = 1, C = 5.$

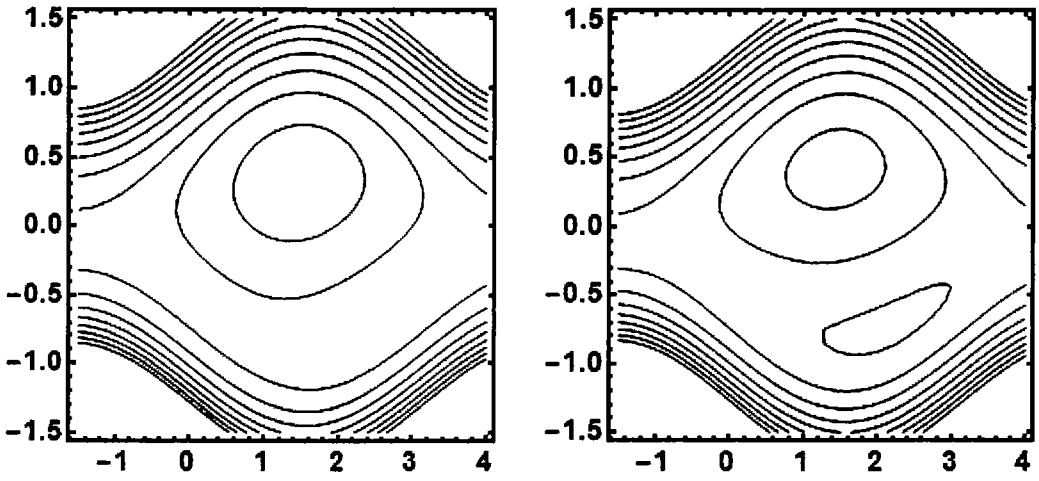

$C = 2$ $C = 3$

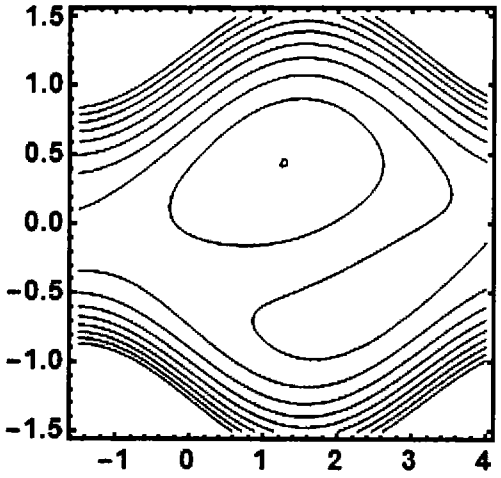

$C = 4$

Figure 9.3: The streamline patterns for the fluid for distinct values of C with $Q = 1.5, \phi = 0.4, Q_s = 1.8, Re = 5, A = 0.8, B = 0.7, \alpha_1 = 2, \delta = 0.01$.

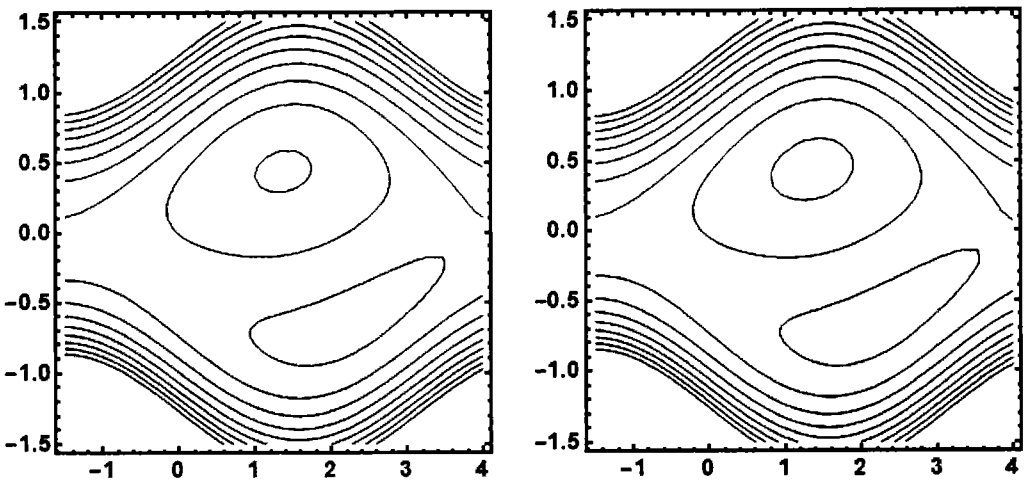

$\alpha_1 = 0$ $\alpha_1 = 1.5$

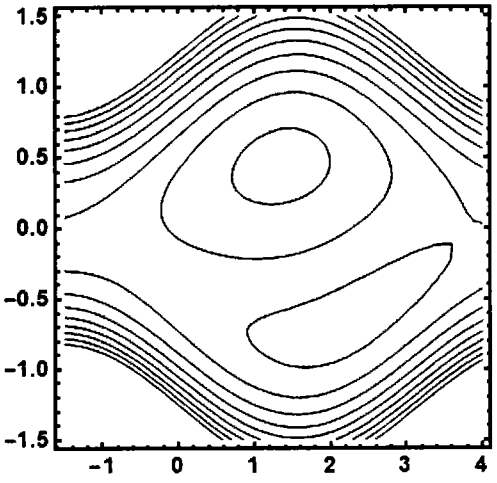

$\alpha_1 = 3$

Figure 9.4: The streamline patterns for the fluid for distinct values of α_1 with $Q = 1.5, \phi = 0.4, Q_s = 1.8, Re = 5, A = 0.8, B = 0.7, C = 3.5, \delta = 0.01$.

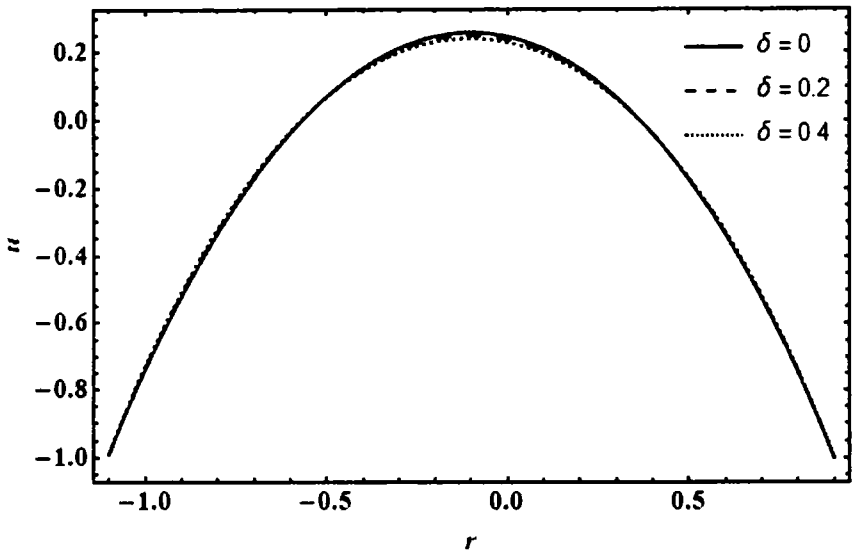

Figure 9.5: The velocity profile for the fluid for distinct values of δ with $\phi = 0.4$,

$Q = 1.5, Q_s = 1.8, Re = 5, A = 0.8, B = 0.7, C = 3.5, \alpha_1 = 1.$

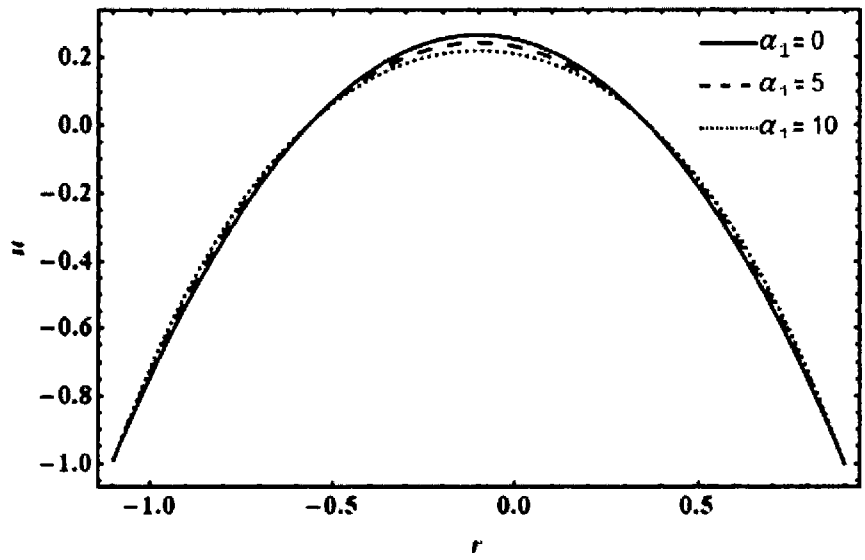

Figure 9.6: The velocity profile for the fluid for distinct values of α_1 with $\phi = 0.4$,

$Q = 1.5, Q_s = 1.8, Re = 5, A = 0.8, B = 0.7, C = 3.5, \delta = 1.$

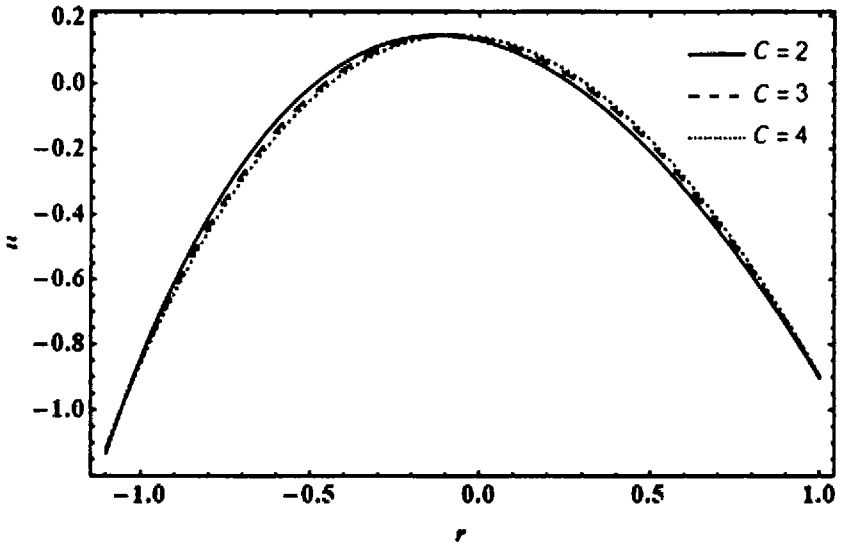

Figure 9.7: The velocity profile for the fluid for distinct values of C with $Q = 1.5$, $\phi = 0.4, Q_s = 1.8, Re = 5, A = 0.8, B = 0.7, \delta = 0.01, \alpha_1 = 1.$

Graphs of Solid Particles

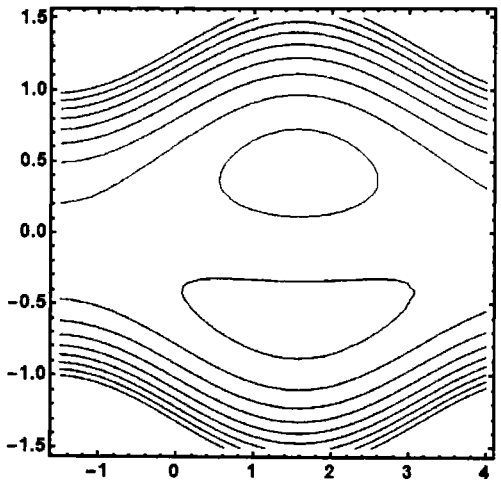

$\delta = 0$

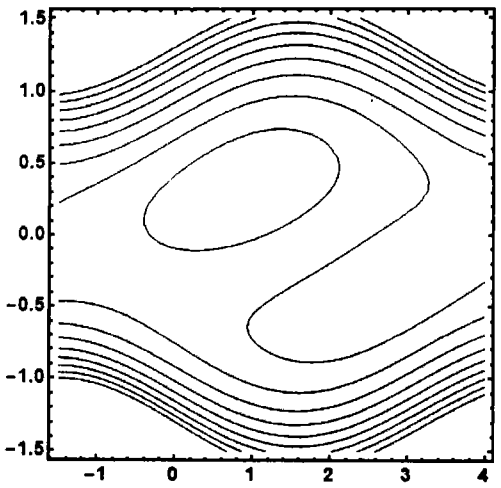

$\delta = 0.01$

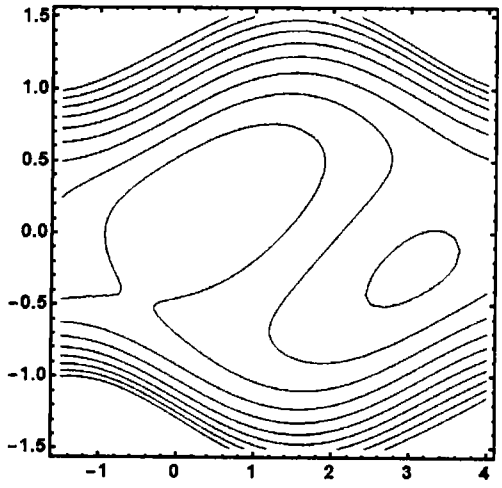

$\delta = 0.02$

Figure 9.8: The streamline patterns for the dust granules for distinct values of δ with $Q = 1.5, \phi = 0.4, Q_s = 1.8, Re = 5, A = 0.8, B = 0.7, C = 5, \alpha_1 = 2.$

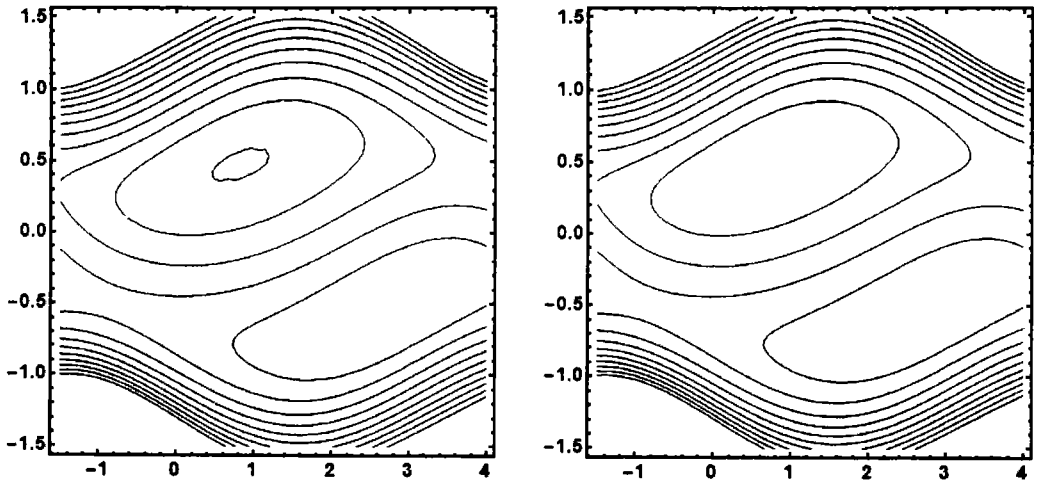

$Re = 0$ $Re = 800$

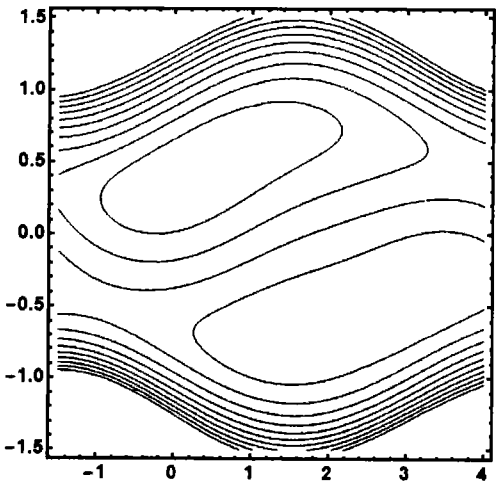

$Re = 1600$

Figure 9.9: The streamline patterns for the dust granules for distinct values of Re with $Q = 1.5, \phi = 0.3, Q_s = 1.8, \delta = 0.02, A = 0.8, B = 0.7, C = 4, \alpha_1 = 3$.

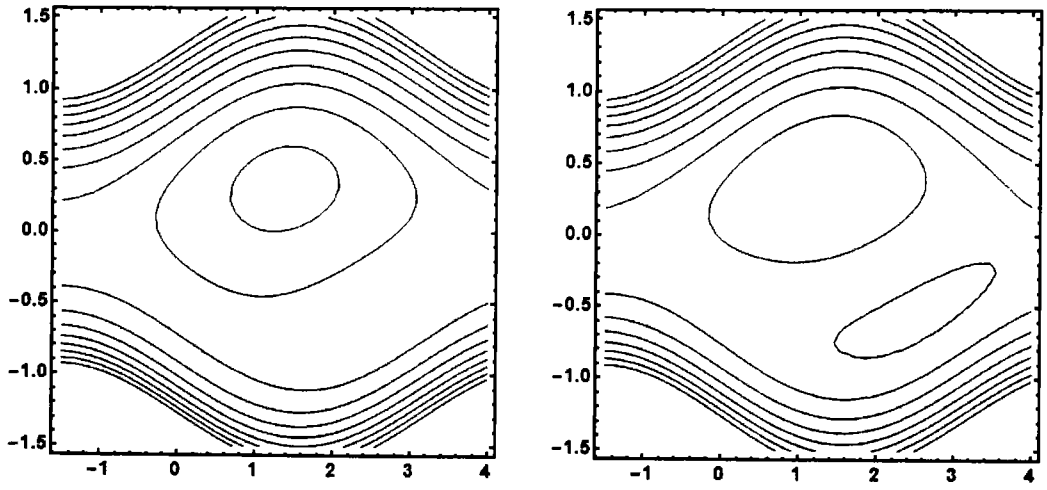

$C = 2$ $C = 3$

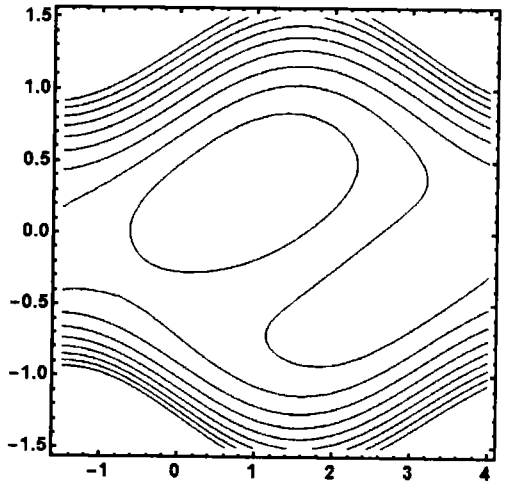

$C = 4$

Figure 9.10: The streamline patterns for the dust granules for distinct values of C with $Q = 1.5, \phi = 0.3, Q_s = 1.8, \delta = 0.01, A = 0.8, B = 0.7, Re = 5, \alpha_1 = 2.$

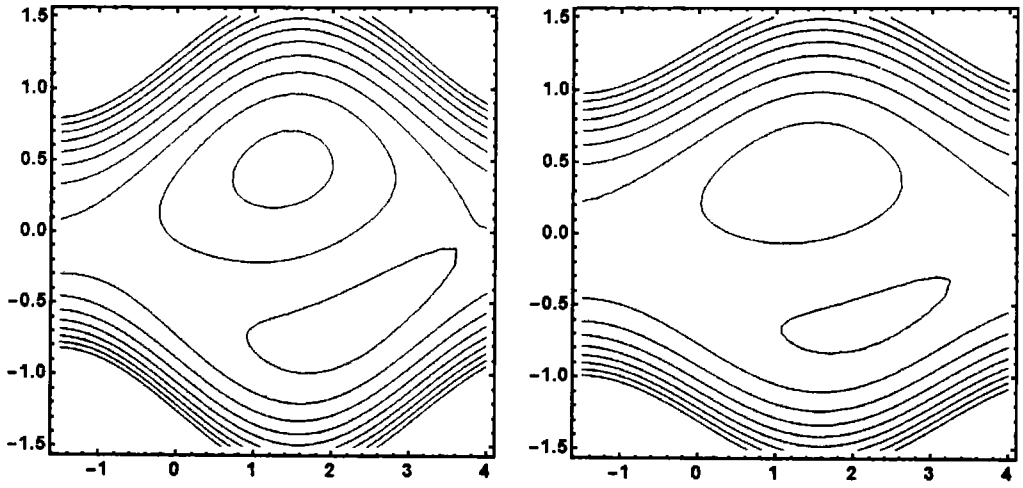

$\alpha_1 = 0$ $\alpha_1 = 2$

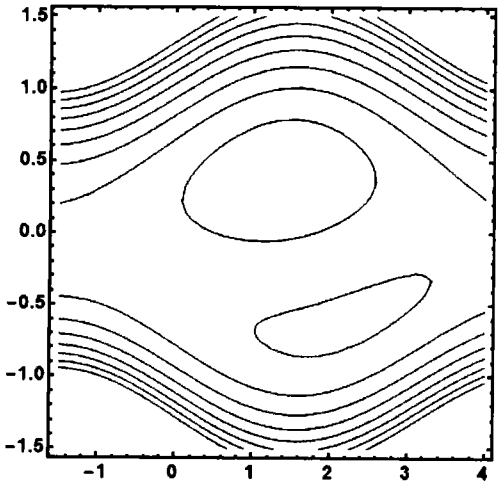

$\alpha_1 = 3$

Figure 9.11: The streamline patterns for the dust granules for distinct values of α_1 with $Q = 1.5, \phi = 0.3, Q_s = 1.8, \delta = 0.01, A = 0.8, B = 0.7, Re = 5, C = 4.$

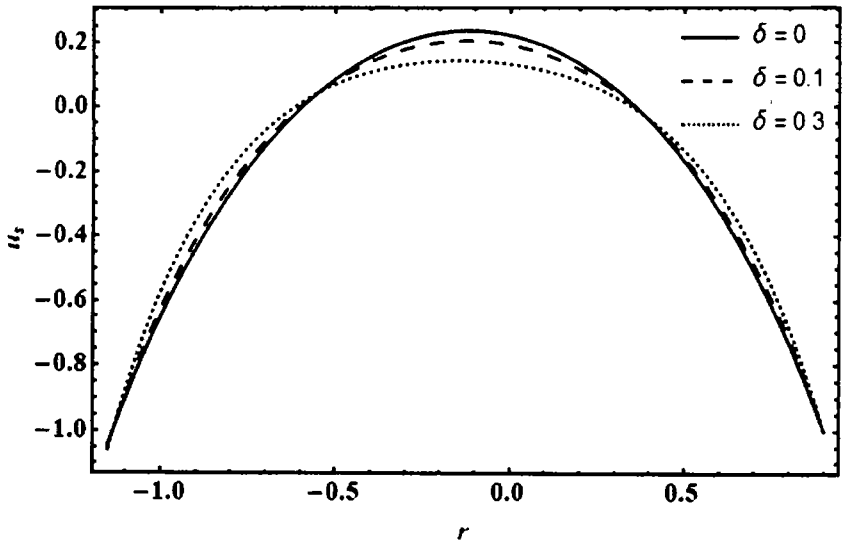

Figure 9.12: The velocity profile for the dust granules for distinct values of δ with

$Q = 1.5, \phi = 0.3, Q_s = 1.8, \alpha_1 = 1, A = 0.8, B = 0.7, Re = 5, C = 4.$

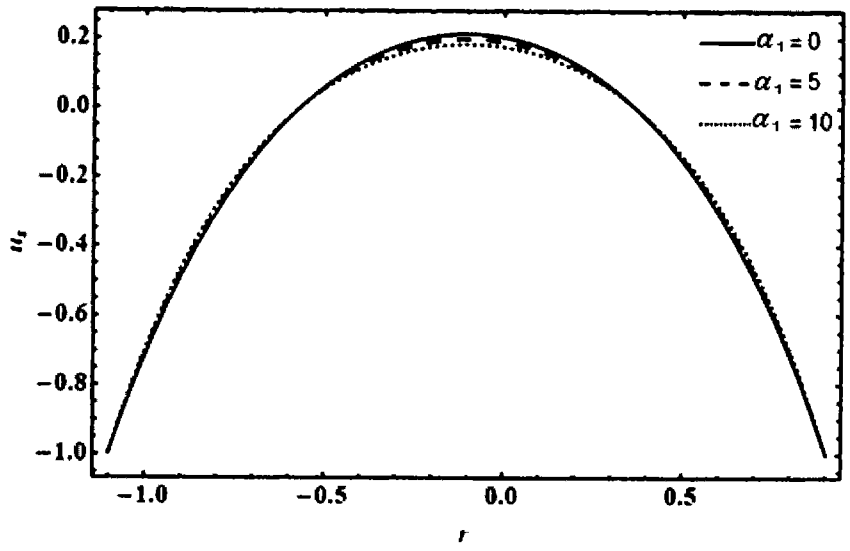

Figure 9.13: The velocity profile for the dust granules for distinct values of α_1 with

$Q = 1.5, \phi = 0.3, Q_s = 1.8, \delta = 0.01, A = 0.8, B = 0.7, Re = 5, C = 4.$

9.6 Conclusion

The peristaltic movement of second-grade dusty fluid in a curved configuration is discussed. Perturbation technique has been employed to get the results. Below are points that are notable.

- The bolus trapped in the lower portion of the passage moves in the direction of the flow as the wave number increases for both fluid and dust particles.
- Bolus forms in the lower portion of the passage as C is increased for both dust particles and fluid.
- Increase in the second-grade parameter contracts the trapped bolus for both solid and fluid particles.
- The velocity decays for both δ and α_1 for both dust granules and fluid.

Chapter 10

Concluding Remarks

This study is performed to examine the peristaltic effect of dusty fluid model flowing past different geometries, with various body forces and boundary conditions. Second-grade dusty fluid model has been studied for asymmetric channel, tube and curved channel. It has been observed that the amplitude of maximum velocity is attained for second-grade parameter and wavenumber in tube as compared to the curved channel. Furthermore, the trapped bolus expands more in an asymmetric channel than the curved channel for the second-grade parameter.

Walter's B fluid model has been studied with the wall properties and for magnetic field in an asymmetric channel. With wall properties effect, there is surge in velocity for the viscoelastic parameter κ while for the asymmetric channel velocity amplitude declines due to magnetic field applied. The porous medium parameter K has been studied for the asymmetric channel and endoscope and it has been concluded that the trapped bolus enhances in both cases.

Appendix

$$C_1 = cosh\left[K^{\frac{1}{2}} h_1\right] - cosh\left[K^{\frac{1}{2}} h_2\right], \qquad C_2 = sinh\left[K^{\frac{1}{2}} h_1\right] - sinh\left[K^{\frac{1}{2}} h_2\right],$$

$$C_3 = cosh\left[K^{\frac{1}{2}} h_1\right] + cosh\left[K^{\frac{1}{2}} h_2\right], \qquad C_4 = sinh\left[K^{\frac{1}{2}} h_1\right] + sinh\left[K^{\frac{1}{2}} h_2\right],$$

$$C_5 = C_2 + 2K\beta C_3, \qquad C_6 = C_1 + 2K\beta C_4,$$

$$C_7 = \frac{C_6 C_1 - C_2 C_5}{(h_2 - h_1)C_5} - \frac{C_6(K^{\frac{1}{2}} sinhKh_1 + K\beta coshKh_1)}{C_5} + K^{\frac{1}{2}} coshK^{\frac{1}{2}} h_1 + K\beta sinhK^{\frac{1}{2}} h_1,$$

$$C_8 = \frac{C_6 coshK^{\frac{1}{2}} h_1}{C_5} - sinhK^{\frac{1}{2}} h_1 - \frac{h_1(C_6 C_1 - C_2 C_5)}{(h_2 - h_1)C_5},$$

$$C_9 = \frac{C_6 coshK^{\frac{1}{2}} h_2}{C_5} - sinhK^{\frac{1}{2}} h_2 - \frac{h_1(C_6 C_1 - C_2 C_5)}{(h_2 - h_1)C_5},$$

$$A_1 = \frac{F_0}{h_1 - h_2} - \frac{(F_0 + h_1 - h_2)(C_6 C_1 - C_2 C_5)}{(h_1 - h_2)C_5},$$

$$A_2 = -\frac{F_0(h_1 + h_2)}{2(h_1 - h_2)} - \frac{(F_0 + h_1 - h_2)C_9}{(h_1 - h_2)C_7},$$

$$A_3 = \frac{(F_0 + h_1 - h_2)C_6}{C_5},$$

$$A_4 = -\frac{(F_0 + h_1 - h_2)}{(h_1 - h_2)C_7},$$

$$B_1 = \frac{(N_0 - BF_0)}{h_1 - h_2}, \qquad B_2 = \frac{(h_1 + h_2)(N_0 - BF_0)}{2(h_2 - h_1)},$$

$$A_{11} = \frac{1}{2}(A_3 A_3' + A_4 A_4'), \qquad A_{12} = \frac{1}{2}(A_3 A_4' + A_4 A_3'),$$

$$\mathrm{A_{13}} = K^{\frac{1}{2}} A_1' A_4; \mathrm{A_{14}} = K^{\frac{1}{2}} A_1' A_3,$$

$$A_{15} = \left(\alpha_1\left(\mathrm{A_1 A_3' K^2 - A_2 A_4 K^{\frac{5}{2}}}\right) - A\left(-\mathrm{B_2' A_4 K^{\frac{3}{2}} + B\left(A_1 A_3' K - A_4 A_2' K^{\frac{3}{2}}\right) + B_1 A_3' K}\right) - Re\left(\mathrm{A_1 A_3' K - A_2' A_4 K^{\frac{3}{2}}}\right)\right),$$

$$A_{16} = \Big(\alpha_1\left(A_1A_4'K^2 - A_3A_2'K^{\frac{5}{2}}\right) - A\left(-A_3B_2'K^{\frac{3}{2}} + B\left(A_1A_4'K - A_3A_2'K^{\frac{3}{2}}\right) + KB_1A_4'\right) - Re\left(KA_1A_4' - A_3A_2'K^{\frac{3}{2}}\right)\Big),$$

$$A_{17} = \left(\alpha_1 KA_{13} - A\left(B_1'A_4K^{\frac{3}{2}} + BA_1'A_4K^{\frac{3}{2}}\right) - Re(A_{13})\right),$$

$$A_{18} = \left(\alpha_1 KA_{14} - A\left(B_1'A_3K^{\frac{3}{2}} + BA_1'A_3K^{\frac{3}{2}}\right) - Re(A_{14})\right),$$

$$A_{19} = \frac{1}{8K^{\frac{5}{2}}}(17A_{18} + 10KA_{15}), \qquad A_{20} = \frac{1}{8K^{\frac{5}{2}}}\left(4KA_{16} + 10K^{\frac{1}{2}}A_{17}\right),$$

$$A_{21} = \frac{1}{8K^{\frac{5}{2}}}(2KA_{18}), \qquad A_{22} = \frac{1}{8K^{\frac{5}{2}}}\left(17A_{17} + 10K^{\frac{1}{2}}A_{16}\right),$$

$$A_{23} = \frac{1}{8K^{\frac{5}{2}}}\left(4KA_{15} + 10K^{\frac{1}{2}}A_{18}\right), \qquad A_{24} = \frac{1}{8K^{\frac{5}{2}}}(2KA_{17}),$$

$$A_{25} = (A_{19} - A_{20}h_1 + A_{21}(h_1)^2)\cosh\left[K^{\frac{1}{2}}h_1\right] + (A_{22} - A_{23}h_1 + A_{24}(h_1)^2)\sinh\left[K^{\frac{1}{2}}h_1\right],$$

$$A_{26} = (A_{19} - A_{20}h_2 + A_{21}(h_2)^2)\cosh\left[K^{\frac{1}{2}}h_2\right] + (A_{22} - A_{23}h_2 + A_{24}(h_2)^2)\sinh\left[K^{\frac{1}{2}}h_2\right],$$

$$A_{27} = K^{\frac{3}{2}}(A_3A_4' - A_4A_3'),$$

$$A_{28} = [\left(A_1A_3'K - A_2'A_4K^{\frac{3}{2}} + 2A_1'A_3K - A_{13}h_1\right)\cosh\left[K^{\frac{1}{2}}h_1\right] + \left(A_1A_4'K - A_3A_2'K^{\frac{3}{2}} + 2A_4A_1'K - A_{14}h_1\right)\sinh\left[K^{\frac{1}{2}}h_1\right] + 2A_{12}\cosh\left[2K^{\frac{1}{2}}h_1\right] + (2A_{11})\sinh\left[2K^{\frac{1}{2}}h_1\right] - A_{27},$$

$$A_{29} = [\left(A_1A_3'K - A_2'A_4K^{\frac{3}{2}} + 2A_1'A_3K - A_{13}h_2\right)\cosh\left[K^{\frac{1}{2}}h_2\right] + \left(A_1A_4'K - A_3A_2'K^{\frac{3}{2}} + 2A_4A_1'K - A_{14}h_2\right)\sinh\left[K^{\frac{1}{2}}h_2\right] + 2A_{12}\cosh\left[2K^{\frac{1}{2}}h_2\right] + (2A_{11})\sinh\left[2K^{\frac{1}{2}}h_2\right] - A_{27},$$

$$A_{30} = \left(-A_{20} + 2h_1A_{21} + K(A_{22} - A_{23}h_1 + A_{24}(h_1)^2)\right)\cosh\left(K^{\frac{1}{2}}h_1\right) + \left(-A_{23} + 2h_1A_{24} + K(A_{19} - A_{20}h_1 + A_{21}(h_1)^2)\right)\sinh\left(K^{\frac{1}{2}}h_1\right),$$

$$A_{31} = \left(-A_{20} + 2h_2A_{21} + K(A_{22} - A_{23}h_2 + A_{24}(h_2)^2)\right)\cosh\left(K^{\frac{1}{2}}h_2\right) + \left(-A_{23} + 2h_2A_{24} + K(A_{19} - A_{20}h_2 + A_{21}(h_2)^2)\right)\sinh\left(K^{\frac{1}{2}}h_2\right),$$

$$A_{32} = \left(2A_{21} + 2K(-A_{23} + 2h_1A_{24}) + K^2(A_{19} - A_{20}h_1 + A_{21}(h_1)^2)\right)\cosh\left(K^{\frac{1}{2}}h_1\right) + \left(2A_{24} + 2K(-A_{20} + 2h_1A_{21}) + K^2(A_{22} - A_{23}h_1 + A_{24}(h_1)^2)\right)\sinh\left(K^{\frac{1}{2}}h_1\right),$$

$$A_{33} = \left(2A_{21} + 2K(-A_{23} + 2h_2A_{24}) + K^2(A_{19} - A_{20}h_2 + A_{21}(h_2)^2)\right)\cosh\left(K^{\frac{1}{2}}h_2\right) + \left(2A_{24} + 2K(-A_{20} + 2h_2A_{21}) + K^2(A_{22} - A_{23}h_2 + A_{24}(h_2)^2)\right)\sinh\left(K^{\frac{1}{2}}h_2\right),$$

$$A_{34} = \beta A_{32} + \alpha_1\beta A_{28}, \qquad A_{35} = \beta A_{33} + \alpha_1\beta A_{29},$$

$$A_{36} = K^{\frac{1}{2}}C_2 + K\beta C_1, \quad A_{37} = K^{\frac{1}{2}}C_1 + K\beta C_2,$$

$$A_{38} = A_{31} - A_{30} - A_{34} - A_{35},$$

$$A_{39} = \frac{1}{(h_1 - h_2)}\left(F_1 - A_{25} + A_{26} - \frac{C_1A_{38}}{A_{36}}\right),$$

$$A_{40} = \frac{C_2A_{36} - C_1A_{37}}{A_{36}(h_1 - h_2)},$$

$$A_{41} = K^{\frac{1}{2}}\sinh\left[K^{\frac{1}{2}}h_1\right] + K\beta\cosh\left[K^{\frac{1}{2}}h_1\right],$$

$$A_{42} = K^{\frac{1}{2}}\cosh\left[K^{\frac{1}{2}}h_1\right] + K\beta\sinh\left[K^{\frac{1}{2}}h_1\right],$$

$$A_{43} = A_{42} - \left(\frac{A_{41}A_{37}}{A_{36}}\right),$$

$$A_{44} = -\left(A_{34} + A_{30} + \frac{A_{41}A_{38}}{A_{36}}\right),$$

$$A_{45} = A_{39} - A_{40}\left(\frac{A_{44} - A_{39}}{A_{43} - A_{40}}\right),$$

$$A_{46} = \frac{A_{38}}{A_{36}} - \frac{A_{37}}{A_{36}}\left(\frac{A_{44} - A_{39}}{A_{43} - A_{40}}\right),$$

$$A_{47} = \left(\frac{A_{44} - A_{39}}{A_{43} - A_{40}}\right),$$

$$A_{48} = \frac{F_1}{2} - A_{45}h_1 - A_{25} - A_{46}\cosh\left[K^{\frac{1}{2}}h_1\right] - A_{47}\sinh\left[K^{\frac{1}{2}}h_1\right],$$

$$A_{49} = A_{46} + A_{19}; A_{50} = A_{22} + A_{47},$$

$$B_{11} = \left(\mathrm{BB}_2'\mathrm{A}_4K^{\frac{3}{2}} - \mathrm{B}\left(\mathrm{BA}_1\mathrm{A}_3'K - \mathrm{A}_4\mathrm{A}_2'K^{\frac{3}{2}}\right) - B\mathrm{B}_1\mathrm{A}_3'K\right),$$

$$B_{12} = \left(B\mathrm{A}_3\mathrm{B}_2'K^{\frac{3}{2}} - \mathrm{B}\left(B\mathrm{A}_1\mathrm{A}_4'K - \mathrm{A}_3\mathrm{A}_2'K^{\frac{3}{2}}\right) - BK\mathrm{B}_1\mathrm{A}_4'\right),$$

$$B_{13} = B\left(\mathrm{B}_1'\mathrm{A}_4K^{\frac{3}{2}} + \mathrm{BA}_1'\mathrm{A}_4K^{\frac{3}{2}}\right),$$

$$B_{14} = B\left(\mathrm{B}_1'\mathrm{A}_3K^{\frac{3}{2}} + B\mathrm{A}_1'\mathrm{A}_3K^{\frac{3}{2}}\right),$$

$$B_{15} = \frac{B_{11}}{K} - \frac{2B_{14}}{K^{\frac{3}{2}}}, \qquad B_{16} = \frac{B_{12}}{K} - \frac{2B_{13}}{K^{\frac{3}{2}}},$$

$$B_{17} = \frac{B_{13}}{K^2}, \quad B_{18} = \frac{B_{14}}{K^2}, \qquad B_{19} = \left(h_1\cosh\left[K^{\frac{1}{2}}h_1\right] - h_2\cosh\left[K^{\frac{1}{2}}h_2\right]\right),$$

$$B_{20} = \left(h_1\sinh\left[K^{\frac{1}{2}}h_1\right] - h_2\sinh\left[K^{\frac{1}{2}}h_2\right]\right), B_{21} = \left(h_1\cosh\left[K^{\frac{1}{2}}h_1\right] + h_2\cosh\left[K^{\frac{1}{2}}h_2\right]\right),$$

$$B_{22} = \left(h_1\sinh\left[K^{\frac{1}{2}}h_1\right] + h_2\sinh\left[K^{\frac{1}{2}}h_2\right]\right),$$

$$B_{23} = \frac{(N_1 - BF_1) + B_{15}C_1 + B_{16}C_2 + B_{17}B_{19} + B_{18}B_{20}}{h_1 - h_2},$$

$$B_{24} = \frac{B_{15}C_3 + B_{16}C_4 + B_{17}B_{21} + B_{18}B_{22} + B_{19}(h_1 + h_2)}{2},$$

$$D_1 = -Re(A_1A_1') + \frac{A}{B}B_{23} - KA_1,$$

$$D_2 = -Re\left(A_1A_4'\sqrt{K} + A_1'A_4\sqrt{K} - A_2'A_3K\right) + \alpha_1\left(A_1A_4'K^{\frac{3}{2}} - A_2'A_3K^2 + A_1'A_4K^{\frac{3}{2}}\right),$$

$$D_3 = Re(A_1'A_3K) - \alpha_1A_1'A_3K^2,$$

$$D_4 = -Re\left(A_1A_3'\sqrt{K} + A_1'A_3\sqrt{K} - A_2'A_4K\right) + \alpha_1\left(A_1A_3'K^{\frac{3}{2}} - A_2'A_4K^2 + A_1'A_3K^{\frac{3}{2}}\right),$$

$$D_5 = Re(A_1' A_4 K) - \alpha_1 A_1' A_4 K^2,$$

$$D_6 = 4\alpha_1 K^2 A_{11}, \qquad D_7 = 4\alpha_1 K^2 A_{12}.$$

References

[1] El Shehawey EF, Mekheimer KS, Kaldas SF, Afifi NAS. Peristaltic transport through a porous medium. J. Biomath. 1999, 14(1): 1-13.

[2] Latham TW. Fluid motions in a peristaltic pump. M. Sc. Thesis, MIT, Cambridge, MA. 1966.

[3] Burns JC, Parkes T. Peristaltic motion. J. Fluid Mech. 1967, 29: 731 – 743.

[4] Fung Y, Yih C. Biofluid mechanics in flexible tubes. Trans. ASME: Journal of Applied Mechanics. 1968, 35(4): 669–675.

[5] Shapiro AH, Jaffrin MY, Weinberg SL. Peristaltic pumping with long wavelengths at low Reynolds number. J. Fluid Mech. 1969, 37(4): 799-825.

[6] Yin FCP, Fung YC. Comparison of theory and experiment in peristaltic transport. Journal of Fluid Mechanics. 1971, 47(1): 93-112.

[7] Barton C, Raynor S. Peristaltic flow in tubes. The Bulletin of mathematical biophysics. 1968, 30(4): 663-680.

[8] Lykoudis PS. Peristaltic pumping: A bioengineering model. In Proceeding Workshop Hydrodynamic Upper Urinary Tract, Nat. Acad. Sci., Washington, DC. 1971.

[9] Lew HS, Fung YC, Lowenstein CB. Peristaltic carrying and mixing of chyme in the small intestine (an analysis of a mathematical model of peristalsis of the small intestine). Journal of Biomechanics. 1971, 4(4): 297-315.

[10] Tong P, Vawter D. An analysis of peristaltic pumping. J. Applied Mech. 1972, 39(4): 857-862.

[11] Li CH. Peristaltic transport in circular cylindrical tubes. Journal of biomechanics. 1970, 3(5): 513-523.

[12] Mittra TK, Prasad SN. Interaction of peristaltic motion with Poiseuille flow. Bulletin of mathematical biology. 1974, 36: 127-141.

[13] Liron N. On peristaltic flow and its efficiency. Bulletin of mathematical biology. 1976, 38(6): 573-596.

[14] Jaffrin MY. Inertia and streamline curvature effects on peristaltic pumping. International Journal of Engineering Science. 1973, 11(6): 681-699.

[15] Gupta BB, Seshadri V. Peristaltic pumping in non-uniform tubes. Journal of Biomechanics. 1976, 9(2): 105-109.

[16] Vishnyakov VI, Pavlov KB, Romanov AS. Peristaltic flow of a non-Newtonian viscoplastic liquid in a slot channel. Journal of engineering physics. 1976, 31(3): 1078-1082.

[17] Manero O, Mena B, Valenzuela R. Further developments on non-Newtonian flow in oscillating pipes. Rheologica Acta. 1978, 17(6): 693-697.

[18] Srivastava LM, Srivastava VP, Sinha SN. Peristaltic transport of a physiological fluid. Biorheology. 1983, 20(2): 153-166.

[19] Böhme G, Friedrich R. Peristaltic flow of viscoelastic liquids. Journal of Fluid Mechanics. 1983, 128: 109-122.

[20] Srivastava LM, Srivastava VP. Peristaltic transport of a two-layered model of physiological fluid. Journal of biomechanics. 1982, 15(4): 257-265.

[21] Takabatake S, Ayukawa K. Numerical study of two-dimensional peristaltic flows. Journal of Fluid Mechanics. 1982, 122: 439-465.

[22] Pozrikidis C. A study of peristaltic flow. Journal of Fluid Mechanics. 1987, 180: 515-527.

[23] Li M, Brasseur JG. Non-steady peristaltic transport in finite-length tubes. Journal of Fluid Mechanics. 1993, 248: 129-151.

[24] Provost AM, Schwarz WH. A theoretical study of viscous effects in peristaltic pumping. Journal of Fluid Mechanics. 1994, 279: 177-195.

[25] Siddiqui AM, Schwarz WH. Peristaltic flow of a second-order fluid in tubes. Journal of Non-Newtonian Fluid Mechanics. 1994, 53: 257-284.

[26] Hayat T, Aslam N, Khan MI, Khan MI, Alsaedi A. Physical significance of heat generation/absorption and Soret effects on peristalsis flow of pseudoplastic fluid in an inclined channel. Journal of Molecular Liquids. 2019, 275: 599-615.

[27] Hino T, Yanagimachi R. Active peristaltic movements and fluid production of the mouse oviduct: their roles in fluid and sperm transport and fertilization. Biology of reproduction. 2019, 101(1): 40-49.

[28] Khan MI, Farooq S, Hayat T, Shah F, Alsaedi A. Numerical simulation for entropy generation in peristaltic flow with single and multi-wall carbon nanotubes. International Journal of Numerical Methods for Heat & Fluid Flow. 2019, 29(12): 4684 – 4705.

[29] Babu VR. Peristaltic flow of Bingham fluid in an inclined tube. International Journal of Engineering Development and Research. 2019, 7(1): 127 – 132.

[30] Formato G, Romano R, Formato A, Sorvari J, Koiranen T, Pellegrino A, Villecco F. Fluid–Structure Interaction Modeling Applied to Peristaltic Pump Flow Simulations. Machines. 2019, 7(3): 50.

[31] Noreen S, Malik A, Rashidi MM. Peristaltic Flow of Shear Thinning Fluid via Temperature-Dependent Viscosity and Thermal Conductivity. Communications in Theoretical Physics. 2019, 71(4): 367.

[32] Mekheimer KS, Shankar BM, Abo-Elkhair RE. Effects of Hall current and permeability on the stability of peristaltic flow. SN Applied Sciences. 2019, 1(12): 1610.

[33] Reddappa B, Parandhama A, Sreenadh S. Peristaltic transport of conducting Williamson fluid in a porous channel. J. Math. Comput. Sci. 2019, 10(2): 277-288.

[34] Manjunatha G, Rajashekhar C, Vaidya H, Prasad KV, Divya BB. Heat transfer analysis on peristaltic transport of a Jeffery fluid in an inclined elastic tube with porous walls. International Journal of Thermofluid Science and Technology. 2020, 7(1): 20070101.

[35] Farooq S, Khan MI, Riahi A, Chammam W, Khan WA. Modeling and interpretation of peristaltic transport in single and multi-walls carbon nanotubes with entropy optimization and Newtonian heating. Computer Methods and Programs in Biomedicine. 2020, 192: 105435.

[36] Vaidya H, Rajashekhar C, Manjunatha G, Prasad KV, Makinde OD, Sreenadh S. Peristaltic motion of non-Newtonian fluid with variable liquid properties in a convectively heated nonuniform tube: Rabinowitsch fluid model. Journal of Enhanced Heat Transfer. 2019, 26(3).

[37] Krzeminski SK, Smialek M, Wlodarczyk M. Numerical analysis of peristaltic MHD flows. IEEE transactions on magnetics. 2000, 36(4): 1319-1324.

[38] Afifi NAS, Gad NS. Interaction of peristaltic flow with pulsatile magneto-fluid through a porous medium. Acta Mechanica. 2001, 149(1-4): 229-237.

[39] Mekheimer KS, Al-Arabi TH. Nonlinear peristaltic transport of MHD flow through a porous medium. International Journal of Mathematics and Mathematical Sciences. 2003, 2003(26): 1663-1682.

[40] Mekheimer KS. Non-linear peristaltic transport of magnetohydrodynamic flow in an inclined planar channel. Arabian Journal for Science and Engineering. 2003, 28(2): 183-202.

[41] El Naby AEHA., El Misery AEM, El Kareem MA. Effects of a magnetic field on trapping through peristaltic motion for generalized Newtonian fluid in channel. Physica A: Statistical Mechanics and its Applications. 2006, 367: 79-92.

[42] Hayat T, Khan M, Siddiqui AM, Asghar S. Non-linear peristaltic flow of a non-Newtonian fluid under effect of a magnetic field in a planar channel. Communications in Nonlinear Science and Numerical Simulation. 2007, 12(6): 910-919.

[43] Hayat T, Ali N. Peristaltically induced motion of a MHD third grade fluid in a deformable tube. Physica A: Statistical Mechanics and its applications. 2006, 370(2): 225-239.

[44] Hayat T, Afsar A, Khan M, Asghar S. Peristaltic transport of a third order fluid under the effect of a magnetic field. Computers & Mathematics with Applications. 2007, 53(7): 1074-1087.

[45] Mekheimer KS. Peristaltic flow of blood under effect of a magnetic field in a non-uniform channel. Applied Mathematics and Computation. 2004, 153(3): 763-777.

[46] Mekheimer KS, Elmaboud YA. Peristaltic flow through a porous medium in an annulus: application of an endoscope. Applied Mathematics & Information Sciences. 2008, 2(1): 103-121.

[47] Tanveer A, Khan M, Salahuddin T, Malik MY, Khan F. Theoretical investigation of peristaltic activity in MHD based blood flow of non-Newtonian material. Computer Methods and Programs in Biomedicine. 2020, 187: 105225.

[48] Khan LA, Raza M, Mir NA, Ellahi R. Effects of different shapes of nanoparticles on peristaltic flow of MHD nanofluids filled in an asymmetric channel. Journal of Thermal Analysis and Calorimetry. 2019, 1-12.

[49] Tanveer A, Hayat T, Alsaedi A, Ahmad B. Heat transfer analysis for peristalsis of MHD Carreau fluid in a curved channel through modified Darcy law. Journal of Mechanics. 2019, 35(4): 527-535.

[50] Vajravelu K, Radhakrishnamacharya G, Radhakrishnamurty V. Peristaltic flow and heat transfer in a vertical porous annulus with long wave approximation. International Journal of Non-Linear Mechanics. 2007, 42(5): 754-759.

[51] Ali N, Sajid M, Javed T, Abbas Z. Heat transfer analysis of peristaltic flow in a curved channel. International Journal of Heat and Mass Transfer. 2010, 53(15-16): 3319-3325.

[52] Srinivas S. Kothandapani M. The influence of heat and mass transfer on MHD peristaltic flow through a porous space with compliant walls. Applied Mathematics and Computation. 2009, 213(1): 197-208.

[53] Hayat T, Hina S, Ali N. Simultaneous effects of slip and heat transfer on the peristaltic flow. Communications in Nonlinear Science and Numerical Simulation. 2010, 15(6): 1526-1537.

[54] Ellahi R, Bhatti MM, Vafai K. Effects of heat and mass transfer on peristaltic flow in a non-uniform rectangular duct. International Journal of Heat and Mass Transfer. 2014, 71: 706-719.

[55] Sinha A, Shit GC, Ranjit NK. Peristaltic transport of MHD flow and heat transfer in an asymmetric channel: Effects of variable viscosity, velocity-slip and temperature jump. Alexandria Engineering Journal. 2015, 54(3): 691-704.

[56] Mekheimer KS, Husseny SZA, Elmaboud YA. Effects of heat transfer and space porosity on peristaltic flow in a vertical asymmetric channel. Numerical Methods for Partial Differential Equations: An International Journal. 2010, 26(4): 747-770.

[57] Khan AA, Usman H, Vafai K, Ellahi R. Study of peristaltic flow of magnetohydrodynamics Walter's B fluid with slip and heat transfer. Scientia iranica. 2016, 23(6): 2650-2662.

[58] Bhatti MM, Ellahi R, Zeeshan A. Study of variable magnetic field on the peristaltic flow of Jeffrey fluid in a non-uniform rectangular duct having compliant walls. Journal of Molecular Liquids. 2016, 222: 101-108.

[59] Mekheimer KS, Husseny SZA, Elmaboud YA. Effects of heat transfer and space porosity on peristaltic flow in a vertical asymmetric channel. Numerical Methods for Partial Differential Equations: An International Journal. 2010, 26(4): 747-770.

[60] Tripathi D, Bég OA. A study of unsteady physiological magneto-fluid flow and heat transfer through a finite length channel by peristaltic pumping. Proceedings of

the institution of mechanical Engineers, Part H: Journal of Engineering in Medicine. 2012, 226(8): 631-644.

[61] Reddy MG. Heat and mass transfer on magnetohydrodynamic peristaltic flow in a porous medium with partial slip. Alexandria Engineering Journal. 2016, 55(2): 1225-1234.

[62] Mehmood OU, Qureshi AA, Yasmin H, Uddin S. Thermo-mechanical analysis of non-Newtonian peristaltic mechanism: Modified heat flux model. Physica A: Statistical Mechanics and its Applications. 2020, 550: 124014.

[63] Noreen S, Kausar T, Tripathi D, Ain QU, Lu DC. Heat transfer analysis on creeping flow Carreau fluid driven by peristaltic pumping in an inclined asymmetric channel. Thermal Science and Engineering Progress. 2020, 17: 100486.

[64] Tanveer A, Hayat T, Alsaedi A, Ahmad B. Heat transfer analysis for peristalsis of MHD Carreau fluid in a curved channel through modified Darcy law. Journal of Mechanics. 2019, 35(4): 527-535.

[65] Riaz A, Alolaiyan H, Razaq A. Convective heat transfer and magnetohydrodynamics across a peristaltic channel coated with nonlinear nanofluid. Coatings. 2019, 9(12): 816.

[66] Makinde OD, Reddy MG. MHD peristaltic slip flow of Casson fluid and heat transfer in channel filled with a porous medium. Scientia Iranica. Transaction B, Mechanical Engineering. 2019, 26(4): 2342-2355.

[67] Ebaid A, Aly EH. Exact analytical solution of the peristaltic nanofluids flow in an asymmetric channel with flexible walls and slip condition: application to the cancer treatment. Computational and mathematical methods in medicine, 2013.

[68] Hayat T, Hussain Q, Ali N. Influence of partial slip on the peristaltic flow in a porous medium. Physica A: Statistical Mechanics and its Applications. 2008, 387(14): 3399-3409.

[69] Ellahi R, Hussain F. Simultaneous effects of MHD and partial slip on peristaltic flow of Jeffery fluid in a rectangular duct. Journal of Magnetism and Magnetic Materials. 2015, 393: 284-292.

[70] Tripathi D, Gupta PK, Das S. Influence of slip condition on peristaltic transport of a viscoelastic fluid with fractional Burger's model. Thermal Science. 2011, 15(2): 501-515.

[71] El-Shehawy EF, El-Dabe NT, El-Desoky IM. Slip effects on the peristaltic flow of a non-Newtonian Maxwellian fluid. Acta Mechanica. 2006, 186(1-4): 141-159.

[72] Nadeem S, Akram S. Slip effects on the peristaltic flow of a Jeffrey fluid in an asymmetric channel under the effect of induced magnetic field. International Journal for Numerical Methods in Fluids. 2010, 63(3): 374-394.

[73] Hayat T, Mehmood OU. Slip effects on MHD flow of third order fluid in a planar channel. Communications in Nonlinear Science and Numerical Simulation. 2011, 16(3): 1363-1377.

[74] Mitra TK, Prasad SN. On the Influence of Wall Properties and Poiseuille Flow in Peristalsis. J. Biomech. 1973, 6: 681-693.

[75] Hayat T, Hina S. The influence of wall properties on the MHD peristaltic flow of a Maxwell fluid with heat and mass transfer. Nonlinear analysis: Real world applications. 2010, 11(4): 3155-3169.

[76] Srinivas S, Gayathri R, Kothandapani M. The influence of slip conditions, wall properties and heat transfer on MHD peristaltic transport. Computer Physics Communications. 2009, 180(11): 2115-2122.

[77] Hayat T, Hina S, Hendi AA, Asghar S. Effect of wall properties on the peristaltic flow of a third-grade fluid in a curved channel with heat and mass transfer. International Journal of Heat and Mass Transfer. 2011, 54(23-24): 5126-5136.

[78] Shahzadi I, Sadaf H, Nadeem S, Saleem A. Bio-mathematical analysis for the peristaltic flow of single wall carbon nanotubes under the impact of variable viscosity and wall properties. Computer methods and programs in biomedicine. 2017, 139: 137-147.

[79] Hina S, Mustafa M, Hayat T, Alsaedi A. Peristaltic flow of pseudoplastic fluid in a curved channel with wall properties. Journal of Applied Mechanics. 2013, 80(2).

[80] Hayat T, Javed M, Hendi AA. Peristaltic transport of viscous fluid in a curved channel with compliant walls. International journal of heat and mass transfer. 2011, 54(7-8): 1615-1621.

[81] Muthu P, Kumar BR, Chandra P. On the influence of wall properties in the peristaltic motion of micropolar fluid. The ANZIAM Journal. 2003, 45(2): 245-260.

[82] Saffman PG. On the stability of laminar flow of a dusty gas. J. fluid Mech. 1962, 13(1): 120-128.

[83] Nayfeh AH. Oscillating two-phase flow through a rigid pipe. AIAA Journal. 1966, 4(10): 1868-1870.

[84] Charya GR. Pulsatile flow of a dusty fluid through a constricted channel. Zeitschrift für angewandte Mathematik und Physik ZAMP. 1978, 29(2): 217-225.

[85] Srinivasacharya D, Radhakrishnamacharya G, Srinivasulu C. The effects of wall properties on peristaltic transport of a dusty fluid. Turkish Journal of Engineering and Environmental Sciences. 2009, 32(6): 357-365.

[86] Kumar SR, Yadhav DP, Kathyayani G, Prasad RS, Rao GP. Peristaltic flow of a dusty couple stress fluid in a flexible channel. Int. J. Open Problems Compt. Math. 2010, 3(5).

[87] Ramamurthy V, Rao US. Flow of a dusty fluid due to wavy motion of a wall for moderately large Reynolds numbers. International Journal of Mathematics and Mathematical Sciences. 1989, 12(3): 559-578.

[88] Rathod VP, Kulkarni P. The influence of wall properties on MHD peristaltic transport of dusty fluid. Advances in Applied Science Research. 2011, 2(3): 265-279.

[89] Muthuraj R, Nirmala K, Srinivas S. Influences of chemical reaction and wall properties on MHD peristaltic transport of a dusty fluid with heat and mass transfer. Alexandria Engineering Journal. 2016, 55(1): 597-611.

[90] Hayat T, Rafiq M, Alsaedi A, Ahmad B. Radiative and Joule heating effects on peristaltic transport of dusty fluid in a channel with wall properties. The European Physical Journal Plus. 2014, 129(10): 225.

[91] Bhatti MM, Zeeshan A, Ijaz N, Bég OA, Kadir A. Mathematical modelling of nonlinear thermal radiation effects on EMHD peristaltic pumping of viscoelastic dusty fluid through a porous medium duct. Engineering science and technology, an international journal. 2017, 20(3): 1129-1139.

[92] Madhura KR, Uma MS. Conducting dusty fluid flow through a constriction in a porous medium. International Journal of Applied Mathematics Research. 2016, 5(1): 29.

[93] Gireesha BJ, Bagewadi CS, Prasannakumar BC. Pulsatile flow of an unsteady dusty fluid through rectangular channel. Communications in Nonlinear Science and Numerical Simulation. 2009, 14(5): 2103-2110.

[94] Ramesh GK, Gireesha B, Bagewadi CS. Unsteady flow of a conducting dusty fluid between two circular cylinders. Acta Math. Univ. Comenianae. 2011, 80(2): 171-184.

[95] Siddiqa S, Begum N, Hossain MA., Mustafa N, Gorla RSR. Two-phase dusty fluid flow along a cone with variable properties. Heat and Mass Transfer. 2017, 53(5): 1517-1525.

[96] Kiran GR, Murthy VR, Radhakrishnamacharya G. Pulsatile flow of a dusty fluid thorough a constricted channel in the presence of magnetic field. Materials Today: Proceedings. 2019, 19(6): 2645-2649.

[97] Kalpana G, Madhura KR, Kudenatti RB. Impact of temperature-dependant viscosity and thermal conductivity on MHD boundary layer flow of two-phase dusty fluid through permeable medium. Engineering Science and Technology, an International Journal. 2019, 22(2): 416-427.

[98] Hasona WM, El-Shekhipy A, Ibrahim MG. Semi-analytical solution to MHD peristaltic flow of a Jeffrey fluid in presence of Joule heat effect by using multi-step differential transform method. New Trends in Mathematical Sciences. 2019, 7(2): 123-137.

[99] Turkyilmazoglu M. Magnetohydrodynamic two-phase dusty fluid flow and heat model over deforming isothermal surfaces. Physics of Fluids. 2017, 29(1): 013302.

[100] Prakash O, Kumar D, Dwivedi YK. Effects of thermal diffusion and chemical reaction on MHD flow of dusty visco-elastic (Walter's liquid model-B) fluid. Journal of Electromagnetic Analysis and Application. 2010, 2: 581-587.

[101] Javed M, Hayat T. Effects of heat transfer on MHD peristaltic transport of dusty fluid in a flexible channel. 14th International Bhurban Conference on Applied Sciences and Technology (IBCAST) IEEE. 2017, 539-550.

[102] Afsar A, Ali N, Hayat T. Effect of an Endoscope on the Peristaltic Transport through a Porous Medium. Journal of Porous Media. 2008, 11(5): 477 – 486.